

Wayne State University Dissertations

January 2022

Phenanthroline-Catalyzed 1,2-Cis Glycosylation: Scope And Mechanism

Jiayi Li
Wayne State University

Follow this and additional works at: https://digitalcommons.wayne.edu/oa_dissertations

 Part of the [Organic Chemistry Commons](#)

Recommended Citation

Li, Jiayi, "Phenanthroline-Catalyzed 1,2-Cis Glycosylation: Scope And Mechanism" (2022). *Wayne State University Dissertations*. 3680.

https://digitalcommons.wayne.edu/oa_dissertations/3680

This Open Access Dissertation is brought to you for free and open access by DigitalCommons@WayneState. It has been accepted for inclusion in Wayne State University Dissertations by an authorized administrator of DigitalCommons@WayneState.

PHENANTHROLINE-CATALYZED 1,2-*CIS* GLYCOSYLATION: SCOPE AND MECHANISM

by

JIAYI LI

DISSERTATION

Submitted to the Graduate School

of Wayne State University,

Detroit, Michigan

in partial fulfillment of the requirements

for the degree of

DOCTOR OF PHILOSOPHY

2022

MAJOR: CHEMISTRY (Organic)

Approved By:

Advisor

Date

© COPYRIGHT BY

JIAYI LI

2022

All Rights Reserved

DEDICATION

To the coin that stayed on my side.

ACKNOWLEDGMENTS

It was a summer night in 2010, a coin decided my journey in America. Firstly, I would like to acknowledge my elder brother who flipped the coin, and my twin sister who chose the other side of the coin (journey to the U.K.). Without them, my path in life would be completely different. Next, I would like to acknowledge my younger brother, who kept me accompanied during my college time. Last but not least, I would like to acknowledge my parents, who gave unconditional love and support to all four of us.

My interest in chemistry began in 2012, the second year after I arrived in America. Here, I would like to thank my parents again for supporting me on a path that was different from their expectations. I quickly adjusted my path and started to look for a new university with a chemical engineering major. Understood the family's financial situation, I covered both coasts on the American map and picked the University of Iowa with my eyes closed.

During my first year at the University of Iowa, I encountered my current advisor, Prof. Hien M. Nguyen, who inspired my interest in organic chemistry, and encouraged me to pursue a higher degree in organic chemistry. In my junior year, I joined Hien's research lab, where I met my fellow mentors Dr. Eric Sletten, Dr. Ravi Loka, and Dr. Fei Yu. Thank you for all the guidance and for being extremely patient with me.

With great enthusiasm for carbohydrate chemistry, I decided to continue my study in Hien's lab, which led me to Wayne State University. I would like to thank all the labmates throughout the years when I stayed in the Nguyen lab. I would also like to acknowledge all the faculties and staffs in the department of chemistry for providing a stable and efficient research environment.

I would also like to acknowledge my committee member: Prof. Jeremy Kodanko, Prof. David Crich, Prof. Long Luo, Prof. Stanislav Groysman, and Prof. Pavel Nagorny, for giving me suggestions on the projects. Special thanks to Prof. H. Bernhard Schlegel for all the guidance on computational chemistry.

In the end, I would like to thank all my family, friends, and acquaintances who have participated in my journey. It has been a wonderful journey with your participation.

TABLE OF CONTENTS

DEDICATION	ii
ACKNOWLEDGMENTS	iii
LIST OF ABBREVIATIONS	viii
LIST OF FIGURES	xiii
LIST OF SCHEMES.....	xvi
LIST OF TABLES	xviii
CHAPTER 1: INTRODUCTION	1
1.1 The Significance of Carbohydrates in Biological Systems.....	1
1.1.1 Metabolism: carbohydrates as an energy source.....	1
1.1.2 Structural building blocks	3
1.1.3 Cellular communication and recognition: glycode and the decoders.....	7
1.2 Carbohydrates and their mimics in drug discovery.....	11
1.2.1 Carbohydrate vaccines	11
1.2.2 Carbohydrate drugs targeting the central dogma of biology.....	12
1.2.3 Glycosidase and glycosyltransferase inhibitors	13
1.2.4 Glycosaminoglycans and their therapeutic applications	14
1.3 Chemical Methods of Carbohydrates Synthesis	15
1.3.1 General pathways of chemical glycosylation.....	16
1.3.2 Substrate-control of stereochemistry.....	18
1.3.3 Reagent-control of stereochemistry	21
1.4 Catalytic Glycosylation.....	24

1.4.1	Beginning of catalytic glycosylation.....	24
1.4.2	Design of stereoselective catalytic glycosylation	25
1.4.3	Catalyst development in stereoselective glycosylation.....	26
1.5	Main objectives.....	40
1.5.1.	Inspiration and hypothesis	40
1.5.2.	Preliminary results and continuation.....	42
1.5.3.	Major Goals	43
CHAPTER 2: SCOPE OF PHENANTHROLINE-CATALYZED 1,2- <i>CIS</i> PYRANOSYLATION.....		44
2.1	First generation phenanthroline catalysis.....	44
2.2	Second generation phenanthroline catalyst.....	45
2.2.1.	Development of a new class of phenanthroline catalyst	45
2.2.2.	Influence of phenanthroline catalyst	49
2.3.	Reaction scope with phenanthroline catalysis.....	51
2.3.1.	Stereoselective glycosylation and limitation.....	51
2.3.2.	Site-selective glycosylation.....	53
2.3.3.	Chemoselective glycosylation.....	54
2.3.4.	Orthogonal glycosylation.....	57
2.4.	Summary	58
CHAPTER 3: MECHANISM OF PHENANTHROLINE-CATALYZED 1,2- <i>CIS</i> PYRANOSYLATION		59
3.1.	β -Glycosyl bromide driven glycosylation?.....	59
3.2.	Double S_N2 mechanism? (Kinetic study).....	60

3.3. Detection of pyranosyl phenanthrolium ion intermediates	64
3.4. Hydrogen bonding in the pyranosyl phenanthrolium ion intermediates	69
3.5. Proposed mechanism	71
3.6. Conclusion	73
CHAPTER 4: EXPLORATION OF PHENANTHROLINE-CATALYZED 1,2-<i>CIS</i> FURANOSYLATION	74
4.1. Introduction.....	74
4.2. Effects of donor anomeric composition	77
4.3. Detection of furanosyl phenanthrolium ion intermediates.....	80
4.4. Reaction progress analysis of phenanthroline-catalyzed furanosylation	83
4.5. Proposed mechanism of phenanthroline-catalyzed furanosylation.....	86
4.5. Conclusion	89
CHAPTER 5: EXPERIMENTAL SECTION	90
5.1. General Information.....	90
5.2. Chapter 2 experimental section.....	91
5.2.1. General procedure and condition in Table 5	91
5.2.2. Standard procedure for catalyst screening	95
5.2.3. Preparation of monosaccharide	96
5.2.4. Standard procedures for C1 or C14-catalyzed glycosylation (Table 9 and Scheme 33).....	102
5.2.5. Standard procedures for C14-catalyzed site-selective glycosylation (Scheme 32).....	108
5.2.5. Standard procedures for C14-catalyzed chemoselective glycosylation (Table 10)	110
5.3. Chapter 3 experimental section.....	114

5.3.1. Kinetic study	114
5.3.2. Mechanistic study	120
5.3.3. Density Functional Theory (DFT) Calculations	128
5.4. Chapter 4 experimental section.....	129
5.4.1. Preparation of 2-deoxy-2-fluoro-3,5-di- <i>O</i> -benzyl-D-furanosyl bromide donors.....	129
5.4.2. NMR study with 2-fluoro xylofuranosyl donor	130
5.4.3. NMR study with 2-fluoro arabinofuranosyl donor	135
APPENDIX A: SYMBOL NOMENCLATURE FOR GLYCANS ²²	140
APPENDIX B: ¹ H, ¹³ C AND ¹⁹ F NMR SPECTRA.....	141
APPENDIX C: LICENSES FROM PUBLISHERS	172
REFERENCES	175
ABSTRACT.....	197
AUTOBIOGRAPHICAL STATEMENT	199

LIST OF ABBREVIATIONS

Ac	Acetyl
ADP	Adenosine diphosphate
AIDS	Acquired immunodeficiency syndrome
Ar	Aryl
ATP	Adenosine triphosphate
AZT	azidothymidine
AZT	Azidothymidine
BINOL	1,1'-Bi-2-naphthol
Bn	Benzyl
BPhen	Bathophenanthroline
bs	broad singlet
Bu ₄ NBr	Tetrabutylammonium bromide
Bz	Benzoyl
C ₆ D ₆	Deuterated benzene
CAC	Citric acid cycle
Cat	Catalyst
CD ₂ Cl ₂	Deuterated dichloromethane
CDCl ₃	Deuterated chloroform
CH ₂ Cl ₂	Dichloromethane
CoA	Coenzyme A
COSY	COrelated SpectroscopY
COVID-19	Coronavirus disease 2019
CRD	Carbohydrate recognition domain

d	Doublet
D ₂ O	Deuterated water
DFT	Density function theory
DMAP	4-(dimethylamino)pyridine
DMF	<i>N,N</i> -dimethylformamide
DNA	Deoxyribonucleic acid
DTBMP	2,6-di- <i>tert</i> -butyl-4-methylpyridine
equiv.	equivalent
ESI	Electrospray ionization
Et	Ethyl
FADH ₂	Flavin adenine dinucleotide
FDA	Food and Drug Administration
GAG	Glycosaminoglycan
GalNac	<i>N</i> -acetylgalactosamine
GBPs	Glycan-binding proteins
Glc	Glucose
gp120	Glycoprotein 120
GTs	Glycosyltransferases
h	Hour
H-bonding	Hydrogen bonding
HBr	Hydrobromic acid
HIV	Human immunodeficiency virus
HIV/AIDS	Human immunodeficiency virus and acquired immunodeficiency syndrome
HRMS	High-Resolution Mass spectrometry

Hz	hertz
IBO	Isobutylene oxide
<i>J</i>	Coupling constant
KDO	3-Deoxy-D-manno-octulosomic acid
LG	Leaving group
LMWH	Low molecular weight heparin
LPS	Lipopolysaccharide
M	Molar
m	Multiplet
Me	Methyl
mg	milligram
min	Minute
mL	milliliter
mmol	millimoles
mol%	mole percent
MTBE	<i>tert</i> -butyl methyl ether
NADH	Nicotinamide adenine dinucleotide
NBS	N-bromosuccinimide
NMR	Nuclear magnetic resonance
NOESY	Nuclear Overhauser Effect Spectroscopy
Nu	Nucleophile
°C	Degree Celsius
PG	Protecting group
Ph	Phenyl

Phen	Phenanthroline
POCl ₃	phosphorus oxychloride
q	quartet
RNA	Ribonucleic acid
ROESY	Rotating frame Overhauser Enhancement Spectroscopy
s	Singlet
SARS-CoV-2	Severe acute respiratory syndrome coronavirus 2
SARS-CoV-2	Severe acute respiratory syndrome coronavirus 2
SMD	solvation model based on density
S _N 1	Nucleophilic substitution unimolecular
S _N 2	Nucleophilic substitution bimolecular
SNFG	Symbol nomenclature for glycans
SPINOL	1,1'-Spirobiindane-7,7'-diol
t	Triplet
TAB	(<i>ortho</i> -tosylamido)benzyl
TAC	Tricarboxylic acid cycle
TBS	<i>tert</i> -Butyldimethylsilyl
TCA	Trichloroacetimidate
Tf	Triflate
TfOH	Trifluoromethanesulfonate acid
THF	Tetrahydrofuran
TLC	Thin-layer chromatography
TMEDA	<i>N,N,N',N'</i> -tetramethylethylenediamine
TMSOTf	Trimethylsilyl triflate

TMSOTf	Trimethylsilyl trifluoromethanesulfonate
Ts	Tosyl
TS2	Second transition state
TsOH	<i>p</i> -Toluenesulfonic acid
WHO	World Health Organization
XyG	Xyloglucan
Xyl	Xylose

LIST OF FIGURES

Figure 1. Examples of carbohydrates in nature.....	1
Figure 2. The structures of starch and cellulose.....	3
Figure 3. Constitution of plant cell wall.....	4
Figure 4. Constitution of bacterial cell wall.....	6
Figure 5. Structure of pyranose.....	7
Figure 6. Symbolic representation of monosaccharides and an example of lipopolysaccharide	8
Figure 7. Glycoconjugates on the cell surface: glycoprotein, glycolipid, and glycoRNA.....	9
Figure 8. Structure of a galactose-specific C-type lectin. PDB: 1JZN.....	10
Figure 9. The design concept of carbohydrate vaccine.....	12
Figure 10. Nucleoside/nucleotide mimetics as carbohydrate-based drugs.....	13
Figure 11. Examples of glycosidase and glycosyltransferase inhibitors.....	14
Figure 12. Structures of heparin and fondaparinux.....	15
Figure 13. Category of glycosides	16
Figure 14. Design concepts for stereoselective catalytic glycosylation.....	26
Figure 15. Kinetics of the reaction of 2-propanol with glucosyl bromide 1 in C ₆ D ₆ at 50 °C	62
Figure 16. Kinetic study in respect to donor concentration	63
Figure 17. Product concentration versus time for the phenanthroline-catalyzed glycosylation with three different phenanthroline catalysts	64
Figure 18. Detection of phenanthrolium intermediate by ¹ H NMR.	65
Figure 19. Mixture of nucleophile 3 and 10 mol% C14 with DTBMP in CD ₂ Cl ₂	66
Figure 20. Conformation of the glycosyl phenanthrolium ion intermediates	67
Figure 21. Conformation of glycosyl phenanthrolium intermediates and NMR evidence	68
Figure 22. Variable-temperature ¹ H NMR spectra and proposed intermediates internal hydrogen bondings	70
Figure 23. Possible mechanism of phenanthroline-catalyzed glycosylation.....	72

Figure 24. Conformation of the 2-deoxy-2-fluoro glycosyl phenanthrolium ion	72
Figure 25. Hexasaccharide motifs found in the cell wall complex of mycobacterial arabinogalactan (AG) and lipoarabinomannan (LAM).	74
Figure 26. Detection of xylofuranosyl phenanthrolium intermediates	81
Figure 27. Detection of arabinofuranosyl phenanthrolium intermediates.....	82
Figure 28. Reaction progress for phenanthroline-catalyzed xylofuranosylation of alcohol acceptor 3	84
Figure 29. Reaction progress for phenanthroline-catalyzed arabinofuranosylation of alcohol acceptor 3	85
Figure 30. Energy diagram of phenanthroline-catalyzed furanosylation for the second nucleophilic substitution.....	86
Figure 31. Possible mechanism for phenanthroline-catalyzed xylofuranosylation.....	87
Figure 32. Possible mechanism for phenanthroline-catalyzed arabinofuranosylation.....	88
Figure 33. Example spectra array for a kinetic experiment with 1 as donor.....	116
Figure 34. Example rate plot: product concentration versus time for a kinetic experiment	116
Figure 35. Product formation versus time at different equivalent of IBO	117
Figure 36. Product formation versus time at 0 mol% catalyst	117
Figure 37. Example spectra array for a kinetic experiment with 2* as donor.....	119
Figure 38. ¹ H NMR of deuterated tetrabenzyl glucosyl bromide 2*	122
Figure 39. ¹ H NMR of deuterated tetrabenzyl glucosyl bromide 2* and C14 at 0 min	122
Figure 40. ¹ H NMR of deuterated tetrabenzyl glucosyl bromide 2* and C14 at 30 min.....	123
Figure 41. ¹ H NMR of deuterated tetrabenzyl glucosyl bromide 2* and C14 with acceptor 3 at 30 min	123
Figure 42. ¹ H NMR of deuterated tetrabenzyl glucosyl bromide 2* and C14 with acceptor 3 at 300 min	124
Figure 43. ¹ H NMR of glucosyl phenanthrolium intermediates (Int₁ and Int₂)	125
Figure 44. ¹ H- ¹ H 2D COSY NMR of glucosyl phenanthrolium intermediates (Int₁ and Int₂)	125
Figure 45. ¹ H- ¹ H 2D ROESY NMR of glucosyl phenanthrolium intermediates (Int₁ and Int₂)	126
Figure 46. Mass spectrum detection of glucosyl phenanthrolium intermediates (Int₁ and Int₂).....	126
Figure 47. ¹ H NMR of 2-deoxy-2-fluoro glucosyl phenanthrolium intermediate (Int₃)	127

Figure 48. ^1H - ^1H 2D COSY NMR of 2-deoxy-2-fluoro glucosyl phenanthrolium intermediate (Int₃)	127
Figure 49. ^1H - ^1H 2D ROESY NMR of 2-deoxy-2-fluoro glucosyl phenanthrolium intermediate (Int₃)	128
Figure 50. Optimized structures of β - and possible α -glycosyl phenanthrolium intermediates	129
Figure 51. ^1H NMR course of furanosylation with 2-fluoro xylofuranosyl bromide 50	130
Figure 52. ^{19}F NMR course of furanosylation with 2-fluoro xylofuranosyl bromide 50	131
Figure 53. ^1H NMR detection of xylofuranosyl phenanthrolium intermediates (Int₄ and Int₅)	132
Figure 54. ^{19}F NMR detection of xylofuranosyl phenanthrolium intermediates (Int₄ and Int₅)	132
Figure 55. ^1H NMR of xylofuranosyl phenanthrolium intermediates (Int₄ and Int₅)	133
Figure 56. ^1H - ^1H COSY NMR of xylofuranosyl phenanthrolium intermediates (Int₄ and Int₅)	133
Figure 57. ^1H - ^1H ROESY NMR of xylofuranosyl phenanthrolium intermediates (Int₄ and Int₅)	134
Figure 58. Mass Spectrum of xylofuranosyl phenanthrolium intermediates (Int₄ and Int₅)	134
Figure 59. ^1H NMR course of furanosylation with 2-fluoro arabinofuranosyl bromide 48	135
Figure 60. ^{19}F NMR course of furanosylation with 2-fluoro arabinofuranosyl bromide 48	136
Figure 61. ^1H NMR detection of arabinofuranosyl phenanthrolium intermediates (Int₆ and Int₇)	137
Figure 62. ^{19}F NMR detection of arabinofuranosyl phenanthrolium intermediates (Int₆ and Int₇)	137
Figure 63. ^1H NMR of arabinofuranosyl phenanthrolium intermediates (Int₆ and Int₇)	138
Figure 64. ^1H - ^1H COSY NMR of arabinofuranosyl phenanthrolium intermediates (Int₆ and Int₇)	138
Figure 65. ^1H - ^1H NOESY NMR of arabinofuranosyl phenanthrolium intermediates (Int₆ and Int₇)	139
Figure 66. Mass Spectrum of xylofuranosyl phenanthrolium intermediates (Int₆ and Int₇)	139

LIST OF SCHEMES

Scheme 1. ATP as a rapid source of energy	2
Scheme 2. Glucose as a source of energy in the biological system.....	3
Scheme 3. The central dogma of biology	12
Scheme 4. Concept of glycosylation	16
Scheme 5. General pathways of glycosylation.....	17
Scheme 6. Neighboring group participation.....	18
Scheme 7. Bimodal anchimeric assistance	19
Scheme 8. Hydrogen bonding mediated aglycone delivery	20
Scheme 9. Use of bicyclic protecting group in stereoselective glycosylation.....	20
Scheme 10. Koenigs-Knorr glycosylation and its development toward 1,2- <i>cis</i> glycosylation	22
Scheme 11. Halide ion catalyzed 1,2- <i>cis</i> glycosylation	22
Scheme 12. Glycosylation through <i>in situ</i> anomerization	23
Scheme 13. Glycosylation through direct S _N 2 substitution with alkoxide	23
Scheme 14. The first catalytic glycosylation by Emil Fischer	24
Scheme 15. First catalytic glycosylation with TCA donors	25
Scheme 16. Glycal as glycosyl donor in catalytic glycosylation.....	26
Scheme 17. Boron trifluoride activation of TCA donor	27
Scheme 18. Synthesis of glycosyl phosphate and inspiration	27
Scheme 19. Development of acid-base catalysis.....	28
Scheme 20. Regioselective activation of glycosyl acceptor.....	29
Scheme 21. Regioselective glycosylation using acid-base catalysis	30
Scheme 22. Cationic palladium(II)-catalyzed stereoselective glycosylation	31
Scheme 23. Brønsted acid-catalyzed glycosylation.....	32
Scheme 24. Kinetic resolution in stereoselective glycosylation using chiral Brønsted acid.....	33

Scheme 25. Site-selective glycosylation by the selection of chiral phosphoric acid.....	34
Scheme 26. Schreiner's thiourea catalyzed 2-deoxy galactoside synthesis	36
Scheme 27. Schreiner's thiourea catalyst as an organo photoacid in catalytic glycosylation.....	37
Scheme 28. Macrocyclic bis-thiourea catalyzed stereospecific glycosylation	39
Scheme 29. Bis-thiourea activation of glycosyl phosphate	39
Scheme 30. Retaining glycosyltransferases-catalyzed stereoretentive glycosylation	40
Scheme 31. Phenanthroline-catalyzed α -1,2- <i>cis</i> -glycosylation	41
Scheme 32. C14-catalyzed site-selective coupling of functionally diverse substrates.....	54
Scheme 33. C14-catalyzed orthogonal glycosylation	58
Scheme 34. Effect of the configuration of glycosyl bromide	60
Scheme 35. Catalytic stereoselective xylofuranosylation	76
Scheme 36. Overview of reaction outcome of phenanthroline catalysis in furanosylation system.....	77
Scheme 37. Catalytic stereoselective arabinofuranosylation.....	78
Scheme 38. Effect of donor anomeric composition in C1-catalyzed furanosylation	79

LIST OF TABLES

Table 1. Chiral Brønsted acid-catalyzed glycosylation.....	32
Table 2. Hidden Brønsted acids catalyzed glycosylation.....	35
Table 3. Urea-catalyzed stereoselective glycosylation.....	38
Table 4. Bathophenanthroline-catalyzed 1,2-cis glycosylation ^[a]	42
Table 5. Bathophenanthroline-catalyzed 1,2-cis glycosylation with electron-rich substrates ^[a]	45
Table 6. Catalyst screening with electron-rich electrophile ^[a]	47
Table 7. Catalyst development in phenanthroline framework ^[a]	48
Table 8. Influence of phenanthroline catalyst ^[a]	50
Table 9. Stereoselective glycosylation using C1 and C14 catalyst ^[a]	52
Table 10. C14 -catalyzed chemoselective glycosylation ^[a]	56

CHAPTER 1: INTRODUCTION

1.1 The Significance of Carbohydrates in Biological Systems

Carbohydrates, also known as glycans, saccharides, or simply sugars, represent a family of compounds with empirical formula $C_m(H_2O)_n$. The term carbohydrate was derived from the French (hydrate de carbone) in the nineteenth century, which later extended to polyhydroxylated aldehydes or ketone containing carbons varying between 3 and 9.¹ Carbohydrates as one of the primary constituents of cells, are the most abundant organic molecules on earth. For example, starch and cellulose are polymers of glucose (**1**), a sugar that contains 6 carbon atoms. DNA (deoxyribonucleic acid) and RNA (ribonucleic acid), the molecules that are responsible for the storage and reading of genetic information, are also built with carbohydrates such as deoxyribose or ribose (**2**), which contain 5 carbon atoms. Sialic acid (**3**), an alpha-keto acid sugar contains 9 carbon backbone that is typically found attached to the outermost ends of *N*-glycans, *O*-glycans, and glycosphingolipid.

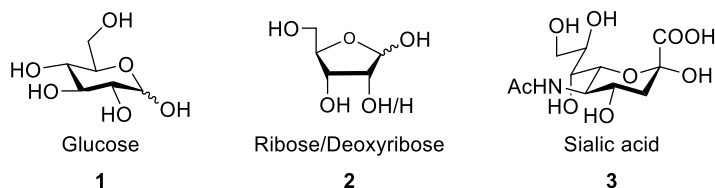


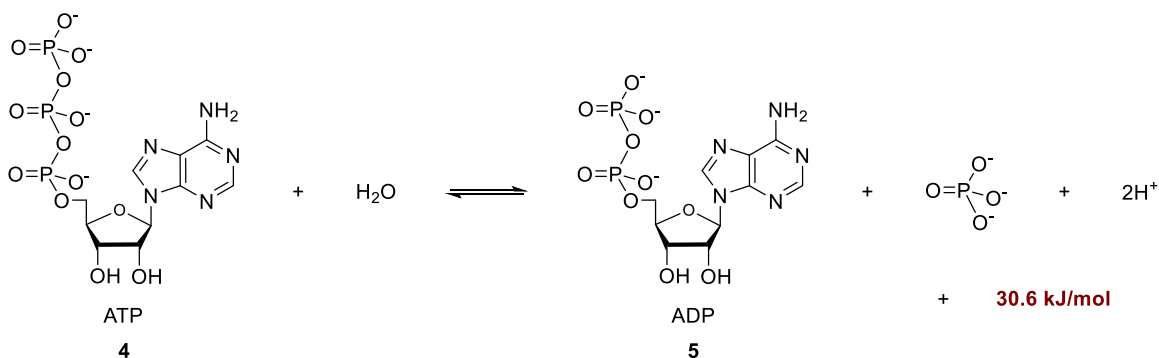
Figure 1. Examples of carbohydrates in nature

Carbohydrates play many central roles in the biological system. It has been long recognized that sugars are an important energy source and structural building blocks for many living organisms. In addition to their participation in metabolism and other intracellular events, carbohydrates also play important roles in intercellular communication or recognition by conjugation to lipids and integral membrane proteins. This section highlights the essential roles of carbohydrates play in the biological system.

1.1.1 Metabolism: carbohydrates as an energy source

Adenosine triphosphate (ATP) **4**, a molecule containing a core of ribose, is a rapidly available energy source in biological systems. ATP is also referred to as the cell's energy currency due to its property of storing and transferring energy in cells. This energy is stored in the phosphodiester bond. Through cleavage

of a phosphodiester bond of ATP, 30.6 kJ/mol of free energy is released in the biological system,¹ and adenosine diphosphate (ADP) **5** is generated (Scheme 1). Similarly, when a phosphate is removed from ADP, energy is also released and leading to the formation of adenosine monophosphate (AMP), which can be recycled into ADP or ATP by regeneration of the phosphodiester bond to restore the energy. ATP, ADP, and AMP are constantly interconverted in the cell to participate in the biochemical processes. In these events, sugars act as carriers during energy storing and transferring.

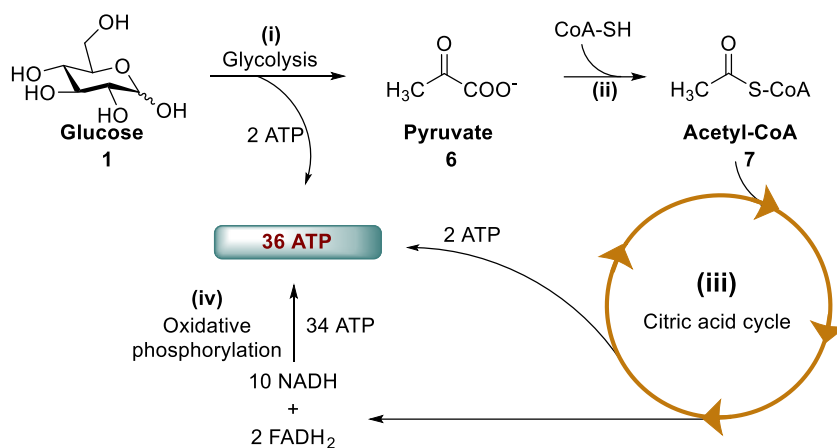


Scheme 1. ATP as a rapid source of energy

The regeneration of ADP from AMP requires ATP; therefore, regeneration of ATP becomes necessary. The major method to regenerate ATP is through phosphorylation of ADP, in which the energy is supplied by the oxidation of glucose. The breakdown of glucose to yield energy-rich ATP involved four stages as shown in Scheme 2.¹

Firstly, glucose **1** undergoes a ten-step sequential process to generate two pyruvates **6** in stage (i). This process is known as glycolysis, where a 6-carbon sugar is dissected into two 3-carbon fragments. During the process of glycolysis, two ATP are generated. In stage (ii), the pyruvates undergo oxidative decarboxylation to form a thioester of acetic acid with coenzyme A (CoA), whose product is known as acetyl-CoA (**7**). Similar to acetyl chloride or acetic anhydride, the S-CoA portion of acetyl-CoA is a good leaving group. Therefore, hydrolysis of the thioester bond is favorable, allowing the acetyl group to enter the stage (iii) – the citric acid cycle (CAC), also known as tricarboxylic acid cycle (TAC) or Krebs' cycle. Through a series of chemical reactions in CAC, the energy stored in the thioester bond is released into 2 ATP and the reduced compounds nicotinamide adenine dinucleotide (NADH) and flavin adenine

dinucleotide (FADH₂). Due to their high reductive potential, NADH and FADH₂ are also strong electron donors. As such, in the oxidative phosphorylation stage (iv), ten NADH and two FADH₂ that are generated in stages (i)-(iii) are fed into the electron transport chain and produce 34 ATP. In total, one glucose molecule produces 36 ATP in the biological system.



Scheme 2. Glucose as a source of energy in the biological system

1.1.2 Structural building blocks

Nature utilizes sugars as building blocks in a polymeric fashion, where the sugars are joining each other covalently through glycosidic linkages.¹⁻² For example, starch (**8**) and cellulose (**9**) are both polymers of D-glucose (Figure 2). Yet, the structural properties of these two polysaccharides are different, where starch is an easily digestible material with no significant structural utility. Cellulose, on the other hand, provides strong structural support to the plant cells, which further developed into materials such as wood and cotton.²

The difference in the structural properties between starch and cellulose simply arises from the anomeric configuration of the glycosidic linkages between the glucose. While starch possesses glycosidic bonds with axial (α) stereochemistry from the C1 anomeric carbon to the C4 oxygen (α -(1 \rightarrow 4) linkage), cellulose

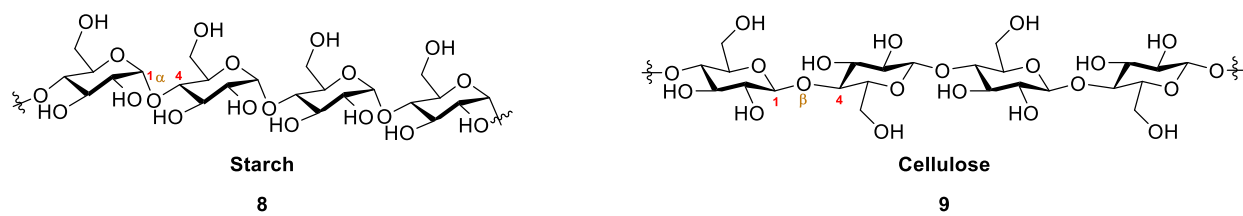


Figure 2. The structures of starch and cellulose

holds equatorial (β) glycosidic bonds (β -(1 \rightarrow 4) linkage). The difference in the anomeric configuration causes variations in the glycosidic torsion angles, where cellulose is less helical compared to starch. As a result, the cellulose strands can pack and interact with each other to form layers, which further turn into fibrils.² As such, while starch develops into the energy storage for plants, cellulose exists as the main construction of cell walls.

The cell wall (Figure 3) is a complex and heterogeneous matrix of polysaccharides that surrounds the plasma membrane of the plant cell, which is the major difference between plant and animal cells (animal cells do not have cell walls).²⁻³ A plant cell wall is a load-bearing network where layers of cellulose are cross-linked by hemicellulose and pectins.⁴⁻⁵ Hemicelluloses are polysaccharides that cross-link between cellulose layers to primarily increase wall strength. Xyloglucan (XyG, **10**) is the most common hemicellulose on earth and has been found in almost every land plant species.⁶ The basic structure of XyG includes a backbone of cellulose, with a branch of D-xylose (Xyl) connecting at the C6 oxygen position of

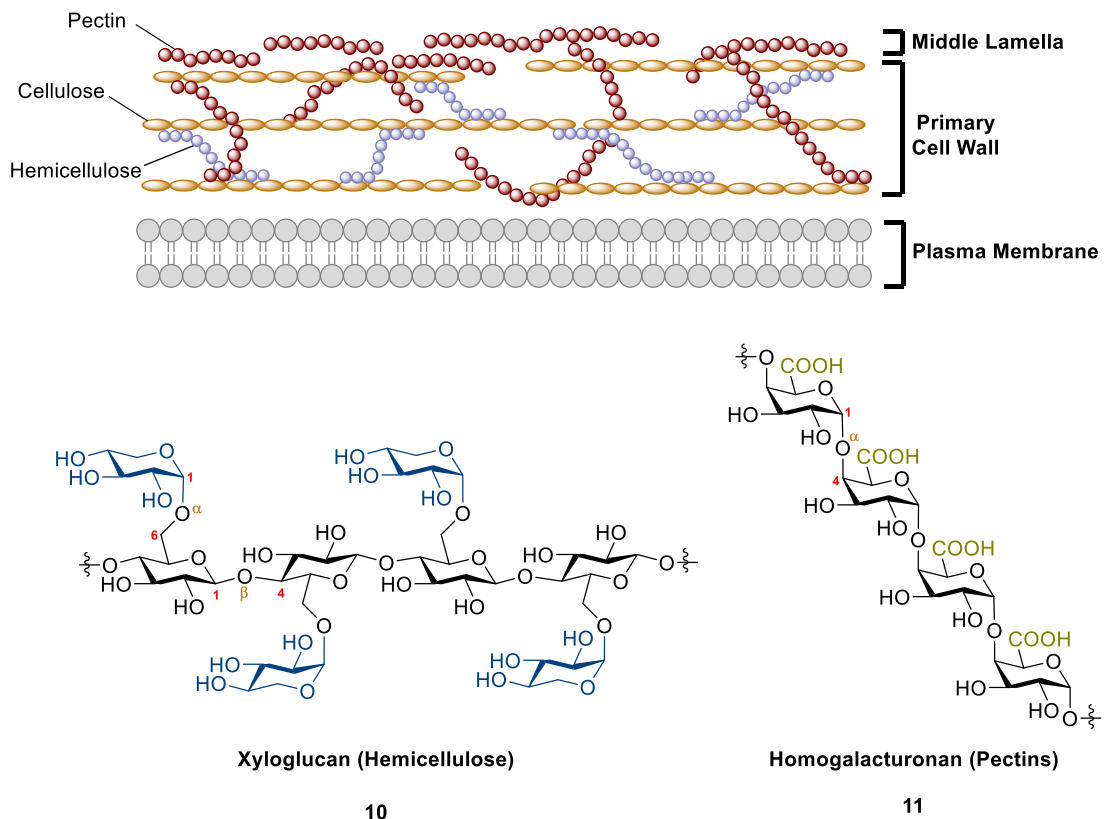


Figure 3. Constitution of plant cell wall

the glucose (Glc) with α anomeric configuration (D-Xyl- α -(1 \rightarrow 6)-Glc). The branching patterns of XyG variate their function such as solubility, which is significant in taxonomy.⁶ The remaining matrix of polysaccharides are pectins, the most structurally and functionally complex polysaccharides in plant cell wall.^{4, 7} The structure and chemical composition of pectins are diverse, yet contain a high degree of galacturonic acid, in which common structures include homogalacturonan (**11**), rhamnogalacturonan I and II, and xylogalacturonan.⁷ Galacturonic acid is a sugar acid derived from galactose, which the carboxyl group is often methylesterified in nature.⁷ The partially methylesterified pectins can form complex hydrated gels, which contribute strength and flexibility to the cell wall and provide connections to the adjacent cells in the middle lamellae (Figure 3).⁴

Unlike plant cell walls, bacterial cell walls are constituted of conjugated polysaccharides. In general, there are two types of bacteria: Gram-positive and Gram-negative bacteria.⁸ Their difference can be determined by Gram staining, where Gram-positive bacteria adopt the crystal violet color, and Gram-negative bacteria appear pink or red after treatment with alcohol.⁹ These staining results are based on the difference in the cell wall structures, whereas Gram-positive bacteria have a thick layer of peptidoglycan in the cell wall, while Gram-negative bacteria surround the peptidoglycan with an outer membrane (Figure 4).⁸ Peptidoglycan (**12**) is a polysaccharide cross-linked by peptides, consisting of repeating disaccharides of *N*-acetylglucosamine (blue) and *N*-acetylmuramic acid (green) carrying short peptides.¹⁰ In Gram-positive bacteria, peptidoglycan provides mechanical strength through the construction of tens of nanometers thick architecture.¹¹⁻¹⁴ On the other hand, Gram-negative bacteria have a thin layer of peptidoglycan surrounded by the plasma membrane and the outer membrane. This double-membrane cellular envelop enables the Gram-negative bacteria to colonize harsh environments. Lipopolysaccharide (LPS) is the main component of most outer membranes, a macromolecule containing up to hundreds of sugars.¹⁵ Figure 4 demonstrates LPS of *E. coli*,¹⁶ where the molecule is categorized in three main components: lipid A, core, and *O*-antigen. Lipid A is the hydrophobic phospholipid anchor of

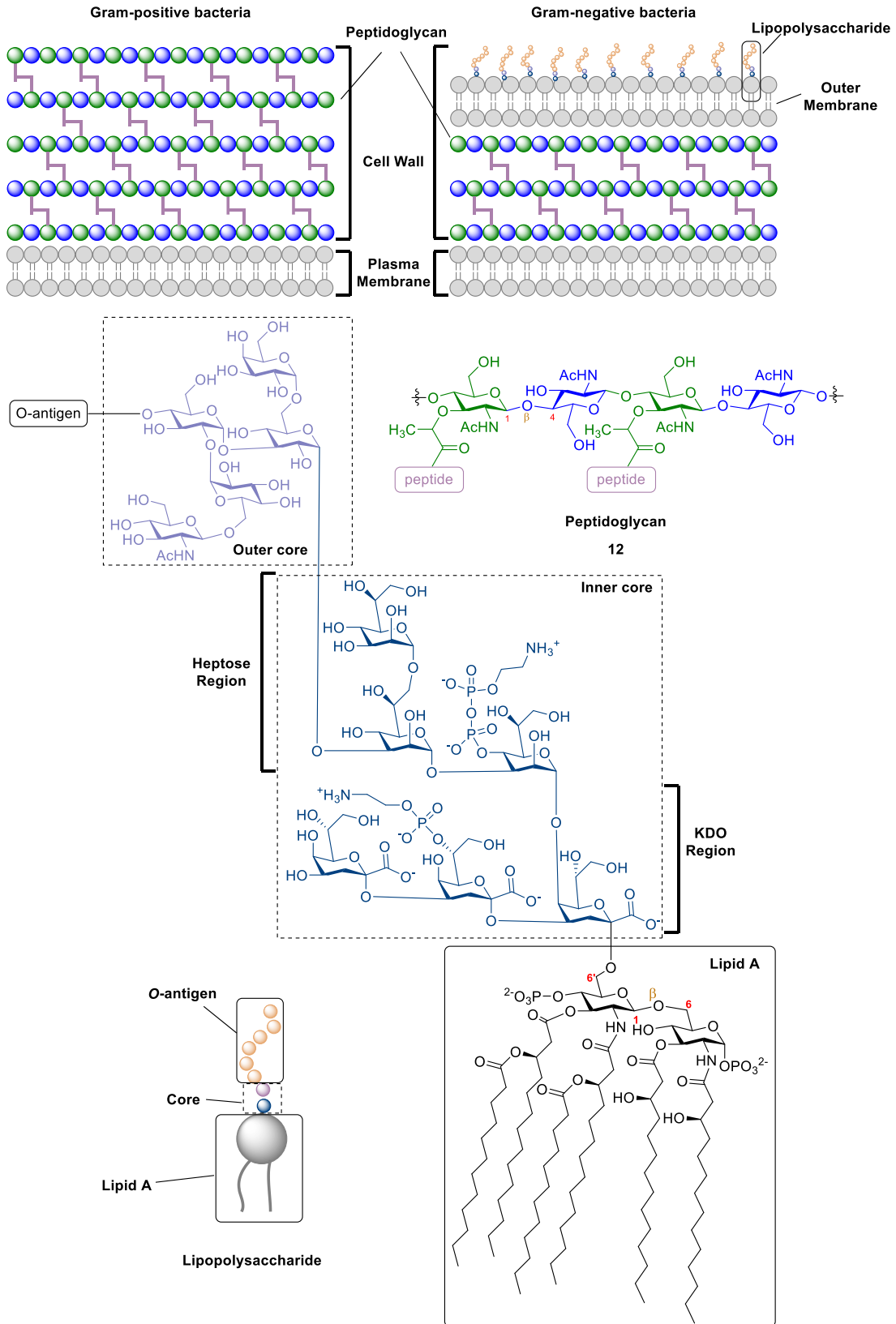


Figure 4. Constitution of bacterial cell wall

LPS containing a β -(1 \rightarrow 6) linked glucosamine disaccharide, which is also known as endotoxin.¹⁵⁻¹⁶ The 6' position of lipid A is glycosylated with a core containing nonrepeating oligosaccharides: a trisaccharide consisting of eight-carbon sugar 3-deoxy-D-manno-octulosomic acid (KDO), a trisaccharide involving seven-carbon sugar L-glycero-D-manno-heptose, and a pentasaccharide comprising of glucose, galactose, and *N*-acetylglucosamine, whereas the KDO region and the heptose region compose the inner core, and the pentasaccharide make up the outer core.¹⁶ At the end, a repetitive glycan is attached to the outer core oligosaccharide designated as *O*-antigen. The *O*-antigens are highly variable in different strains of bacteria, which are targets for recognition by host antibodies in the immune system.¹⁷

1.1.3 Cellular communication and recognition: glycode and the decoders

In the first half of the 20th century, research on carbohydrates in biological systems is primarily focused on metabolism and structural function. Until the 1970s, the studies of glycans lagged far behind other major classes of biomolecules such as nucleotides and peptides.¹⁸ This was due to the inherent complications in the structure of carbohydrates. For example, Figure 5 demonstrates the structure of a pyranose, a six-carbon monosaccharide where the six-membered ring consists of five carbon atoms and one oxygen atom. The first complication arises from the ring size, where the six-membered ring can be contracted into a five-membered ring, which is known as a furanose. Secondly, each carbon on the ring can have an *R* or *S* configuration. In addition, each hydroxyl group can react with another sugar through glycosylation. Therefore, glycans exist in both linear and branch forms, in contrast to the linear nature of nucleotides and peptides. A calculation was performed to show 1.05×10^{12} possible oligosaccharides structures for a reducing hexasaccharide, whereas a hexamer of DNA (a basis set of 4) may form 4096 different combinations, and a hexapeptide (a basis set of 20) may have 6.4×10^7 isomers.^{1,19} Besides, each hydroxyl group can be decorated with sulfates,

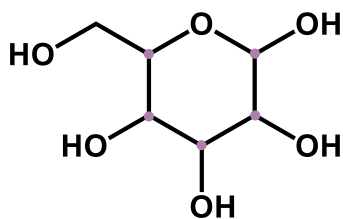


Figure 5. Structure of pyranose

phosphates, methyls, or acyls, and more than one hydroxyl group can be modified on the same sugar.¹ As such, the information that the glycans can convey is enormous. Glycomics, a systematic and comprehensive study of the total glycan structures (glycome) in the biological system, emerged. The molecular messages cracked from this study are called glycode, also known as sugar code.²⁰

Given the complexity of many glycans, a schematic glycan representation is necessary. In the late 1970s, Kornfeld and colleagues first presented a symbolic representation of vertebrate glycans, which quickly gained popularity and was adopted by the community of glycoscience.²¹⁻²² Figure 6 demonstrates some monosaccharides symbols (the full universal symbol nomenclature for glycans (SNFG) can be found in Appendix A),²² where both shapes and colors are utilized to overcome the diversity of carbohydrates. Utilizing this SNFG, the structure of lipopolysaccharides in Figure 4 can be simplified (Figure 6).

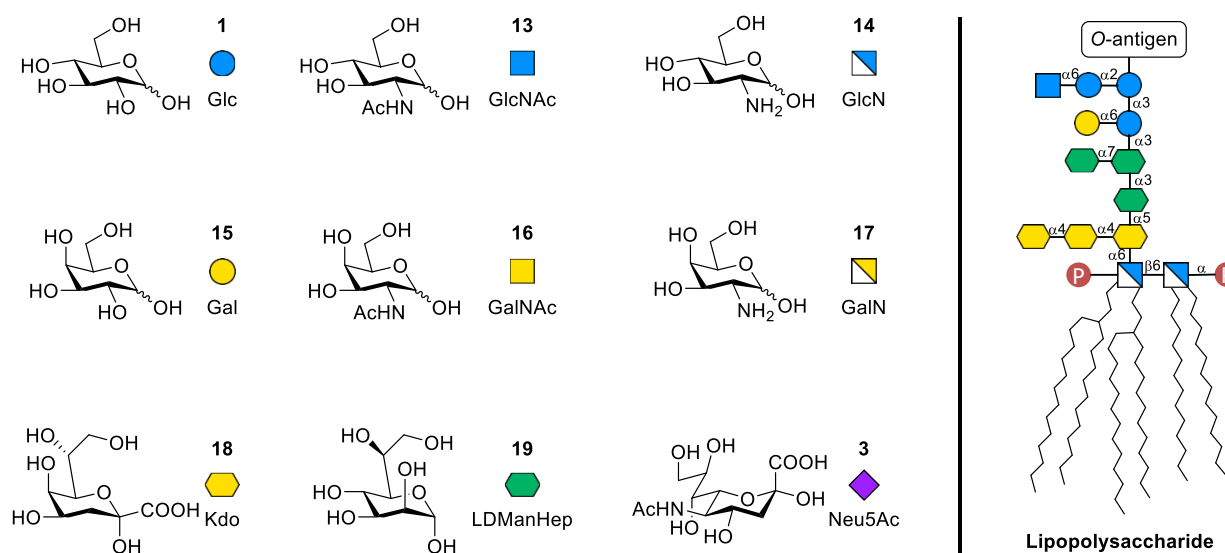


Figure 6. Symbolic representation of monosaccharides and an example of lipopolysaccharide

The cell surface was first observed as a polysaccharide coat by electron microscopy.¹⁸ These glycans on the cell surface exist in the conjugated form, in which the glycans are covalently bonded to non-carbohydrate molecules (aglycone). Increasing research has shown that these glycoconjugates play crucial roles in cellular function, especially in the events on the cell surface.¹⁸ Three classes of glycoconjugates were found on the cell surface (Figure 7): glycoprotein, glycolipid, and glycoRNA (a new class of glycoconjugate discovered recently by Flynn and colleagues²³).

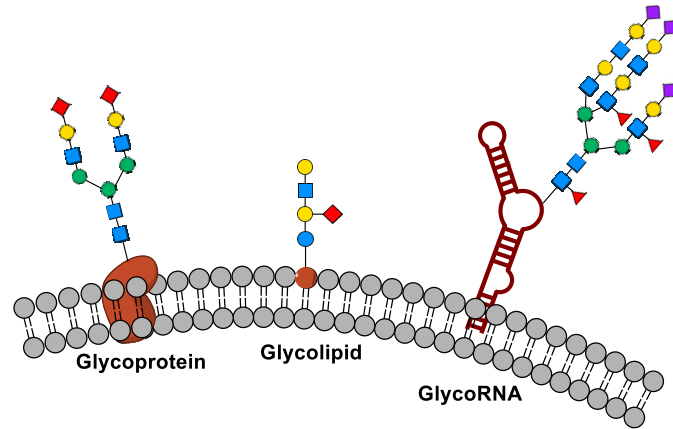


Figure 7. Glycoconjugates on the cell surface: glycoprotein, glycolipid, and glycoRNA

A glycoprotein is a glycoconjugate in which a protein covalently carries one or more glycans, usually through the side chain of the amino acids such as asparagine (*N*-linkage) or serine/threonine (*O*-linkage). Similar to *O*-glycans (*O*-linked oligosaccharides), glycosaminoglycans (GAG) attached to the core protein through glycosylation to the hydroxyl group of a serine residue, and these glycoconjugates are also known as proteoglycans. The main difference between an *O*-linked glycoprotein and a proteoglycan is at the core region, where an *O*-linked glycoprotein links to the glycan via *N*-acetylgalactosamine (GalNAc), while a proteoglycan connects to the protein through a xylose residue.¹⁸ These glycans decorated proteins also change in their properties such as increasing solubility, altering the antigenicity, and preventing the proteins from degradation.^{1, 24-25} Unlike nucleotides and proteins, the biosynthesis of glycans is non-templated. Therefore, glycoproteins naturally occur in forms with different glycosylation, and these various forms are known as glycoforms.^{1, 24}

Glycolipid, also known as glycosphingolipid, consists of a glycan (polar) attached to a nonpolar moiety. The nonpolar moiety is ceramide, which is composed of sphingosine (a long chain base) and fatty acid. The glucose or galactose from the glycan connects to the terminal primary hydroxyl group of the ceramide through a glycosidic linkage.¹⁸ Typically, the hydrophobic lipid positions itself at the outer lipid layer to allow the hydrophilic glycans to face outside of the cell.¹ Consequently, glycolipids can play essential roles in cellular recognition, such as mediating cell-cell interactions or modulating activities of proteins in the same membrane.²⁶

GlycoRNA is a class of glycoconjugate that only appeared in discussion in the past decade. RNA as an essential biopolymer participates in many events in the biological system, including coding, decoding, regulation, and expression of genes. Until 2011, the first membrane-bound non-coding RNAs were discovered in bacteria,²⁷⁻²⁸ declaring their essential membrane function. As such, associations of membrane RNA with glycans seem possible. In 2021, Flynn and colleagues first reported glycoRNA on living cell surface,²³ opening a new chapter on cell surface glycoconjugates.

The aforementioned glycoconjugates on the cell surface encrypt an enormous amount of information. To crack these encrypted codes on the cell surface, nature has designed specific decoders: the glycan-binding proteins (GBPs). Two main categories are included in the GBPs: lectins (Figure 8) and sulfated GAG-binding proteins.²⁹ Lectins typically recognized the terminal sugar on a glycan by fitting the sugar molecule into its shallow but highly specific binding pockets through hydrogen bonding, while sulfated GAG-binding proteins bind to sulfated GAGs (negatively charged) through ionic interaction with clusters of positively charged residues in the binding pocket.^{1, 29} To overcome the weak hydrogen bonding interaction, many lectins have multiple carbohydrate recognition domains (CRDs). For example, Figure 8 demonstrates a galactose specific C-type lectin (PDB: 1JZN),³⁰ in which the protein resembles a pentamer

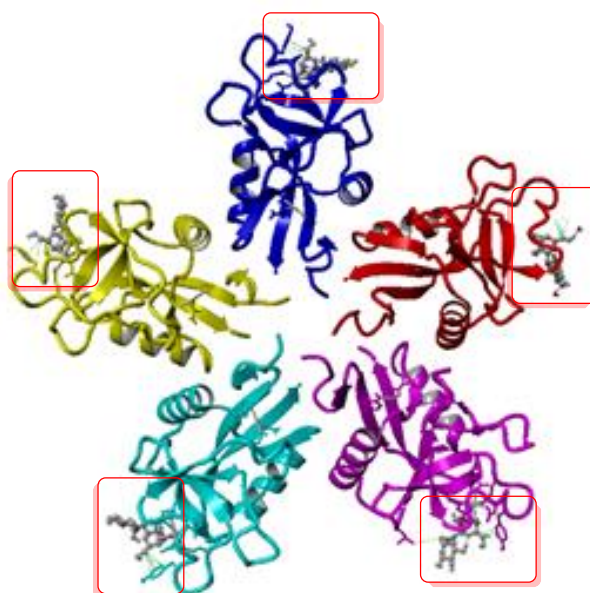


Figure 8. Structure of a galactose-specific C-type lectin.³⁰ PDB: 1JZN

with five CRDs (red boxed). This setting increases the chance of binding and allows multiple glycans binding at the same time, consequently increasing its specificity. This avidity effect is also known as the multivalent effect.^{1,29}

1.2 Carbohydrates and their mimics in drug discovery

1.2.1 Carbohydrate vaccines

Vaccines are preparations to stimulate the body's immune response against one or several diseases, typically containing agents that resemble the pathogen such as a deactivated microbe, or its toxins or surface proteins.³¹ The pathogens' and malignant cells' surfaces often consist of unique glycan structures, which makes carbohydrates an attractive vaccine target.³² The history of carbohydrate vaccines dates back to 1930 when oligosaccharides decorated proteins were used as a vaccine against pneumonia.^{1, 33-34} Unfortunately, this research was limited due to the complicated process to isolate natural oligosaccharides and the lack of synthetic methods.¹ Until the 1970s, advances in glycan analysis, synthesis, and structure determination contribute significantly to carbohydrate vaccine development, which promoted the first commercialized polysaccharide vaccine PNEUMOVAX launching in 1983.^{1, 32} This vaccine contains capsular polysaccharides isolated from 14 pneumonia serotypes, which protect people against approximately 90% of infections caused by these pathogens.³² Unfortunately, this unconjugated capsular polysaccharide vaccine did not induce sufficient protection to the high-risk group (children under 2-year-old, and immunocompromised elderly),³⁵ which is now well understood that these polysaccharides need to be conjugated to immunogenic proteins to induce long-lasting protection for the high-risk group.^{32, 36-37}

The modern design of carbohydrate-based glycoconjugate vaccine consists of four parts: the antigen (poly-/oligo saccharide), the linker, the carrier (protein, glycolipids, or nanoparticles), and the adjuvant (alum or self-adjuvanting) (Figure 9).³⁸ Traditionally, carbohydrate vaccines are naturally derived. However, due to the economic challenges of meeting quality control and safety standards required by the U.S. Food and Drug Administration (FDA), movements toward synthetic carbohydrate vaccines are in progress.^{32, 38}

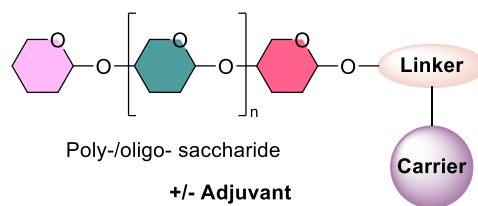
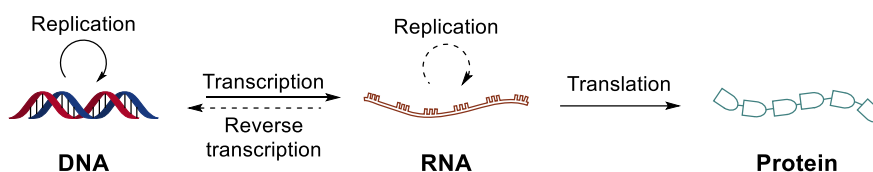


Figure 9. The design concept of carbohydrate vaccine

1.2.2 Carbohydrate drugs targeting the central dogma of biology

The central dogma of biology explains the flow of genetic information within a biological system, which is demonstrated in Scheme 3.³⁹ Therefore, nucleoside/nucleotide mimetics that interrupt the replication of pathogens gained lots of spotlight in the antiviral battle. However, it is easy to forget that nucleosides/nucleotides are made of carbohydrates, where the core molecule contains the pentose D-ribose (Section 1.1). As such, these nucleoside/nucleotide analogs contain carbohydrate moiety in the structures.



Scheme 3. The central dogma of biology

Human immunodeficiency virus and acquired immunodeficiency syndrome (HIV/AIDS) is an ongoing epidemic spread to the U.S. between 1966 and 1972.⁴⁰⁻⁴¹ Azidothymidine (**20**, AZT, Figure 10) is the first antiretroviral drug for the treatment of AIDS approved by the FDA in March of 1987.⁴² AZT is a reverse transcriptase inhibitor, which stops retroviruses such as HIV from replication. After treatment of AZT, the reverse transcriptase incorporates the nucleoside analogs into its DNA during the reverse transcription process, which causes termination of the DNA elongation due to the lack of 3'-hydroxyl group (it is azide group in AZT).⁴³

In December 2019, coronavirus disease 2019 (COVID-19), an acute respiratory disease emerged and quickly spread globally, which was declared as a pandemic in March 2020 by the World Health Organization (WHO).⁴⁴ This pandemic was caused by a new strain of coronavirus: severe acute respiratory syndrome coronavirus 2 (SARS-CoV-2). Remdesivir (**21**, Figure 10), a nucleotide analog was authorized

for emergency use as a post-infection treatment for COVID-19.⁴⁵ Coronaviruses contain a large family of single-stranded RNA viruses that are characterized by their spherical shapes.⁴⁶ Remdesivir as an RNA-dependent RNA polymerase inhibitor, causes a decrease in viral RNA production. As such, prior to treatment for COVID-19, Remdesivir was used in the investigation of other viral diseases such as Ebola virus disease and showed promising therapeutic efficacy.⁴⁷ In December 2021, the first orally available COVID-19 antiviral medication Molnupiravir (**22**, Figure 10) was approved by the U.S. FDA.⁴⁸ Unlike AZT and Remdesivir, Molnupiravir inhibits viral reproduction by promoting mutation during viral RNA replication.⁴⁹

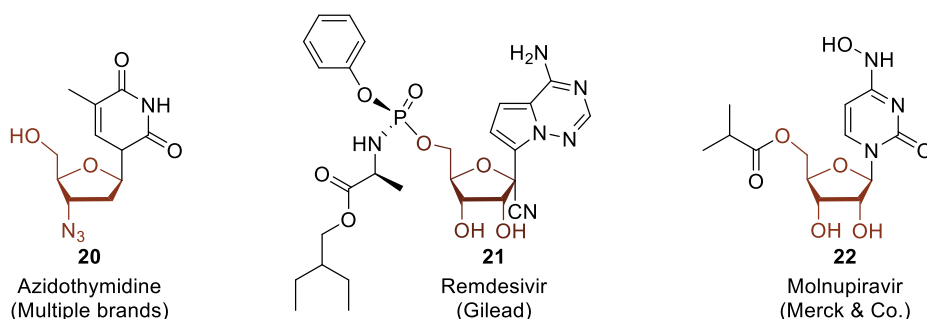


Figure 10. Nucleoside/nucleotide mimetics as carbohydrate-based drugs

1.2.3 Glycosidase and glycosyltransferase inhibitors

Glycosidases and glycosyltransferases are two types of carbohydrate processing enzymes utilized by nature to construct all the carbohydrate structures in all biological systems. Through inhibition of these enzymes, the biosynthesis or degradation of some carbohydrate structures can be controlled.¹ For example, Miglustat (**23**, Figure 11) is a ceramide glucosyltransferase inhibitor that is used to treat Gaucher disease, a genetic disorder of glucosylceramide accumulation in cells and organs.⁵⁰⁻⁵¹ Inhibition of ceramide glucosyltransferase might also alter the membrane surface glycoconjugate. Therefore, Miglustat was also studied for HIV/AIDS treatment and found reduced infection of white blood cells by HIV due to the inefficient binding to gp120 (glycoprotein found on virus surface).⁵²⁻⁵³ Unfortunately, Miglustat showed limited efficacy in phase II clinical trial for HIV/AIDS due to low potency and difficulty to achieve steady-state therapeutic concentration.⁵⁴⁻⁵⁵

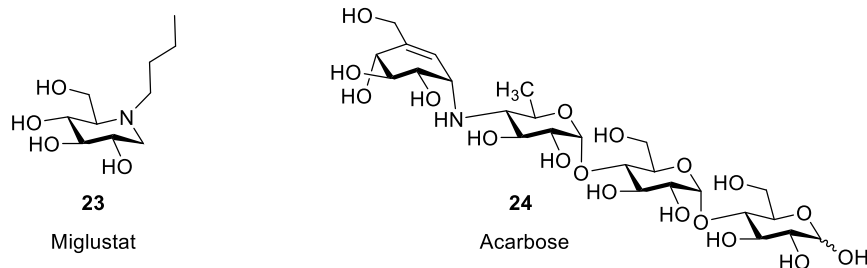


Figure 11. Examples of glycosidase and glycosyltransferase inhibitors

On the other hand, Acarbose (**24**, Figure 11) is a pseudo-tetrasaccharide consisting of multiple α -(1 \rightarrow 4) linkages that acts as an α -glucosidase inhibitor. α -Glucosidase is an intestinal enzyme that releases glucose from breaking down the large carbohydrates with α -(1 \rightarrow 4) linkage. Therefore, Acarbose is used as a treatment for Type 2 diabetes and showed great efficacy in Asian patients, in which the efficacy is likely due to the high carbohydrate diet.⁵⁶⁻⁵⁸

1.2.4 Glycosaminoglycans and their therapeutic applications

Today, one of the most widely prescribed drugs is the anticoagulant heparin (**25**, Figure 12), a highly sulfated glycosaminoglycan containing repeating units of glucuronic acid/iduronic acid and glucosamine. Antithrombin is a protease inhibitor of the coagulation cascade, which is triggered by tissue trauma or vascular injury.⁵⁹ Activation of antithrombin leads to rapid inhibition of thrombin and factor Xa, shutting down the production of fibrin clots, eventually limits the blood's ability to clot.⁶⁰ Heparin binds and activates antithrombin, therefore, it is often prescribed for patients after surgeries to prevent and treat thrombosis (blood clotting).⁵⁹ Low molecular weight heparin (LMWH) is a fractionated heparin derived by chemical or enzymatic cleavage of heparin, which has replaced unfractionated heparin in developed countries as a therapeutic of choice due to its fewer secondary complication (thrombocytopenia induced by heparin and antibodies).⁶⁰ To further eliminate the secondary complication, a synthetic heparin mimic pentasaccharide fondaparinux (**26**, Figure 12) was developed. Fondaparinux specifically and irreversibly binds to antithrombin and is used to prevent deep-vein thrombosis and pulmonary embolism. Nevertheless, the high cost of production has prevented fondaparinux from larger success therapeutic.⁶⁰

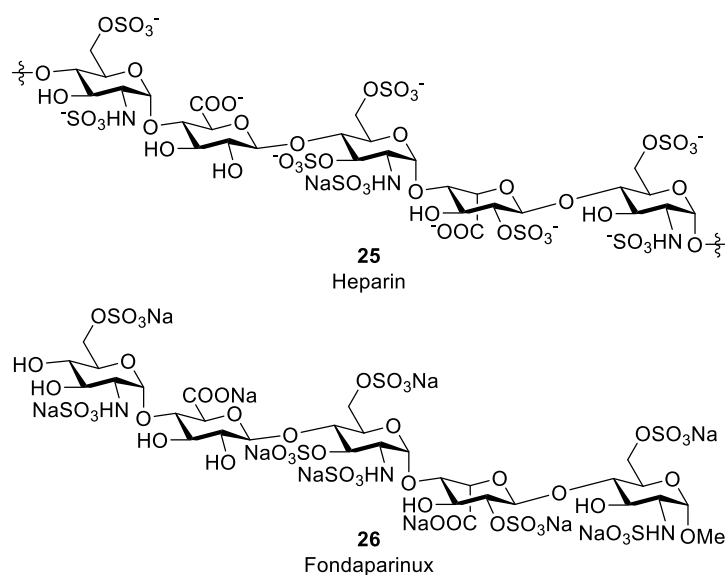
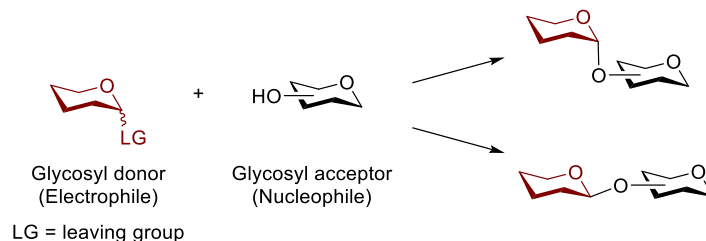


Figure 12. Structures of heparin and fondaparinux

1.3 Chemical Methods of Carbohydrates Synthesis

Although impressive progress has been achieved in the field of glycoscience, the major bottleneck is the lack of homogeneous forms of oligosaccharide as well as scalable methods of oligosaccharide synthesis. Unlike nucleic acids and proteins, the biosynthesis of carbohydrates is not templated, which leads to a variety of complicated carbohydrates products. As most bioactive carbohydrates used in clinics are isolated from natural sources, the inconsistency of natural products becomes problematic. In 2008, heparin was contaminated by a heparin-like compound, oversulfated chondroitin sulfate, which caused nearly 100 deaths⁶¹⁻⁶². As such, a scalable method that allows us to produce well-defined glycans is currently demanded.

Glycosylation is the fundamental method for constructing complex glycans, in which a glycosyl donor (sugar that donates the anomeric carbon) reacts with a glycosyl acceptor (the molecule that accepts the anomeric carbon) to form a glycoside through the newly formed glycosidic linkage. Scheme 4 demonstrates the glycosylation of pyranosyl donor and acceptor as well as the formation of two possible glycosides, where the glycosidic linkage can be either axial or equatorial.



Scheme 4. Concept of glycosylation

There are two general methods of glycosylation: chemical and chemoenzymatic glycosylation. It is envisioned that the combination of chemical and chemoenzymatic tools is a promising solution to the construction of complex natural or designed glycans. This section will focus on chemical glycosylation.

1.3.1 General pathways of chemical glycosylation

Glycosylation is a substitution reaction at the anomeric (C1) position. Although the concept of glycosylation is extremely simple, the operation has been frustrating. The challenges arise from carbohydrate molecules' inherent poly-hydroxyl nature, which leads to problems with regioselectivity and stereoselectivity. To avoid problems with regioselectivity, protecting groups are often used on the sugar molecules. The other main challenge is the stereochemical outcome at the anomeric center, which is considered the most challenging in carbohydrate synthesis.¹ The stereoselectivity at the anomeric center can be viewed in respect to the C2 position (Figure 13), where 1,2-*cis* and 1,2-*trans* glycosides could be possibly formed in glycosylation. In the case of 2-deoxy glycoside, an α and β mixture of glycosides is often found after glycosylation.

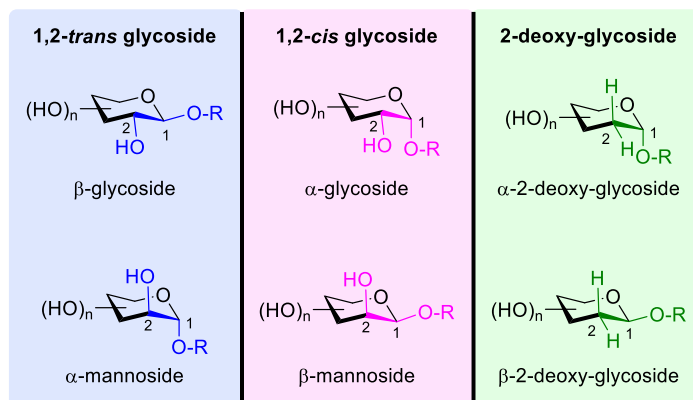
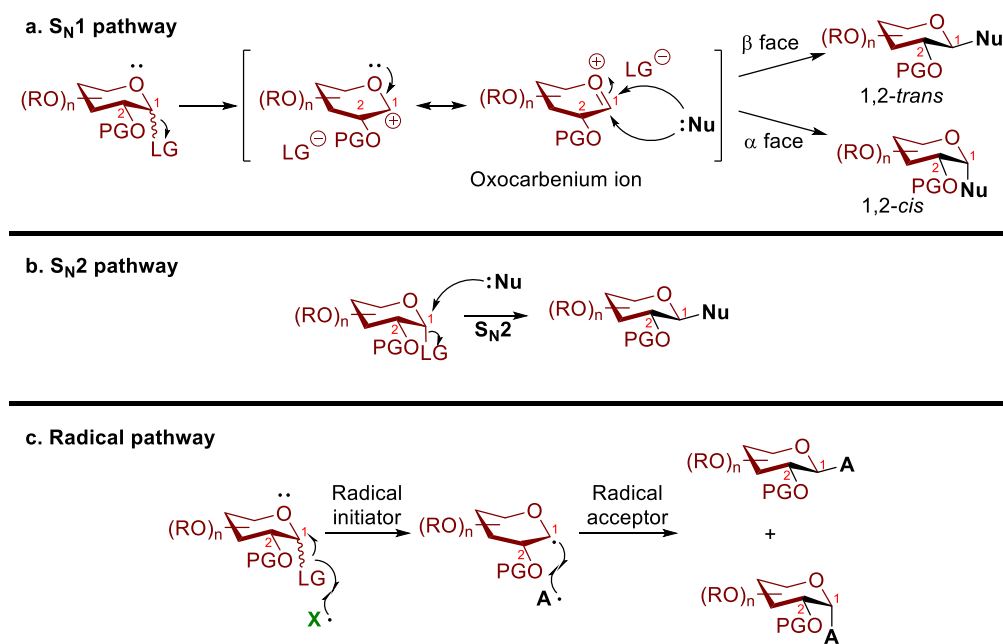


Figure 13. Category of glycosides

To solve the stereoselectivity problem of glycosylation, it is necessary to consider the possible mechanisms, which generally include three pathways: the S_N1 , S_N2 , and free radical pathways (Scheme 5). Chemical glycosylation is commonly seen as a nucleophilic substitution reaction, where the glycosyl donor is an electrophile, and the glycosyl acceptor is a nucleophile. As such, S_N1 and S_N2 pathways are often processed in chemical glycosylation. Yet, the complication of glycosylation rises from the ring oxygen, which facilitates the S_N1 pathway.¹ As demonstrated in Scheme 5a, upon the departure of the leaving group, the lone pair on the ring oxygen can stabilize the carbocation through resonance, and generate an oxocarbenium ion. A nucleophile can approach the anomeric center from either α or β face, which leads to two possible products. On the other hand, glycosylation undergoing the S_N2 pathway gives a clean inversion of configuration at the anomeric center (Scheme 5b).

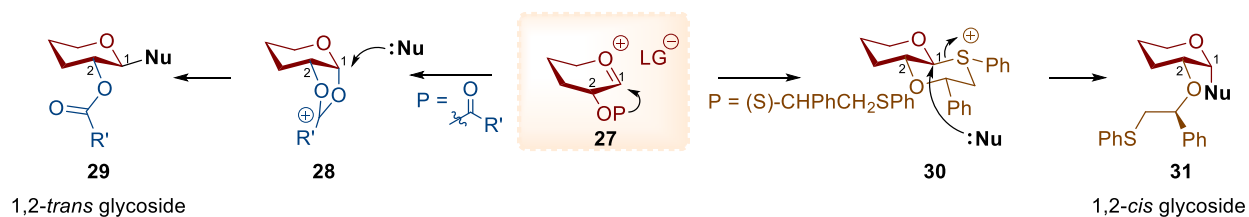
Another less mentioned pathway in glycosylation is the radical pathway (Scheme 5c). Propagation of anomeric glycosyl radicals followed by termination with glycosyl acceptor radicals, the radical pathway in glycosylation allows efficient access to C-glycosides, sugars with a carbon substituent at the anomeric center.



Scheme 5. General pathways of glycosylation

1.3.2 Substrate-control of stereochemistry

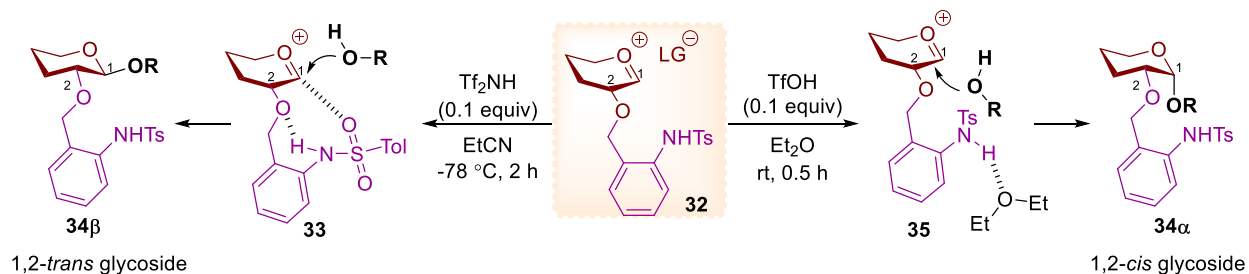
The ability to forge glycosidic bonds in a stereoselective fashion is not easily predictable due to the reaction's high degree of variables and shifting S_N1 - S_N2 mechanistic paradigm (Scheme 5a-b).⁶³⁻⁶⁵ Many factors influence the stereochemical outcome of glycosylation, such as the substrate itself, additives to the reaction, the temperature, and even the solvents and the concentration of the reaction.^{1, 66} Most established methods to achieve stereoselective glycosylation reactions have focused on tuning the steric and electronic nature of the protecting group on the electrophilic partners⁶⁷⁻⁷³. The most reliable approach is based on the *O*-acyl participatory protecting group at C2 of the glycosyl electrophile for construction of the 1,2-*trans* glycosidic linkage (Scheme 6).^{67, 74} Upon the formation of oxocarbenium ion **27**, the C2-*O*-acyl protecting group leads to a more stable 1,2-*cis* acyloxonium bridged intermediate **28**. Subsequent nucleophilic attack at the anomeric center leads to 1,2-*trans* glycoside **29**. To achieve 1,2-*cis* glycoside, Boons and coworkers have developed (1*S*)-phenyl-2-(phenylsulfanyl)ethyl chiral auxiliary as a C2 participatory protecting group.⁶⁸⁻⁶⁹ To minimize the steric and electronic interference, a 1,2-*trans* decalin sulfonium intermediate **30** is formed. Following the displacement of the sulfonium ion by a nucleophile at the anomeric center leads to 1,2-*cis* glycoside **31**.



Scheme 6. Neighboring group participation

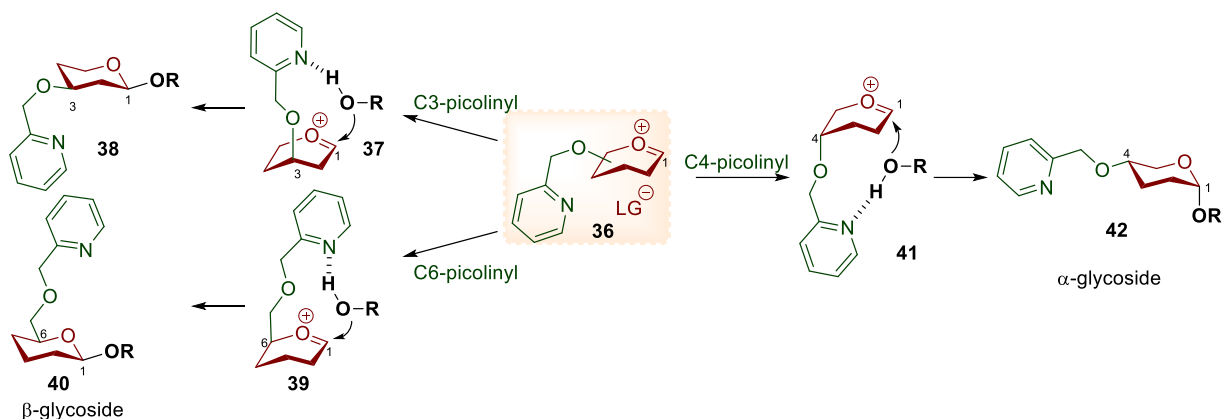
Besides participation in constructing a stable intermediate, the C2-neighboring group is also capable of bimodal assistance in stereoselective glycosylation. In 2018, Ding, Ishiwata, and Ito discovered that the C2-*O*-(*ortho*-tosylamido)benzyl (TAB) protecting group enables access to α - or β -anomeric product under specific reaction conditions (Scheme 7).⁷⁵ TAB group is a functional group designed for anchimeric assistance in glycosylation. With a catalytic amount of triflimide in the reaction, and propionitrile as the solvent, the TAB protecting group proceeds intramolecular hydrogen bonding between the tosylamido

proton and C2-oxygen resembles a phthalimide moiety. Following anchimeric assistance of the sulfonyl oxygen leads to the formation of a stable 1,2-*cis* cyclic intermediate **33**. A final nucleophilic substitution by the alcohol glycosyl acceptor at the anomeric center on **33** eventually yields 1,2-*trans* glycoside **34 β** . On the other hand, when diethyl ether is used as the solvent, the intramolecular hydrogen bonding that resembles the phthalimide moiety is disrupted. After activation by a catalytic amount of triflic acid, an oxocarbenium ion **35** is formed, leading to the thermodynamically favored α -product **34 α** .



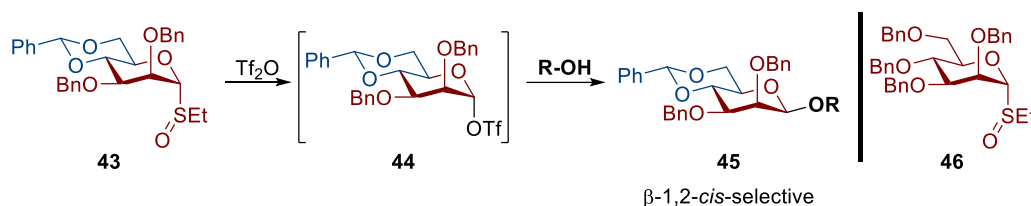
Scheme 7. Bimodal anchimeric assistance

Apart from functionalization on the C2 position, the remote positions on the sugar molecule could also participate in glycosylation. In 2012, Yasomanee and Demchenko utilized *O*-picolinyl and *O*-picoloyl groups at remote positions to control facial selectivity for the nucleophilic attack of the alcohol glycosyl acceptor, which is known as hydrogen bond-mediated aglycone delivery (Scheme 8).⁷⁰ When a picolinyl group is functionalized at the C3 or the C6 position, the formation of the oxocarbenium ion **37** or **39** shifts the picolinyl group to the β -face. Hydrogen bonding between the picolinyl group and the alcohol delivers the glycosyl acceptor to the β -face eventually generates the β -glycosides **38** or **40**. Conversely, functionalization of the picolinyl group at the C4 position directs the alcohol glycosyl acceptor to the α -face, leading to α -glycoside **42** as the major product.



Scheme 8. Hydrogen bonding mediated aglycone delivery

The utilization of conformationally constraining bicyclic protecting groups is another effective method to control the diastereoselectivity of glycosylation. For example, the Crich group demonstrated the use of the 4,6-*O*-benzylidene group on mannosyl sulfoxides (**43**) give superior β -selectivity compared to the conformationally mobile donor (**46**, Scheme 9).⁷⁶⁻⁷⁷ Extensive mechanistic study showed that an α -mannosyl triflate (**44**) is formed upon activation with triflic anhydride.⁷⁸ Subsequent displacement by the nucleophile leads to the β -mannoside product (**45**). On the other hand, the minor α -mannoside product arises from an oxocarbenium-like intermediate, which is destabilized due to the conformationally constrained 4,6-*O*-benzylidene protecting group.



Scheme 9. Use of bicyclic protecting group in stereoselective glycosylation

These substrate-controlled methods, however, are highly specialized for each electrophilic partner. In addition, some technical issues are particularly difficult to avoid. For example, low temperature is typically required to achieve the desired selectivity. Besides, a dilute concentration of reaction is preferred to allow proper hydrogen bonding denoting that more solvent is required in the reaction. Additionally, sterically hindered nucleophiles are less effective in the hydrogen bonding mediated aglycone delivery methods.⁷⁹

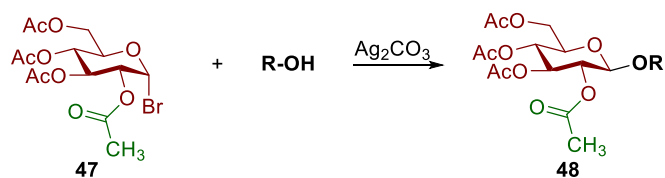
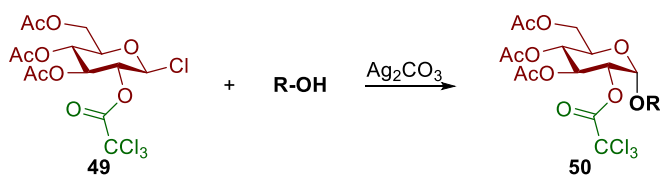
Furthermore, the undesired byproduct is hard to avoid in some cases. For instance, in C2-*O*-acyl neighboring group participation, the carbocation is competing with the anomeric center leading orthoester as a byproduct when a weak nucleophile is used.⁸⁰ Alternatively, reagent-controlled glycosylation has emerged as a way to eliminate the need for specific protecting groups.

1.3.3 Reagent-control of stereochemistry

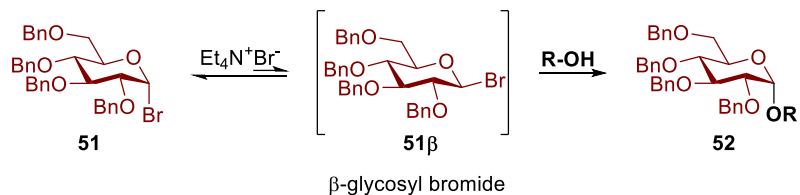
Since the first glycosylation was reported in 1879,⁸¹ C2-*O*-acyl neighboring group participation has been utilized to access 1,2-*trans* glycosides. It was until 2005 that the Boons group have developed the sulfanyl chiral auxiliary as a C2-participatory group which allowed access to 1,2-*cis* glycosides through the substrate-controlled method (Scheme 8a).⁶⁸⁻⁶⁹ Aiming to stereoselectively synthesize 1,2-*cis* glycosides, chemists had diversified their focus in controlling the stereochemical outcome of glycosylation.

The first step to access 1,2-*cis* glycosides was to eliminate the C2-*O*-acyl anchimeric assistance. In 1901, Koenigs and Knorr reported glycosylation through the displacement of glycosyl halide **47** with alcohol under excess Ag₂CO₃ to achieve β-1,2-*trans* glycoside **48** (Scheme 10a).⁸² The Koenigs-Knorr glycosylation has then developed into one of the most common methods to synthesize oligosaccharides and glycoconjugates. It was later understood that the silver assisted the bromide to leave and concerted nucleophilic substitution of alcohol led to the glycoside product with inversion of configuration at the anomeric center. In 1926, Brigl and Keppler demonstrated the first 1,2-*cis* glycosylation using the Koenigs-Knorr method (Scheme 10b).⁸³ In this reaction, a β-glycosyl chloride (**49**) was used as the glycosyl donor. To eliminate the C2-*O*-acyl anchimeric competition, a trichloroacetyl protecting group, in which the carbonyl oxygen is less nucleophilic, was installed at the C2 position. Under the excess amount of Ag₂CO₃, the alcohol successfully displaced β-glycosyl chloride **49** resulting in the desired α-1,2-*cis* glycoside **50**.

a. Koenigs-Knorr glycosylation, 1901

b. Brigl-Kepler 1,2-*cis* glycosylation, 1926**Scheme 10.** Koenigs-Knorr glycosylation and its development toward 1,2-*cis* glycosylation

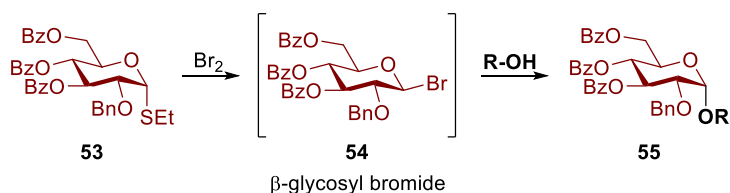
Breakthrough toward 1,2-*cis* glycosylation was made in 1975 by Lemieux and coworkers, where tetraethylammonium bromide was added to control the diastereoselectivity of glycosylation (Scheme 11).⁸⁴ This extraordinary work allowed efficient, and more importantly, reproducible stereoselective synthesis of 1,2-*cis* glycoside for the first time.⁸⁵ The central concept of this work is to anomerize the α -glycosyl bromide **51** to the more reactive β -glycosyl bromide **51 β** *in situ* with excess bromide ion, subsequent S_N2 -like displacement with alcohol leads to the desired 1,2-*cis* glycoside **52**.

**Scheme 11.** Halide ion catalyzed 1,2-*cis* glycosylation

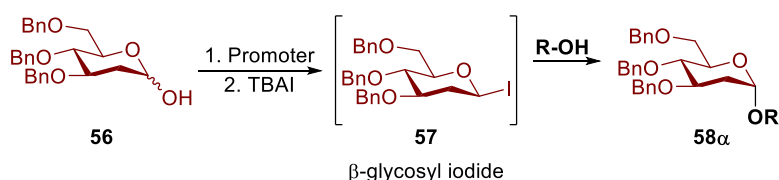
The concept of *in situ* anomerization has a strong impact on the chemical synthesis of α -1,2-*cis* glycosylation, and it is not limited to glycosyl halide as starting material. For example, Demchenko and coworkers employed bromine to activate the inert thioglycoside **53**, and the formation of the reactive β -glycosyl bromide **54** leads to α -1,2-*cis* glycoside **55** as the major product (Scheme 12a).⁸⁶ Lemieux's concept is also applicable to 2-deoxy sugars, which neighboring groups are inherently null. For example, Bennett and coworkers generated β -2-deoxy glycosyl iodide **57** *in situ* through activation of the inert 2-

deoxy glycosyl hemiacetal **56**, followed by the addition of tetrabutylammonium iodide (TBAI). Subsequent reaction of **57** with alcohol eventually leads to a majority of α -selective products **58 α** (Scheme 12b).⁸⁷

a. Demchenko, 2012



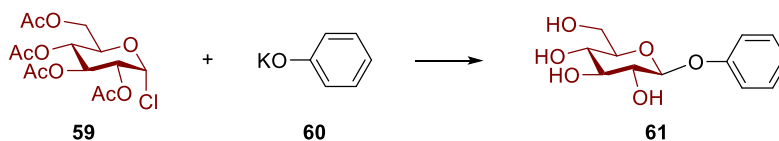
b. Bennett, 2011



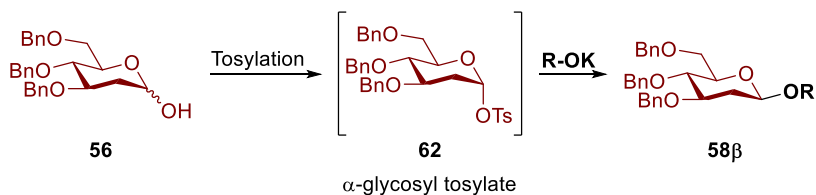
Scheme 12. Glycosylation through *in situ* anomerization

Direct $\text{S}_{\text{N}}2$ substitution is an efficient way of controlling the stereochemical outcome of glycosylation, as an inversion of configuration is expected at the reaction center. As demonstrated by Arthur Michael in 1879 (Scheme 13a),⁸¹ a phenoxide anion (**60**) substituted the α -glycosyl chloride (**59**) from the β -face, resulting in β -glycoside **61** as the product. Although the acetyl protecting groups were removed under the reaction condition, it was the first successful glycosylation in history.

a. First glycosylation in history by Michael, 1879



b. β -specific dehydrative glycosylation, 2013



Scheme 13. Glycosylation through direct $\text{S}_{\text{N}}2$ substitution with alkoxide

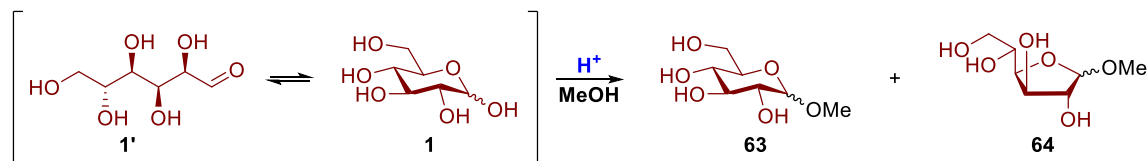
This direct S_N2 substitution method at the anomeric center with alkoxide is convenient for 2-deoxy sugars, in which the C2 position is free of manipulation. In 2013, the Bennett group developed a dehydrative method to access β -linked 2-deoxy-sugars (Scheme 13b).⁸⁸ Firstly, the inert 2-deoxy glycosyl hemiacetal **56** is converted into α -glycosyl tosylate **62** *in situ*. Subsequent addition of alkoxide or thiolate displaces the tosylate leaving group, leading to β -2-deoxy glycoside **58 β** as the glycosylated product. These dehydrative protocols together with the *in situ* anomerization method (Scheme 12b) and the direct S_N2 method (Scheme 13b) allow stereocontrol in the direct synthesis of 2-deoxy glycosides using bench stable glycosyl hemiacetals.

Reagent-controlled glycosylation is an effective method to bias the stereochemical outcome in the absence of anchimeric assistance. However, these reagent-controlled methods that require the addition of excess reagents are not efficient from the environmental and industrial perspectives. Therefore, catalytic glycosylation has emerged to meet the demand for the environment and economy.

1.4 Catalytic Glycosylation

1.4.1 Beginning of catalytic glycosylation

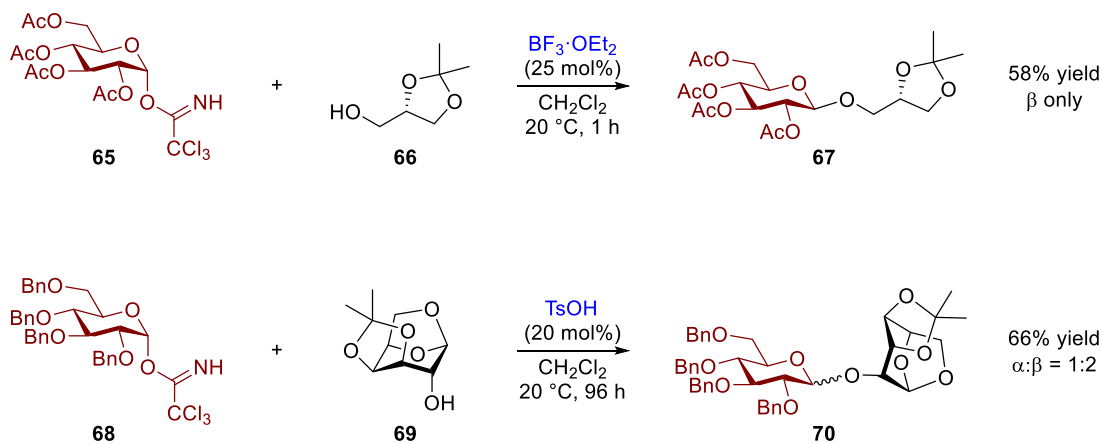
The first catalytic glycosylation was reported in 1893 by Emil Fischer, in which glycosylation was carried out through the reaction of aldose (**1'**) and alcohol (MeOH) in the presence of a catalytic amount of acid (Scheme 14).⁸⁹ This is also known as Fischer glycosylation. Nevertheless, the Fischer glycosylation undergoes an equilibrium process which leads to a mixture of ring size isomers such as **63** and **64**.



Scheme 14. The first catalytic glycosylation by Emil Fischer

Although Fischer glycosylation is still the preferred method to make simple glycoside nowadays, it is not practical for oligosaccharide synthesis.⁹⁰ Until 1980, Michel and Schmidt demonstrated catalytic activation of the trichloroacetimidate (TCA) in glycosyl donors with either Lewis acid or Brønsted acid

(Scheme 15),⁹¹ leading to the blooming of catalytic glycosylation. One problem at a time, the early stage of catalytic glycosylation focuses on the ability of coupling. For instance, Michel and Schmidt employed anchimeric assistance from the C2 acyl protecting group to achieve β -glycoside **67** in a practical yield with absolute stereocontrol. However, when a non-participatory protecting group was used in donor **68**, the diastereoselectivity of coupled glycoside **70** reduced to 1:2 (α : β). Since then, chemists began to take the challenge in stereocontrol of glycosylation through the development of catalysts. Nowadays, in addition to the coupling ability, the focus on catalyst design in glycosylation has extended into stereocontrol and regiocontrol.



Scheme 15. First catalytic glycosylation with TCA donors

1.4.2 Design of stereoselective catalytic glycosylation

Despite reaction conditions and substituent effects, three components are considered in catalytic glycosylation: the glycosyl donor that donates the anomeric carbon, the glycosyl acceptor that accepts the anomeric center, and the catalyst. Aiming at successful glycosylation, the catalyst must interact with either the glycosyl donor or the glycosyl acceptor, or both. Considering catalytic *O*-glycosylation through the coupling of alcohol with glycosyl donor bearing a leaving group, it can be simplified as alcohol substitution at one reaction center. There are five possible interactions between the catalyst and the glycosyl donor or the glycosyl acceptor (Figure 14). Interactions between the catalyst and the glycosyl donor include direct displacement, insertion, and induced departure. On the other hand, the catalyst interacts with the glycosyl

acceptor through hydrogen bonding or insertion in the OH group. For the outcome of catalytic glycosylation to be selective, chemists have elaborated these aforementioned interactions and designed catalysts that allow collaboration with both the glycosyl donor and acceptor.

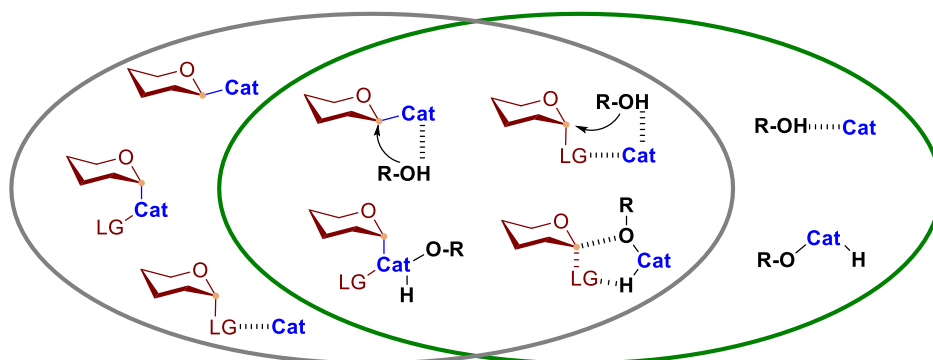
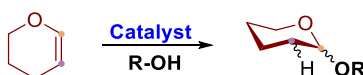


Figure 14. Design concepts for stereoselective catalytic glycosylation

Another common method of glycosylation is through the coupling of glycal with alcohol (Scheme 16). Unlike glycosyl donors with leaving groups, the glycal contains a double bond between the anomeric carbon and C2. In other words, there are two reaction centers upon activation of the glycal. This type of glycosyl donor is preferred in the synthesis of 2-deoxy glycosides as the ring oxygen bias regioselectivity, and the stereochemistry at C2 can be neglected.



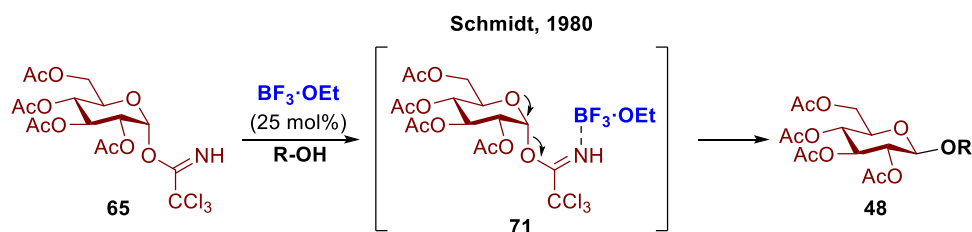
Scheme 16. Glycal as glycosyl donor in catalytic glycosylation

1.4.3 Catalyst development in stereoselective glycosylation

1.4.3.1 From Lewis acid to acid-base catalysis (complexation with nucleophilic acceptor)

The early approach in catalytic glycosylation began with the activation of glycosyl donors. For example, in Schmidt's first reported catalytic glycosylation (Scheme 17),⁹¹ boron trifluoride diethyl etherate ($\text{BF}_3 \cdot \text{OEt}_2$) acted as a Lewis acid accepting electrons from the imidate nitrogen, which promoted the departure of the TCA leaving group, leading to the formation of a carbocation. With the assistance of the

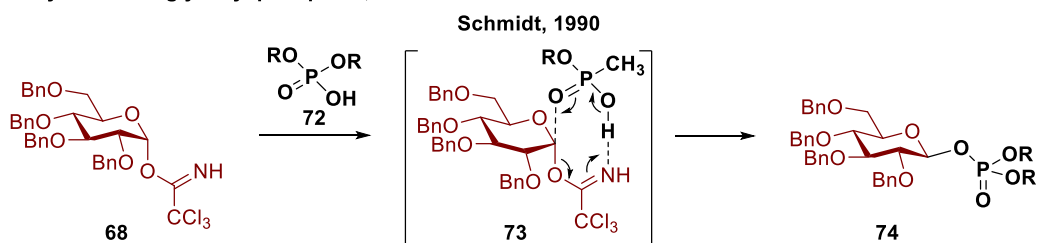
C2-acyl protecting group, β -glycoside was obtained as the product. Although glycosyl fluorides have been detected in this glycosylation,⁹⁰ the mechanism of BF_3 activation of TCA donor is still debatable.



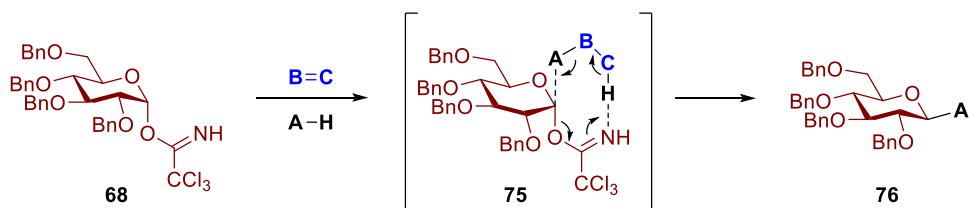
Scheme 17. Boron trifluoride activation of TCA donor

An interesting phenomenon was observed by the Schmidt group in 1982 when mixing perbenzylated glucosyl TCA donor and phosphoric acid mono- or di-esters, where α -glucosyl TCA **68** led to β -glucosyl phosphate **74** with absolute stereocontrol in the absence of a catalyst (Scheme 18a).⁹² In 1990, a cyclohexane-like eight-membered cyclic transition state (**73**) was proposed for this stereospecific glycosylation leading to a new concept of catalysis.⁹³ The Schmidt group proposed that a catalyst ($B = C$) would generate an $A - B - C - H$ intermediate *in situ* with an alcohol acceptor ($A - H$), which would resemble the 6-membered ring-like transition state (**75**) and lead to stereospecific glycosylation (Scheme 18b).

a. Synthesis of glycosyl phosphate, 1982

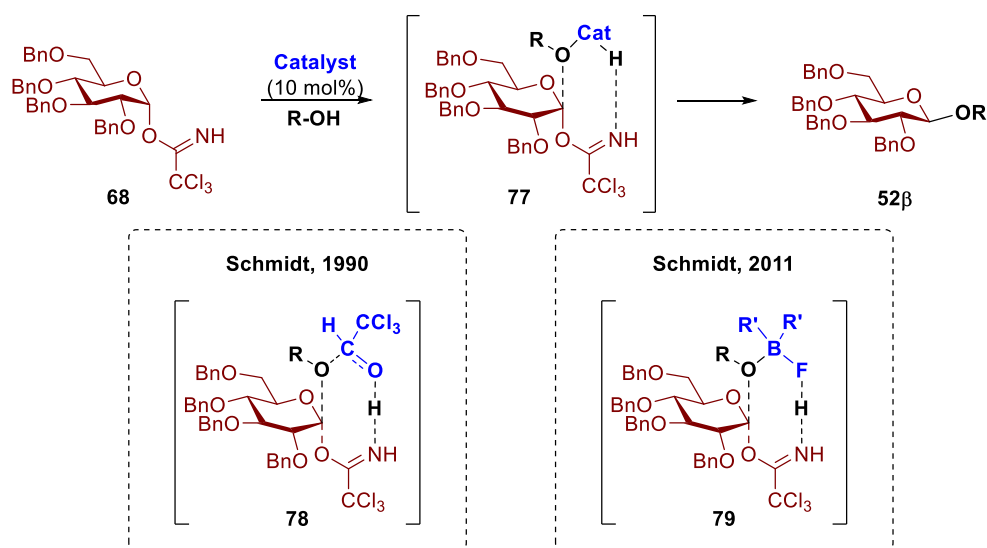


b. Inspiration of acid-base catalysis



Scheme 18. Synthesis of glycosyl phosphate and inspiration

After testing a series of carbonyl compounds, chloral (**78**, Scheme 19) was able to catalyze glycosylation with TCA donor and alcohol acceptor.⁹³ Although the temperature, solvent, and catalyst concentration affect the rate, yield, and diastereoselectivity of the glycosylation dramatically, the concept of acid-base catalysis through complexation with acceptor in stereoselective glycosylation was first established. Twenty years later, the Schmidt group reinvestigated the complexation concept and demonstrated boron-centered catalysts (**79**, Scheme 19)⁹⁴ for stereospecific glycosylation.

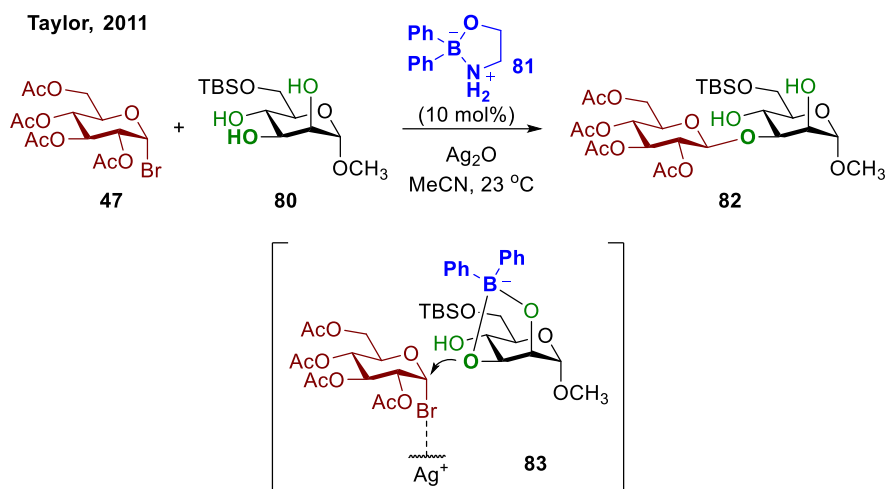


Scheme 19. Development of acid-base catalysis

Several key criteria were listed for the activation through precomplexation: (1). A fast equilibrium between the alcohol acceptor and the $A - B - C - H$ intermediate; (2). Increased acidity of alcohol acceptor after complexation; (3). The catalyst cannot react with glycosyl TCA in the absence of the acceptor; (4). Increased nucleophilicity of the alcohol after complexation.

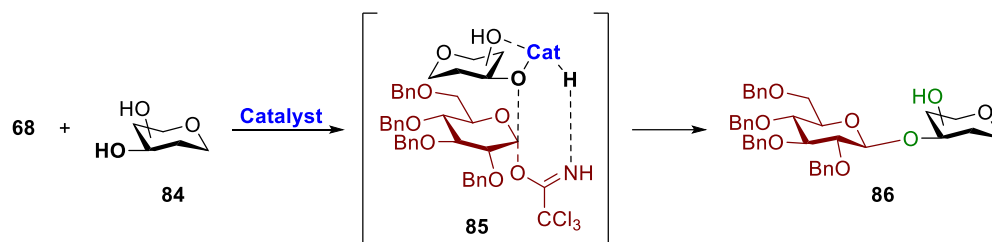
In 2011, the Taylor group demonstrated the utility of commercially available diarylborinic acid derivatives in catalyzing regioselective Koenigs-Knorr glycosylation (Scheme 20), in which the regioselectivity was accomplished through complexation of acceptor and catalyst.⁹⁵ The borinate ester **81** is a precatalyst, as the ethanolamine ligand is replaced by the diol during the reaction. Coordination of a 1,2-*cis* diol (**80**) to the boron catalyst leads to a tetracoordinate boron-acceptor adduct (**83**), which alternates the nucleophilicity of the alcohols. Eventually, the most nucleophilic complexed equatorial alcohol (C3

alcohol) leads to the final product **82**. This method is a big step forward in chemical glycosylation as it allows regioselective glycosylation with the catalytic addition of a simple small molecule. Yet, this glycosylation still relies on an equivalent amount of silver oxide to activate the glycosyl bromide **47**.

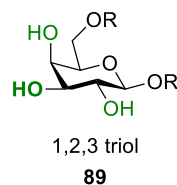
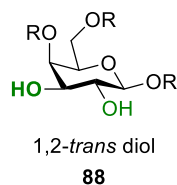
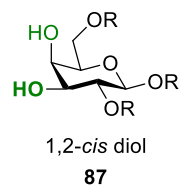


Scheme 20. Regioselective activation of glycosyl acceptor

Since then, Schmidt and coworkers exercised their acid-based catalysis system on regioselective glycosylation (Scheme 21).⁹⁶⁻⁹⁸ In 2012, the Schmidt group successfully coupled the complexed equatorial alcohol in a 1,2-*cis* diol to the TCA donor with a catalytic amount of PhSiF_3 . Similar to the boron-centered catalysts **79**, silicon has a higher affinity to fluorine and oxygen than nitrogen. However, unlike the boron-centered catalyst **77**, the silicon-center allows penta- or hexacoordination.^{96, 99} In other words, the PhSiF_3 catalyst can coordinate to more than one alcohol. Elaborating on this concept, Peng and Schmidt later reported gold(III)⁹⁷ and platinum(IV)⁹⁸ catalyzed glycosylation allowing regioselective coupling of the complexed equatorial alcohol in 1,2-*cis* diols and 1,2-*trans* diols (PtCl_4 only).

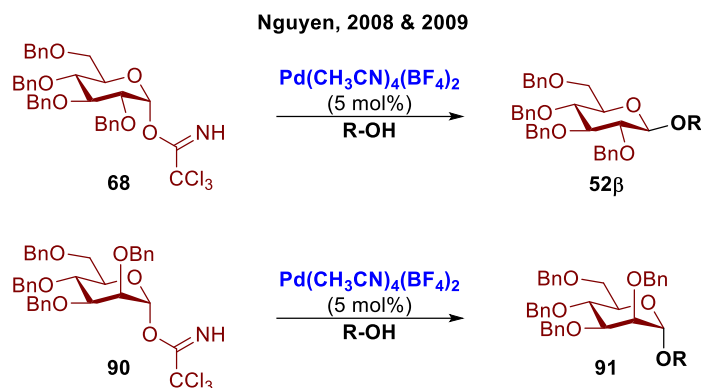


Schmidt, 2012	PhSiF_3	1,2-cis diols, 1,2,3 triols
Peng and Schmidt, 2015	AuCl_3	1,2-cis diols, 1,2,3 triols
Peng et al., 2021	PtCl_4	1,2-cis diols, 1,2-trans diols, 1,2,3 triols



Scheme 21. Regioselective glycosylation using acid-base catalysis

Transition metals are frequently Lewis acid. Previous to Peng and Schmidt's work on gold(III) and platinum(IV), the Nguyen group has reported activation of TCA donors utilizing commercially available cationic palladium(II) as the catalyst (Scheme 22).¹⁰⁰⁻¹⁰¹ More importantly, this cationic palladium(II) catalyzed glycosylation expressed great stereocontrol, as 1,2-trans glycosides are expected even without anchimeric assistance. Furthermore, this chemistry has effectively coupled a wide scope of donors including glucose (**68**), mannose (**90**), and galactose to a variety of acceptors including primary and secondary alcohols, as well as phenols¹⁰². Although the mechanism of this palladium(II)-catalyzed glycosylation is still unclear, it is believed that the catalyst interacts with both the donor and acceptor.

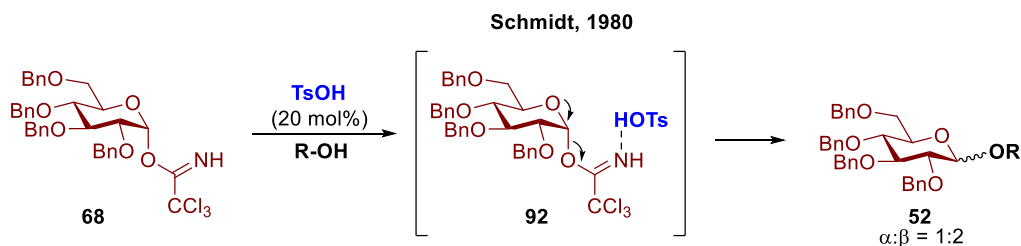


Scheme 22. Cationic palladium(II)-catalyzed stereoselective glycosylation

Summary: Begin with $\text{BF}_3 \cdot \text{OEt}_2$ ⁹¹, Lewis acids catalyzed glycosylation has elaborated beyond simple activation of TCA donor. Through observation from the synthesis of glycosyl phosphates⁹², the Schmidt group hypothesized acid-base catalysis and developed several organo-catalysts allowing stereoselective glycosylation.⁹³⁻⁹⁴ The stereocontrol arises from the formation of a six-membered ring-like complex during the transition state, where the catalyst inserts in the alcohol acceptor leading to simultaneously increased acidity and nucleophilicity of the complexed alcohol. Later, the Nguyen group demonstrated stereocontrol in glycosylation using TCA donors and transition metal catalyst¹⁰⁰⁻¹⁰², along with the Taylor group presented regiocontrol in glycosylation using a small molecule catalyst.⁹⁵ These successful studies have eventually led to stereocontrol and regiocontrol in glycosylation through the use of one catalyst.⁹⁶⁻⁹⁸

1.4.3.2 From Brønsted acid to chiral acid catalysis (cooperative catalysis)

Dated back in 1980, Schmidt and coworkers also reported activation of the TCA donor using 20 mol% *p*-toluenesulfonic acid (TsOH).⁹¹ In this glycosylation, TsOH acts as a Brønsted acid donating a proton to the imidate nitrogen, which promotes the departure of the TCA leaving group, leading to the formation of an oxocarbenium ion (Scheme 23). Due to the lack of C2-neighboring group participation, the stereochemical outcome of the glycosylation was uncontrollable and led to α : β at 1:2.



Scheme 23. Brønsted acid-catalyzed glycosylation

Fast forward to thirty years later, the Fairbanks group revisited the Brønsted acid-catalyzed glycosylation and added chirality as an element of diastereocontrol in catalytic glycosylation. Inspired by asymmetric synthesis¹⁰³⁻¹⁰⁴ and activation of TCA leaving group on a non-carbohydrate compound¹⁰⁵ using chiral Brønsted acids as catalysts, the Fairbanks group sought solutions for stereoselective glycosylation in BINOL-derived phosphoric acid catalysis (Table 1).¹⁰⁶ In the glycosylation of galactosyl TCA donor **93** with alcohol acceptor, the chiral BINOL-derived phosphoric acids **94** (entry 2 and 3) catalyzed glycosylation with superior diastereocontrol than TMSOTf (entry 1) and better yield than the achiral diphenyl phosphate (PhO)₂P(O)OH (entry 4). In addition, the catalyst configuration significantly affects the diastereoselectivity of the glycosylation, as (*S*)-**94** catalyzed the glycosylation with $\beta:\alpha$ ratio of 7:1, while reduced anomeric selectivity was observed with the (*R*)-enantiomer ($\beta:\alpha = 2:1$).

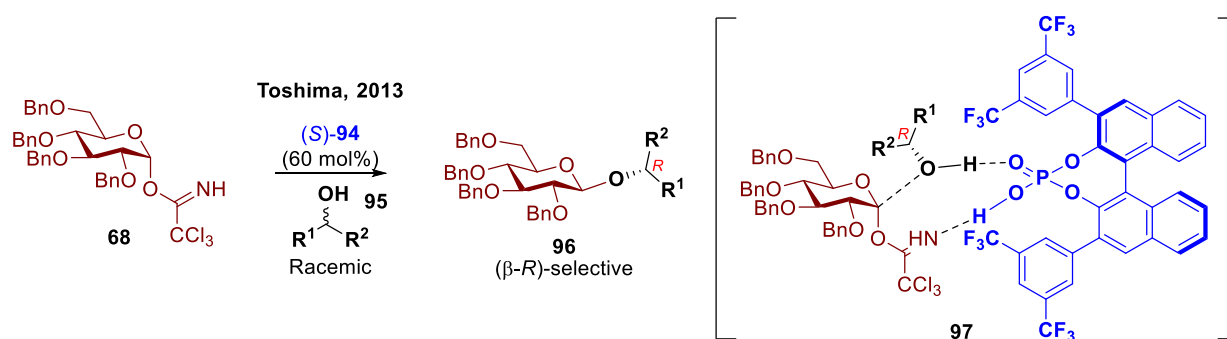
Table 1. Chiral Brønsted acid-catalyzed glycosylation

Fairbanks, 2010

Entry	Catalyst	Yield (%)	$\alpha:\beta$
1	TMSOTf	98	1.2:1
2	(<i>S</i>)- 94	80	1:7
3	(<i>R</i>)- 94	88	1:2
4	(PhO) ₂ P(O)OH	19	1:1.9

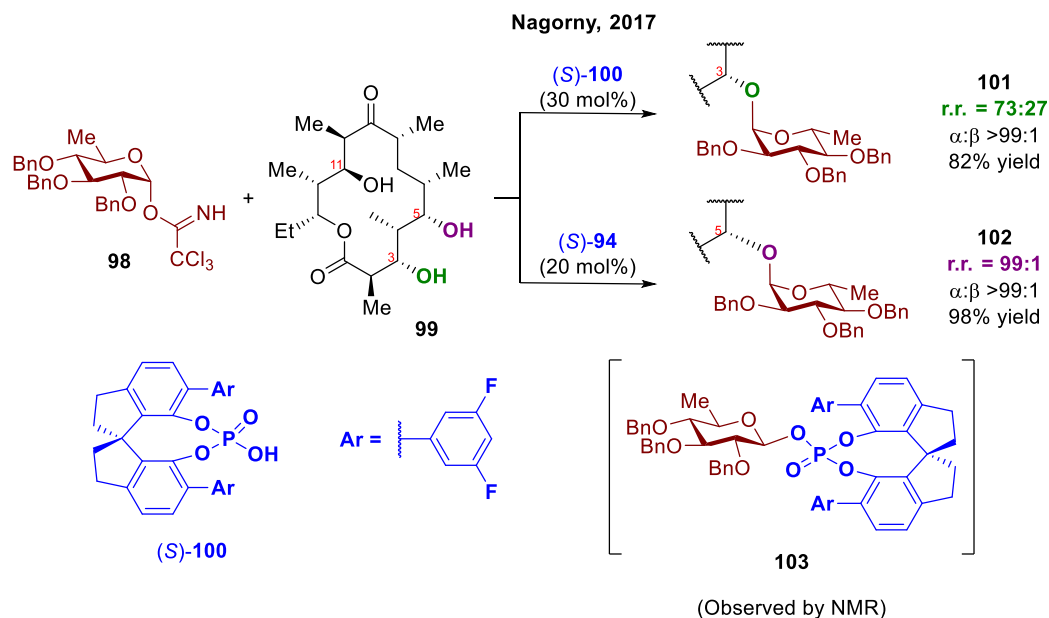
In 2013, Toshima and coworkers extended the work on chiral phosphoric acid-catalyzed glycosylation further to kinetic resolution of racemic alcohol acceptors (Scheme 24).¹⁰⁷ Taking advantage of the chirality

on the catalyst, only the alcohol with *R*-configuration was recognized by (*S*)-**94**. In the glycosylation catalyzed by (*S*)-**94**, the glucosyl TCA donor **68** and racemic alcohol acceptors **95** lead to coupled glycoconjugate **96** with (β -*R*)-selectivity. Based on this observation, the Toshima group proposed a cooperative mechanism: while the chiral BINOL-derived phosphoric acid (*S*)-**94** plays its role as a Brønsted acid to activate the TCA donor, it also acts as a hydrogen bond acceptor to guide the alcohol acceptor to the anomeric carbon (**97**). Overall, an S_N2 mechanism was proposed to explain the high β -selective, although the mechanism on the diastereoselectivity remains unknown.



Scheme 24. Kinetic resolution in stereoselective glycosylation using chiral Brønsted acid

In 2017, the Nagorny group reported site-selective glycosylation of 6-deoxyerythronolide B acceptor **99** through the selection of chiral phosphoric acids as catalysts (Scheme 25).¹⁰⁸ While SPINOL-based phosphoric acid **100** catalyzes the glycosylation at the C3 position of macrolactone **99**, the BINOL-based phosphoric acid **94** prefers to catalyze at the C5 position of **99**. In the mechanistic study, covalent glycosyl phosphate intermediates were observed through NMR. While β -glycosyl phosphate **103** was detected in the 6-deoxy glucosyl substrate **98**, α -intermediates were found in the D- and L- fucose cases, indicating the formation of glycosyl phosphate intermediate may not always be S_N2 -like (contrasting Scheme 18a). In addition, the same stereochemical outcomes of glycosylation were observed despite the anomeric compositions of the TCA donor. As the β -glycosyl phosphate intermediate led to the α -glycoside product (vice versa in fucose substrates), it was proposed that the anomeric composition of the glycosyl phosphate intermediate was responsible for the stereochemical outcome of the glycosylation.



Scheme 25. Site-selective glycosylation by the selection of chiral phosphoric acid

Although transition metals are often Lewis acid, some of which could be “hidden Brønsted acids”.¹⁰⁹⁻

¹¹¹ In 2019, the Nguyen group conducted a thorough mechanism investigation on nickel(II) triflate ($\text{Ni}(\text{OTf})_2$) catalyzed 1,2-*cis* glycosylation of *N*-phenyl trifluoroacetimidate donor (**104**), in which experimental evidence pointed toward triflate acid (TfOH) as the active catalyst in the system (Table 2).¹¹² A correlation was found between the catalytic activity of the metal triflates and their hydrolysis constant (pK_h). For metal salts with pK_h less than 10.1, the cationic metals are generally easy to hydrolyze when the anion is weakly coordinating. As such, the catalytic glycosylation proceeded with similar yield and selectivity when $\text{Ni}(\text{OTf})_2$ ($pK_h = 9.86$), $\text{Zn}(\text{OTf})_2$ ($pK_h = 8.96$), and $\text{In}(\text{OTf})_3$ ($pK_h = 4.00$) were used as the catalyst (entry 1-3). On the other hand, AgOTf cannot catalyze glycosylation since the pK_h of $\text{Ag}(\text{I})$ is 12 (entry 4). ¹⁹F NMR observation on the mixture of glycosyl donor **104** and $\text{Ni}(\text{OTf})_2$ confirmed and quantified the formation of TfOH . In the end, the glycosylation was successfully repeated with only 1 mol% TfOH added to the reaction (entry 5). In the variable temperature NMR study, glycosyl triflate **106** was identified leading to a Curtin-Hammett scenario to explain the high diastereoselectivity of the catalytic glycosylation.

Table 2. Hidden Brønsted acids catalyzed glycosylation

Nguyen, 2019

Entry	Catalyst	Yield (%)	α : β
1	Ni(OTf) ₂	90	10:1
2	Zn(OTf) ₂	91	10:1
3	In(OTf) ₃	95	9:1
4	AgOTf (30 mol%)	<6	n/a
5	TfOH (1 mol%)	78	10:1

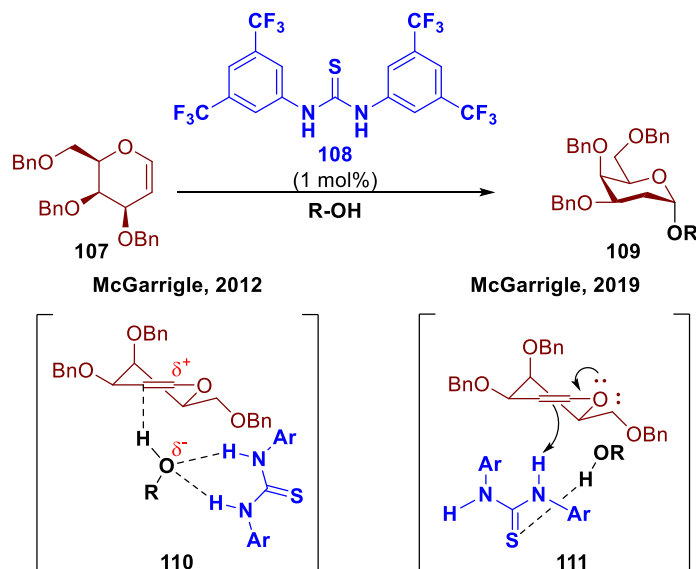
(Observed by NMR)

Summary: The ability of Brønsted acid-catalyzed glycosylation has first been shown in 1980⁹¹, albeit with poor stereoselectivity. Until recently, improved stereoselectivity was observed with chiral Brønsted acid.¹⁰⁶ Although the role of chirality in stereocontrol remains unclear, the ability of kinetic resolution during glycosylation is presented.¹⁰⁷ Further NMR observation of glycosyl phosphate intermediate suggested the stereocontrol of the chiral Brønsted acid-catalyzed glycosylation arises from the anomeric composition of the intermediate.¹⁰⁸ Besides the aforementioned chiral Brønsted acids, some metal triflates are considered “hidden Brønsted acid”, where TfOH is the active catalyst in the metal-catalyzed glycosylation system.¹¹² Although the mechanism of diastereocontrol with TfOH in catalyzing glycosylation remains unresolved, a Curtin-Hammett scenario is generally accepted.

1.4.3.3 From thiourea to bis-thiourea catalysis (cooperative catalysis)

Similar to phosphoric acid, thiourea is also an important class of small molecule that has successfully catalyzed a variety of asymmetric chemical transformations.¹¹³ The utilization of thiourea as a catalyst in glycosylation was first reported by McGarrigle and coworkers in 2012 (Scheme 26).¹¹⁴ Inspired by Kotke and Schreiner’s acetalization,¹¹⁵ McGarrigle and coworkers applied the Schreiner’s thiourea catalyst **108** to the synthesis of 2-deoxy galactoside through the coupling of galactal and alcohol. Under the influence of 1 mol% thiourea **108**, the alkyl and silyl ether protected galactals react with a variety of primary and

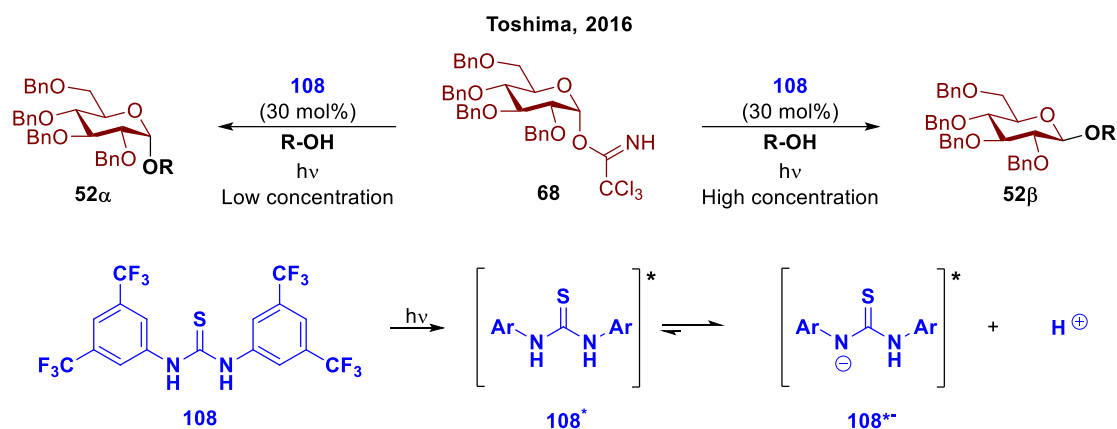
secondary glycosyl alcohols in *syn* fashion, leading to the formation of α -2-deoxygalactosides as the products. The originally proposed mechanism involved the formation of an alcohol-thiourea complex (**110**) through double hydrogen bonding, where the thiourea catalyst **108** acted as the hydrogen bond donor. Yet, the subsequent mechanistic study in 2019 revealed that the thiourea catalyst played a role as Brønsted acid in glycosylation of galactal donor and alcohol acceptor (**111**).¹¹⁶



Scheme 26. Schreiner's thiourea catalyzed 2-deoxy galactoside synthesis

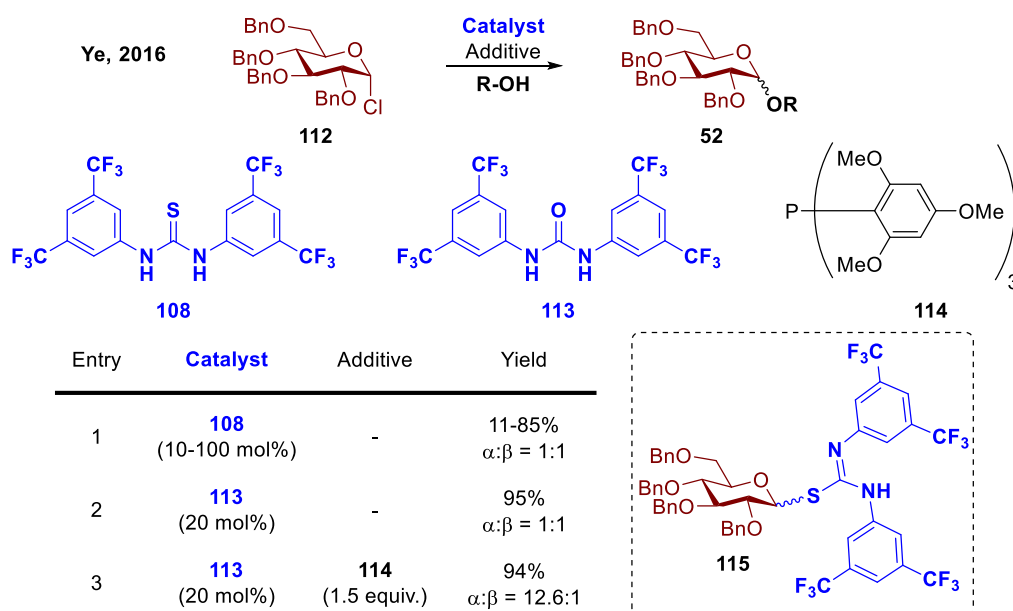
Using thiourea derivative as a Brønsted acid in catalyzing glycosylation was reported before 2019. In 2016, Toshima and coworkers envisioned the conjugate base of aryl thiourea (nitrogen anion) should be rather stable due to the resonance effect, which translated into increased acidity of aryl thiourea upon photoirradiation. As such, the group demonstrated the use of Schreiner's thiourea catalyst **108** as an organo photoacid in catalyzing glycosylation with glycosyl TCA donor (Scheme 27).¹¹⁷ Upon irradiation at 365 nm, a proton (H^+) was released from the excited thiourea **108*** and activated the glycosyl TCA donor. Additionally, the Toshima group discovered that this photoinduced catalytic glycosylation proceeded with β -selectivity at high reaction concentration (1-2 M), indicating the reaction underwent an S_N2 -type mechanism. Conversely, an S_N1 -type mechanism was expected at low reaction concentration, which led to

α -selectivity in the stereochemical outcome. As expected, the photoinduced catalytic glycosylation proceeded with α -selectivity at 0.005-0.1 M.

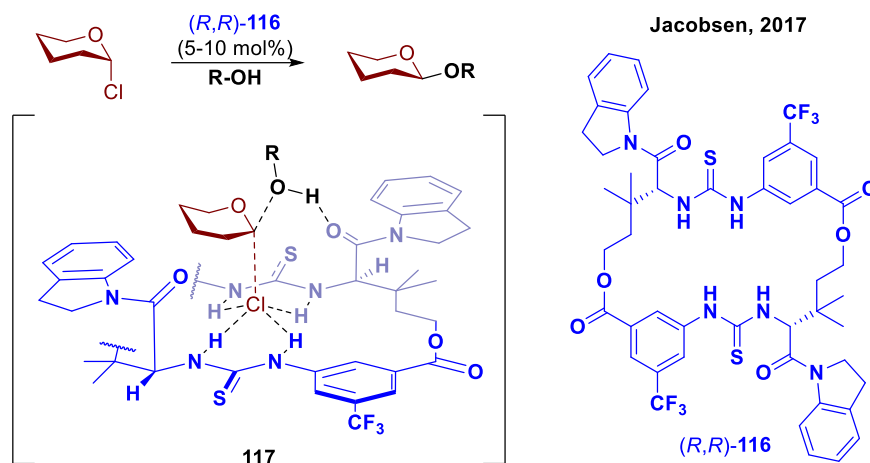


Scheme 27. Schreiner's thiourea catalyst as an organo photoacid in catalytic glycosylation

On the other hand, thiourea derivatives as hydrogen bond donors have proven to activate halogenated compounds.¹¹⁸ In 2016, Ye and coworkers attempted to activate perbenzylated glucosyl chloride **112** utilizing thiourea **108** as a catalyst (Table 3).¹¹⁹ However, a diminished yield was collected when using a catalytic amount of thiourea **108**, where 10 mol% catalyst loading led to an 11% yield (entry 1). In addition, the S-glycosylated byproduct **115** was isolated in all reactions with thiourea **108**. The urea-derived catalyst **113** was used to avoid this side reaction and led to an excellent yield (95%), albeit poor stereoselective (α : β = 1:1, entry 2). However, this catalytic reaction with galactosyl, mannosyl, rhamnosyl, and glucosaminyl donor proceeded with high α -selectivity. To solve the stereoselectivity issue with the glucose substrate, a phosphine additive (**114**) was added to the catalytic reaction, and the anomeric selectivity improved to 12.6:1 α / β (entry 3). NMR mechanistic study revealed that the glycosyl chloride was activated by urea **113** through a dual hydrogen bonding as the chemical shift of the urea protons shifted upfield upon mixing with glycosyl chloride **112**. Although the function of phosphine additive **114** is still unclear, a complex of glycosyl chloride with both catalyst **113** and additive **114** was indicated based on the NMR study.

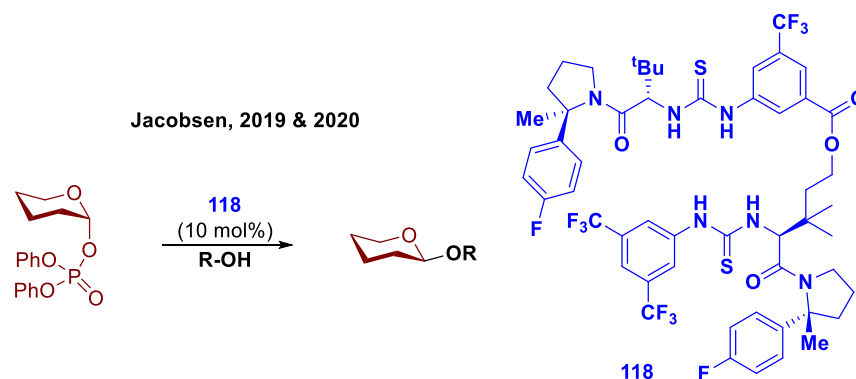
Table 3. Urea-catalyzed stereoselective glycosylation

In 2017, the Jacobsen group designed a dimeric, macrocyclic thiourea catalyst to promote stereospecific glycosylation with glycosyl chlorides (Scheme 28).¹²⁰ Aiming to catalyze glycosylation in an S_N2 pathway, cooperative activation of both glycosyl donor and acceptor through a catalyst was pursued. The cyclic design of bis-thiourea **116** weakens the C-Cl bond through quadruple hydrogen bonding. Meanwhile, the Lewis base interaction between the alcohol acceptors and the indoline amides adjacent to the thiourea increases the acceptors' nucleophilicity (**117**). More importantly, the C_2 symmetric design of **116** not only simplifies the catalyst synthesis but also allows the alcohol nucleophile to approach the anomeric carbon at a broader angle. As such, both enantiomers of **116** expressed similar reactivity and diastereoselectivity in glycosylation. Through simultaneous activation of α -glycosyl chloride and alcohol acceptors, the Jacobsen group has successfully demonstrated the synthesis of *trans*-1,2-, *cis*-1,2-, and 2-deoxy- β -glycosides in good yield and high stereoselectivity using bis-thiourea catalyst **116**.



Scheme 28. Macrocyclic bis-thiourea catalyzed stereospecific glycosylation

Besides glycosyl chlorides, the Jacobsen group later designed another bis-thiourea catalyst enabling the activation of glycosyl phosphates (Scheme 29).¹²¹⁻¹²² Since the phosphate leaving group exhibited a stronger Lewis basic character than the chloride, a quadruple hydrogen bonding is no longer needed. As such, the new catalyst **118** adopted a linear design to accommodate the spatial need of the phosphate leaving group. Kinetic study showed a 16-fold improvement in catalytic efficiency when using glycosyl phosphate as the donor compare to that of glycosyl chloride. In addition, since the thiourea catalyst **118** binds stronger to the phosphate leaving group, a larger scope of nucleophiles, including thiol and phenol, can be used in the reaction.



Scheme 29. Bis-thiourea activation of glycosyl phosphate

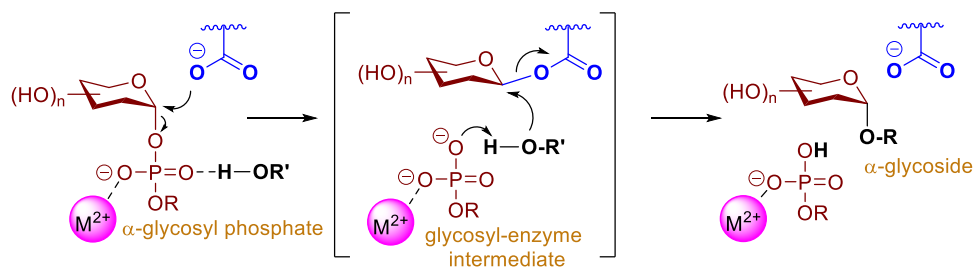
Summary: While thiourea derivatives are commonly known as dual hydrogen bond donors, they can serve a role as Brønsted acids, such as activation of galactal using Schreiner's thiourea catalyst.¹¹⁴ Upon

photo-irradiation, the Schreiner's thiourea catalyst becomes more acidic, which is capable of activating the TCA donor.¹¹⁷ Certainly, the Schreiner's thiourea/urea catalysts serving as dual hydrogen bond donors enable activation of glycosyl chlorides, although the diastereoselective depends on the nature of substrates or additives in the reaction.¹¹⁹ In the end, Jacobsen's bis-thiourea catalyst demonstrated simultaneous activation of glycosyl donor and nucleophilic displacement, leading to stereospecific glycosylation.¹²⁰⁻¹²²

1.5 Main objectives

1.5.1. Inspiration and hypothesis

It has been reported that enzymatic glycosylation undergoes an S_N2 pathway. While inverting glycosyltransferases (GTs) proceed a direct S_N2 displacement to provide the products with inversion of anomeric configuration, the retaining GTs proceed a double S_N2 mechanism to generate the products with net retention of anomeric stereochemistry (Scheme 30)¹²³. The nucleophilic residue of the retaining glycosyltransferase reacts with α -glycosyl phosphate to generate a covalent β -glycosyl-enzyme intermediate with inversion of stereochemistry. Inverted substitution by a nucleophile affords the corresponding α -glycoside product with net retention of anomeric stereochemistry.



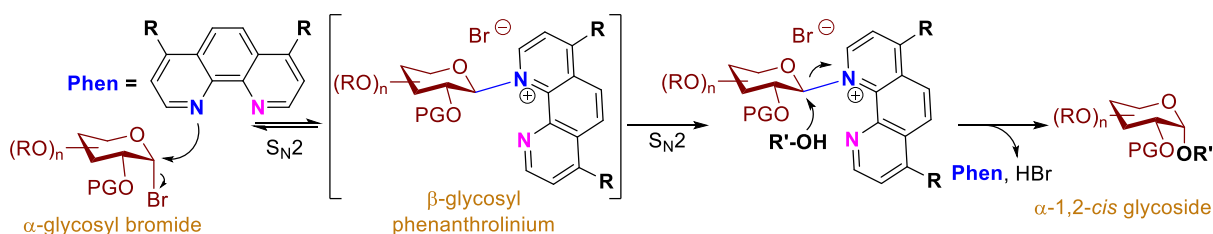
Scheme 30. Retaining glycosyltransferases-catalyzed stereoretentive glycosylation

Hypothesis: Inspired by the effectiveness of retaining GTs, it is envisioned that a small molecule catalyst capable of acting like GTs to provide 1,2-*cis* glycosides, via a double S_N2 displacement with predictable α -selectivity and in high yields, would likely find broad applications.

It was first reported by Lemieux and Morgan that pyridine could serve as a nucleophile to displace the anomeric leaving group to afford a glycosyl pyridinium complex.¹²⁴⁻¹²⁵ To minimize the steric and electrostatic interactions, the pyridinium ion intermediate prefers to position at the equatorial face on the

glycosyl electrophile. The nucleophilic attack is more likely to take place at the axial position of the pyridinium ion complex to provide an axial (α) glycosidic bond. However, pyridine is not bulky enough to form an exclusively equatorial intermediate. As an axial glycosyl pyridinium intermediate could also be generated in the reaction¹²⁴⁻¹²⁵, the stereoselectivity of the coupling product would be detrimentally affected. To overcome this inherent problem, we sought to identify a catalyst that would be able to form an exclusively equatorial intermediate.

The commercially available pyridine-like compound, phenanthroline, appealed to us with great interest. As demonstrated in Scheme 31, it is hypothesized that the first nitrogen atom of phenanthroline (Phen) could serve as the nucleophile to displace the anomeric bromide leaving group, generating a covalent β -glycosyl phenanthroline intermediate. Meanwhile, the two fused pyridine rings of phenanthroline could sterically prevent the formation of α -glycosyl phenanthroline intermediate. In addition, the second nitrogen could cooperate to promote glycosylation, either by directing the alcohol nucleophile to α -face or non-covalently interacting with the carbohydrate moiety. All these advantages of phenanthroline have driven us to explore its ability as the catalyst to promote the reactions that afford high-yielding 1,2-*cis* products with predictable stereoselectivity.

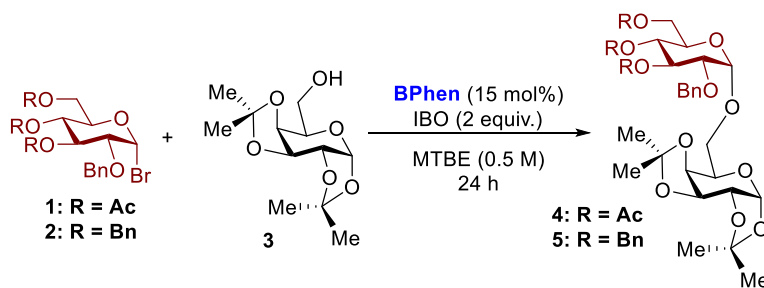


Scheme 31. Phenanthroline-catalyzed α -1,2-*cis*-glycosylation

1.5.2. Preliminary results and continuation

The initial investigation was performed by Dr. Fei Yu utilizing α -glycosyl bromide **1** as the model electrophile and 1,2:3,4-di-*O*-isopropylidene- α -D-galactopyranose (**3**) as the nucleophile to afford the disaccharide **4**. After a series of catalyst screening and reaction optimization, use of 15 mol% bathophenanthroline (**BPhen**) and 2 equivalent of isobutylene oxide (IBO) as an acid scavenger of hydrogen bromide (HBr) in *tert*-butyl methyl ether (MTBE) at 50 °C for 24 h were found to be the most effective at promoting the reaction (Table 4, entry 1, **4**: 73% yield, α : β > 20:1)¹²⁶. However, when the reaction temperature decreased to 25 °C (room temperature), the glycosylation did not proceed (Table 4, entry 2). It has been determined that the protecting groups on glycosyl electrophile and nucleophiles could affect the efficiency and selectivity of the coupling product^{64, 73}. As such, 2,3,4,6-tetra-*O*-benzyl- α -D-glucopyranosyl bromide (**2**, entries 3 and 4), which is to promote glycosylation via the S_N1 pathway, was then explored as part of my Ph.D. work. As expected, under standard conditions at 50 °C, the glycosylation proceeded to provide 82% yield of the disaccharide **5** with reduced α -selectivity (α : β = 6:1, entry 3). This result suggested that the S_N1-S_N2 reaction paradigm was slightly shifted. On the other hand, when the reaction was conducted at room temperature (entry 4), the coupling product was obtained with excellent

Table 4. Bathophenanthroline-catalyzed 1,2-cis glycosylation^[a]



entry	R	Temp. (°C)	yield ^b (α : β) ^c
1*	Ac	50	73% (>20:1)
2*	Ac	25	-
3	Bn	50	82% (6:1)
4	Bn	25	55% (16:1)

^[a] All reactions were conducted with 0.1 mmol glycosyl bromide and 0.2 mmol glycosyl acceptor. ^[b] Yield of isolated products. ^[c] Diastereoselectivity (α : β) was determined by ¹H NMR. *Result from Dr. Fei Yu.

selectivity ($\alpha:\beta = 16:1$) albeit in lower yield (55%). The high selectivity with tetrabenzyl glycosyl substrate indicates that the ability of the catalyst overrides the inherent substrate's selectivity preference. The coupling of glycosyl nucleophile **3** with electrophilic partner **2** to yield the disaccharide **5** was later optimized to 95% yield by using 20 mol% of **BPhen** catalyst.¹²⁶

1.5.3. Major Goals

My graduate works have mainly focused on exploring the phenanthroline catalysis system. The first part was to investigate the utility of **BPhen** on electron-rich glycosyl donors. As the S_N1 - S_N2 reaction paradigm shifts toward the S_N1 direction with the electron-rich substrates, a more practical catalyst was highly desirable. This has led to the second part of the study: identify an efficient catalyst within and beyond the phenanthroline framework allowing stereoselective glycosylation in a shorter time with the electron-rich electrophilic donors. The successful identification of an efficient catalyst led to the expansion of substrate scope. Chapter 2 of this dissertation contains substrate scope and catalyst screening. Another main focus of the exploration was to investigate the mechanism of the phenanthroline catalytic system (Chapter 3), which includes kinetic studies, NMR studies, and computational studies.

Furanoses are more prone to proceed at the S_N1 - S_N2 boundary than their pyranose counterparts due to their conformational flexibility and electronic properties.¹²⁷ As Dr. Hengfu Xu explored the stereoselective 1,2-*cis* furanosylation method promoted by phenanthroline catalyst, the mechanism was unclear. The last part of my dissertation is focused on the mechanistic study of phenanthroline-catalyzed stereoselective 1,2-*cis* furanosylation (Chapter 4).

CHAPTER 2: SCOPE OF PHENANTHROLINE-CATALYZED 1,2-*CIS* PYRANOSYLATION

2.1 First generation phenanthroline catalysis

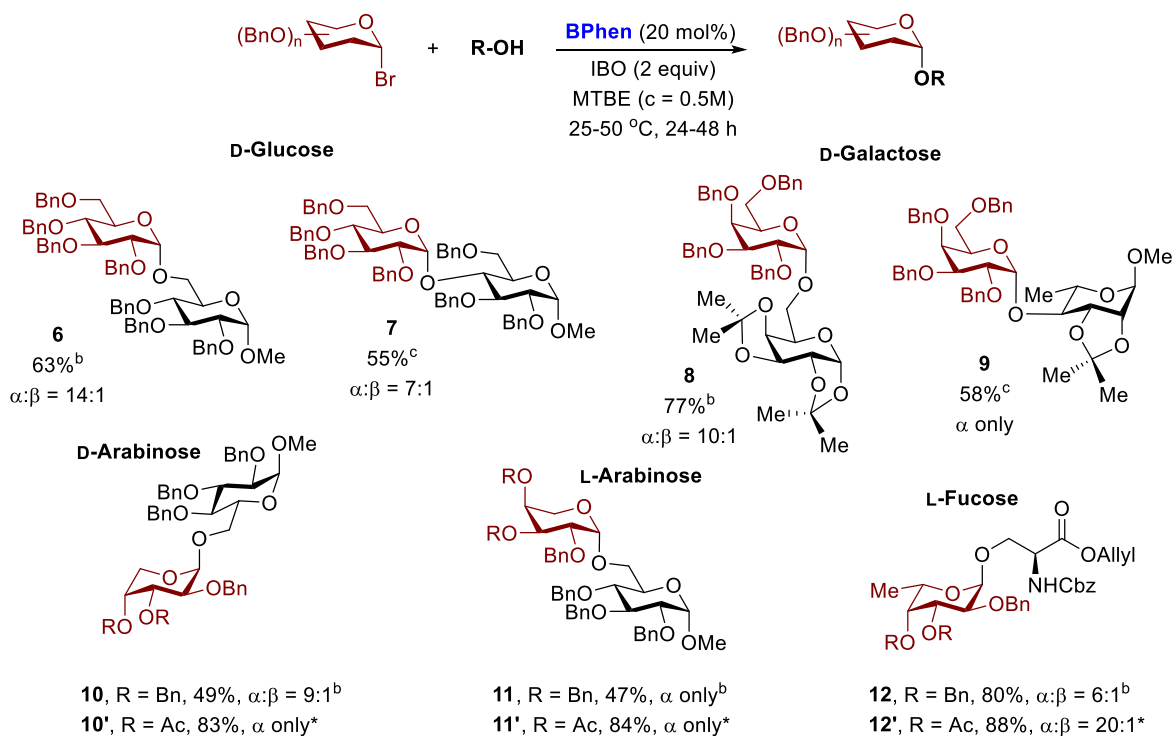
Several underlying factors potentially influence the efficiency and the selectivity of the glycosylated products, including the protecting group nature of glycosyl electrophiles,^{64, 68, 90, 128} the reactivity of nucleophiles, and the reaction conditions. To explore the utility of this phenanthroline catalysis system on electron-rich donor substrates, a series of glycosylation were performed to prepare a variety of disaccharides and glycoconjugate (Table 5). For example, while AgBF₄ promoted glycosylation provided the disaccharide **6** with $\alpha:\beta$ ratio of 2.4:1¹²⁹, or TMSOTf-mediated coupling with trichloroacetimidate electrophiles provided **6** with marginal a selectivity ($\alpha:\beta = 1:1.2-4:1$)¹³⁰, our catalysis system generated the coupling product **6** with $\alpha:\beta = 14:1$. Extremely hindered secondary alcohol nucleophile is also amendable to provide the disaccharide **7** with good selectivity ($\alpha:\beta = 7:1$), for which the S_N1-S_N2 reaction paradigm was slightly shifted.

In addition to glucosyl electrophile **2**, a number of different sugar substrates were adapted into glycosyl bromide electrophiles to prepare disaccharides **8** – **11** and glycoconjugate **12**. It has been reported that D-galactose favors β -product compared to D-glucose.¹³¹ Nevertheless, phenanthroline-catalyzed glycosylation with galactosyl bromide produced disaccharide **8** with excellent α -selectivity ($\alpha:\beta = 10:1$). In contrast, the amide-promoted reaction provided **8** with $\alpha:\beta = 3:1$.¹³² In addition, the phenanthroline catalysis system produces disaccharide **9** with excellent diastereoselectivity (α only).

Arabinose is a more challenging substrate due to its lability with electron-rich protecting groups. Use of D- or L-tribenzyl arabinosyl bromide in the phenanthroline catalyzed glycosylation reaction provides disaccharide **10** or **11** with excellent diastereoselectivity ($\alpha:\beta = 9:1$ and α only, respectively), albeit with low yield (<50%) due to decomposition of the arabinosyl bromide during the reaction. The yield could be improved with the use of acetyl protecting groups (**10'**: 83%, **11'**: 84%). Similarly, while tribenzyl L-

fucofucosyl bromide afforded **12** with $\alpha:\beta = 6:1$, the use of triacetyl L-fucofucosyl bromide provided exclusively α -isomer **12'**. Both **12** and **12'** are key units of a thrombospondin type 1 compound associated with an autosomal recessive disorder.¹³³

Table 5. Bathophenanthroline-catalyzed 1,2-cis glycosylation with electron-rich substrates^[a]



^[a] All reactions were conducted with 0.1-0.3 mmol glycosyl bromide. Yields of isolated products. Diastereoselectivity ($\alpha:\beta$) was determined by ¹H NMR analysis. ^[b] 20 mol% **BPhen** at 25 °C. ^[c] 20 mol% **BPhen** at 50 °C. *Result from Dr. Fei Yu, 15-30 mol% **BPhen** at 50 °C for 24-48 h.

2.2 Second generation phenanthroline catalyst

2.2.1. Development of a new class of phenanthroline catalyst

To improve the practicality of this glycosylation on electron-rich substrates, we sought to re-screen the commercially available catalyst with the reactive donors. (Table 6). We selected 2,3,4,6-tetra-*O*-benzyl- α -D-glucopyranosyl bromide (**2**) as an electrophilic donor and 1,2:3,4-di-*O*-isopropylidene- α -D-galactopyranoside (**3**) as the nucleophilic model coupling partners in catalyst screening because they are the most reactive coupling partners.¹²⁶ Previously, we reported the reaction of glycosyl bromide **2** and hydroxyl nucleophile **2** with 20 mol% 4,7-diphenyl-1,10-phenanthroline (**C1** or **BPhen**) catalyst in the

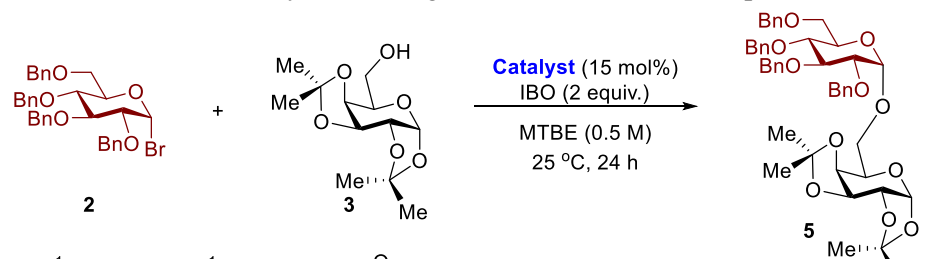
presence of IBO as an acid scavenger in MTBE at 25 °C for 24 h yielded disaccharide **5** (95%) with outstanding diastereoselectivity ($\alpha:\beta = 15:1$).¹²⁶ This effective glycosylation model was adapted in this investigation. To distinguish the reactivity of different catalysts, we decreased the catalyst loading to 15 mol% and kept the reaction time at 24 h.

In the absence of the catalyst, only a trace amount of the product was detected (entry 1), and 98% of starting material **3** was recovered. As for the phenanthroline derivatives (**C1** – **C5**), we first investigated how the electronic nature of the substituents on the catalyst would vary the reaction outcome. Interestingly, use of the non-substituted 1,10-phenanthroline (**C2**, entry 3) delivered comparable yield (54% vs 55%) and selectivity ($\alpha:\beta = 18:1$ vs 16:1) as 4,7-diphenyl-1,10-phenanthroline (**C1**, entry 2). However, with Dr. Yu's triacetate substrate, the yields of the coupling product with the use of catalysts **C1** and **C2** differed by 20% (73% and 53% yield respectively), while the selectivity was comparable ($\alpha:\beta >20:1$)¹²⁶. This is probably due to the electron-rich nature of the tetrabenzyl glycosyl electrophile overcomes the marginal difference in nucleophilicity of the catalyst. Therefore, when we utilized bromine as a substituent on the *para*-position of the catalyst **C3** (entry 4), the yield was not affected. The methoxy group is known as an electron-donating substituent; however, the use of 4,7-dimethoxyl-1,10-phenanthroline (**C4**, entry 5) did not further improve the yield of the disaccharide **5**. This might be due to the inductive effect of the oxygen atom that decreases the nucleophilicity of the catalyst. As such, the electron-rich tetramethyl substituted phenanthroline was used (**C5**, entry 6), and the glycosylation proceeded with a significantly higher yield (76%) than those with other phenanthroline derivatives (54 – 58%).

Furthermore, we investigated the necessity of the phenanthroline framework on coupling efficiency and selectivity (Table 6, entry 7-13). The performance with the non-phenanthroline-based catalysts varied in the glycosylation. For example, when we free the two nitrogen from the planar configuration by using 2,2'-bipyridine type catalyst (**C6** and **C7**), the yield and selectivity reduced significantly (entries 7 and 8) compared to **C1** (entry 2). Similarly, increasing the number of pyridines on the catalyst (**C8**, entry 9) did not improve the yield or selectivity (23% yield, $\alpha:\beta = 8:1$). Meanwhile, maintaining the planar structure of

the catalyst preserved the glycosylation outcome. In the case of 4,5-diazafluoren-9-one as the catalyst (**C9**, entry 10), the yield of the glycosylation is similar to that of **C2**, albeit with lower α -selectivity, which is likely due to the change in the distance and angle between the two nitrogen on the catalyst.

Table 6. Catalyst screening with electron-rich electrophile ^[a]



entry	Catalyst	yield (%) ^b	α : β ^c
1	-	Trace	-
2	C1	55	16:1
3	C2	54	18:1
4	C3	58	10:1
5	C4	56	10:1
6	C5	76	10:1
7	C6	24	10:1
8	C7	33	9:1
9	C8	23	8:1
10	C9	50	13:1
11	C10	43	12:1
12	C11	73	14:1
13	C12	93	11:1

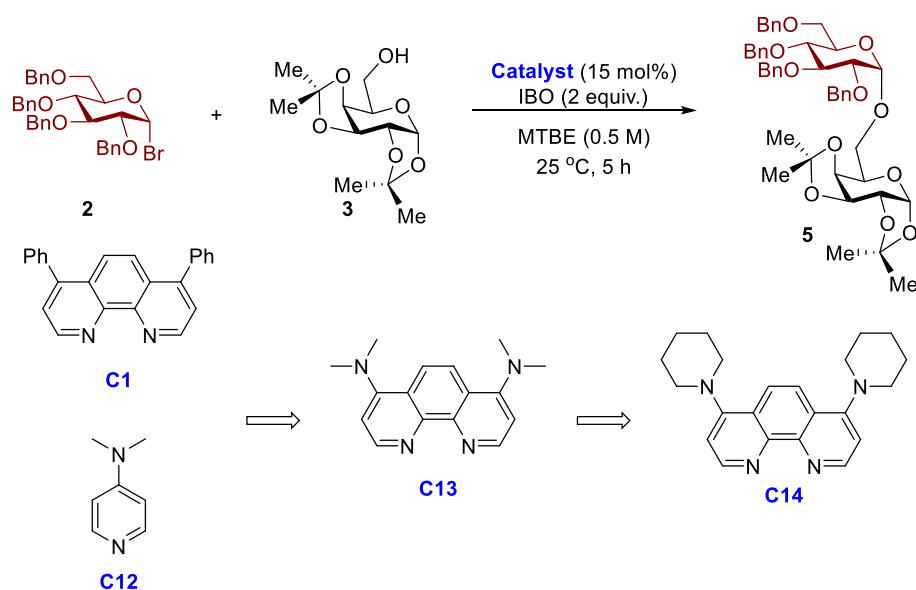
^[a] All reactions were conducted with 0.2 mmol glycosyl bromide **2** and 0.1 mmol glycosyl acceptor **3**. ^[b] Yields of isolated products. ^[c] Diastereoselectivity (α : β) was determined by ¹H NMR analysis.

In addition, 5-membered fused rings were also of interest. Similar to the bi- or tri-pyridine catalysts, the imidazole substituted pyridine catalyst (**C10**, entry 11) did not proceed to completion. Since the tertiary amine is more nucleophilic than pyridine, we attempted *N,N,N',N'*-tetramethylethylenediamine (TMEDA, **C11**) bearing two tertiary amine groups (entry 12). The yield of TMEDA-catalyzed glycosylation increased as expected; however, the reaction did not proceed to completion after 24 hours. In the end, we anticipated that dimethylamino substituents on the *para*-position would drastically improve the glycosylation outcome.

As expected, the use of 4-(dimethylamino)pyridine (DMAP, **C12**) provided the desired disaccharide **5** in 93% yield (entry 13) with good α -selectivity (α : β = 11:1) in 24 h. This result led to further design on the phenanthroline catalyst.

To further improve the catalyst performance, the dimethylamino substituents were installed onto the phenanthroline framework (**C13**, Table 7). Catalyst **C13** was prepared over 2 steps from commercially available 4,7-dihydroxy-1,10-phenanthroline. First, treatment of dihydroxyl phenanthroline with phosphorus oxychloride (POCl_3) at 60 °C for 2 h allowed functional group interconversion to produce the 4,7-dichloro-1,10-phenanthroline. After removal of excess POCl_3 , the dichlorophenanthroline was then treated with *N,N*-dimethylformamide (DMF) at 160 °C for 60 h to afford catalyst **C13**.

Table 7. Catalyst development in phenanthroline framework^[a]



entry	Catalyst	yield (%) ^b	α : β ^c
1	C1	40	13:1
2	C12	63	11:1
3	C13	61	15:1
4	C14	67	12:1

^[a] All reactions were conducted with 0.2 mmol glycosyl bromide **2** and 0.1 mmol glycosyl acceptor **3**. ^[b] Yields of isolated products. ^[c] Diastereoselectivity (α : β) was determined by ¹H NMR analysis.

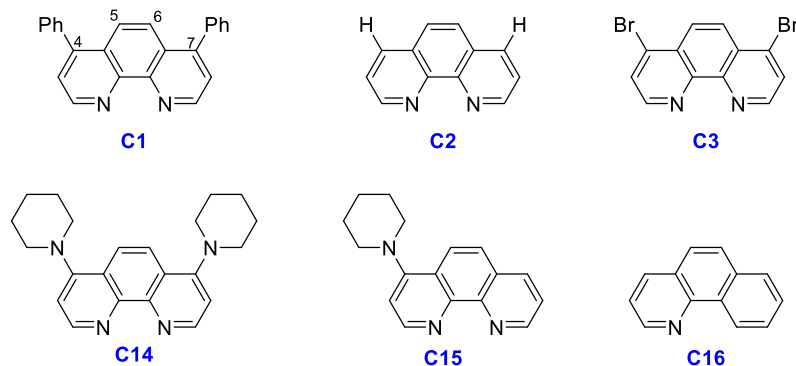
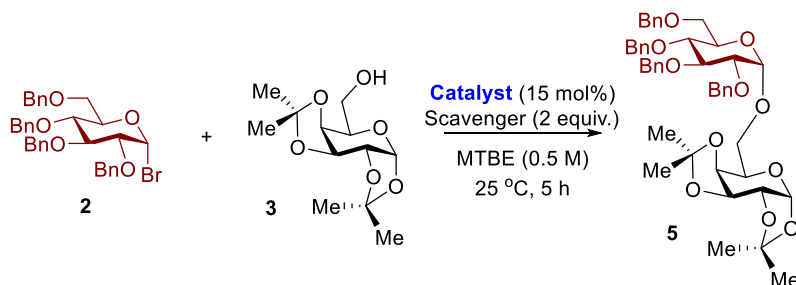
To distinguish the efficiency of the catalysts, the reaction time was reduced to 5 h. As illustrated in Table 7, the glycosylation catalyzed by BPhen (**C1**) only proceeded with a 40% yield of disaccharide **5** at 5 h, while DMAP (**C12**) catalyzed the glycosylation with 63% yield. Expectedly, the glycosylation catalyzed by catalyst **C13** (entry 3) is more efficient than **C1** (BPhen, entry 1) and **C12** (DMAP, entry 2), as the yield of glycosylation with **C13** is higher than that with BPhen (61% vs 40%), and the diastereocontrol is better than DMAP (15:1 vs 11:1). However, catalyst **C13** is not suitable in the synthesis of 2-deoxy-2-fluoro glycoside, as only a trace amount of disaccharide was observed in the reaction.¹³⁴ This is likely due to competition of the dimethylamine in the reaction leading to many side products. As such, the sterically hindered piperidine substituents (**C14**) were installed to replace the dimethylamino substituents (**C13**). Gratifyingly, catalyst **C14** promoted glycosylation of 2-deoxy-2-fluoro-glycosyl electrophile with high yield and excellent levels of diastereoselectivity¹³⁴, and the effectiveness of **C14** with the electron-rich glycosyl electrophile remains remarkable (entry 4, 67% yield, $\alpha:\beta = 12:1$).

2.2.2. Influence of phenanthroline catalyst

Next, we evaluated the electronic and structural effects of phenanthroline (Table 8). Use of **C1** provided disaccharide **3** in 40% yield with $\alpha:\beta = 13:1$ (entry 1). Meanwhile, the use of **C14** provided **3** in higher high yield due to the electron-donating *para*-piperidine substituents increasing the nucleophilicity of the catalyst (67%, entry 3). In contrast, electron-withdrawing *para*-bromide substituted phenanthroline **C3** reduced glycosylation reactivity, providing 9% of the desired disaccharide **3** (entry 6). Predictably, the non-substituted phenanthroline **C2** yielded slightly less product compared to **C1** (35% vs. 40%, entry 5 vs. 1). We next evaluated the mono-piperidine substituted phenanthroline **C15**, and a reduced yield (24%, entry 7) was obtained in comparison to the symmetrical catalysts **C14** (entry 3) and **C2** (entry 5), confirming the C₂-symmetry of phenanthroline plays a critical role in glycosylation reactivity. Benzo[h]quinoline (**C16**, entry 8) catalyst containing only one pyridine ring is less reactive and α -selective compared with the two fused pyridine **C2** catalyst (entry 5), suggesting the importance of the second nitrogen atom on the phenanthroline framework. Further exploration revealed that replacement of IBO with 2,6-di-*tert*-butyl-4-

methypyridine (DTBMP) as acid scavenger resulted in improved α -selectivity while maintaining comparable yield (entries 2 and 4 vs 1 and 3). We rationalized that utilizing DTBMP as an acid scavenger would preserve bromide ion in the reaction, which further facilitates the equilibrium between the glycosyl phenanthroline ion intermediate and the α -glycosyl bromide (Scheme 31).¹³⁴

Table 8. Influence of phenanthroline catalyst^[a]



entry	Catalyst	Scavenger	yield ^b (α : β) ^c
1	C1	IBO	40% (13:1)
2	C1	DTBMP	31% (19:1)
3	C14	IBO	67% (12:1)
4	C14	DTBMP	63% (14:1)
5	C2	IBO	35% (14:1)
6	C3	IBO	9% (10:1)
7	C15	IBO	24% (13:1)
8	C16	IBO	6% (5:1)

^[a] All reactions were conducted with 0.2 mmol glycosyl bromide **2** and 0.1 mmol glycosyl acceptor **3**. ^[b] Yields of isolated products. ^[c] Diastereoselectivity (α : β) was determined by ¹H NMR analysis.

Overall, we have identified that increasing nucleophilicity on phenanthroline facilitates the glycosylation reaction, as well as the critical role of the symmetrical phenanthroline framework in catalyzing glycosylation.

2.3. Reaction scope with phenanthroline catalysis

2.3.1. Stereoselective glycosylation and limitation

Previously, we focused on 4,7-diphenyl-1,10-phenanthroline (**C1**)-catalyzed glycosylation reactions with electron-withdrawing glycosyl bromides, providing α -1,2-*cis* products in good yield with high levels of α -selectivity (Section 2.1).¹²⁶ This **C1** catalyst, however, is not effective at promoting the glycosylation of the highly hindered C4-hydroxyls of D-glucoside and L-rhamnoside acceptors **16** – **18** (Table 9) with electron-donating glycosyl bromide donors. For instance, coupling of **16** with 2,3,4,6-tetra-*O*-benzyl- α -D-glucosyl bromide **2**, under the influence of **C1**, provided disaccharide **7** in 55% yield with moderate α -selectivity (α : β = 7:1, entry 1).¹²⁶ This result suggests that the S_N1-S_N2 reaction paradigm is slightly shifted in the presence of the hindered alcohol **16**. The use of DTBMP as an acid scavenger led to a slight increase in yield (55%→71%) and α -selectivity (7:1→ 10:1) in favor of α -1,2-*cis* glycoside **7**. The use of **C14** as the catalyst maintained the yield and diastereoselectivity (entry 1). Although the α / β selectivity of the resulting disaccharide **7** was determined by the standard ¹H NMR analysis, it can be challenging due to the overlap of the anomeric protons with the benzyl protons. This issue was overcome by introducing the 4-fluorobenzyl group onto C6 of glucoside acceptor **17**, wherein the α / β selectivity of the resulting disaccharide **22** was determined using ¹⁹F NMR (entry 2).¹³⁵ The ArF-resonance of α -isomer **22** appeared at δ_F = -115.07 ppm while β -isomer counterpart appeared at δ_F = -114.49 ppm. The diastereoselectivity of product **22** through coupling of **17** with glucosyl bromide **2** was significantly improved using **C14** catalyst (10:1 → 20:1, entry 2). Notably, when we coupled galactosyl bromide **13** to C4-hydroxyl nucleophile **17** under the influence of both **C1** and **C14** catalysts, the yield of the coupling product **23** increased while α -selectivity remained excellent compared to glucosyl bromide **2** (entry 3). Again, the **C14** catalyst is more α -selective than the **C1** catalyst.

Table 9. Stereoselective glycosylation using **C1** and **C14** catalyst ^[a]

entry	Donors	Acceptors	Products	C1 Catalyst	C14 Catalyst
1				IBO , 50 °C ^b 55% (α:β = 7:1) DTBMP , 50 °C ^b 71% (α:β = 10:1)	DTBMP , 50 °C ^b 54% (α:β = 10:1)
		16 : R = Bn; 17 : R = 4-F-Bn	7 : R = Bn		
2		17	22 : R = 4-F-Bn	DTBMP , 50 °C ^b 79% (α:β = 10:1)	DTBMP , 50 °C ^b 72% (α:β = 20:1)
3		17		DTBMP , 50 °C ^b 92% (α:β = 11:1)	DTBMP , 50 °C ^b 90% (α:β = 13:1)
		13	23 : R = 4-F-Bn		
4				IBO , 50 °C ^c 58% (α:β = 4:1) DTBMP , 25 °C ^c 37% (α:β = 5:1)	DTBMP , 25 °C ^c 46% (α:β = 12:1)
		14	18		
5				IBO , 25 °C ^b 80% (α:β = 6:1) DTBMP , 25 °C ^b 85% (α:β = 6:1)	DTBMP , 25 °C ^b 99% (α:β = 11:1)
		19	12		
6		20 (R = Bn)			DTBMP , 25 °C ^{b,f} 90% (α:β = 8:1)
		20 (R = Bn)	6 (R = Bn)		
7		21 (R = Bz)			DTBMP , 25 °C ^{b,f} 88% (α:β = 16:1)
		21 (R = Bz)	25 (R = Bz)		
8		16		IBO , 50 °C ^c 11% (α:β = 5:1) DTBMP , 50 °C ^c 17% (α:β = 17:1)	DTBMP , 50 °C ^c 27% (α:β > 20:1)
		15	26		

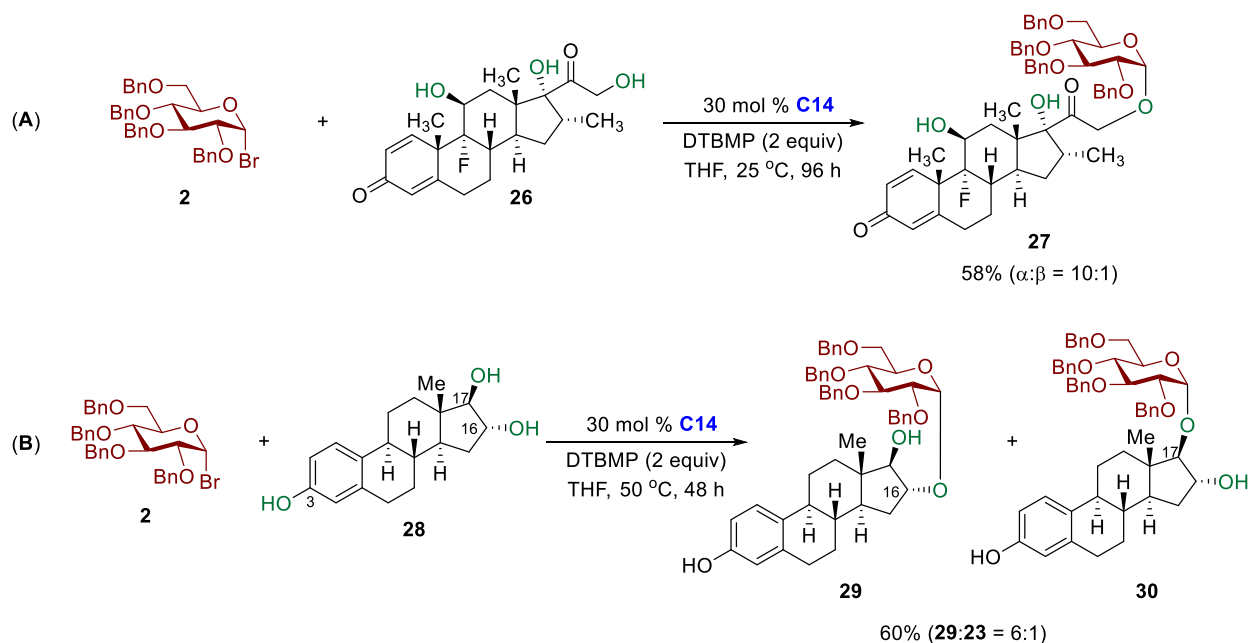
^[a] All reactions were conducted with glycosyl bromide (0.2 mmol) and glycosyl acceptor (0.1 mmol) in MTBE (0.5 M). ^[b] Reaction complete at 24 h. ^[c] Reaction was allowed to stir for 48 h. ^[d] Yields of isolated products. ^[e] Diastereoselectivity (α:β) was determined either by ¹H or ¹⁹F NMR analysis. ^[f] Reaction was run in CH₂Cl₂.

Next, we examined the glycosylation of challenging C4-hydroxyl rhamnose acceptor **18** with L-fucosyl bromide **14** (Table 9, entry 4). Under the influence of **C1** catalysts, the coupling product **24** (entry 4) was obtained in moderate α -selectivity ($\alpha:\beta = 5:1$). The diastereoselectivity of disaccharide **24** significantly improved ($5:1 \rightarrow 12:1$) with the use of **C14** catalyst. An important consequence of **C14** catalyst is its effectiveness with many different coupling partners. For example, **C1**-catalyzed glycosylation of serine residue **19** with fucosyl bromide **14** provided glycoconjugate **12** with moderate α -selectivity ($\alpha:\beta = 6:1$, entry 5). In contrast, the use of **C14** in the analogous reaction substantially increased in selectivity from 6:1 to 11:1 in favor of α -1,2-*cis* glycoside **12**. We also noted that **C14** catalyst is more selective with electron-withdrawing acceptor **21** ($\alpha:\beta = 16:1$, entry 7) than with electron-donating acceptor **20** ($\alpha:\beta = 8:1$, entry 6). We rationalized that the less reactive nucleophile **21** allows the equilibrium of the reactive glycosyl intermediates shifts toward β -glycosyl phenanthrolium ion, further enhancing the diastereoselectivity of the final product **25**. Unfortunately, the phenanthroline system proved to be less robust with the combination of highly unreactive donor **15** and highly hindered C4-hydroxyl acceptor **16** (entry 8). Although **C14** was found more efficient to promote the coupling of **16** with **15** than that of **C1**, the glycosylated product **26** was isolated in only 27% yield, albeit with excellent levels of α -selectivity ($\alpha:\beta > 20:1$).

2.3.2. Site-selective glycosylation

Next, we sought to evaluate the performance of functionally complex nucleophiles under **C14**-catalyzed site-selective reaction (Scheme 32). Dexamethasone **26**, bearing a variety of functional groups and three hydroxyls, is an anti-inflammatory and immunosuppressive corticosteroid that has been used as the drug to treat severe COVID-19 patients.¹³⁶⁻¹³⁷ Although there are three potential coupling sites in dexamethasone **26**, we hypothesized that a primary hydroxyl would be the preferred site. As expected, a 58% yield of the coupling product **27** was obtained with high α -diastereoselectivity ($\alpha:\beta = 10:1$) and complete site-selectivity (Scheme 32A) when **C14** was applied to the glycosylation of **26** with glucosyl bromide **2**. Estriol **28**, bearing three hydroxyl groups at the C3, C16, and C17 positions, was then evaluated to furnish a 6:1 mixture of regioisomers **29** and **30** (Scheme 32B) in 60% yield with almost

exclusive α -selectivity. In this reaction, the C16-hydroxyl is the preferred site for glycosylation forming **29** as a major product while the more hindered C17-hydroxyl site afforded minor product **30**. Importantly, the glycosylation at the C3-phenol site was not observed in the reaction, suggesting that an alkyl hydroxyl can be site-selectively coupled in the presence of a phenol nucleophile. These results demonstrate the applicability of **C14** catalyst in the site-selective α -1,2-*cis* glycosylation to afford synthetically useful yields of complex carbohydrates.



Scheme 32. **C14**-catalyzed site-selective coupling of functionally diverse substrates

2.3.3. Chemoselective glycosylation

In typical approaches to the synthesis of oligosaccharides, a glycosyl electrophile is glycosylated with a nucleophile in the presence of external reagents or catalysts, and the resulting disaccharide then undergoes additional steps for selective anomeric deprotection followed by installation of an anomeric latent leaving group after each glycosylation. In principle, the **C14**-controlled approach could streamline the needs for anomeric deprotection and protecting group manipulations. We envisioned that a glycosyl bromide is activated by **C14** catalyst and subsequently coupled to a carbohydrate acceptor incorporated with an alkyl hydroxyl as well as an unprotected C1-hemiacetal functionality. Ideally, the primary or secondary alkyl

hydroxyl is chemoselectively glycosylated in the presence of the C1-hydroxyl to generate the hemiacetal-terminated disaccharide, which can be directly converted into a glycosyl donor or is directly used as a glycosyl donor for another coupling iteration to selectively furnish the corresponding oligosaccharide. The key issue of glycosylation chemoselectivity relies on the nucleophilic difference between the alkyl hydroxyls and the C1-hydroxyl within the carbohydrate acceptor itself. Due to the inductive effect of the pyranose ring oxygen, we hypothesized that an alkyl hydroxyl is likely to be more nucleophilic than a C1-hydroxyl functionality. The influence of donor reactivity in chemoselective glycosylation reactions has been well-documented.¹³⁸ In contrast, our chemoselective strategy focuses on the effect of acceptor nucleophilicity, which has been underdeveloped.¹³⁹ Although the chemoselective coupling of an alkyl hydroxyl in the presence of a free C1-hydroxyl within a carbohydrate acceptor has been reported using dehydrative glycosylation method,¹⁴⁰ the process is neither catalytic nor diastereoselective.

We aimed to address these limitations by examining the efficacy of the **C14** catalyst to promote both stereo- and chemoselective coupling of carbohydrate diol acceptors. Furthermore, the concept of chemoselectivity can only be realized under conditions that do not promote oligomerization of the carbohydrate diol acceptor. To validate the critical questions of stereo- and chemoselectivity, a coupling of 1,6-diol acceptor **32** with glycosyl bromide **2** was examined under the influence of **C14** catalyst (Table 10, entry 1). We selected diol **32** to test the feasibility of the chemoselective concept because it incorporates a relatively unhindered C6-hydroxyl as the preferred site for glycosylation. In addition, the aryl fluorine helps to determine the chemoselectivity and diastereoselectivity of the final product via ¹⁹F NMR. Under optimal **C14**-catalyzed conditions, the desired hemiacetal-terminated disaccharide **34** was obtained in 63% yield with excellent diastereoselectivity ($\alpha:\beta = 11:1$) and complete chemoselectivity (entry 1). Importantly, self-coupling of diol acceptor **32** to form 1,1'-linked disaccharide was not observed in the reaction. We next examined fluorinated diol acceptor **32** in glycosylation with glycosyl bromide donors **31** and **14** (entries 2 and 3), the yields and α -diastereoselectivities of these reactions were excellent (80%, $\alpha:\beta \geq 20:1$). Notably, these reactions proceeded with complete chemoselectivity.

Table 10. C14-catalyzed chemoselective glycosylation^[a]

entry	Donors	Acceptors	Products	yield ^c ($\alpha:\beta$) ^d
1	2	32	34	63% ($\alpha:\beta = 11:1$)
2	31	32	35	80% ($\alpha:\beta = 20:1$)
3	14	32	36	80% ($\alpha:\beta > 20:1$)
4	1	33	37	70% ^b ($\alpha:\beta = 11:1$)

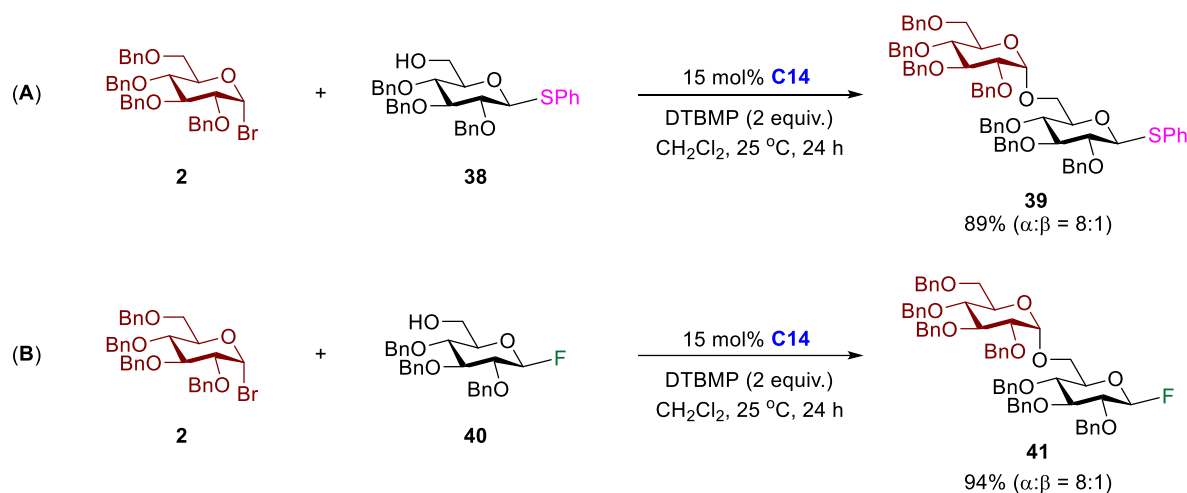
^[a] All reactions were conducted with glycosyl bromide (0.1 mmol) and diol acceptor (0.15 mmol) in MTBE (0.5 M). ^[b] Reaction were conducted with 0.3 mmol diol acceptor. ^[c] Yields of isolated products. ^[d] Diastereoselectivity ($\alpha:\beta$) was determined either by ¹H or ¹⁹F NMR analysis.

Having demonstrated that the **C14**-catalyzed stereo- and chemoselective couplings of primary alcohols within carbohydrate acceptors in the presence of free C1-hydroxyls, this chemistry was further explored with secondary alcohol within carbohydrate acceptor **33** (Table 10, entries 4). The diol **33** incorporates a highly hindered C4-hydroxyl as the preferred site for the coupling to take place. To our excitement, coupling of diol acceptor **33** with electron-withdrawing glycosyl bromide **1** (entry 4) also proceeded with complete chemoselectivity to afford the corresponding 1,4-linked disaccharide **37** in 70% yield with high levels of

diastereoselectivity ($\alpha:\beta = 11:1$). More importantly, self-coupling of 1,4-diol acceptor **33** to form 1,1-linked disaccharide was also not observed in the reactions. Overall, these results demonstrate that the **C14** catalyst effectively promotes the stereo- and chemoselective coupling of an alkyl hydroxyl in the presence of a free C1-hydroxyl functionality within a carbohydrate acceptor.

2.3.4. Orthogonal glycosylation

The concept of orthogonal glycosylation reaction focuses on the relative reactivities of glycosyl donors, which can be modulated by protecting groups and anomeric latent leaving groups. Successful glycosylation requires the anomeric leaving group of each carbohydrate coupling partner to be chemically distinct and activated by different reagents.¹⁴¹⁻¹⁴³ The orthogonal glycosylation strategy streamlines the need for anomeric derivatization steps as the coupling products are directly used as glycosyl donors for subsequent glycosylation. In addition, it has been illustrated to provide solutions for the synthesis of complex oligosaccharides.¹⁴¹⁻¹⁴³ However, subtle changes to the structures of carbohydrate coupling partners and protecting groups could impact glycosylation selectivity and reactivity. In addition, the process is not catalytic. We sought to assess the efficiency of **C14** catalyst to promote the couplings of carbohydrate coupling partners possessing chemically distinct anomeric leaving groups. Thioglycoside **38** and glycosyl bromide **2** was used in the first combination (Scheme 33A) as their anomeric leaving groups can be activated by different sets of external reagent and catalyst. The **C14** catalyzed orthogonal reaction was evaluated under optimized standard conditions with the use of dichloromethane as a solvent because thioglycoside **38** was partially soluble in MTBE. The disaccharide product **39** (Scheme 33A) was obtained in 89% yield with good α -selectivity ($\alpha:\beta = 8:1$). Similarly, the combination of glycosyl fluoride **40** and glycosyl bromide **2** under the influence of **C14** catalyst provided disaccharide **41** (Scheme 33B) in good yield and diastereoselectivity.



Scheme 33. C14-catalyzed orthogonal glycosylation

2.4. Summary

Several trends were obtained from this phenanthroline catalysis: (1) while reactions with α -glycosyl bromide donors containing the electron-withdrawing groups require to be conducted at 50 °C, their electron-donating counterparts can proceed at 25 °C; (2) reactions with primary alcohols proceeds faster than sterically hindered secondary alcohols. Furthermore, while primary alcohols could couple to reactive glycosyl donors at 25 °C, the sterically hindered secondary alcohol needs to proceed at 50 °C for the coupling to occur; (3) phenanthroline derived catalysts are more efficient compared to pyridine derived catalysts, and (4) C4- and C7-heterocyclic nitrogen substituted phenanthroline catalysts increase the reaction reactivity and improve diastereomeric outcome.

Limitations of the phenanthroline catalysis on coupling of highly unreactive glycosyl bromide and sterically hindered C4-hydroxyl acceptors was overcome by introducing piperidine substituents on the C4- and C7 position on the phenanthroline. The utility of this phenanthroline catalysis is expanded to sterically hindered hydroxyl nucleophiles and chemoselective coupling of an alkyl hydroxyl group in the presence of free C1-hemiacetal functionality. The phenanthroline-based catalyst also has a pronounced effect on site-selective couplings of triol motifs and orthogonally activates the anomeric bromide leaving group over the fluoride and sulfide counterparts.

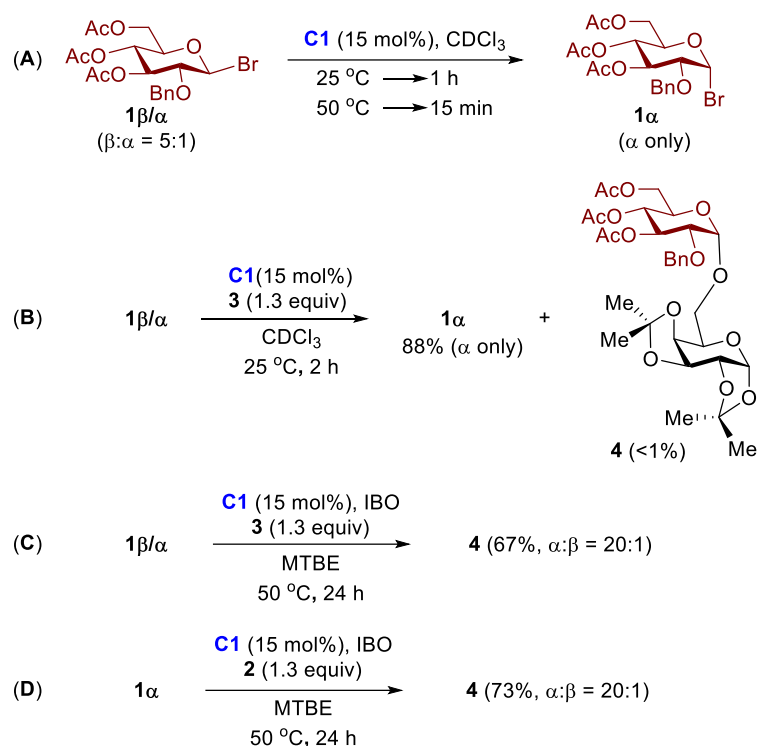
CHAPTER 3: MECHANISM OF PHENANTHROLINE-CATALYZED 1,2- *CIS* PYRANOSYLATION

Phenanthroline has been utilized extensively as a powerful ligand for metals and a binding agent for DNA/RNA.¹⁴⁴⁻¹⁴⁵ However, there was no report on the use of phenanthroline as a nucleophilic catalyst in organic reactions or stereoselective glycosylation until our recent discovery.¹²⁶ Our initial proposed mechanism evolved from a basic principle: two pyridine nitrogen atoms are positioned to act cooperatively (Scheme 31, Chapter 2). The first nitrogen atom acts as a catalytic nucleophile to displace the C1-anomeric bromide leaving group of a glycosyl donor, via an S_N2-like pathway, to generate an equatorial (β) phenanthroline ion intermediate preferentially to avoid the steric interactions associated with positioning that group in the axial (α) orientation. The second nitrogen atom could interact with carbohydrate moiety to further stabilize the phenanthroline ion intermediate. Subsequent S_N2-like substitution by a hydroxyl nucleophile leads to the formation of α -1,2-*cis* glycosides.

3.1. β -Glycosyl bromide driven glycosylation?

The preferential formation of α -glucosides from α -glucosyl bromide in the presence of added bromide ion (Bu₄NBr) was first described by Lemieux and attributed to the enhanced reactivity of the higher energy β -glycosyl bromide.⁸⁴ As such, we evaluated if the stereochemistry of the α -1,2-*cis* product would be dictated by the configuration of glycosyl bromide at the anomeric carbon.¹²⁶ Because it is difficult to obtain β -isomer of glycosyl bromide in a pure form, a 5:1 mixture of β - and α -isomers of glycosyl bromide **1 β / α** with β -isomer being a major diastereomer was used as a model substrate (Scheme 34).¹²⁶ We observed that a 5:1 β / α mixture of starting material **1 β / α** slowly anomerized to the corresponding a 2:1 α / β mixture in the absence of the phenanthroline catalyst after 24 h. However, a 5:1 β / α mixture **1 β / α** converted exclusively to the corresponding α -isomer **1 α** in the presence of 15 mol% of **C1** catalyst within 1 h at 25 °C (Scheme 34A). We also performed the reaction of a 5:1 β / α mixture **1 β / α** with galactoside acceptor **3** under the influence of **C1** catalyst at 25 °C. We observed isomerization of this 5:1 β / α mixture to α -isomer

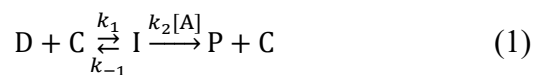
1 α is faster than formation of the coupling product **4** at 25 °C (Scheme 34B). On the other hand, coupling of **3** with this 5:1 β/α mixture **1 β/α** under standard **C1**-catalyzed conditions provided **4** (Scheme 34C) in comparable yield and α -selectivity to that obtained with α -isomer **1 α** (Scheme 34D). Collectively, these results suggest that β -isomer of glycosyl bromide is not the reacting partner in the phenanthroline-catalyzed reaction. This catalysis, which derives its α -stereoselectivity from the highly reactive β -covalent phenanthrolium ion intermediate, is different from the Lemieux system.⁸⁴



Scheme 34. Effect of the configuration of glycosyl bromide

3.2. Double $\text{S}_{\text{N}}2$ mechanism? (Kinetic study)

To further verify the glycosylation reaction undergoes double $\text{S}_{\text{N}}2$ -like mechanism, we conducted kinetic investigation based on the mechanism outlined for phenanthroline-catalyzed glycosylation in Scheme 31 (Chapter 2), the overall reaction can be described as equation (1), wherein k_1 and k_{-1} defined the pre-equilibrium in the first nucleophilic substitution between the reactants, glycosyl bromide donor (D) and catalyst (C), and the intermediate (I). An irreversible nucleophilic attack (k_2) by a hydroxyl acceptor (A) then leads to formation of the coupling product (P) and regeneration of catalyst.



Applying steady-state approximation, the rate of product formation can be derived as equation (2).

$$\frac{d[P]}{dt} = \frac{k_1 k_2 [D][A][C]_0}{k_{-1} + k_1 [D] + k_2 [A]} \quad (2)$$

For fixed donor and acceptor concentration, the rate of product formation in respect to catalyst concentration is simplified in equation (3):

$$\frac{d[P]}{dt} = k' [C]_0 \quad (3)$$

where $k' = \frac{k_1 k_2 [D][A]}{k_{-1} + k_1 [D] + k_2 [A]}$.

For fixed donor and catalyst concentration, the rate of product formation in respect to acceptor concentration is illustrated in equation (4):

$$\frac{d[P]}{dt} = \frac{k_a [A]}{k_b + k_2 [A]} \quad (4)$$

where $k_a = k_1 k_2 [D][C]_0$, and $k_b = k_{-1} + k_1 [D]$.

In the end, for fixed acceptor and catalyst concentration, the rate of product formation in respect to donor concentration is shown in equation (5):

$$\frac{d[P]}{dt} = \frac{k_c [D]}{k_d + k_1 [D]} \quad (5)$$

where $k_c = k_1 k_2 [A][C]_0$, and $k_d = k_{-1} + k_2 [A]$.

The kinetic studies were conducted at 50 °C, using C₆D₆ as the reaction solvent and toluene as a quantitative internal standard, with 3,4,6-tri-acetyl-2-*O*-benzyl- α -glucopyranosyl bromide (**1**) and 2-propanol (**1A**) as coupling partners in the presence of IBO and **C1**. The product (**1P**) formation was monitored by ¹H NMR over the course of 60 h. The rates of reaction were then plotted as functions of the concentration of **C1** (Figure 15a) and 2-propanol (Figure 15b).

Overall, the rate of the reaction is both catalyst- and acceptor-dependent. At fixed donor and acceptor concentration (Figure 15a), a linear correlation was observed in the plot of rate vs catalyst concentration, which was predicted by equation (3). On the other hand, a biphasic kinetic was observed from the plot of rate vs acceptor concentration (Figure 15b). This biphasic kinetic suggests a shift in the rate-determining step (RDS) at different concentrations of 2-propanol. At high concentration of 2-propanol, the RDS is formation of the phenanthrolium ion (first step in Scheme 31), and is further supported by the linear dependence of rate on catalyst concentration (Figure 15a). At low concentration of 2-propanol, nucleophilic attack (second step in Scheme 31) is the RDS. The biphasic kinetic is also predicted by equation (4).

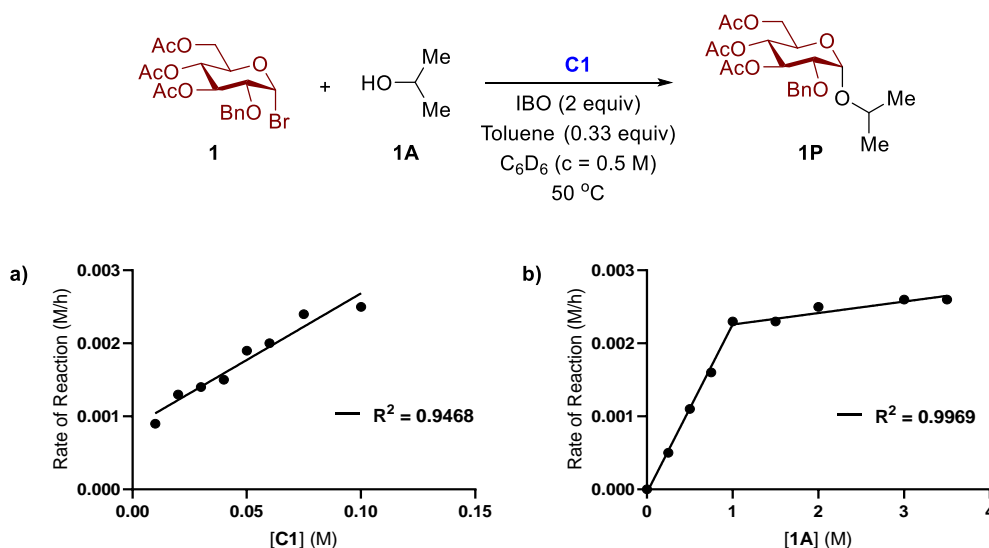


Figure 15. Kinetics of the reaction of 2-propanol with glucosyl bromide **1** in C_6D_6 at 50 °C: (a) Initial rate of reaction vs **C1**; reaction condition: glucosyl bromide **1** (0.5 M), 2-propanol (1.5 M), IBO (1 M), catalyst **C1** (0-20 mol%); (b) Initial rate of reaction vs 2-propanol; reaction condition: glucosyl bromide **1** (0.5 M), 2-propanol (0.25 – 3.5 M), IBO (1 M), catalyst **C1** (15mol%).

However, due to solubility issue, we were not able to conduct the kinetic study with high concentration of glucosyl bromide **1**. In addition, we were not able to lower the glucosyl bromide concentration as the experiment required 60 h to obtain sufficient data under standard **C1**-catalyzed conditions.

To verify the glycosylation is first-order dependent in the concentration of glucosyl bromide, we adapted the optimal reagent system in Table 8, and conducted kinetic experiment at varying glucosyl bromide concentration. To obtain a clear view on the product anomeric region (4.5 – 5.0 ppm) in 1H NMR,

2,3,4,6-tetra-benzyl-d₇-glucopyranosyl bromide **2**^{*} was used as the model electrophile. The kinetic experiments were carried at 25 °C in CD₂Cl₂, with glucosyl bromide **2**^{*} and glycosyl nucleophile **3** as the coupling partners, using phenanthroline **C14** as the catalyst, DTBMP as acid scavenger, and mesitylene as internal standard. As illustrated in Figure 16a, the coupling product concentration appeared linear relationship to time (apparent zero-order kinetics in substrates), and induction period was not observed. In addition, the rate of product formation increases as the concentration of glucosyl bromide **2**^{*} increases. The initial rate of reaction in Figure 16b showed first-order dependence on glucosyl bromide **2**^{*}. Unfortunately, due to limiting amount of **2**^{*}, we were not able to observe the saturation behavior in glucosyl bromide concentration. However, the collective kinetic studies suggest that the phenanthroline catalyzed α -selective glycosylation undergoes associative mechanisms (likely double S_N2).

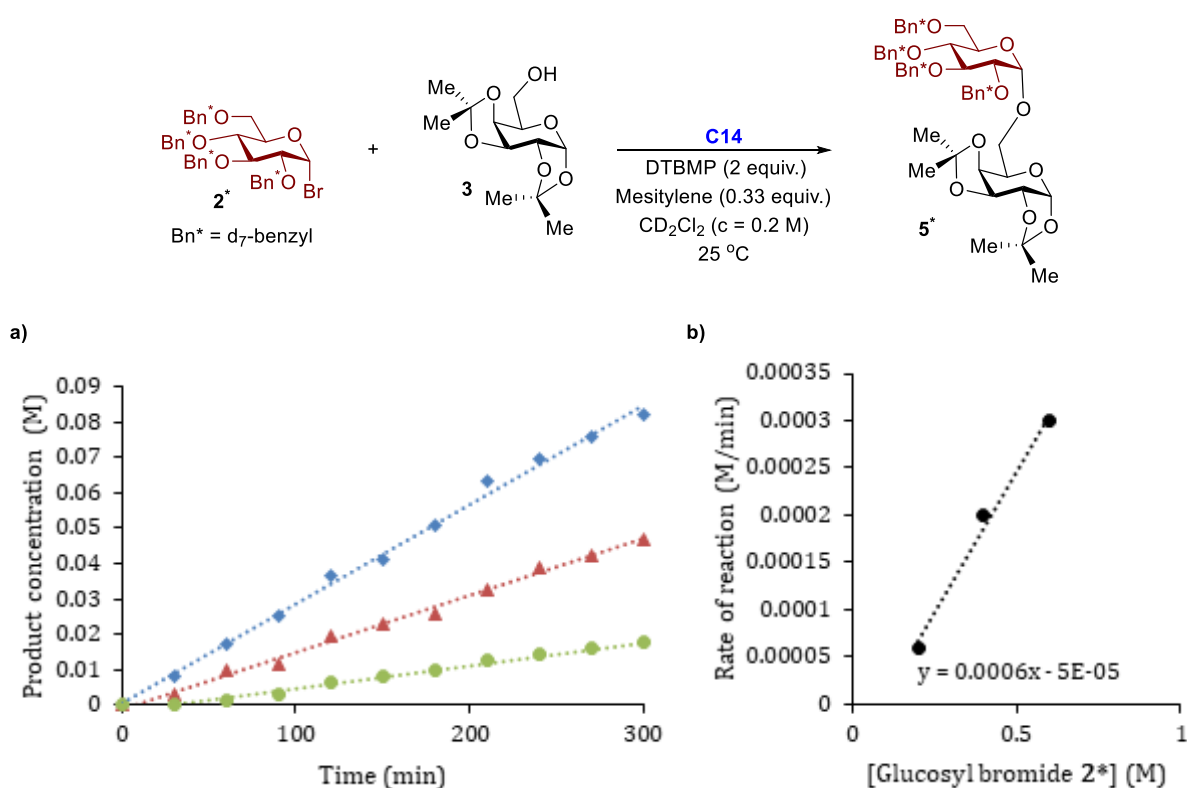


Figure 16. Kinetic study in respect to donor concentration: (a) Product concentration versus time for phenanthroline-catalyzed (**C14**, 0.02M) glycosylation with varying donor concentration: 0.2 M **2**^{*} (●, green), 0.4 M **2**^{*} (▲, red) and 0.6 M **2**^{*} (◆, blue). Reaction conditions: donor **2**^{*} (0.2 – 0.6 M), acceptor **3** (0.2 M), **C14** (0.02 M), DTBMP (0.4 M), CD₂Cl₂ (0.5 mL), 25 °C; (b) the initial rate of reaction is dependent on the concentration of **2**^{*}.

The rates of phenanthroline-catalyzed reactions with different substituents on the phenanthroline framework were also investigated. As illustrated in Figure 17, all three phenanthroline catalysts provide similar rate profile, where the overall rates are apparent zero-order kinetics in substrates and showing no induction period. Due to the electron donating effect of the piperidine substituents, the rate of **C14**-catalyzed glycosylation should be faster than that of **C1** and **C2**. As predicted, the **C14**-catalyzed reaction is more rapid than both **C1**- and **C2**-catalyzed reaction. On the other hand, both **C1** and **C2** showed similar rate, complementary to the observation in Table 8 (Chapter 2).

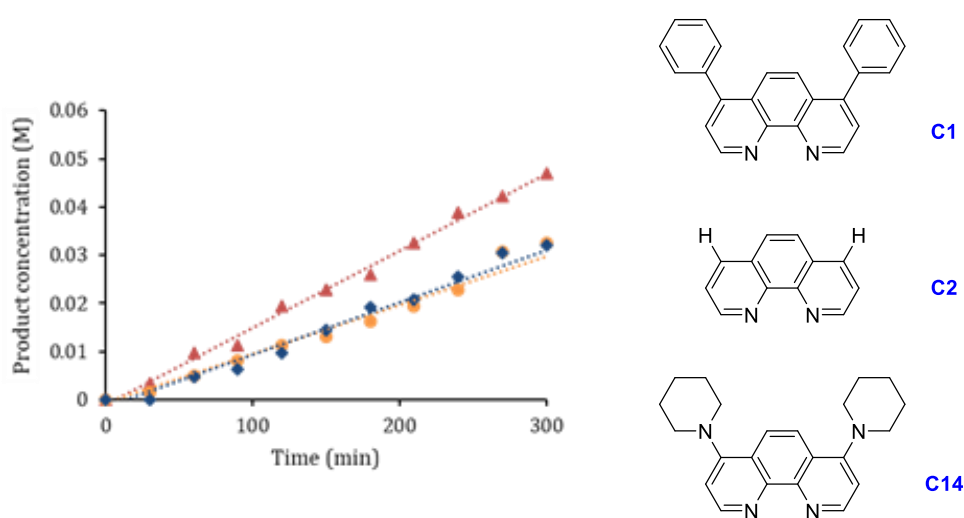


Figure 17. Product concentration versus time for the phenanthroline-catalyzed glycosylation with three different phenanthroline catalysts: **C1** (●, orange), **C2** (◆, dark blue) and **C14** (▲, red). Reaction condition: **2*** (0.4 M), **3** (0.2 M), catalyst (0.02 M), DTBMP (0.4 M), CD₂Cl₂ (0.5 mL), 25 °C

3.3. Detection of pyranosyl phenanthrolium ion intermediates

For the phenanthroline-catalyzed glycosylation to yield α -1,2-*cis* product, the catalyst must associate with either or both substrates in the reaction. In our proposed mechanism (Scheme 31), phenanthroline displaces the bromide leaving group to form a glycosyl phenanthrolium ion intermediate. Unlike sugars, phenanthroline is a rigid and planar organic compound with a C₂ symmetry. However, if phenanthroline is coupled with a sugar molecule, the symmetry will be destroyed. As a result, our first objective was to perform ¹H NMR study to observe the symmetry on phenanthroline (Figure 18). To obtain a clear view on the aromatic region in ¹H NMR, 2,3,4,6-tetra-benzyl-d₇-glucopyranosyl bromide **2*** was used as an

electrophile, wherein the chemical shift of anomeric proton (H_1) resonance appeared at $\delta_H = 6.55$ ppm in CD_2Cl_2 (Figure 18a). Piperidine substituted phenanthroline **C14** was chosen for our NMR study because it is the most effective catalyst¹³⁴ compared to other catalysts,¹²⁶ implying formation of the reactive glycosyl intermediates is more favorable. In addition, the chemical shift of the piperidyl substituents would not appear in the aromatic region. To avoid any possible side reaction with by-product of isobutyl oxide (IBO),¹³⁴ di-*tert*-butylmethylpyridine (DTBMP) was chosen as the acid scavenger in the later NMR experiment (Figure 18).

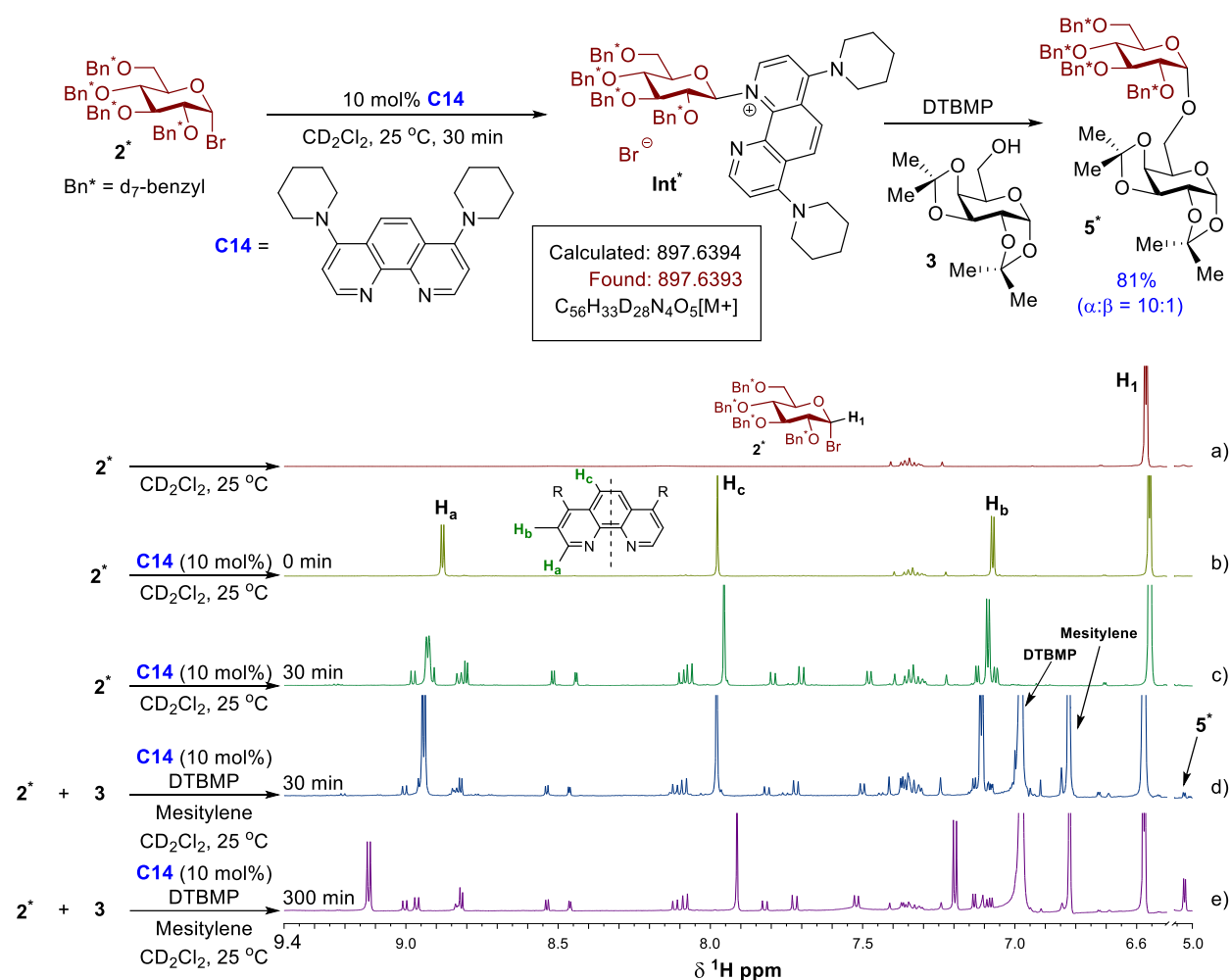


Figure 18. Detection of phenanthroline intermediate by 1H NMR: (a) Deuterated *tetra*-benzyl glucosyl bromide 2^* in CD_2Cl_2 ; (b) 2^* and 10 mol% **C14** at 0 min; (c) 2^* and **C14** at 30 min, new signals emerging around phenanthroline aromatic region; (d) 2^* , **3**, **C14** at 30 min, disaccharide 5^* emerging; and (e) 2^* , **3**, **C14** at 300 min, more disaccharide 5^* formed in the reaction. See Section 5.3.2 for full spectrum.

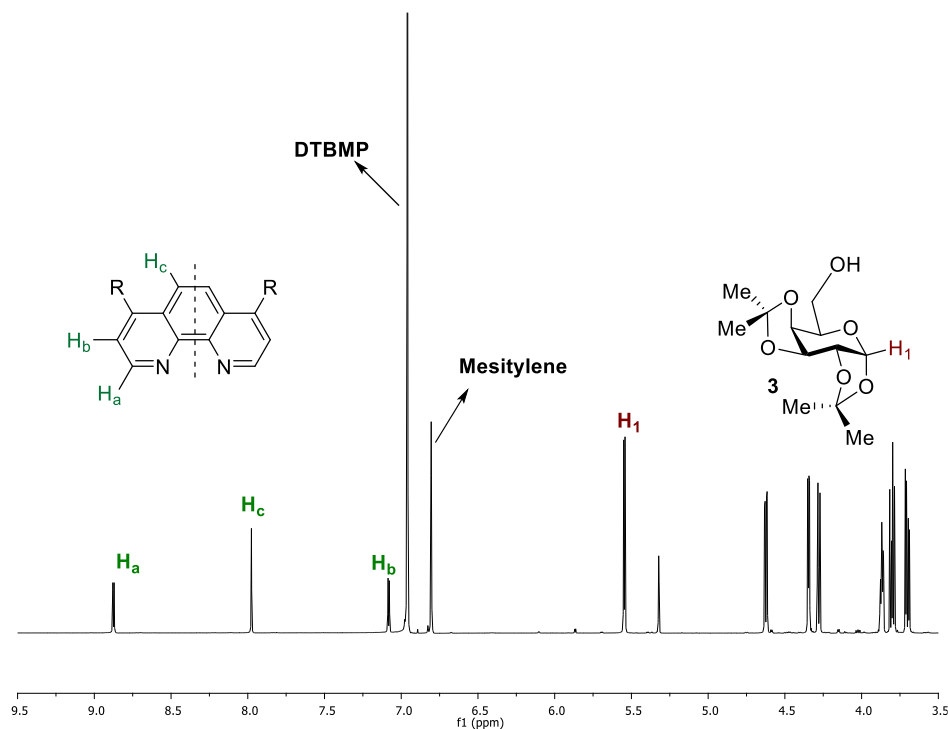


Figure 19. Mixture of nucleophile **3** and 10 mol% **C14** with DTBMP in CD₂Cl₂, and mesitylene as internal standard

Upon addition of 10 mol% of **C14** to the deuterated glycosyl bromide **2**^{*}, three new signals appeared at $\delta_{\text{H}} = 8.88$ ppm (H_a, d, $J = 5.0$ Hz) and $\delta_{\text{H}} = 7.07$ ppm (H_b, d, $J = 5.1$ Hz) and the singlet at $\delta_{\text{H}} = 7.98$ ppm (H_c) represented the symmetry of **C14** catalyst (Figure 18b). Within 30 min, new signals emerged around the phenanthroline region (Figure 18c). These new signals were not detected in the mixture of nucleophile **3** and **C14** (Figure 19). An aliquot of the reaction mixture was subjected to electrospray ionization (ESI) mass spectrometry and returned m/z ratio of 897.6393 (Figure 46), confirming the presence of the intermediate **Int**^{*} (Figure 18) which resembled a phenanthrolium ion. Hydroxyl nucleophile **3** was subsequently added to the reaction mixture along with DTBMP and mesitylene (internal standard). After 30 min, new signals still surrounded the aromatic region (Figure 18d) along with the appearance of the disaccharide product whose anomeric proton appeared at $\delta_{\text{H}} = 5.03$ ppm (d, $J = 3.6$ Hz, Figure 18d). At 5 h, more product was formed and the new peaks remained at the aromatic region (Figure 18e). The reaction mixture was allowed to stir overnight at 25 °C. The product **5**^{*} was isolated in comparable yield (80%) and selectivity ($\alpha:\beta = 10:1$) to that of disaccharide **5** (Table 8, entry 4). Several key observations were obtained

from this NMR experiment: (1) the new signals appeared to be doublets, indicating the newly-formed phenanthroline species did not maintain their symmetry; (2) the number of signals suggests that there are two possible phenanthroline species (**Int₁** and **Int₂**) present in the solution (Figure 20); (3) the population of unbound phenanthroline **C14** and the two phenanthroline species (**Int₁** and **Int₂**) shifted from 76:14:10 (**C14**: **Int₁**: **Int₂**) to 81:12:7 upon addition of alcohol **2**, suggesting the equilibrium of the catalyst states had shifted toward regeneration of **C14**, likely through formation of the coupling product; and (4) the integration of the signals suggested that an extra hydrogen atom appeared on the phenanthroline aromatic region for each newly-formed species, which was subsequently identified as a C1-proton of the sugar unit (Figure 20).

To further identify the presence of the two newly-formed species upon mixing deuterated glycosyl bromide **2*** with **C14**, a 1:1 stoichiometry ratio of **2*** and **C14** catalyst was employed. As the concentration of **C14** increased, the equilibrium shifted toward the two new intermediates, wherein the population of unbound **C14** catalyst, **Int₁** and **Int₂** became 55%, 30%, and 15%, respectively (see Section 5.3.2 for ¹H

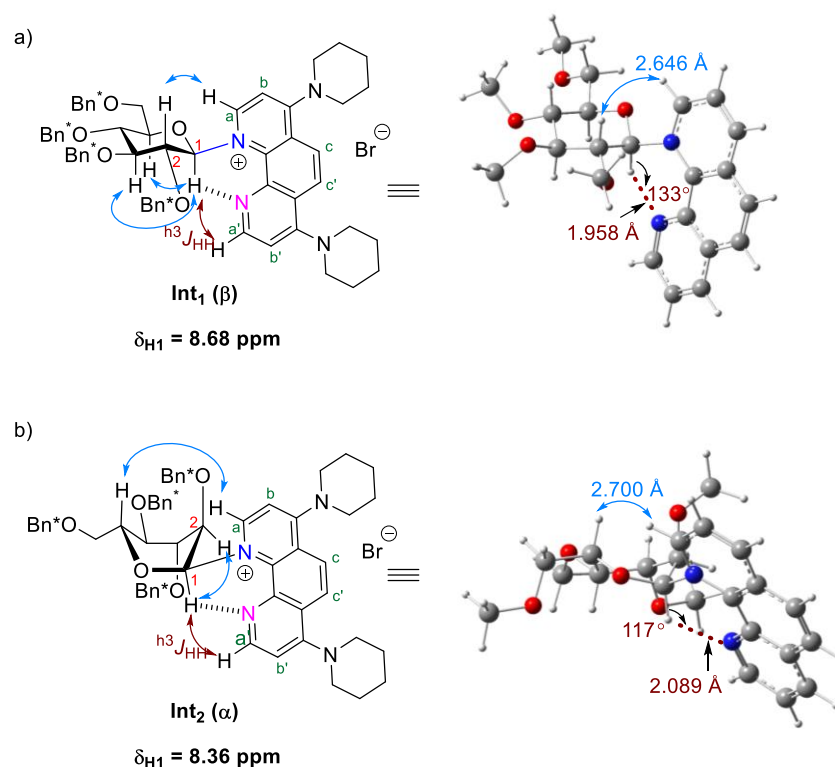


Figure 20. Conformation of the glycosyl phenanthroline ion intermediates: 1H-1H 2D COSY (red) and ROESY (blue) NMR evidence as well as DFT calculation structures.

NMR spectra). Variable temperature ^1H , ^1H - ^1H 2D COSY and ROESY NMR spectra at 0 °C were subsequently obtained. density functional theory (DFT) calculations were employed to assist the deconvolution of these intermediates. The geometries of possible intermediates' structures were optimized and vibrational frequencies were calculated at the B3LYP/6-31+G(d,p) level¹⁴⁶⁻¹⁵⁶ with the SMD implicit solvent model¹⁵⁷ and the GD3BJ empirical dispersion correction¹⁵⁸⁻¹⁵⁹. All calculations were carried out with Gaussian 09.¹⁶⁰ In our DFT calculations, tetramethyl glucosyl bromide was used as a model electrophile to reduce computational cost (Figure 20). The DFT calculation results are consistent with our NMR data.

Employing 2D COSY NMR, the newly formed protons in the phenanthroline aromatic region resided at $\delta_{\text{H}} = 8.68$ ppm (d, $J = 8.1$ Hz) and $\delta_{\text{H}} = 8.36$ ppm (d, $J = 3.6$ Hz) were identified to be the C1 protons of the anomeric mixture of **Int**₁ (β) and **Int**₂ (α), in a ratio of 2:1 (β : α) (Figure 20 and Figure 21c). Suggested

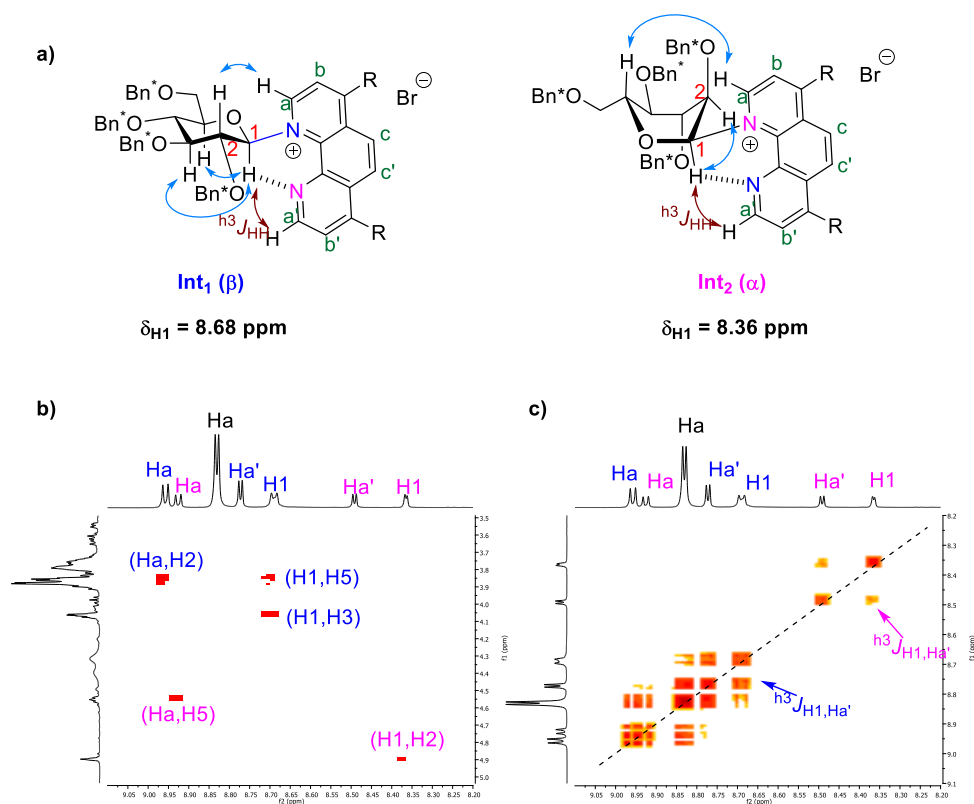


Figure 21. Conformation of glycosyl phenanthrolium intermediates and NMR evidence: (a) Conformation of β - and α -phenanthrolium intermediates; (b) ^1H - ^1H 2D ROESY NMR spectrum; (c) ^1H - ^1H 2D COSY NMR spectrum.

by DFT calculations (Figure 20), while H_a proton on the phenanthroline is spatially closed to the C2 proton for the β -isomer **Int**₁ (2.646 Å), the H_a proton for the α -isomer **Int**₂ is closed to the C5 proton (2.700 Å) on the sugar ring. These spatial interactions were also observed through 2D ROESY NMR (Figure 21b), which consolidate the anomeric configurations for the two detected intermediates. Similar to the glycosyl pyridinium ion,¹⁶¹⁻¹⁶³ the major phenanthroline ion intermediate is a β -configured isomer (**Int**₁) and exists in the ⁴C₁ chair conformation while the minor α -isomer (**Int**₂) exists in the B_{2,5} boat conformation to avoid stereo- and electronic effect from the ring.

3.4. Hydrogen bonding in the pyranosyl phenanthroline ion intermediates

Several NMR evidences were found below to support hydrogen bonding (H-bonding) interaction between the second nitrogen of phenanthroline and the C1 anomeric proton. In general, for H-bonding involving an electronegative acceptor such as oxygen or nitrogen, the donor nucleus experiences a deshielding effect.¹⁶⁴ Conversely, if the C1 anomeric proton is hydrogen bonding to the second nitrogen of phenanthroline, the chemical shift should appear more downfield in the ¹H NMR. It has been reported that the anomeric proton of β -glucosyl pyridinium bromide resonances at $\delta_{\text{H}} = 6.10$ ppm in D₂O.¹⁶⁵ In addition, Gin and coworker established anomeric mixture of glycosyl pyridinium species, wherein the anomeric protons resonance at $\delta_{\text{H}} = 6.63$ and 6.49 ppm in CD₂Cl₂ at -60 °C.¹⁶⁶ However, the ¹H NMR spectra of a 1:1 mixture of glycosyl bromide **2**^{*} and **C14** taken at -60 °C (Figure 22) showed the anomeric protons of the intermediates, **Int**₁ (β) and **Int**₂ (α), resonance at $\delta_{\text{H}} = 8.44$ and 8.18 ppm, respectively. The downfield shift of the anomeric protons of glycosyl phenanthroline ion intermediates compare to that of the reported glycosyl pyridinium species is likely due to an intramolecular hydrogen bonding between the anomeric proton and second nitrogen on phenanthroline.

A more direct hydrogen bonding observation is through hydrogen bond scalar coupling.¹⁶⁴ The scalar interaction arises from electron cloud between nuclei, such as covalent bonds. Upon formation of H-bonding, the redistribution of electron density of the nuclei associate with H-bonding allows us to observe

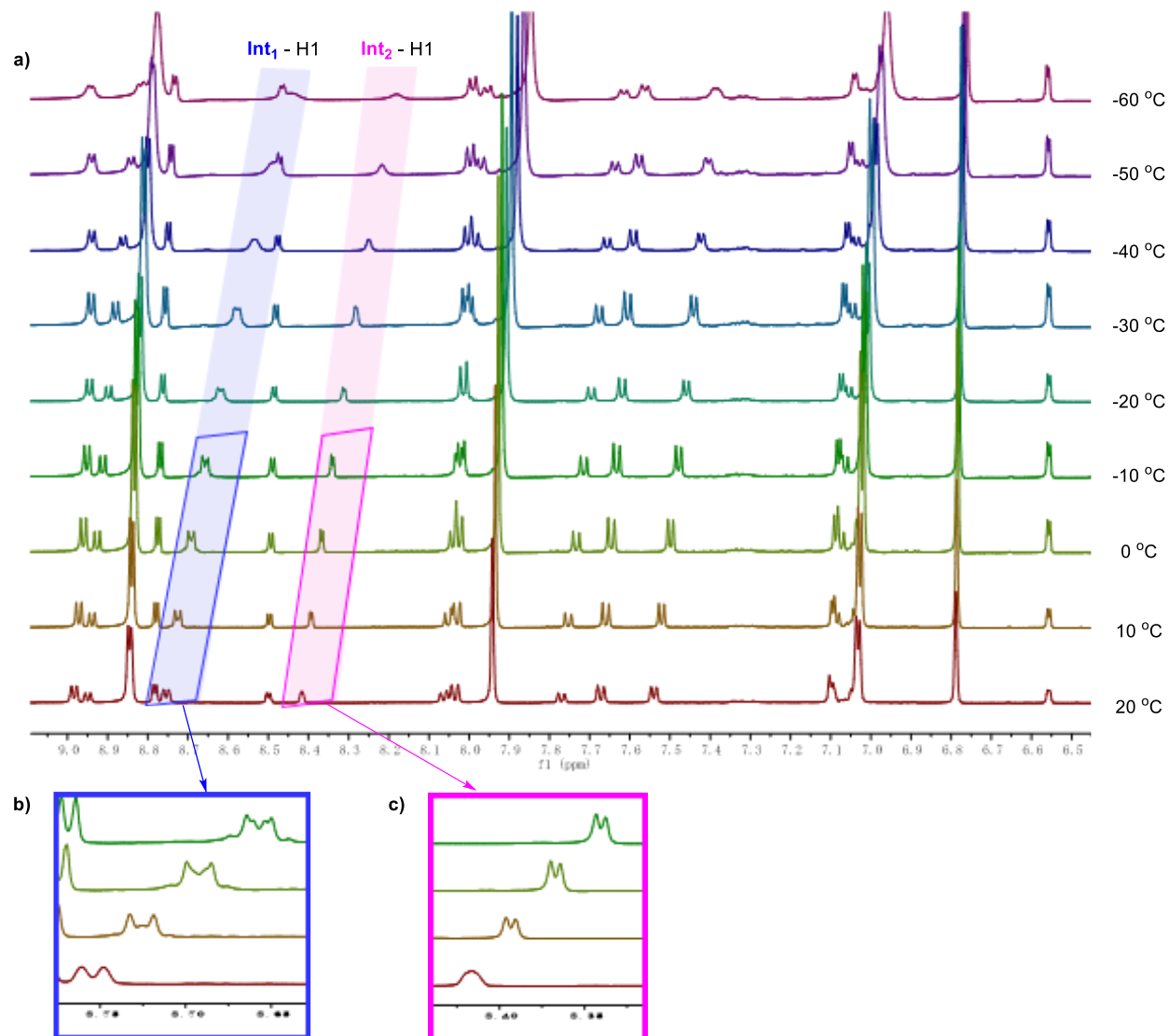


Figure 22. Variable-temperature ¹H NMR spectra and proposed intermediates internal hydrogen bondings: (a) VT-NMR spectra of glucosyl bromide **2*** and **C14** (1 equiv.) in CD₂Cl₂ with mesitylene as internal standard; (b). Zoomed-in spectra of anomeric protons for **Int₁** and (c) **Int₂**.

the scalar coupling using COSY experiment.¹⁶⁴ As shown in Figure 21, scalar couplings (^{h3}J_{HH}) between the anomeric proton and H_{a'} on the phenanthroline were observed for both intermediates **Int₁** and **Int₂**. These scalar interactions mediated by the lone pair electrons on the second pyridine nitrogen of phenanthroline and the conjugated system are evidential for H-bonding between the anomeric proton and the second nitrogen of phenanthroline. In order to obtain a clear view of the hydrogen bond coupling in ¹H NMR, a rigid H-bonding network is required.¹⁶⁷⁻¹⁶⁸ As hydrogen bond formation is highly dependent on

temperature,¹⁶⁹ we cooled the 1:1 mixture of glucosyl bromide **2*** and **C14** in CD₂Cl₂ to -60 °C and gradually warm to room temperature. The ¹H NMR spectra were taken at 10 °C interval and combined (Figure 22a). The ¹H NMR spectrum was at highest resolution at -10 °C. The C1-anomeric proton of **Int₁** (β) showed a defined allylic splitting at -10 °C (Figure 22b). Further, DFT optimized structures (Figure 20) for anomeric mixtures of the phenanthrolium intermediates are consistent with the NMR observation: for **Int₁** (β) the H1–N' distance is 1.958 Å and the C1–H1---N angle is 133°, while those for **Int₂** (α) are 2.089 Å and 117°.

3.5. Proposed mechanism

Based on the NMR study and DFT calculations,¹³⁴ a proposed mechanism for the phenanthroline-catalyzed α-1,2-*cis* glycosylation is illustrated in Figure 3. We hypothesize that the first pyridine nitrogen atom of the phenanthroline catalyst **C14** displaces the anomeric α-bromide leaving group of glycosyl donor to form the β-phenanthrolium ion intermediate. This phenanthrolium ion positions equatorially to avoid the steric and electrostatic interactions. Our recent DFT calculations suggest that formation of the β-covalent phenanthrolium ion intermediate is reversible.¹³⁴ The β-covalent glycosyl intermediate adopts the ⁴C₁ chair conformation and is in equilibrium with the α-glycosyl intermediate whose exists in the B_{2,5} boat conformation. Our NMR study showed that these two key intermediates, a major ⁴C₁ β-phenanthrolium ion conformer (**Int₁**) and a minor B_{2,5} α-phenanthrolium ion conformer (**Int₂**) were formed in the reaction (Figure 20). To obtain high levels of diastereoselectivity, a Curtin-Hammett situation must be established: interconversion of the ⁴C₁ chair-like β-conformer and B_{2,5} boat-like α-conformer via an oxocarbenium ion intermediate is rapid and much faster than the subsequent nucleophilic attack (Figure 23). In the NMR study, these two intermediates were formed and equilibrated within 30 min while the product formation typically required more than 1 h to be observable. To rationalize the diastereoselectivity for the major α-1,2-*cis* product, hydroxyl acceptor preferentially approaches to the α-face of the ⁴C₁ chair conformation of the β-glycosyl phenanthrolium ion intermediate via an S_N2 pathway. This would the

reaction proceeding through a disfavored B_{2,5} boat conformation of the α intermediate, which leads to the minor β -1,2-*trans* product. preclude

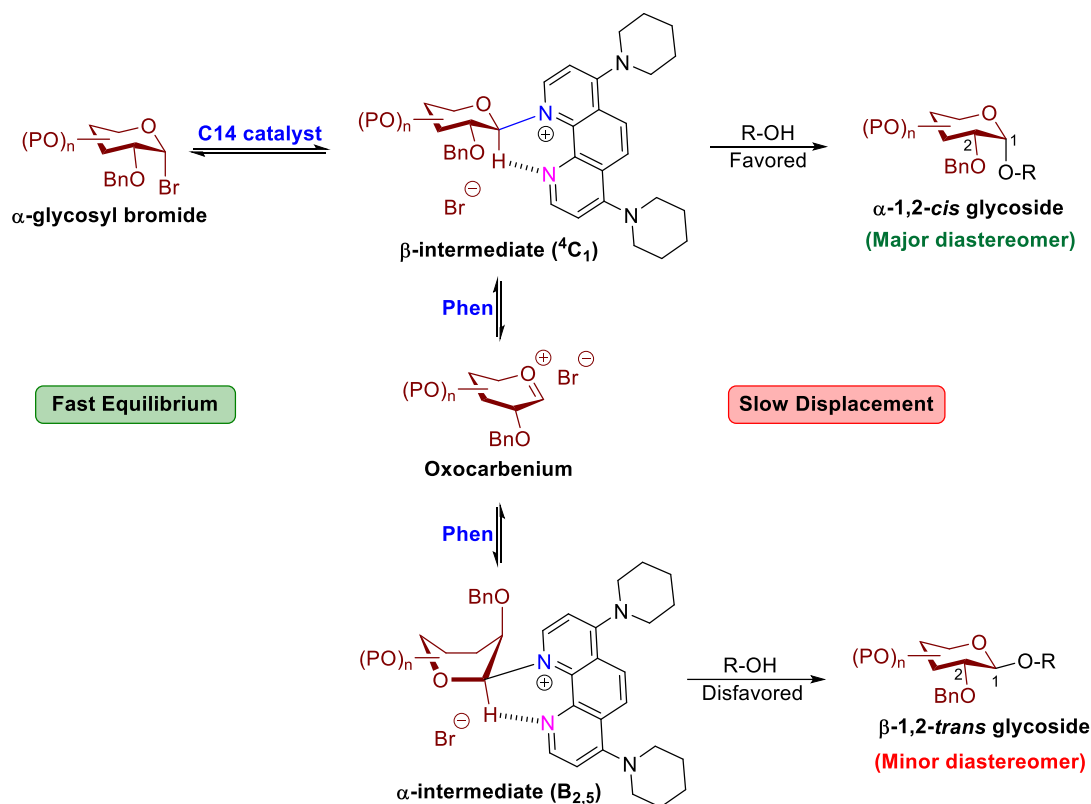


Figure 23. Possible mechanism of phenanthroline-catalyzed glycosylation

To further verify that the 4C_1 chair-like β -glycosyl phenanthrolium is indeed the reactive intermediate, we sought to detect the intermediates for 2-deoxy-2-fluoro glycosyl bromide donor. The highly reactive tribenzyl 2-fluoro galactosyl bromide **31** was chosen as a model electrophile (Figure 24). The transient glycosyl phenanthrolium ion intermediate (**Int₃**) was detected by ${}^1\text{H}$ NMR within several minutes using

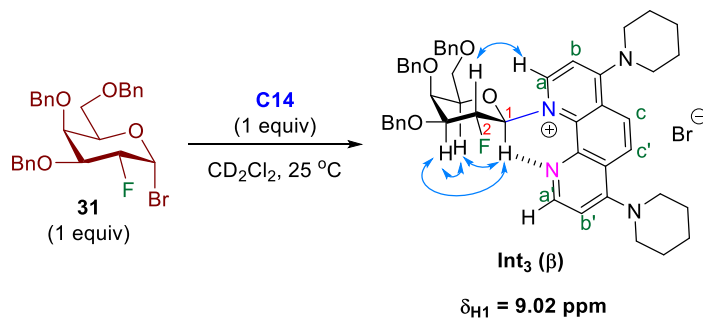


Figure 24. Conformation of the 2-deoxy-2-fluoro glycosyl phenanthrolium ion and ROESY (blue) NMR evidence (see Section 5.3.2 for full spectrum).

a 1:1 mixture of 2-fluoro glycosyl bromide **31** and **C14** catalyst at 25 °C. Importantly, only the β -glycosyl phenanthrolium ion intermediate **Int₃** (Figure 24) existing in the 4C_1 chair conformation was observed. In addition, more than 90% of **31** were converted to the **Int₃** intermediate within 2 h. Unlike the tetrabenzyl glycosyl bromide donor **2***, which produces highly interconvertible intermediates (**Int₁** and **Int₂**, Figure 20), the 2-fluoro galactosyl bromide **31** generates a more stable intermediate (**Int₃**), which results in either formation of the products or reverts to the reactant **31**. This observation was further supported by DFT calculations.¹³⁴

3.6. Conclusion

A systematic mechanistic investigation of the 4,7-dipiperidine substituted phenanthroline **C14** catalyzed-stereoselective α -1,2-cis glycosylation reaction with α -glycosyl bromide donor was performed employing variable temperature NMR (1H , COSY, and ROESY) experiments. In this respect, NMR studies have showed that activation of deuterated tetrabenzyl glucosyl bromide with **C14** catalyst can readily form the two phenanthrolium ion intermediates: the β -isomer adopts a 4C_1 chair conformation while the α -isomer adopts a $B_{2,5}$ boat conformation. These two glycosyl intermediates exist in a ratio of 2:1 favoring the 4C_1 chair-like β -phenanthrolium ion. The 1H and COSY NMR studies indicate that there is an intramolecular hydrogen bonding between the anomeric C1- proton of the carbohydrate moiety and the second pyridine nitrogen of phenanthroline framework for the two glycosyl phenanthrolium ion intermediates. The coupling is governed by Curtin-Hammett principles and proceeds through the more reactive 4C_1 chair-like β -phenanthrolium ion. The α -anomeric selectivity is rationalized by a model in which nucleophilic attack takes place from the α -face of the β -covalent glycosyl phenanthrolium ion intermediate. Kinetic study suggested that the phenanthroline-catalyzed reaction operates by associative mechanisms.

CHAPTER 4: EXPLORATION OF PHENANTHROLINE-CATALYZED 1,2-*CIS* FURANOSYLATION

4.1. Introduction

The interest in the stereoselective synthesis of furanose-containing glycans has been growing rapidly over the past decade¹⁷⁰⁻¹⁷⁵ as furanoses are key constituents of many pathogenic microorganisms and plants.¹⁷⁶⁻¹⁷⁹ Oligosaccharides and polysaccharides containing 1,2-*trans* and 1,2-*cis* furanosidic linkages (Figure 25) are generally present in the cell walls of the microorganisms and play critical roles in disease progression and interaction with the host immune system.¹⁷⁶⁻¹⁷⁹ As a result, they are targets for therapeutic intervention.¹⁸⁰⁻¹⁸¹ The 1,2-*trans* furanosides are obtained through neighboring group participation of the C2-*O*-acyl protecting group. On the other hand, the ability to access 1,2-*cis* furanosides requires furanosyl donors with a non-assisting functionality at C2. The use of these electrophilic donors often leads to the formation of a mixture of two stereoisomers that differ in the configuration of the anomeric center.¹⁷⁰⁻¹⁷⁵

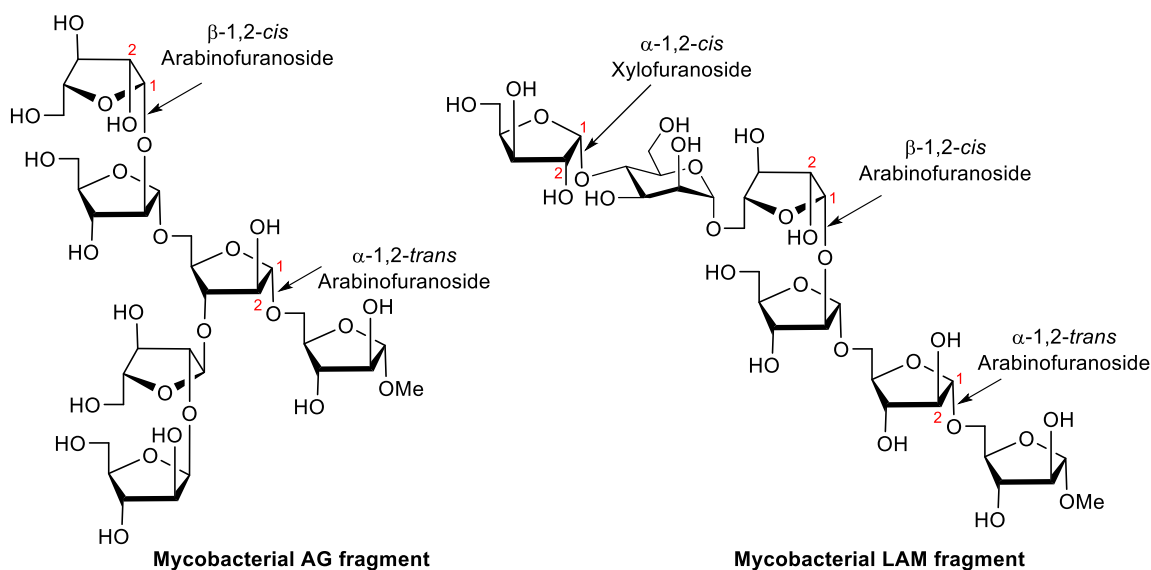


Figure 25. Hexasaccharide motifs found in the cell wall complex of mycobacterial arabinogalactan (AG) and lipoarabinomannan (LAM).

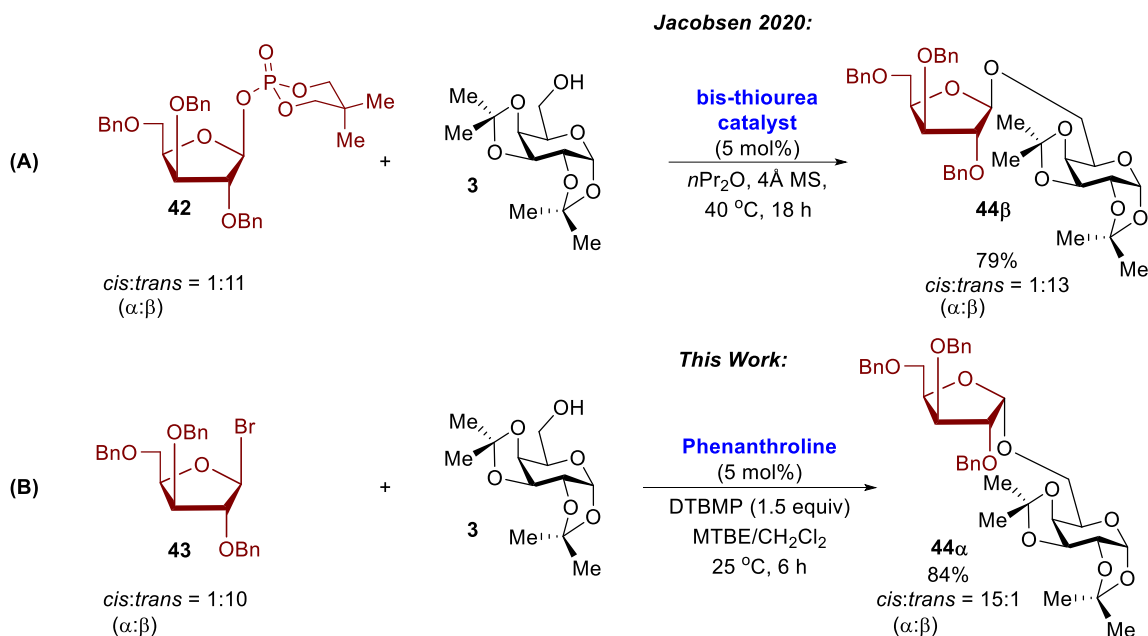
The furanosides react closer to the S_N1 end of the S_N1 - S_N2 boundary than their pyranoside counterparts due to their conformational flexibility and electronic properties.¹²⁷ To overcome these inherent challenges,

several groups have employed conformationally blocked furanosyl donors that provide 1,2-*cis* furanosides with high levels of selectivity.¹⁸²⁻¹⁸⁷ The introduction of 1,2-*cis*-furanosidic,¹⁸⁸⁻¹⁹⁰ remote participation of the acyl protecting group at C3 or C5,¹⁹¹⁻¹⁹² hydrogen bonding-assisted coupling,¹⁹³ and regioselective opening of the 2,3-anhydrofuransoyl donor.¹⁹⁴⁻¹⁹⁵ While these substrate-controlled methods have been successful to provide solutions to a number of 1,2-*cis* furanosylation challenges in the oligosaccharide synthesis,¹⁹⁶⁻²⁰² achieving the desired stereoselectivity remains system-dependent. Subtle changes to the structure of carbohydrate coupling partners have pronounced effects on the furanosylation selectivity and reactivity.

Methods that enable catalytic stereoselective glycosylation are a powerful means of rapidly introducing 1,2-*cis* furanosidic linkages into biologically relevant oligosaccharides, obviating the need to rely on substrate control. The catalysis with small organic molecules to expand the chemical space of stereoselective 1,2-*cis* furanosylation reaction is of interest. The area of organocatalysis has become a highly dynamic area of research as small organic molecules are capable of catalyzing a wide range of organic reactions.²⁰³⁻²¹⁴ Recently, Jacobsen and coworkers reported the use of small molecule catalysts, bis-thiourea hydrogen-bond donors, to mediate the formation of 1,2-*cis* furanosides in high yields and diastereoselectivities.²¹⁵ In their investigation, 1,2-*trans* furanosyl phosphate donors undergo substitution with a variety of hydroxyl acceptors to provide access to 1,2-*cis* products.²¹⁵ However, when β -1,2-*trans* xylofuranosyl phosphate donor (**42**, *cis:trans* = 1:11) was employed in the reaction (Scheme 35A), the β -1,2-*trans* product **44 β** was obtained as the major product with the net retention of anomeric configuration (*cis:trans* = 1:13).²¹⁵ This is a unique case when compared to other furanosyl phosphates under bis-thiourea-catalyzed selective furanosylation conditions.

Our group recently discovered that phenanthroline, a rigid and planar organic compound with two pyridine rings fused to a benzene ring, effectively acts as a nucleophilic catalyst to promote the stereoselective glycosylation with α -pyranosyl bromide donors providing α -1,2-*cis* pyranosides with net retention of anomeric configuration.^{126, 134, 216} The reaction is governed by Curtin-Hammett principles and

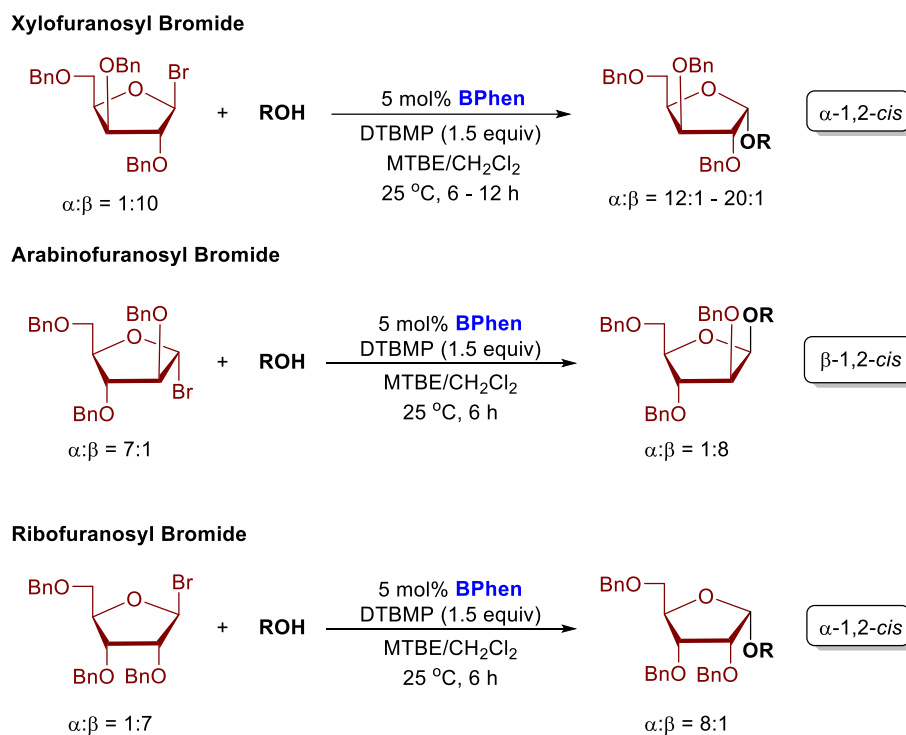
proceeds through the more reactive β -pyranosyl phenanthrolium ion intermediate. The α -1,2-*cis* selectivity is rationalized by a model in which nucleophilic attack takes place from the α -face of the β -glycosyl phenanthrolium ion.²¹⁶ Given the paucity of catalytic stereoselective 1,2-*cis* furanosylation reports, we saw an opportunity to demonstrate the utility of our catalytic strategy toward furanose substrates. Dr. Hengfu Xu has investigated the commercially available phenanthroline-catalyzed stereoselective glycosylation of a variety of hydroxyl nucleophiles with furanosyl bromide donors to provide access to the challenging 1,2-*cis* furanoside products with high levels of anomeric selectivity. Unlike the pyranose substrates, the reaction with furanose substrates proceeds with inversion of stereochemistry.



Scheme 35. Catalytic stereoselective xylofuranosylation

As illustrated in Scheme 35B, reaction of 1,2:3,4-di-*O*-isopropylidene- α -D-galactopyranoside **3** with β -1,2-*trans* xylofuranosyl bromide donor (**43**, *cis:trans* = 1:10) using 15 mol% 4,7-diphenyl-1,10-phenanthroline (**C1**) provided the α -1,2-*cis* product **44 α** with excellent selectivity (*cis:trans* = 15:1). This result is the opposite of Jacobsen's observation (Scheme 35A).²¹⁵ This catalysis system has also been extended to a number of furanosyl bromide donors. While arabinofuranosyl bromide provides β -1,2-*cis* products as the major stereoisomers, xylo- and ribofuranosyl donors favor α -1,2-*cis* products (Scheme 36).

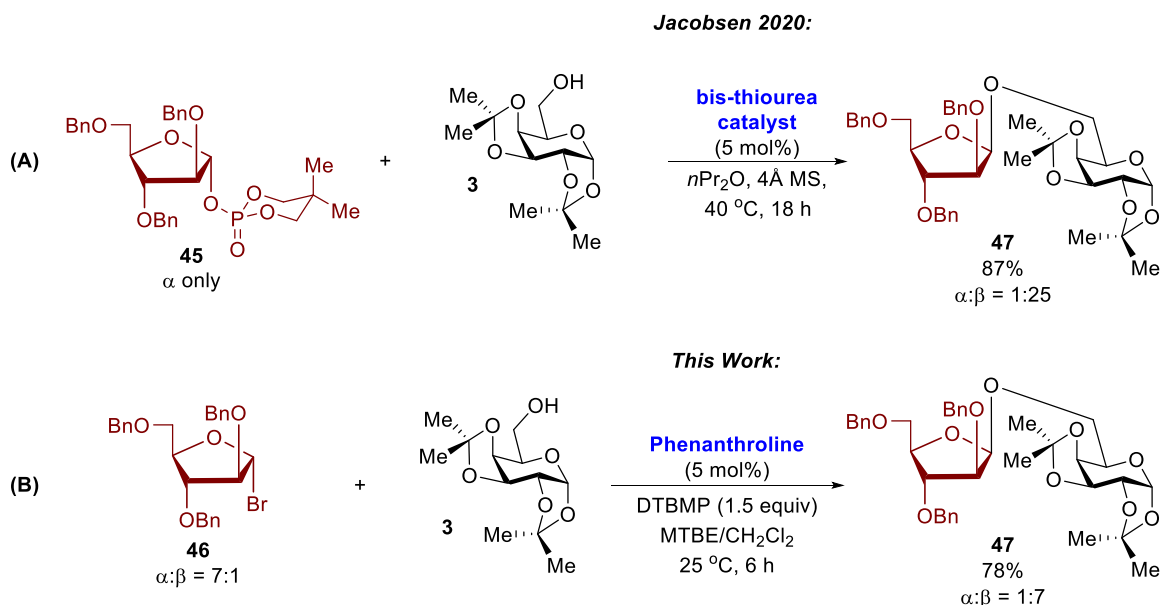
To understand the behavior of phenanthroline in the furanosylation system, an extensive mechanistic investigation was initiated.



Scheme 36. Overview of reaction outcome of phenanthroline catalysis in furanosylation system

4.2. Effects of donor anomeric composition

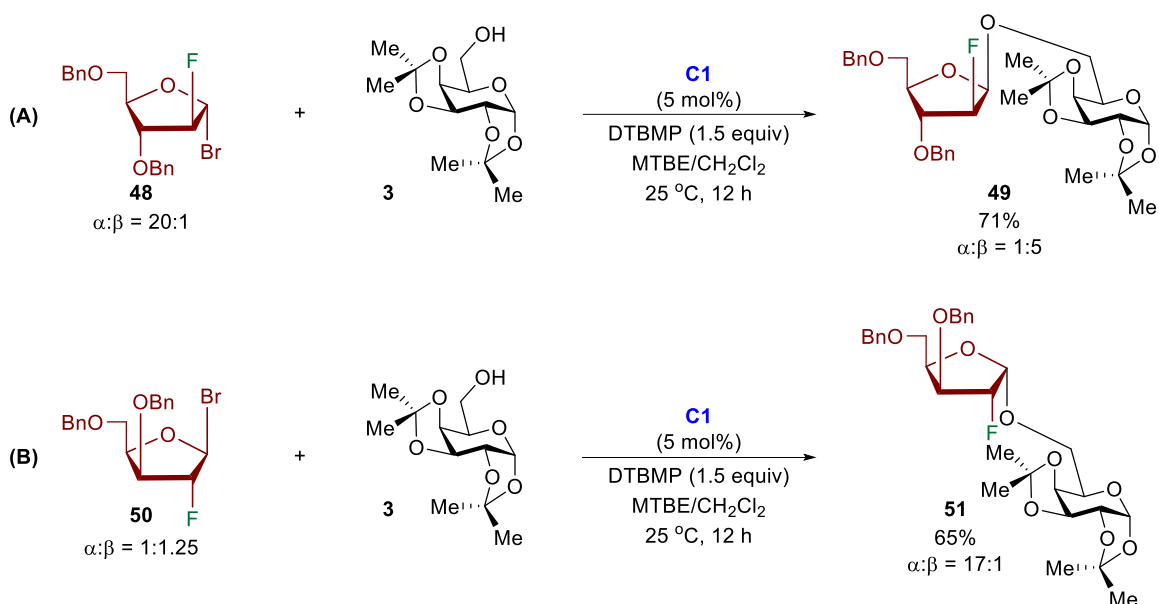
Jacobsen and coworkers have reported that the anomeric composition of the furanosyl phosphate donors had a pronounced effect on the reaction outcome under bis-thiourea-catalyzed furanosylation conditions.²¹⁵ For example, the coupling of alcohol acceptor **3** with α -arabinofuranosyl phosphate **45** provided disaccharide **47** with $\alpha:\beta = 1:25$ (Scheme 37A).²¹⁵ In contrast, the use of an 8:1 α/β mixture of arabinofuranosyl phosphate donor led to a decrease in selectivity, affording **47** with $\alpha:\beta = 1:10$ which is comparable with our **C1** catalysis conditions ($\alpha:\beta = 1:7$, Scheme 37B).



Scheme 37. Catalytic stereoselective arabinofuranosylation

Since we were unable to obtain α -D-arabinofuranosyl bromide **46** in a high α -form, it is unclear how the anomeric composition of this donor could impact the stereochemical outcome under phenanthroline-catalyzed furanosylation conditions and whether the furanosylation operates by associative mechanisms.^{126, 134, 216} To determine if the stereochemical outcome of the reaction is dependent on the anomeric configuration of the electrophilic partner, we proposed to replace the C2-oxygen of arabinose with a fluorine atom to generate 2-fluoro-arabinofuranosyl bromide since this donor has been obtained with high α -selectivity.²¹⁷ As anticipated, 2-fluoro arabinosyl bromide **48** (Scheme 38A) was primarily isolated as the α -furanosyl donor ($\alpha:\beta = 20:1$). Although the reaction of donor **48** with primary alcohol acceptor **3** provided disaccharide **49** in 71% yield (Scheme 38A), a decrease in β -1,2-*cis* selectivity ($\alpha:\beta = 1:5$) was observed in comparison to the result obtained for a 7:1 α/β mixture of arabinofuranosyl bromide donor **46** ($\alpha:\beta = 1:7$, Scheme 37B). Interestingly, similar anomeric selectivity ($\alpha:\beta = 1:5$) was also obtained for 1,2-*cis* product **49** in the coupling of alcohol **3** with 2-fluoro arabinosyl phosphate mediated by the bis-thiourea catalyst.²¹⁵ Next, we replace C2-oxygen of xylose with a fluorine atom to form 2-fluoro xylofuranosyl bromide donor **50** (Scheme 38B). Interestingly, while donor **50** was primarily isolated as a 1:1 α/β mixture, the coupling product **51** was obtained with excellent levels of *cis/trans* diastereoselectivity ($\alpha:\beta = 17:1$).

Taken together, the data obtained in Scheme 38 suggest that furanosyl donor anomeric composition is not responsible for the reaction anomeric selectivity.



Scheme 38. Effect of donor anomeric composition in **C1**-catalyzed furanosylation

The use of 2-fluorofuranosyl bromide donors **48** and **50** (Scheme 38) also allows to study the effect of C2-fluorine atom on the reaction selectivity as the directing role of fluorine at C2 on 1,2-*trans* glycosylation with pyranosyl donors has been reported.²¹⁸ Two mechanistic S_N1 and S_N2 scenarios have been proposed.²¹⁸ For the S_N1 pathway, the C2-F bond of pyranosyl donor adopts a quasi-axial arrangement to allow maximum orbital overlap for σ_{C-F}^* and the incoming alcohol nucleophile in the transition state.²¹⁸ As such, if the C2-fluorine directs furanosylation, 1,2-*trans* products should be obtained as the major products. However, in both the phenanthroline system and the bis-thiourea system²¹⁵, 1,2-*cis* products **49** and **51** (Scheme 38) were observed as the major products, suggesting either the reaction did not undergo S_N1 pathway or the catalyst overrides the C2-fluorine directing effect. For the S_N2 pathway, it has been proposed that the C2-fluorine may induce an electrostatic attraction between the pyranosyl donors and alcohol nucleophiles.²¹⁸ If the reaction proceeds through S_N2 pathway, the final coupling product should be in the opposite stereochemistry of the glycosyl electrophile. In the 2-fluoro-arabinofuranosylation case, we used furanosyl bromide **48** with 20:1 of $\alpha:\beta$ ratio, but only obtained 1:5 of $\alpha:\beta$ ratio for the coupling products

49 (Scheme 38A). On the other hand, in the 2-fluoro-xylofuranosylation case, although a 1:1 anomeric mixture of furanosyl bromide **50** was used in the reaction, a high α : β ratio (17:1) of the coupling product **51** (Scheme 38B) was obtained. These results suggest that the furanosylation does not undergo direct S_N2 pathway. The data are also consistent with our recent report on the phenanthroline-catalyzed stereoselective construction of 2-fluoroglycosides, in which phenanthroline catalyst overrides the C2-fluorine directing effect and gives access to the corresponding 1,2-*cis*-2-fluoro glycosides.¹³⁴

4.3. Detection of furanosyl phenanthrolium ion intermediates

With the possibility that the reaction goes through covalent phenanthrolium ion intermediates, NMR spectroscopy was employed to detect the putative intermediates. To minimize the proton signals on the aromatic region, **C14** was chosen as a catalyst of choice. In addition, both 2-fluoro xylosyl **50** and arabinosyl **48** bromides were chosen as model donors in our NMR study as we have established their anomeric composition (see Scheme 38).

With the previous knowledge that the covalent phenanthrolium ion intermediates form within 30 min upon combining the pyranosyl donor with **C14**,²¹⁶ the first step in our study was to add **C14** (0.13 mmol) to the 1:1.25 α / β mixture of 2-fluoro xylofuranosyl bromide **50** (0.10 mmol) at 25 °C. Within 1 h, new signals appeared around the phenanthroline region (7.0 – 9.1 ppm) and the sugar region (5.4 – 6.0 ppm) (Figure 26). An aliquot of the reaction mixture was then analyzed by electrospray ionization (ESI) mass spectrometry with an m/z ratio of 661.3548 (Figure 26 and Figure 58), confirming the formation of the phenanthrolium ion. Furthermore, the number of new signals in both ^1H and ^{19}F NMR indicates that there are two possible intermediates, **Int₄** and **Int₅**, present in a ratio of 2:1 in the reaction (Figure 26, Figure 53 and Figure 54). In ^1H - ^1H COSY (Figure 56) and ROESY (Figure 57) NMR analysis, the C1 protons of the anomeric mixture of **Int₄** and **Int₅** were identified to reside at $\delta_{\text{H}} = 7.63$ ppm and $\delta_{\text{H}} = 8.02$ ppm, respectively. On the other hand, the C2-fluorine of **Int₄** and **Int₅** resides at $\delta_{\text{F}} = -188.01$ ppm (ddd, $J = 45.7, 16.1, 8.4$ Hz) and $\delta_{\text{F}} = -189.64$ ppm (ddd, $J = 52.2, 17.9, 14.0$ Hz), respectively, in the ^{19}F NMR (Figure 54). Through 2D

ROESY NMR analysis, the major **Int₄** was identified as a β -phenanthrolium ion and exists in the 3E envelop conformation while the minor **Int₅** was an α -phenanthrolium ion and adopts the E_3 envelop conformation (Figure 26, Figure 55 and Figure 57).

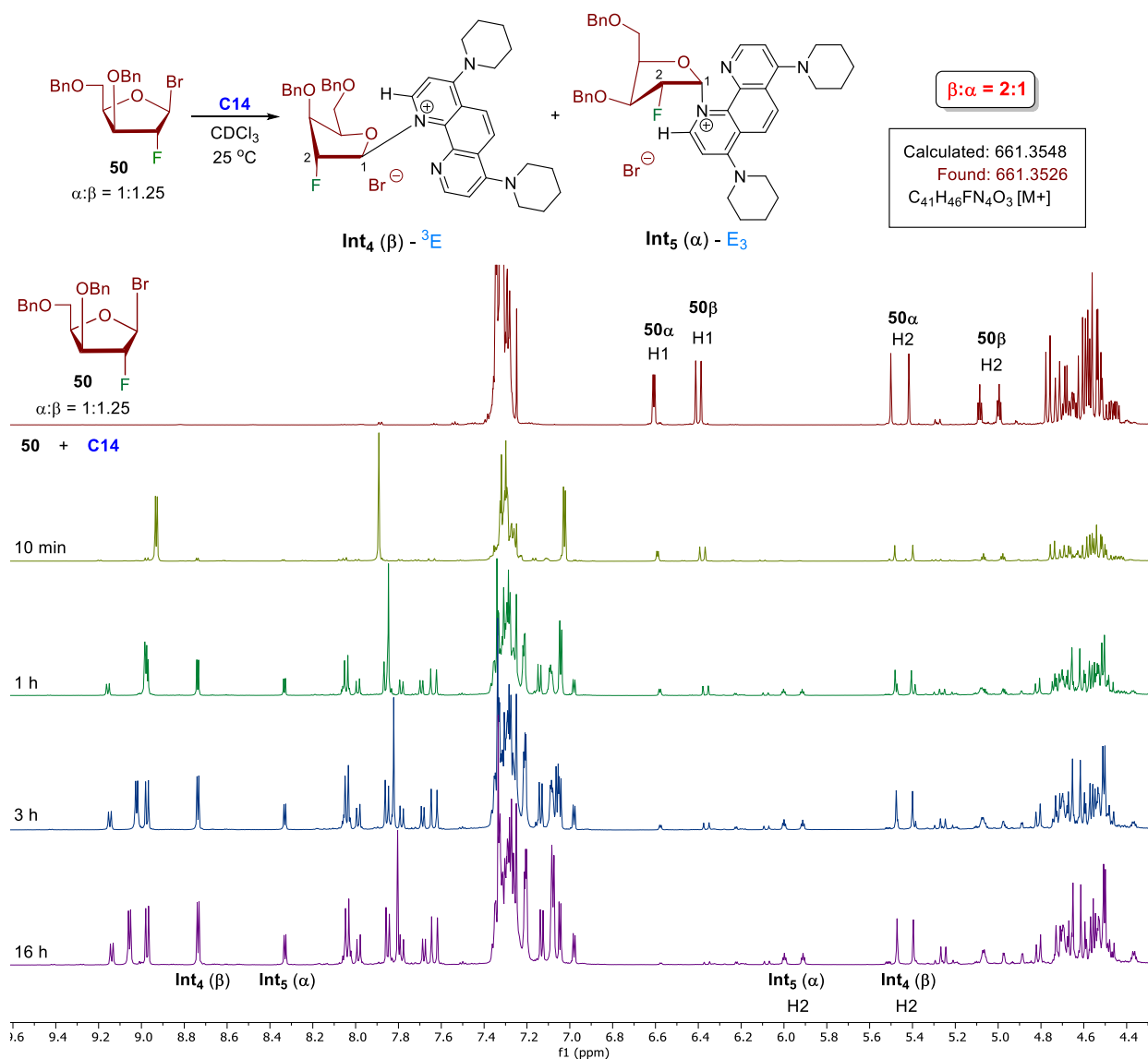


Figure 26. Detection of xylofuranosyl phenanthrolium intermediates

In the case of 2-fluoro arabinofuranosyl bromide **48** ($\alpha:\beta = 20:1$, Figure 27), our NMR study of the 1:1 stoichiometry ratio of donor **48** and **C14** mixture shows that two key intermediates, a major 3E β -phenanthrolium ion conformer (**Int₆**) and a minor E_3 α -phenanthrolium ion conformer (**Int₇**), were also formed in a ratio of 2:1 β/α mixture (Figure 27, Figure 59 and Figure 60). The formation of the arabinosyl

phenanthroline ion intermediate was also confirmed using electrospray ionization (ESI) with an m/z ratio of 661.3541 (Figure 27 and Figure 66). From the 2D NMR study (Figure 64 and Figure 65), the C1 protons of the anomeric mixture of **Int₆** and **Int₇** were identified to reside at $\delta_H = 7.99$ ppm and $\delta_H = 8.05$ ppm, whereas the C2-fluorine resides at $\delta_F = -192.53$ ppm (ddd, $J = 51.3, 20.5, 11.8$ Hz) and $\delta_F = -186.34$ ppm (dt, $J = 46.0, 13.3$ Hz), respectively (Figure 62).

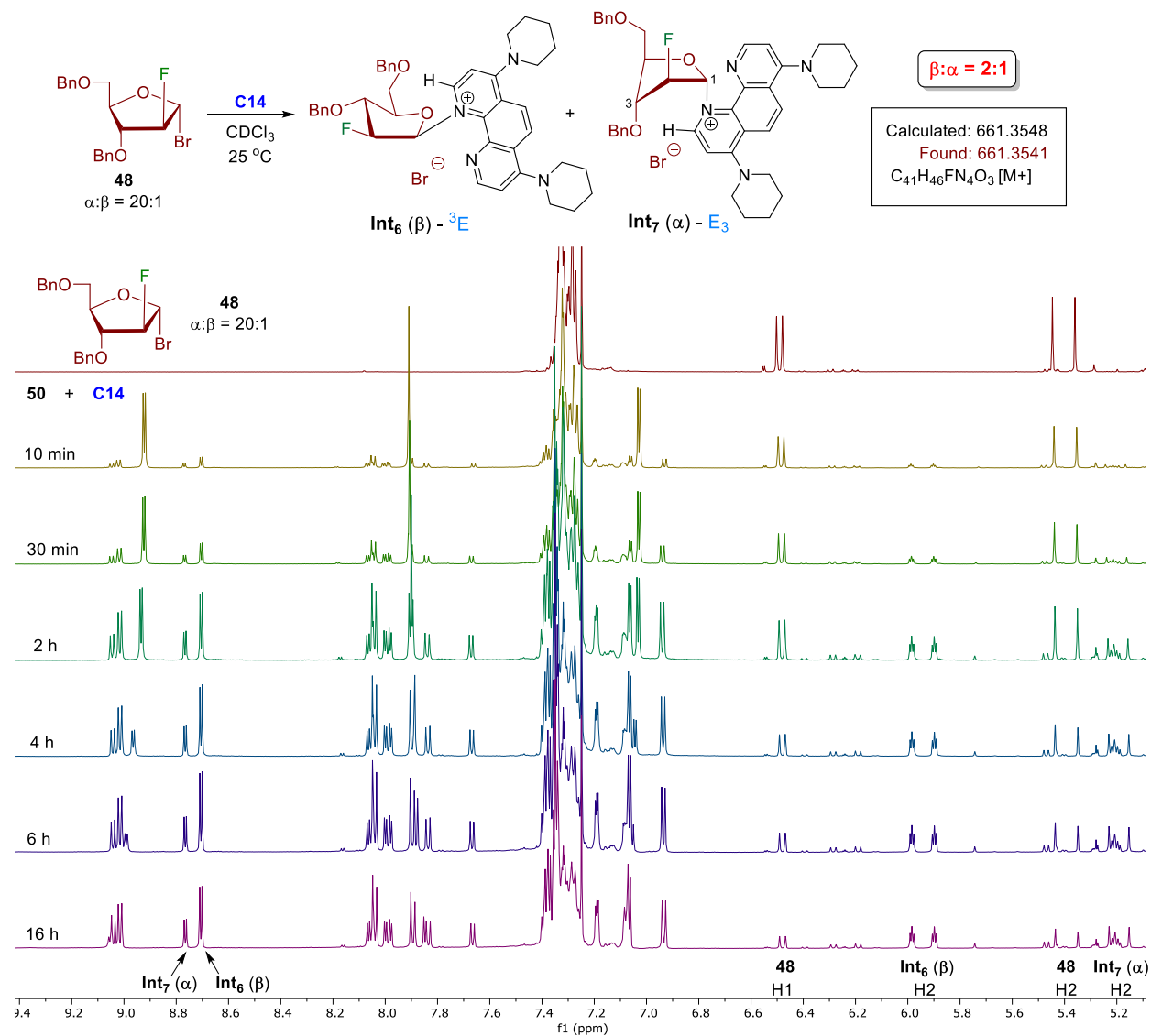


Figure 27. Detection of arabinofuranosyl phenanthroline intermediates

Collectively, the discovery of both α/β intermediates in the NMR study further illustrated that the phenanthroline-catalyzed furanosylation does not proceed through a stereospecific substitution. However,

to obtain high levels of 1,2-*cis* selectivity, the reaction is likely to proceed through a Curtin-Hammett scenario, wherein interconversion of the β -phenanthroline intermediate and its corresponding α -conformer must be more rapid than nucleophilic addition of alcohol acceptor. To further investigate this potential mechanism, we next performed reaction progress analysis using NMR spectroscopy.

4.4. Reaction progress analysis of phenanthroline-catalyzed furanosylation

In the reaction progress analysis, both 2-fluoro xylose **50** and arabinose **48** were again chosen as furanosyl bromide donors (0.3 M), and primary alcohol **3** (0.1 M) was chosen as the acceptor since we have established the α/β selectivity of the resulting products **51** and **49** (Scheme 38). The reactions were carried in deuterated chloroform (CDCl_3) with 15 mol% **C14** and 1.5 equivalent of DTBMP as the acid scavenger. Taking advantage of the C2-fluorine, the reaction progress was monitored using ^{19}F NMR for 20 – 24 h, and the relative concentrations of furanosyl bromide, covalent phenanthroline intermediates, and the disaccharide products were then determined (Figure 28 and Figure 29).

Firstly, we monitored the reaction progress for 2-fluoro xylofuranosyl bromide donor **50** ($\alpha:\beta = 1:1.25$) 30 minutes after mixing **50** with 5 mol% **C14** using both ^1H (Figure 51) and ^{19}F (Figure 52) NMR. Interestingly, **Int₄(β)** and **Int₅(α)** appeared with a ratio of 1:8 (Figure 52). After alcohol acceptor **3** had been added to the reaction mixture for 1 h, a new sharp fluorine signal resided at $\delta_{\text{F}} = -204.18$ ppm (dd, $J = 52.9, 16.2$ Hz) was verified to be the disaccharide **51 α** (α -isomer, Figure 52). Meanwhile, an indistinct fluorine peak located at $\delta_{\text{F}} = -193.02$ ppm (ddd, $J = 50.2, 17.5, 14.3$ Hz) was later confirmed to be the β -isomer of **51 β** (Figure 52). Overall, the α/β selectivity of the disaccharides **51** was determined to be 21:1 after 24 h. The reaction progress analysis of xylofuranosyl donor **51** and alcohol acceptor **3** was also quantified as a kinetic profile in a concentration vs time graph (Figure 28). The linear relationship in Figure 28a between the concentrations and time in the kinetic profile revealed that the xylofuranosylation was in apparent zero-order kinetics in the first 7 h. Interestingly, although the anomeric mixture of xylofuranosyl bromides disappeared at similar rates, the two products appeared at significantly different rates – the rate of **51 α** formation was 16 times faster than that of **51 β** (Figure 28a). Meanwhile, increasing concentration

of **Int₅(α)** was also observed in the kinetic profile of the xylofuranosyl phenanthroline intermediates (Figure 28b) while **Int₄(β)** concentration maintained at a low level. These kinetic profiles suggested that the consumption rate of **Int₄(β)**, which led to the major product **51 α** , was much faster than that of **Int₅(α)**. As more products were formed in the reaction, the consumption rate of **Int₄(β)** decreased, and a slight downward slope of product formation was observed at 7 h. This ratio of **Int₄(β)** and **Int₅(α)** maintained at 1:16 until the end of the reaction course (24 h), likely due to hydrolysis in the reaction.

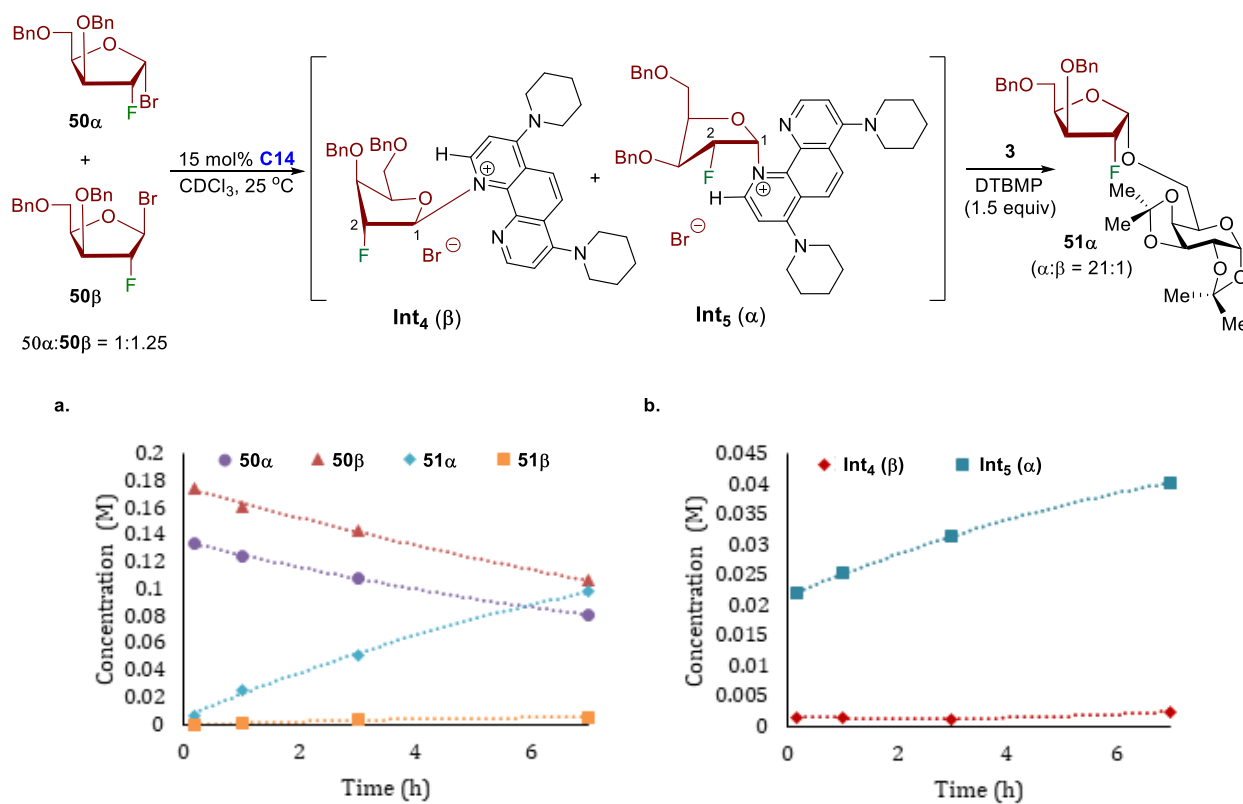


Figure 28. Reaction progress for phenanthroline-catalyzed xylofuranosylation of alcohol acceptor **3** using ^{19}F NMR: (a) xylofuranosyl bromide **50** and products **51**; (b). xylofuranosyl-phenanthroline intermediates **Int₄(β)** and **Int₅(α)**

On the other hand, in the reaction progress of 2-fluoro arabinofuranosyl bromide **48** (Figure 29), the ratio of intermediates **Int₆(β)** and **Int₇(α)** only increased to 3:1 upon addition of primary alcohol **3** (Figure 60). Meanwhile, the α/β selectivity of the disaccharides **49** slowly decreased from 1:7 at 1 h to 1:5 at 6 h

(Figure 29a, Figure 59 and Figure 60). This 1:5 α/β ratio maintained until the end of the course of the reaction (20 h). Like the 2-fluoro-xylofuranosylation reaction, the kinetic profile of the 2-fluoro arabinofuranosylation also expressed apparent zero-order kinetics in the first 6 h. The disappearance rate of **48 α** was 24 times faster than that of **48 β** (Figure 29a), likely due to the higher concentration of starting material **48 α** , which further resulted in the higher concentration of **Int₆(β)**. However, unlike xylofuranosylation, the consumption rates of the two intermediates (**Int₆(β)** and **Int₇(α)**, Figure 29b) in the arabinofuranosylation were similar, which eventually led to a lower selectivity in the coupling products **49**.

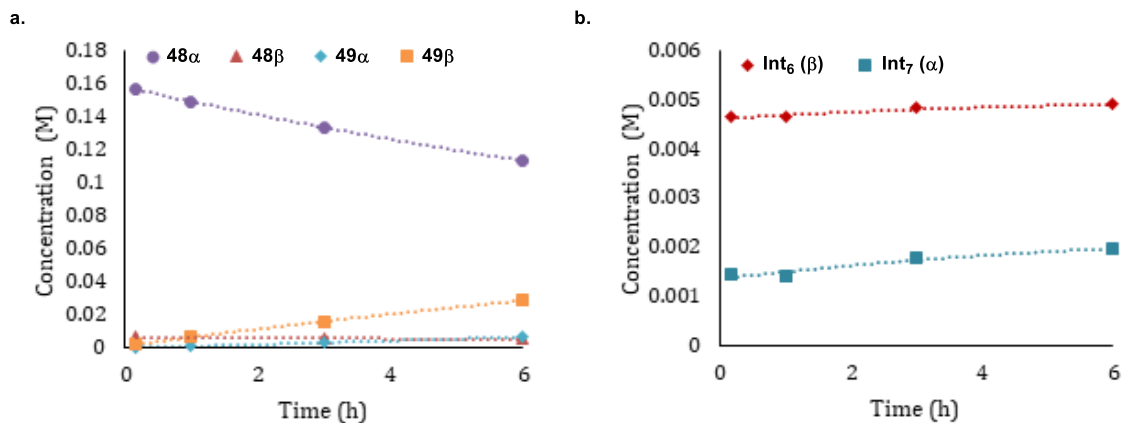
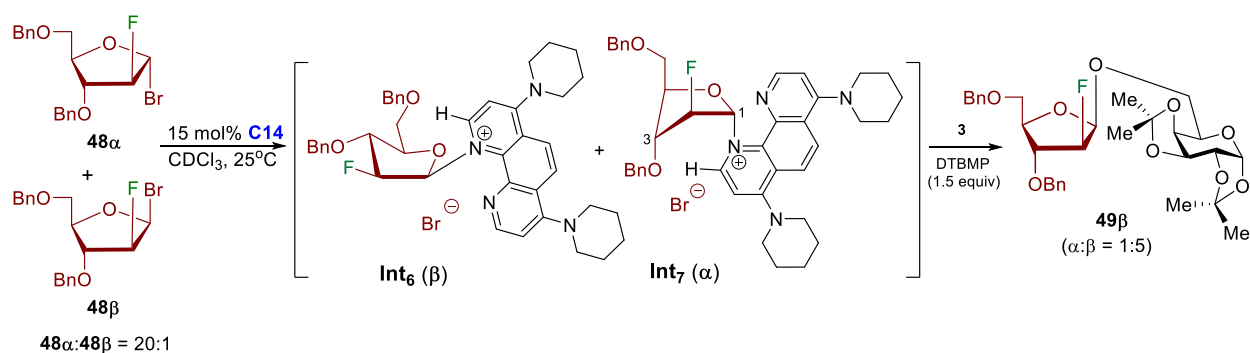


Figure 29. Reaction progress for phenanthroline-catalyzed arabinofuranosylation of alcohol acceptor **3** using ^{19}F NMR: (a) arabinofuranosyl bromide **48** and coupling products **49**; (b) arabinofuranosyl-phenanthroline intermediates **Int₆(β)** and **Int₇(α)**.

4.5. Proposed mechanism of phenanthroline-catalyzed furanosylation

To obtain high levels of 1,2-*cis* selectivity, a Curtin-Hammett situation must be established such that equilibration of **Int**(β) and **Int**(α) is rapid and much faster than the subsequent nucleophilic attack. The hypothesis, that the rate-determining step takes place after the phenanthroline intermediates are formed, was confirmed by kinetic analysis (Figure 28b and Figure 29b), as the kinetic profiles for both xylose and arabinose showed an accumulation (positive slope) of the intermediates.

To provide further insight into the mechanism and selectivity, Dr. Richard N. Schaugaard performed density functional theory (DFT) calculations to examine the key transition states and intermediates along the reaction pathway. DFT calculations indicate that the second transition state (Figure 30) – the nucleophilic attack of alcohol onto the faster reacting phenanthroline ion intermediate – determines the stereochemistry of the product. As illustrated in Figure 30, TS2 indicates the second transition state that leads to the major product, while TS2' represents the route to the minor product. The difference between TS2 and TS2' ($\Delta\Delta G^\ddagger$) of xylofuranosylation was calculated as 4.0 kcal/mol, which results in a high product ratio (**51** α :**51** β = 21:1, Figure 30a). Meanwhile, the $\Delta\Delta G^\ddagger$ of arabinofuranosylation was only 1.6 kcal/mol, which leads to a moderate product ratio as **49** α :**49** β = 1:5 (Figure 30b).

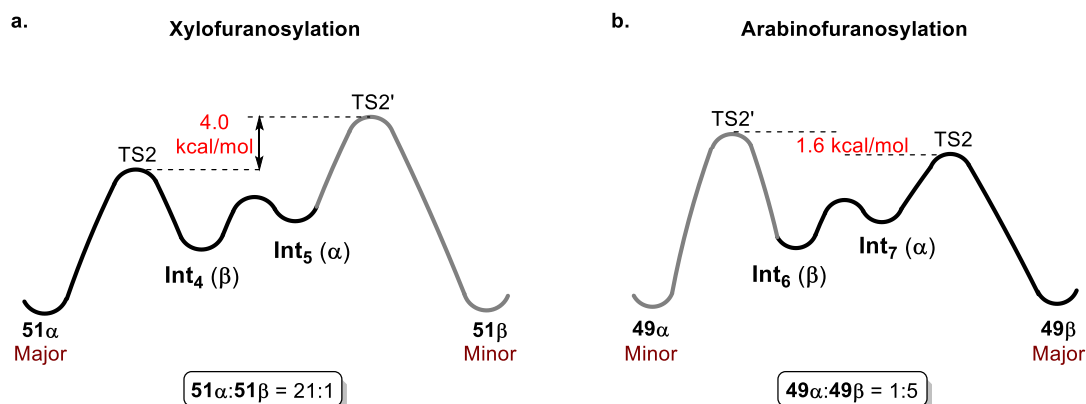


Figure 30. Energy diagram of phenanthroline-catalyzed furanosylation for the second nucleophilic substitution: (a) xylofuranosylation (b) arabinofuranosylation

Based on the NMR data, kinetic profile (Figure 28), and computational results (Figure 30a) for xylofuranosyl bromide donor **50**, we propose the following mechanistic rationale for the observed α -1,2-*cis* stereochemistry (Figure 31). Since α - and β -isomers of xylofuranosyl bromide **50** exist as a 1:1.25 mixture, displacement of their anomeric bromide leaving group with NPhen via an S_N2 -like pathway would generate 3E β -phenanthroline ion conformer **Int₄(β)** and E_3 α -phenanthroline ion conformer **Int₅(α)**, respectively, with the preference of the **Int₄(β)** intermediate. Calculations predict that **Int₅(α)** is 0.4 kcal/mol less stable than **Int₄(β)**, likely due to eclipsing interaction between C2-F and C1-N in **Int₅(α)**. Nucleophilic attack of alcohol acceptor **3** onto **Int₄(β)**, via an S_N2 -like pathway, would provide the α -xylofuranoside product **51 α** . To obtain high levels of 1,2-*cis* selectivity, a Curtin-Hammett situation must be established such that equilibration of **Int₄(β)** and **Int₅(α)** is rapid and much faster than the subsequent nucleophilic attack. The hypothesis, that the rate-determining step takes place after the phenanthroline

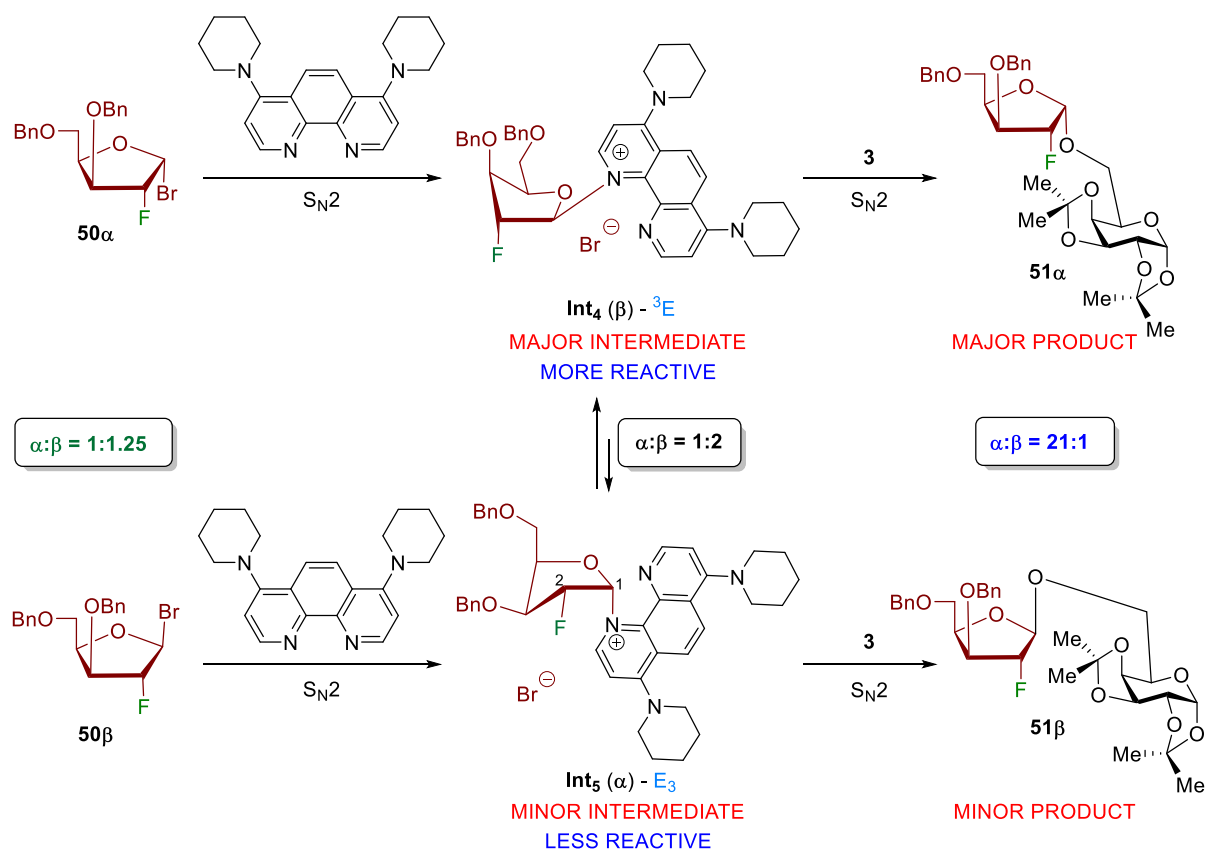


Figure 31. Possible mechanism for phenanthroline-catalyzed xylofuranosylation

intermediates are formed, was confirmed by kinetic analysis (Figure 28b) and computational observation (Figure 30a). It is also observed that **Int₄(β)** is not only the more stable intermediate than **Int₅(α)** by 0.4 kcal/mol, but also is the faster-reacting conformer (Figure 30a). Indeed, the calculated TS2 transition state for the formation of the α -xyloside product resulted from **Int₄(β)** is 4.0 kcal/mol more favorable than the analogous formation of the β -xyloside product (Figure 30a). Collectively, the α -1,2-*cis* xyloside product **51 α** resulted from the nucleophilic attack of alcohol **3** onto the major intermediate **Int₄(β)** should prevail and will not reflect the equilibrium distribution of **Int₄(β)** and **Int₅(α)**.

In the case of arabinose (Figure 32), the kinetic profile (Figure 29), and DFT calculations (Figure 30b) for arabinofuranosyl bromide suggest that (1) the donor anomeric composition would not reflect the intermediate distribution; and (2) although **Int₇(α)** is the minor intermediate observed by both NMR study (Figure 29b) and DFT calculation (Figure 30b), it is the fast-reacting conformer that reacts with alcohol

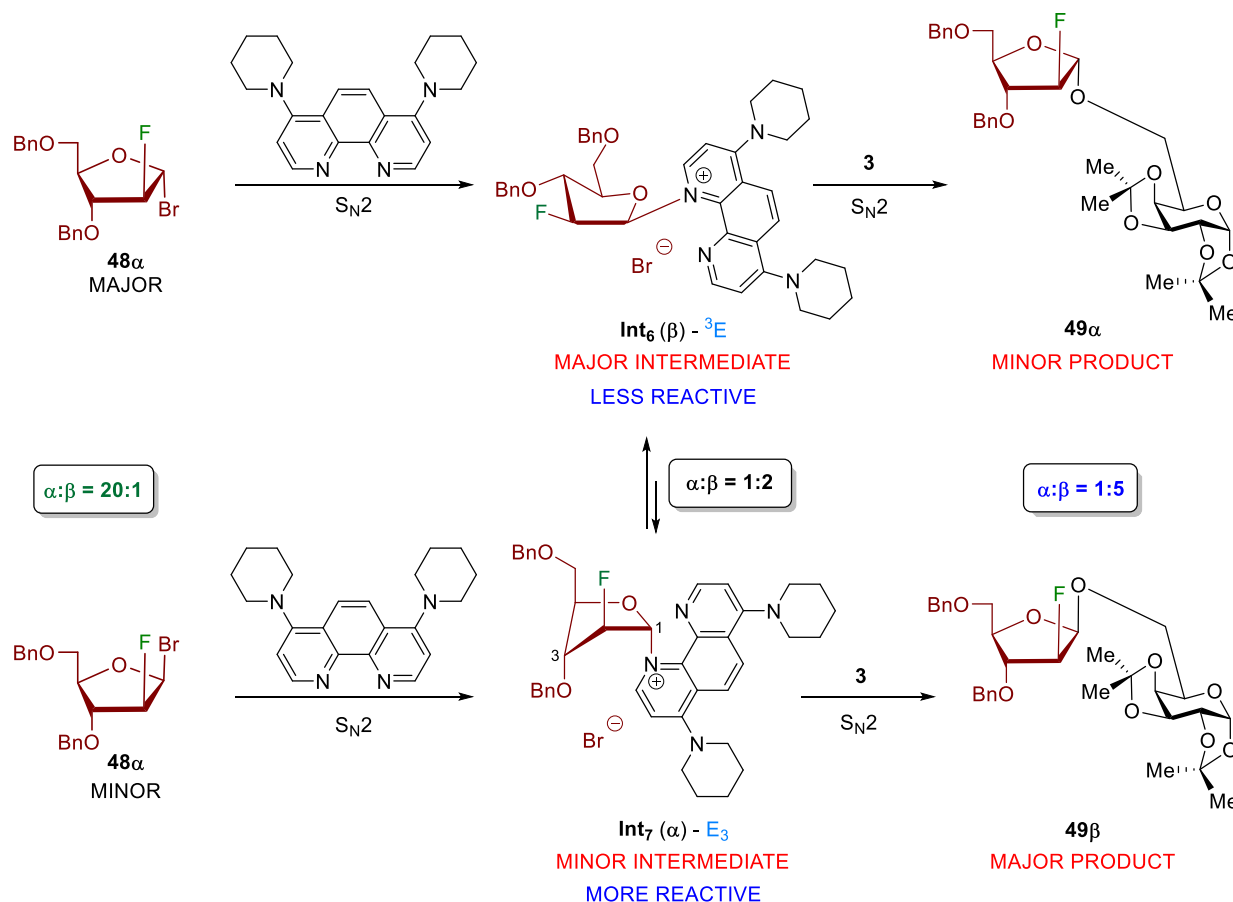


Figure 32. Possible mechanism for phenanthroline-catalyzed arabinofuranosylation

acceptor to form the major β -1,2-*cis*-arabinoside product (see the proposed mechanism in Figure 32). Kinetic analysis (Figure 29b) shows that the rate of the nucleophilic substitution of **Int**₇(α) is also faster than that of the more stable one **Int**₆(β). As a result, as soon as **Int**₇(α) is consumed, it is replenished from **Int**₆(β) as the energy barrier for interconversion of **Int**₆ and **Int**₇ is low. The difference of the energy barrier for the two transition states ($\Delta\Delta G^\ddagger$) is about 1.6 kcal/mol (Figure 30b), further supporting the experimental result that a mixture of 1,2-*cis*- and 1,2-*trans*-arabinoside products (5:1) was obtained in the reaction.

4.5. Conclusion

A phenanthroline-catalyzed stereoselective furanosylation is developed to achieve access to the challenging 1,2-*cis* furanosidic linkages. Substitution of xylofuranosyl bromide donor with a variety of primary and secondary hydroxyl acceptors affords α -1,2-*cis* linked products in high yields and with excellent levels of *cis/trans* diastereoselectivity. This phenanthroline catalysis method is also applicable to other furanosyl donors. Experiments with 2-fluoro-xylofuranosyl and -arabinofuranosyl bromide donors indicate that furanosyl donor anomeric composition is not responsible for the reaction selectivity. Importantly, the furanosylation reaction is unlikely to proceed through a stereospecific substitution. NMR experiments, kinetic profile, and DFT calculations indicate that the second transition state – the nucleophilic attack of alcohol onto the faster reacting phenanthrolium ion intermediate – determines the stereochemistry of the product. Collectively, the results obtained highlight the unique features of phenanthroline to catalyze the highly stereoselective furanosylation reactions. The utility of this new method is currently extending to other carbohydrate electrophiles as well as nitrogen and sulfur carbohydrate nucleophiles.

CHAPTER 5: EXPERIMENTAL SECTION

5.1. General Information

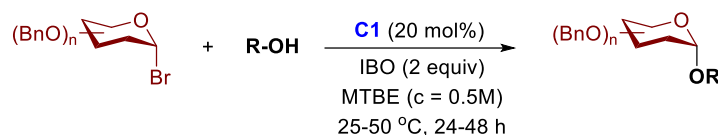
Methods and Reagents. All reactions were performed in oven-dried flasks fitted with septa under a positive pressure of nitrogen atmosphere. Organic solutions were concentrated using a Buchi rotary evaporator below 40 °C at 25 torr. Analytical thin-layer chromatography was routinely utilized to monitor the progress of the reactions and performed using pre-coated glass plates with 230-400 mesh silica gel impregnated with a fluorescent indicator (250 nm). Visualization was then achieved using UV light, iodine, or ceric ammonium molybdate. Flash column chromatography was performed using 40-63 μm silica gel (SiliaFlash F60 from Silicycle) or a Biotage Isolera One system using normal phase pre-column cartridges and SNAP Ultra 10g column. Purifications were performed using ethyl acetate/n-hexanes eluting with a step gradient method starting from 0% ethyl acetate and ending at 30% ethyl acetate. Dry solvents were obtained from a SG Waters solvent system utilizing activated alumina columns under an argon pressure. All other commercial reagents were used as received from Sigma Aldrich, Alfa Aesar, Acros Organics, TCI, and Combi-Blocks, unless otherwise noted.

Instrumentation. All new compounds were characterized by Nuclear Magnetic Resonance (NMR) spectroscopy and High-Resolution Mass spectrometry (HRMS). All ^1H NMR spectra were recorded on either Agilent 400 or 600 MHz spectrometers. All ^{13}C NMR spectra were recorded on either Agilent 100 or 150 MHz spectrometer. All ^{19}F NMR spectra were recorded on either Agilent 376 or 564 MHz spectrometer. Chemical shifts are expressed in parts per million (δ scale) downfield from tetramethylsilane and are referenced to the residual proton in the NMR solvent (CDCl_3 : δ 7.26 ppm, δ 77.00 ppm; CD_2Cl_2 : δ 5.20 ppm, δ 54.00 ppm). Data are presented as follows: chemical shift, multiplicity (s = singlet, d = doublet, t = triplet, q = quartet, m = multiplet, and bs = broad singlet), integration, and coupling constant in hertz (Hz).

High resolution (ESI-TOF) mass spectrometry was performed at Wayne State University Chemistry Lumigen Center.

5.2. Chapter 2 experimental section

5.2.1. General procedure and condition in Table 5



Condition A: A 10 mL Schlenk flask was charged with glycosyl bromide (0.4 mmol, 2.0 equiv), alcohol (0.2 mmol, 1.0 equiv), catalyst **C1** (0.06 mmol, 30 mol%), IBO (0.4 mmol, 2.0 equiv.) and MTBE (0.4 mL). The resulting solution was stirred at 50 °C for 24 h, diluted with toluene, and purified by silica gel flash chromatography (toluene/ethyl acetate: 9/1→4/1) to give the desired product.

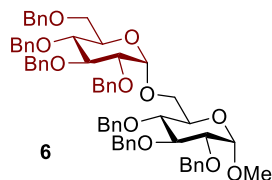
Condition B: A 10 mL Schlenk flask was charged with glycosyl bromide (0.2 mmol, 2.0 equiv), alcohol (0.1 mmol, 1.0 equiv), catalyst **C1** (0.02 mmol, 20 mol%), IBO (0.2 mmol, 2.0 equiv.) and MTBE (0.2 mL). The resulting solution was stirred at 25 °C for 24 h, diluted with toluene, and purified by silica gel flash chromatography (toluene/ethyl acetate: 9/1→4/1) to give the desired product.

Condition C: A 10 mL Schlenk flask was charged with glycosyl bromide (0.2 mmol, 2.0 equiv), alcohol (0.1 mmol, 1.0 equiv), catalyst **C1** (0.02 mmol, 20 mol%), IBO (0.2 mmol, 2.0 equiv.) and MTBE (0.2 mL). The resulting solution was stirred at 25 °C for 48 h, diluted with toluene, and purified by silica gel flash chromatography (toluene/ethyl acetate: 9/1→4/1) to give the desired product.

Condition D: A 10 mL Schlenk flask was charged with glycosyl bromide (0.2 mmol, 1.0 equiv), alcohol (0.6 mmol, 3.0 equiv), catalyst **C1** (0.04 mmol, 20 mol%), IBO (0.4 mmol, 2.0 equiv.) and MTBE (0.4 mL). The resulting solution was stirred at 25 °C for 24 h, diluted with toluene, and purified by silica gel flash chromatography (toluene/ethyl acetate: 9/1→4/1) to give the desired product.

Condition E: A 10 mL Schlenk flask was charged with glycosyl bromide (0.2 mmol, 1.0 equiv), alcohol (0.6 mmol, 3.0 equiv), catalyst **C1** (0.04 mmol, 20 mol%), IBO (0.4 mmol, 2.0 equiv.) and MTBE (0.4 mL). The resulting solution was stirred at 50 °C for 24 h, diluted with toluene, and purified by silica gel flash chromatography (toluene/ethyl acetate: 9/1→4/1) to give the desired product.

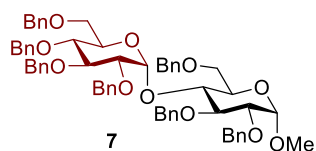
Note: The α/β ratio of the desired products were determined by ^1H NMR analysis based on the ratio of the anomeric protons of both α - and β -anomers. When the anomeric protons are overlapped, other protons of both anomers were analyzed. In some cases, we utilized prep-TLC to separate the α -anomer from the β -anomer so that we can accurately determine the α/β ratio of the mixture.



Conditions D: 63% (124.2 mg), $\alpha:\beta = 14:1$

^1H and ^{13}C NMR of disaccharide **6** has been reported.²¹⁹

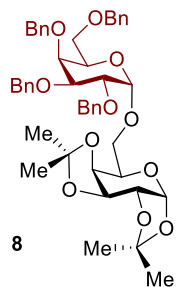
^1H NMR (400 MHz, CDCl_3): δ 7.44 – 7.16 (m, 35H), 5.08 – 4.97 (m, 4H), 4.93 – 4.83 (m, 3H), 4.81 – 4.70 (m, 4H), 4.67 – 4.61 (m, 3H), 4.56 – 4.46 (m, 2H), 4.10 – 4.01 (m, 2H), 3.93 – 3.83 (m, 3H), 3.82 – 3.66 (m, 4H), 3.65 – 3.58 (m, 2H), 3.52 (dd, $J = 9.6, 3.6$ Hz, 1H), 3.43 (s, 3H). ^1H NMR matches with the literature report.²¹⁹



Conditions A: 55% (54.3mg), $\alpha:\beta = 7:1$

^1H and ^{13}C NMR of disaccharide **7** has been reported.²¹⁹

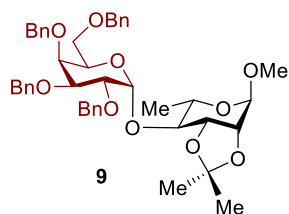
^1H NMR (400 MHz, CDCl_3): δ 7.37 – 7.05 (m, 35H), 5.69 (d, $J = 3.5$ Hz, 1H), 5.03 (d, $J = 11.6$ Hz, 1H), 4.91 – 4.39 (m, 13H), 4.27 (d, $J = 12.2$ Hz, 1H), 4.11 – 4.01 (m, 2H), 3.93 – 3.80 (m, 3H), 3.74 – 3.69 (m, 1H), 3.67 – 3.56 (m, 3H), 3.51 – 3.46 (m, 2H), 3.41 – 3.39 (m, 1H), 3.37 (s, 3H). ^1H NMR matches with the literature report.²¹⁹



Conditions D: 77% (120.4mg), $\alpha:\beta = 10:1$

^1H and ^{13}C NMR of disaccharide **8** has been reported.²²⁰

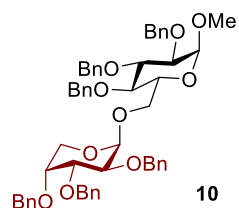
^1H NMR (400 MHz, CDCl_3): δ 7.43 – 7.10 (m, 20H), 5.53 (d, $J = 5.0$ Hz, 1H), 5.03 (d, $J = 3.6$ Hz, 1H), 4.95 (d, $J = 11.4$ Hz, 1H), 4.85 (d, $J = 11.7$ Hz, 1H), 4.78 – 4.72 (m, 3H), 4.62 – 4.56 (m, 2H), 4.52 – 4.40 (m, 2H), 4.35 – 4.29 (m, 2H), 4.10 – 3.95 (m, 5H), 3.84 – 3.73 (m, 2H), 3.62 – 3.51 (m, 2H), 1.54 (s, 3H), 1.45 (s, 3H), 1.35 – 1.29 (m, 6H). ^1H NMR matches with the literature report.²²⁰



Conditions E: 58% (86.4mg), α only

^1H and ^{13}C NMR of disaccharide **9** has been reported.²¹⁹

^1H NMR (CDCl_3 , 400 MHz): $\delta = 7.39 - 7.21$ (m, 20H), 4.98 – 4.92 (m, 2H), 4.87 – 4.81 (m, 2H), 4.75 – 4.68 (m, 3H), 4.59 (d, $J = 11.3$ Hz, 1H), 4.48 (d, $J = 11.9$ Hz, 1H), 4.39 (d, $J = 11.9$ Hz, 1H), 4.24 (dd, $J = 9.2, 4.5$ Hz, 1H), 4.16 – 4.04 (m, 4H), 3.96 (dd, $J = 10.2, 2.7$ Hz, 1H), 3.77 – 3.60 (m, 2H), 3.50 (dd, $J = 8.3, 4.6$ Hz, 1H), 3.36 – 3.27 (m, 4H), 1.37 (s, 3H), 1.30 (d, $J = 6.3$ Hz, 3H), 1.25 (s, 3H). ^1H NMR matches with the literature report.²¹⁹

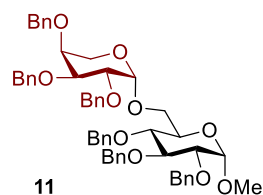


Conditions C: 48% (62mg), $\alpha:\beta = 9:1$

$^1\text{H NMR}$ (CDCl_3 , 400 MHz): $\delta = 7.42\text{--}7.22$ (m, 30 H), 5.00–4.60 (m, 14 H), 4.03–3.56 (m, 10 H), 3.50 (dd, $J = 8.0, 4.0$ Hz, 1 H), 3.32 (s, 3 H).

$^{13}\text{C NMR}$ (CDCl_3 , 100 MHz): $\delta = 138.7, 138.62, 138.58, 138.4, 138.3, 138.2, 128.4, 128.31, 128.28, 128.2, 128.1, 1287.94, 127.90, 127.83, 127.75, 127.7, 127.6, 127.5, 98.3, 97.9, 82.0, 80.0, 77.7, 76.2, 75.7, 74.9, 73.7, 73.4, 73.2, 72.3, 71.7, 70.0, 66.4, 60.4, 55.0$.

HRMS (ESI): calc. for $\text{C}_{54}\text{H}_{58}\text{O}_{10}\text{Na}$ ($\text{M}+\text{Na}$): 889.3922; found: 889.3959.

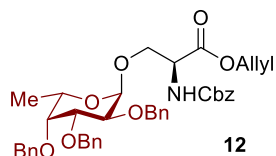


Conditions C: 47% (61mg), α only

$^1\text{H NMR}$ (CDCl_3 , 400 MHz): $\delta = 7.42\text{--}7.22$ (m, 30 H), 5.00–4.60 (m, 14 H), 4.03–3.96 (m, 2 H), 3.88–3.58 (m, 8 H), 3.46 (dd, $J = 12.0, 4.0$ Hz, 1 H), 3.32 (s, 3 H).

$^{13}\text{C NMR}$ (CDCl_3 , 100 MHz): $\delta = 138.82, 138.76, 138.6, 138.4, 138.3, 138.1, 128.32, 128.26, 128.24, 128.18, 127.91, 127.89, 127.8, 127.6, 127.4, 98.3, 97.8, 82.0, 80.0, 77.9, 76.3, 76.2, 75.6, 74.9, 73.9, 73.3, 72.8, 72.4, 71.6, 70.2, 66.4, 60.5, 54.9$.

HRMS (ESI): calc. for $\text{C}_{54}\text{H}_{58}\text{O}_{10}\text{Na}$ ($\text{M}+\text{Na}$): 889.3922; found: 889.3943.

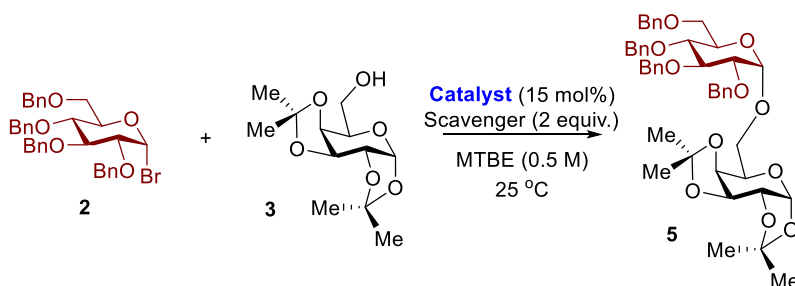


Conditions B: 80% (55.7 mg), $\alpha:\beta = 6:1$

$^1\text{H NMR}$ (400 MHz, CDCl_3): $\delta = 7.42 - 7.19$ (m, 20H), 6.08 (d, $J = 9.0$ Hz, 1H), 5.90 – 5.80 (m, 1H), 5.29 (d, $J = 17.2$ Hz, 1H), 5.21 – 5.12 (m, 3H), 4.97 (d, $J = 11.6$ Hz, 1H), 4.85 – 4.77 (m, 2H), 4.73 – 4.53 (m, 7H), 4.20 (dd, $J = 9.9, 2.2$ Hz, 1H), 4.01 (dd, $J = 10.1, 3.6$ Hz, 1H), 3.80 (dd, $J = 10.1, 2.7$ Hz, 1H), 3.73 (q, $J = 6.4$ Hz, 1H), 3.60 – 3.52 (m, 2H), 1.07 (d, $J = 6.4$ Hz, 3H).

$^{13}\text{C NMR}$ (CDCl_3 , 100 MHz): $\delta = 170.0, 156.2, 138.8, 138.5, 138.4, 136.3, 131.6, 128.5, 128.4, 128.3, 128.2, 128.1, 127.8, 127.6, 127.5, 118.6, 98.9, 79.0, 77.6, 76.4, 74.8, 73.3, 73.2, 69.0, 67.0, 66.8, 66.0, 54.4, 16.5$.

5.2.2. Standard procedure for catalyst screening



To a 10 mL oven-dried Schlenk flask, added alcohol **3** (0.1 mmol, 1.0 equiv.), catalyst (0.015 mmol, 15 mol%), acid scavenger (IBO or DTBMP, 0.2 mmol, 2.0 equiv.), then transferred glycosyl bromide **2** (0.2 mmol, 2 equiv.) with MTBE (0.2 mL). The resulting solution was stirred at 25 °C for 5 - 24 h, then directly subjected to Biotage Isolera One purification system to give **5** as a colorless syrup.

^1H and ^{13}C NMR of disaccharide **5** has been reported.²¹⁹

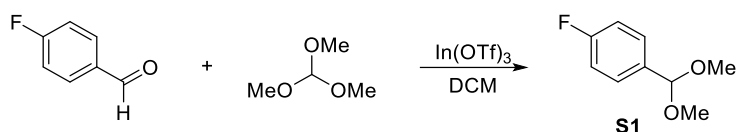
$^1\text{H NMR}$ (600 MHz, CDCl_3) $\delta = 7.38 - 7.23$ (m, 18H), 7.15 – 7.11 (m, 2H), 5.51 (d, $J = 5.0$ Hz, 1H), 4.99 (d, $J = 3.5$ Hz, 1H), 4.97 (d, $J = 10.9$ Hz, 1H), 4.80 (dd, $J = 12.5, 11.1$ Hz, 2H), 4.74 (d, $J = 11.9$ Hz, 1H), 4.68 (d, $J = 11.9$ Hz, 1H), 4.62 (d, $J = 12.1$ Hz, 1H), 4.59 (dd, $J = 7.9, 2.2$ Hz, 1H), 4.48 (d, $J = 7.9$ Hz, 1H),

4.46 (d, $J = 9.3$ Hz, 1H), 4.35 (dd, $J = 7.9, 1.6$ Hz, 1H), 4.30 (dd, $J = 5.0, 2.3$ Hz, 1H), 4.05 – 4.01 (m, 1H), 3.98 (t, $J = 9.3$ Hz, 1H), 3.84 – 3.80 (m, 1H), 3.80 – 3.72 (m, 3H), 3.69 – 3.62 (m, 2H), 3.58 (dd, $J = 9.6, 3.6$ Hz, 1H), 1.53 (s, 3H), 1.44 (s, 3H), 1.32 (s, 3H), 1.30 (s, 3H).

^1H NMR matches with the literature report.²¹⁹

5.2.3. Preparation of monosaccharide

Preparation of Methyl 6-*O*-(4-Fluorobenzyl)-2,3-bis-*O*-Benzyl- α -D-Glucopyranoside (17)



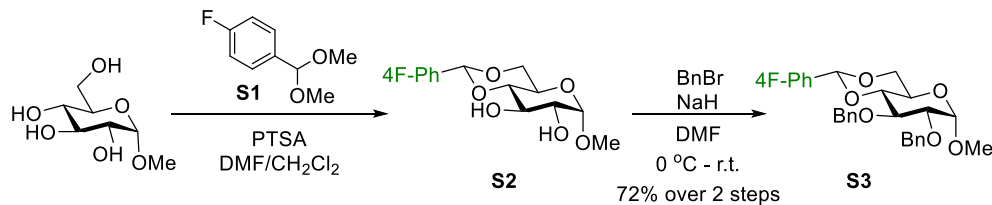
4-Fluorobenzaldehyde dimethyl acetal (**S1**) was prepared according to literature procedure.²²¹

To a 250 mL round-bottom flask, added CH_2Cl_2 (40 mL), 4-fluorobenzaldehyde (2.2 mL, 21 mmol) and trimethyl orthoformate (4.6 mL, 42 mmol), then stirred the mixture at room temperature. 5 minutes later, indium triflate (59 mg, 0.105 mmol) was added to the flask, and stirred for 10 minutes. Upon completion (monitored by TLC), the mixture was passed through a short plug of neutral alumina which was washed with additional CH_2Cl_2 (2 x 50 mL). The combined solution was concentrated *in vacuo*, and the resulting residue (**S1**) was directly used in the next step.

^1H NMR (400 MHz, CDCl_3): δ 7.38 (dd, $J = 8.5, 5.6$ Hz, 2H), 7.00 (t, $J = 8.7$ Hz, 1H), 5.32 (s, 1H), 3.26 (s, 3H).

^{19}F NMR (376 MHz, CDCl_3): δ -114.11 (tt, $J = 8.8, 5.5$ Hz).

^1H NMR matches with the literature report.²²²



To a 250 mL round-bottom flask with **S1** residue (21 mmol) in it, added methyl α -D-glucopyranoside (2g, 10.3 mmol), DMF (50 mL) and *p*-toluenesulfonic acid monohydrate (1 g, 5.15 mmol). The mixture was stirred at room temperature overnight, and then put on rotary evaporators to remove byproduct (MeOH) and excess solvent. Upon completion (monitored by TLC), the mixture was diluted with 300 mL ethyl acetate, and then washed with 100 mL deionized water, followed by 100 mL saturated sodium bicarbonate solution twice, and 100 mL brine. The organic solution was then dried over sodium sulfate, and concentrated *in vacuo* overnight to give **S2** as a white solid. The resulting residue (**S2**) was directly used in the next step.

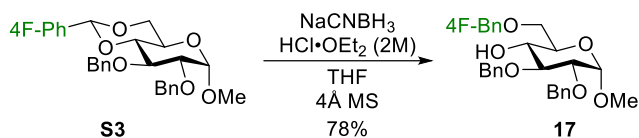
¹H NMR (400 MHz, CDCl₃): of crude δ 4.81 (d, J = 3.9 Hz, 1H- α).

The white residue **S2** was charged to a 500 ml round-bottom flask, and then DMF (75 mL) and benzyl bromide (3.7 mL, 31 mmol) were added to the flask. The solution was then cooled to 0 °C in an ice bath and sodium hydride (60% in mineral oil) (1.24 g, 31 mmol) was added in 3 portions. The mixture was stirred in ice bath overnight. The resulting solution was poured into chipped ice (~ 200 mL), and extracted with 300 mL ethyl acetate. The organic solution was washed with brine, dried over sodium sulfate, and then concentrated *in vacuo*. The residue was then subjected to Biotage Isolera One purification system to give 3.56 g (72% over two steps) of **S3** as a white solid.

¹H NMR (600 MHz, CDCl₃): δ 7.44 (dd, J = 8.4, 5.6 Hz, 2H), 7.38 – 7.24 (m, 10H), 7.04 (t, J = 8.6 Hz, 2H), 5.50 (s, 1H), 4.89 – 4.81 (m, 3H), 4.69 (d, J = 12.1 Hz, 1H), 4.58 (d, J = 3.6 Hz, 1H), 4.24 (dd, J = 10.2, 4.8 Hz, 1H), 4.02 (t, J = 9.3 Hz, 1H), 3.80 (td, J = 10.0, 4.8 Hz, 1H), 3.68 (t, J = 10.3 Hz, 1H), 3.57 (d, J = 9.6 Hz, 1H), 3.54 (dd, J = 9.5, 3.9 Hz, 1H), 3.39 (s, 3H).

^{13}C NMR (151 MHz, CDCl_3): δ 138.65, 138.08, 128.42, 128.28, 128.09, 127.95, 127.94, 127.90, 127.89, 127.57, 115.13, 114.99, 100.65, 99.20, 81.99, 79.20, 78.53, 75.31, 73.76, 69.01, 62.23, 55.35.

^{19}F NMR (376 MHz, CDCl_3): δ -113.01 (tt, $J = 8.7, 5.5$ Hz).



Methyl 6-*O*-(4-Fluorobenzyl)-2,3-bis-*O*-Benzyl- α -D-Glucopyranoside (**17**) was prepared according to literature procedure.²²³

To a 100 mL round-bottom flask, added **S3** (1 g, 2.08 mmol), THF (15 mL), and 4Å molecular sieves (1.5 g), stirred at room temperature for 30 minutes. Then sodium cyanoborohydride (1.3 g, 20.8 mmol) was added to the solution. Upon all solid dissolved (~ 15 min), hydrogen chloride solution (2.0 M in diethyl ether) was added dropwise until the evolution of gas ceased (~ 10 mL). Upon completion (~5 min, monitored by TLC), the mixture was diluted with 150 mL ethyl acetate, and then washed with 50 mL saturated sodium bicarbonate solution three times. The organic solution was dried over sodium sulfate, and concentrated *in vacuo*. The residue was then subjected to Biotage Isolera One purification system to give **17** as a colorless syrup.

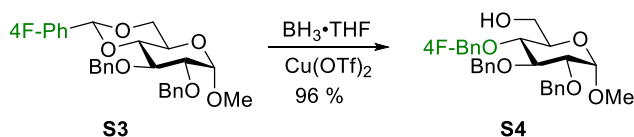
^1H NMR (600 MHz, CDCl_3): δ 7.37 – 7.24 (m, 12H), 6.99 (t, $J = 8.7$ Hz, 2H), 5.00 (d, $J = 11.5$ Hz, 1H), 4.76 (d, $J = 12.1$ Hz, 1H), 4.72 (d, $J = 11.5$ Hz, 1H), 4.65 (d, $J = 12.1$ Hz, 1H), 4.63 (d, $J = 3.5$ Hz, 1H), 4.53 (d, $J = 12.0$ Hz, 1H), 4.49 (d, $J = 12.0$ Hz, 1H), 3.77 (t, $J = 9.2$ Hz, 1H), 3.69 (dt, $J = 9.6, 3.7$ Hz, 1H), 3.65 (d, $J = 3.8$ Hz, 2H), 3.57 (t, $J = 9.3$ Hz, 1H), 3.52 (dd, $J = 9.6, 3.5$ Hz, 1H), 3.37 (s, 3H).

^{13}C NMR (151 MHz, CDCl_3) δ 163.23, 161.60, 138.87, 138.13, 133.90, 133.88, 129.45, 129.40, 128.71, 128.58, 128.22, 128.10, 128.07, 127.98, 115.36, 115.22, 98.29, 81.54, 79.74, 75.52, 73.24, 72.96, 70.63, 70.03, 69.52.

^{19}F NMR (564 MHz, CDCl_3): δ -114.91 – -114.97 (m).

HRMS (ESI): calc. for $\text{C}_{28}\text{H}_{31}\text{O}_6\text{FNa}$ ($\text{M}+\text{Na}$): 505.1997; found: 505.1999.

Preparation of 2,3-bis-*O*-Benzyl-4-*O*-(4-Fluorobenzyl)-*D*-Glucopyranose (**S2**)



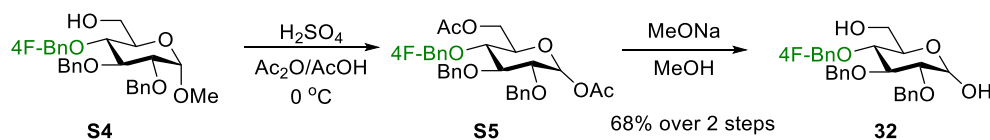
Methyl 2,3-bis-*O*-Benzyl-4-(4-Fluorobenzyl)- α -*D*-Glucopyranoside (**S4**) was prepared according to literature procedure.²²⁴

To a 25 mL Schlenk flask, under nitrogen, added **S3** (500 mg, 1.04 mmol) and borane tetrahydrofuran complex solution (1 M in THF), and then stirred at room temperature for 10 minutes. Next, copper(II) trifluoromethanesulfonate (18 mg, 0.05 mmol) was added to the flask. Upon completion (monitored by TLC), the reaction was cooled to 0 °C, and sequentially quenched with triethylamine and methanol (*Caution: hydrogen gas evolved!*). The solution was then concentrated *in vacuo* and subjected to Biotage Isolera One purification system to give 483.4 mg (96%) of **S4** as a colorless syrup.

¹H NMR (400 MHz, CDCl₃) δ 7.39 – 7.19 (m, 12H), 6.99 (t, J = 8.7 Hz, 2H), 5.00 (d, J = 11.0 Hz, 1H), 4.85 – 4.76 (m, 3H), 4.66 (d, J = 12.1 Hz, 1H), 4.59 (d, J = 12.8 Hz, 1H), 4.57 (d, J = 3.7 Hz, 1H, H-1 α), 3.99 (t, J = 9.3 Hz, 1H), 3.78 (d, J = 11.4 Hz, 1H), 3.72 – 3.62 (m, 2H), 3.54 – 3.47 (m, 2H), 3.37 (s, 3H), 1.70 (brs, 1H, -OH).

¹³C NMR (101 MHz, CDCl₃) δ 138.70, 138.05, 129.73, 129.65, 128.47, 128.40, 128.11, 127.95, 127.85, 127.62, 115.38, 115.17, 98.14, 81.86, 79.99, 77.39, 75.70, 74.26, 73.40, 70.58, 61.85, 55.20.

¹⁹F NMR (376 MHz, CDCl₃) δ -114.26 – -114.77 (m).



To a 50 mL round-bottom flask, added **S4** (483.4 mg, 1 mmol), acetic acid (2.5 mL), and acetic anhydride (2.5 mL). The mixture was cooled to 0 °C in an ice bath, and then concentrated sulfuric acid

(0.11 mL, 2 mmol) was added to the reaction. Upon completion (~15 min, monitored by TLC), the mixture was diluted with 150 mL ethyl acetate, and then washed with 50 mL saturated sodium bicarbonate solution three times, followed by 50 mL brine. The organic solution was dried over sodium sulfate, and concentrated *in vacuo* overnight to give **S5** a colorless syrup. The resulting residue (**S5**) was directly used in the next step.

¹H NMR (499 MHz, CDCl₃) of α/β (5/1) mixture (crude) δ 6.32 (d, $J = 3.5$ Hz, 1H- α), 5.61 (d, $J = 8.2$ Hz, 1H- β).

To a 50 mL round-bottom flask with **S5** inside, added dry methanol (5 mL) and sodium methoxide (27 mg, 0.5 mmol). The mixture was stirred at room temperature overnight. Upon completion (monitored by TLC), the reaction was neutralized with Amberlyst® 15 hydrogen form, then filtered. The resulting solution was then concentrated *in vacuo* and subjected to Biotage Isolera One purification system to give 320.1 mg (66% over two steps) of **32** as a white solid.

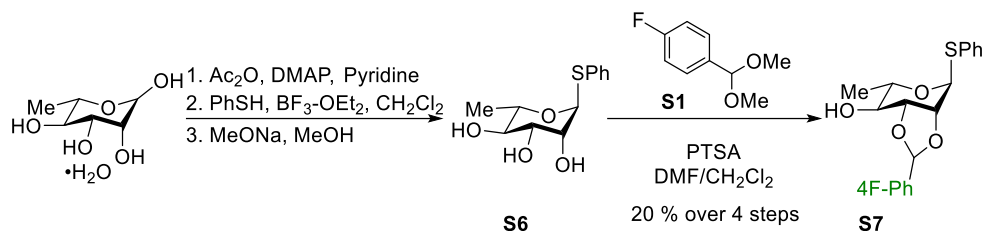
¹H NMR (600 MHz, CDCl₃) of $\alpha:\beta = 2:1$ mixture δ 7.37 – 7.26 (m, 28H), 7.24 – 7.18 (m, 6H), 7.02 – 6.95 (m, 6H), 5.18 (d, $J = 3.5$ Hz, 2H, H-1 α), 4.96 – 4.90 (m, 4H), 4.84 – 4.73 (m, 10H), 4.68 (d, $J = 11.7$ Hz, 2H), 4.63 – 4.57 (m, 3H), 3.95 (t, $J = 9.2$ Hz, 2H), 3.93 – 3.89 (m, 2H), 3.85 (dd, $J = 12.0, 2.4$ Hz, 1H), 3.79 (dd, $J = 11.9, 2.5$ Hz, 2H), 3.73 – 3.64 (m, $J = 18.2, 14.1, 6.4$ Hz, 4H), 3.58 – 3.50 (m, 5H), 3.42 – 3.38 (m, 1H), 3.36 (dd, $J = 9.1, 7.8$ Hz, 1H), 3.32 (brs, 1H, β -OH, hemiacetal), 3.00 (brs, 2H, α -OH, hemiacetal), 2.02 (brs, 1H, β -OH), 1.74 (brs, 2H, α -OH).

¹³C NMR (151 MHz, CDCl₃) δ 138.52, 138.36, 138.13, 137.63, 133.89, 133.87, 129.75, 129.70, 129.65, 128.54, 128.44, 128.41, 128.10, 128.07, 128.02, 127.82, 127.77, 127.72, 127.68, 127.67, 115.38, 115.35, 115.24, 115.21, 97.38, 91.24, 84.36, 83.14, 81.47, 80.15, 77.35, 75.63, 75.29, 74.82, 74.25, 73.34, 70.97, 61.88, 61.75.

¹⁹F NMR (376 MHz, CDCl₃, ¹H decoupled) δ -114.32 (s, β), -114.44 (s, α).

HRMS (ESI): calc. for C₂₇H₂₉O₆FNa (M+Na): 491.1840; found: 491.1846

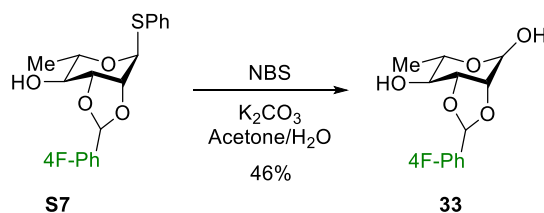
Preparation of 6-Deoxy-2,3-O-(4-Fluorobenzylidene)-L-Mannopyranose (**33**)



Procedures of **S6** → **S7** refer to synthesis of **S2**.

¹H NMR (400 MHz, CDCl₃) of diastereomer mixture (~1:1.5) δ 7.53 – 7.39 (m, 11H), 7.36 – 7.28 (m, 8H), 6.14 (s, 2H), 5.93 (s, 1H), 5.87 (s, 1H), 5.78 (s, 2H), 4.43 (dd, *J* = 7.0, 4.8 Hz, 3H), 4.33 (d, *J* = 5.3 Hz, 2H), 4.29 – 4.24 (m, 1H), 4.22 – 4.09 (m, 3H), 3.62 (dd, *J* = 9.8, 7.6 Hz, 2H), 3.45 (dd, *J* = 9.7, 7.3 Hz, 1H), 2.24 (s, 2H), 1.30 (d, *J* = 6.2 Hz, 5H), 1.24 (d, *J* = 6.2 Hz, 3H).

¹⁹F NMR (376 MHz, CDCl₃) δ -111.94 (tt, *J* = 8.5, 5.4 Hz), -112.34 (tt, *J* = 8.7, 5.4 Hz).



To a 100 mL round-bottom flask with **S7** (2.07 g, 5.7 mmol) inside, added acetone (50 mL), deionized water (7 mL), N-bromosuccinimide (2.03 g, 11.4 mmol) and potassium carbonate (3.93 g, 28.5 mmol). The mixture was stirred at room temperature overnight. Upon completion (monitored by TLC), the mixture was diluted with 250 mL ethyl acetate, and then washed with 100 mL saturated sodium bicarbonate solution three times. The organic solution was dried over sodium sulfate, and concentrated *in vacuo*. The residue was then subjected to Biotage Isolera One purification system to give **33** as a white solid.

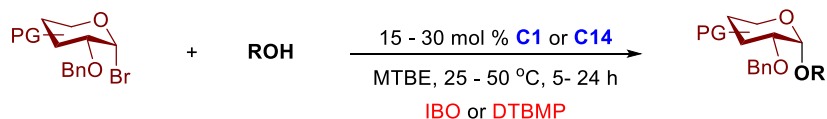
¹H NMR (400 MHz, CDCl₃) δ 7.44 (dd, *J* = 8.6, 5.4 Hz, 2H), 7.07 (t, *J* = 8.6 Hz, 2H), 5.93 (s, 1H), 5.57 (s, 1H), 5.00 (dd, *J* = 5.4, 3.9 Hz, 1H), 4.77 (d, *J* = 5.6 Hz, 1H), 4.13 (td, *J* = 12.6, 6.3 Hz, 1H), 4.00 (dd, *J* = 8.0, 3.7 Hz, 1H), 2.45 (s, 1H), 2.35 (s, 1H), 1.39 (d, *J* = 6.3 Hz, 3H).

^{13}C NMR (151 MHz, CDCl_3) δ 128.65, 128.59, 115.51, 115.36, 105.02, 101.28, 85.05, 84.15, 80.03, 66.22, 20.32.

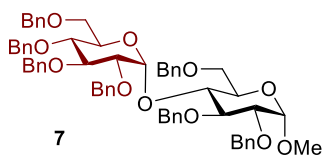
^{19}F NMR (376 MHz, CDCl_3) δ -111.46 (tt, $J = 8.7, 5.4$ Hz).

HRMS (ESI): calc. for $\text{C}_{13}\text{H}_{16}\text{O}_5\text{F}$ (M+H): 271.0976; found: 271.0975.

5.2.4. Standard procedures for C1 or C14-catalyzed glycosylation (Table 9 and Scheme 33)



To a 10 mL oven-dried Schlenk flask, added alcohol **2** (0.1 mmol, 1.0 equiv.), catalyst (**C1** or **C14**, 0.015 – 0.03 mmol, 15 – 30 mol%), acid scavenger (IBO or DTBMP, 0.2 mmol, 2.0 equiv.), then transferred glycosyl bromide (0.2 mmol, 2 equiv.) with MTBE or CH_2Cl_2 (0.2 mL). The resulting solution was stirred at 25 - 50 °C for 24 - 48 h, then directly subjected to Biotage Isolera One purification system to give desired products.

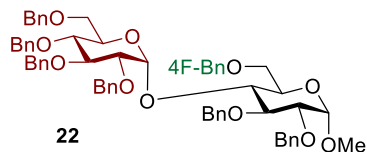


Reaction was conducted with 30 mol% catalyst at 50 °C.

^1H and ^{13}C NMR of disaccharide **7** has been reported.²¹⁹

^1H NMR (600 MHz, CDCl_3) δ 7.35 – 7.25 (m, 33H), 7.17 – 7.13 (m, 2H), 5.74 (d, $J = 3.6$ Hz, 1H), 5.08 (d, $J = 11.6$ Hz, 1H), 4.93 (d, $J = 10.8$ Hz, 1H), 4.87 – 4.80 (m, 3H), 4.74 (d, $J = 12.1$ Hz, 1H), 4.66 – 4.53 (m, 7H), 4.47 (d, $J = 10.9$ Hz, 1H), 4.33 (d, $J = 12.2$ Hz, 1H), 4.14 (t, $J = 9.0$ Hz, 1H), 4.10 (t, $J = 9.0$ Hz, 1H), 3.96 (t, $J = 9.3$ Hz, 1H), 3.92 – 3.87 (m, 2H), 3.79 – 3.75 (m, 1H), 3.73 – 3.67 (m, 2H), 3.64 (dd, $J = 9.3, 3.5$ Hz, 2H), 3.56 – 3.53 (m, 2H), 3.46 – 3.43 (m, 1H), 3.42 (s, 3H).

^1H NMR matches with the literature report.²¹⁹



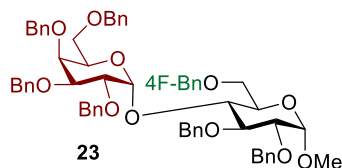
Reaction was conducted with 30 mol% catalyst at 50 °C.

¹H NMR (600 MHz, CDCl₃) δ 7.31 – 7.15 (m, 30H), 7.11 – 7.08 (m, 2H), 6.90 (t, *J* = 8.6 Hz, 2H), 5.67 (d, *J* = 3.5 Hz, 1H), 5.02 (d, *J* = 11.6 Hz, 1H), 4.88 (d, *J* = 10.8 Hz, 1H), 4.80 (d, *J* = 3.4 Hz, 1H), 4.77 (d, *J* = 10.6 Hz, 2H), 4.69 (d, *J* = 12.1 Hz, 1H), 4.60 – 4.50 (m, 5H), 4.43 – 4.41 (m, 3H), 4.31 (d, *J* = 12.2 Hz, 1H), 4.07 (t, *J* = 9.1 Hz, 1H), 4.01 (t, *J* = 9.2 Hz, 1H), 3.89 (t, *J* = 9.3 Hz, 1H), 3.85 – 3.79 (m, 2H), 3.70 (d, *J* = 10.0 Hz, 1H), 3.66 – 3.60 (m, 2H), 3.58 (dd, *J* = 9.5, 3.5 Hz, 1H), 3.50 – 3.45 (m, 2H), 3.39 – 3.37 (m, 1H), 3.37 (s, 3H).

¹³C NMR (151 MHz, CDCl₃) δ 162.92, 161.29, 138.92, 138.72, 138.43, 137.95, 137.88, 133.86, 128.96, 128.91, 128.40, 128.30, 128.27, 128.25, 128.20, 128.17, 127.95, 127.90, 127.85, 127.76, 127.69, 127.64, 127.60, 127.56, 127.47, 127.07, 126.73, 115.08, 114.94, 97.76, 96.59, 82.01, 81.97, 80.19, 79.46, 77.64, 75.50, 74.97, 74.41, 73.47, 73.35, 73.22, 72.43, 72.29, 70.98, 69.47, 69.04, 68.19, 55.13.

¹⁹F NMR (564 MHz, CDCl₃) δ -115.15 – -115.24 (m).

HRMS (ESI): calc. for C₆₂H₆₅O₁₁FNa (M+Na): 1027.4403; found: 1027.4436.



Reaction was conducted with 30 mol% catalyst at 50 °C.

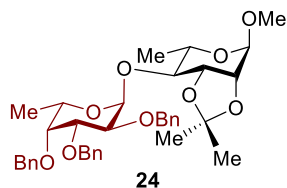
¹H NMR (600 MHz, CDCl₃) δ 7.35 – 7.18 (m, 32H), 6.95 (t, *J* = 8.6 Hz, 2H), 5.76 (d, *J* = 3.8 Hz, 1H), 4.98 (d, *J* = 11.5 Hz, 1H), 4.89 (d, *J* = 11.4 Hz, 1H), 4.84 (d, *J* = 11.4 Hz, 1H), 4.73 (d, *J* = 11.7 Hz, 1H), 4.71 – 4.66 (m, 3H), 4.59 – 4.53 (m, 5H), 4.38 (d, *J* = 12.1 Hz, 1H), 4.30 (dd, *J* = 27.2, 11.6 Hz, 3H), 4.08 (t, *J* = 9.1 Hz, 1H), 4.02 (dd, *J* = 10.3, 3.8 Hz, 1H), 3.98 – 3.93 (m, 2H), 3.89 – 3.82 (m, 3H), 3.71 (dd, *J* = 10.6,

4.7 Hz, 1H), 3.63 (dd, $J = 10.6, 1.9$ Hz, 1H), 3.56 (dd, $J = 9.6, 3.5$ Hz, 1H), 3.51 (t, $J = 8.2$ Hz, 1H), 3.44 (dd, $J = 8.8, 5.5$ Hz, 1H), 3.39 (s, 3H).

^{13}C NMR (151 MHz, CDCl_3) δ 162.95, 161.33, 138.97, 138.56, 138.55, 138.27, 137.99, 137.95, 134.11, 134.09, 129.26, 129.20, 128.40, 128.36, 128.32, 128.30, 128.23, 128.23, 128.18, 128.17, 127.89, 127.84, 127.77, 127.73, 127.61, 127.46, 127.38, 127.04, 126.74, 115.09, 114.95, 97.75, 97.57, 81.97, 80.16, 79.18, 75.61, 74.77, 74.53, 74.37, 73.84, 73.46, 73.37, 72.92, 72.71, 72.36, 69.93, 69.47, 69.39, 68.75, 55.11.

^{19}F NMR (564 MHz, CDCl_3) δ -115.03 – -115.11 (m).

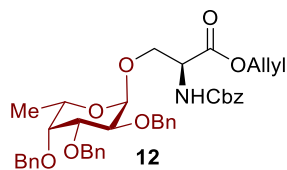
HRMS (ESI): calc. for $\text{C}_{62}\text{H}_{65}\text{O}_{11}\text{FNa}$ ($\text{M}+\text{Na}$): 1027.4403; found: 1027.4434.



Reaction was conducted with 30 mol% catalyst at 25 °C.

^1H NMR (600 MHz, CDCl_3) δ 7.43 – 7.23 (m, 15H), 5.66 (d, $J = 3.9$ Hz, 1H), 4.97 (d, $J = 11.6$ Hz, 1H), 4.89 (d, $J = 11.7$ Hz, 1H), 4.85 (s, 1H), 4.81 (d, $J = 11.5$ Hz, 1H), 4.76 – 4.70 (m, 2H), 4.66 (d, $J = 11.6$ Hz, 1H), 4.31 (dd, $J = 7.2, 5.9$ Hz, 1H), 4.11 – 4.03 (m, 2H), 3.91 (q, $J = 6.5$ Hz, 1H), 3.86 (dd, $J = 10.2, 2.8$ Hz, 1H), 3.74 (dq, $J = 12.4, 6.2$ Hz, 1H), 3.69 – 3.65 (m, 1H), 3.56 (dd, $J = 9.9, 7.4$ Hz, 1H), 3.34 (s, 3H), 1.51 (s, 3H), 1.35 (s, 3H), 1.24 (d, $J = 6.2$ Hz, 4H), 1.10 (d, $J = 6.5$ Hz, 3H).

^{13}C NMR (151 MHz, CDCl_3) δ 139.01, 138.55, 138.48, 128.51, 128.31, 128.23, 128.13, 127.54, 127.54, 127.41, 127.39, 109.26, 98.02, 95.92, 79.27, 78.68, 77.55, 77.38, 76.13, 76.06, 74.69, 73.39, 72.91, 66.56, 63.82, 54.63, 27.96, 26.42, 18.03, 16.60.

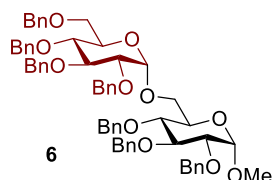


Reaction was conducted with 20 mol% catalyst at 25 °C.

^1H and ^{13}C NMR of **20** has been reported.²²⁵

^1H NMR (600 MHz, CDCl_3) δ 7.42 – 7.19 (m, 20H), 6.05 (d, $J = 9.0$ Hz, 1H), 5.85 (dq, $J = 10.9, 5.7$ Hz, 1H), 5.28 (d, $J = 17.2$ Hz, 1H), 5.18 (d, $J = 10.4$ Hz, 1H), 5.16 – 5.11 (m, 2H), 4.96 (d, $J = 11.6$ Hz, 1H), 4.80 (t, $J = 12.2$ Hz, 2H), 4.70 (d, $J = 11.8$ Hz, 1H), 4.68 (d, $J = 3.4$ Hz, 1H), 4.64 – 4.59 (m, 4H), 4.58 – 4.54 (m, 1H), 4.19 (dd, $J = 9.9, 2.0$ Hz, 1H), 4.00 (dd, $J = 10.1, 3.6$ Hz, 1H), 3.80 (dd, $J = 10.1, 2.7$ Hz, 1H), 3.72 (q, $J = 6.3$ Hz, 1H), 3.58 – 3.54 (m, 2H), 1.07 (d, $J = 6.5$ Hz, 3H).

^1H NMR matches with the literature report.²²⁵

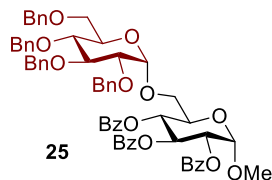


Reaction was conducted with 20 mol% catalyst at 25 °C.

^1H and ^{13}C NMR of disaccharide **6** has been reported.²¹⁹

^1H NMR (600 MHz, CDCl_3) δ 7.40 – 7.24 (m, 33H), 7.19 – 7.16 (m, 2H), 5.04 (d, $J = 3.4$ Hz, 1H), 5.02 (d, $J = 10.9$ Hz, 1H), 4.99 (t, $J = 6.7$ Hz, 1H), 4.97 (d, $J = 11.1$ Hz, 1H), 4.87 (dd, $J = 10.8, 8.4$ Hz, 2H), 4.83 (d, $J = 10.9$ Hz, 1H), 4.76 (d, $J = 12.0$ Hz, 1H), 4.72 – 4.68 (m, 3H), 4.64 – 4.60 (m, 3H), 4.51 (d, $J = 11.0$ Hz, 1H), 4.47 (d, $J = 12.1$ Hz, 1H), 4.04 (t, $J = 7.2$ Hz, 1H), 4.01 (t, $J = 7.2$ Hz, 1H), 3.88 (dd, $J = 11.6, 4.5$ Hz, 1H), 3.85 – 3.81 (m, 2H), 3.79 – 3.75 (m, 1H), 3.73 – 3.66 (m, 3H), 3.62 – 3.58 (m, 2H), 3.49 (dd, $J = 9.6, 3.5$ Hz, 1H), 3.40 (s, 3H).

^1H NMR matches with the literature report.²¹⁹

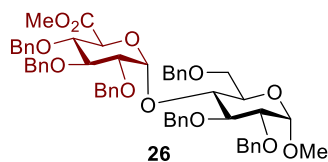


Reaction was conducted with 20 mol% catalyst at 25 °C.

^1H and ^{13}C NMR of disaccharide **25** has been reported.²²⁶

^1H NMR (600 MHz, CDCl_3) δ 8.03 – 8.00 (m, 2H), 7.99 – 7.97 (m, 2H), 7.91 – 7.88 (m, 2H), 7.51 (q, $J = 7.6$ Hz, 2H), 7.45 – 7.21 (m, 25H), 7.17 (d, $J = 6.6$ Hz, 2H), 6.19 (t, $J = 9.7$ Hz, 1H), 5.58 (t, $J = 9.9$ Hz, 1H), 5.28 – 5.23 (m, 2H), 4.95 (d, $J = 10.9$ Hz, 1H), 4.86 (d, $J = 11.0$ Hz, 1H), 4.83 – 4.77 (m, 3H), 4.66 (d, $J = 12.2$ Hz, 1H), 4.58 (d, $J = 12.1$ Hz, 1H), 4.49 (d, $J = 11.0$ Hz, 1H), 4.41 (d, $J = 12.1$ Hz, 1H), 4.38 – 4.33 (m, 1H), 4.01 (t, $J = 9.3$ Hz, 1H), 3.92 – 3.86 (m, 2H), 3.70 – 3.65 (m, 2H), 3.63 (dd, $J = 11.0, 1.9$ Hz, 1H), 3.58 (dd, $J = 9.7, 3.5$ Hz, 1H), 3.54 (dd, $J = 10.6, 1.7$ Hz, 1H), 3.47 (s, 3H).

^1H NMR matches with the literature report.²²⁶

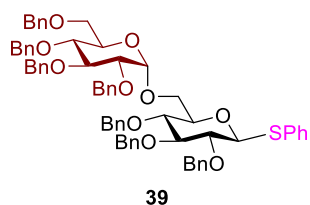


Reaction was conducted with 30 mol% catalyst at 50 °C.

^1H NMR (600 MHz, CDCl_3) δ 7.34 – 7.15 (m, 30H), 5.75 (d, $J = 3.6$ Hz, 1H), 5.02 (d, $J = 11.7$ Hz, 1H), 4.85 (d, $J = 10.9$ Hz, 1H), 4.80 – 4.75 (m, 3H), 4.68 (d, $J = 12.1$ Hz, 1H), 4.65 (d, $J = 12.3$ Hz, 1H), 4.61 (d, $J = 3.4$ Hz, 1H), 4.60 (d, $J = 8.6$ Hz, 1H), 4.57 – 4.54 (m, 2H), 4.52 (d, $J = 9.1$ Hz, 1H), 4.50 (d, $J = 8.8$ Hz, 1H), 4.30 (d, $J = 9.9$ Hz, 1H), 4.11 – 4.05 (m, 2H), 3.94 (t, $J = 9.3$ Hz, 1H), 3.89 – 3.83 (m, 2H), 3.72 (t, $J = 9.5$ Hz, 2H), 3.59 (dd, $J = 8.7, 2.9$ Hz, 1H), 3.52 (dd, $J = 9.7, 3.6$ Hz, 1H), 3.46 (s, 3H), 3.39 (s, 3H).

^{13}C NMR (151 MHz, CDCl_3) δ 170.31, 139.06, 138.55, 138.44, 138.11, 138.03, 137.89, 128.54, 128.46, 128.44, 128.42, 128.34, 128.32, 128.30, 128.04, 127.91, 127.88, 127.74, 127.73, 127.72, 127.41, 127.35,

127.18, 126.72, 97.87, 97.29, 81.87, 81.26, 80.30, 79.89, 78.88, 77.37, 77.16, 76.95, 75.71, 75.19, 74.42, 73.55, 73.45, 73.31, 71.24, 69.44, 69.09, 55.33, 52.29.

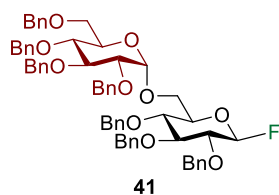


Reaction was conducted with 15 mol% catalyst at 25 °C.

^1H and ^{13}C NMR of disaccharide **39** has been reported.²²⁷

^1H NMR (600 MHz, CDCl_3) δ 7.63 – 7.60 (m, 2H), 7.48 (d, $J = 7.2$ Hz, 2H), 7.44 – 7.27 (m, 32H), 7.25 – 7.18 (m, 4H), 5.11 (d, $J = 3.5$ Hz, 1H), 5.06 (d, $J = 10.9$ Hz, 1H), 4.95 (dd, $J = 11.1, 3.7$ Hz, 2H), 4.93 – 4.85 (m, 5H), 4.81 (d, $J = 12.1$ Hz, 1H), 4.75 (d, $J = 11.1$ Hz, 1H), 4.71 (d, $J = 9.9$ Hz, 1H), 4.68 (d, $J = 5.3$ Hz, 1H), 4.67 (d, $J = 7.2$ Hz, 1H), 4.55 (d, $J = 11.0$ Hz, 1H), 4.51 (d, $J = 12.1$ Hz, 1H), 4.06 (t, $J = 9.3$ Hz, 1H), 3.96 – 3.90 (m, 2H), 3.87 – 3.84 (m, 1H), 3.80 – 3.71 (m, 4H), 3.70 – 3.65 (m, 2H), 3.57 (ddd, $J = 9.8, 4.7, 1.5$ Hz, 1H), 3.34 (dd, $J = 9.7, 8.8$ Hz, 1H).

^1H NMR matches with the literature report.²²⁷



Reaction was conducted with 15 mol% catalyst at 25 °C.

^1H and ^{13}C NMR of disaccharide **41** has been reported.²²⁸

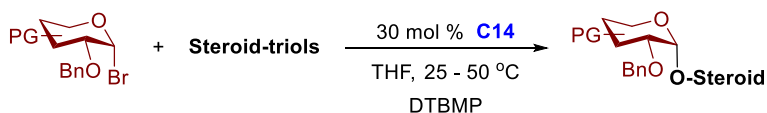
^1H NMR (600 MHz, CDCl_3) δ 7.54 – 7.09 (m, 35H), 5.28 (dd, $J = 52.9, 6.8$ Hz, 1H), 5.08 (d, $J = 3.5$ Hz, 1H), 5.04 (d, $J = 10.9$ Hz, 1H), 4.93 (dd, $J = 11.1, 4.7$ Hz, 2H), 4.90 (d, $J = 10.9$ Hz, 1H), 4.86 (d, $J = 10.9$ Hz, 1H), 4.82 (d, $J = 11.1$ Hz, 2H), 4.82 (d, $J = 11.1$ Hz, 2H), 4.79 (d, $J = 7.6$ Hz, 2H), 4.72 (d, $J = 11.2$ Hz, 1H), 4.65 (d, $J = 12.3$ Hz, 2H), 4.54 (d, $J = 10.9$ Hz, 1H), 4.50 (d, $J = 12.1$ Hz, 1H), 4.05 (t, $J = 9.3$ Hz,

1H), 3.92 (dd, $J = 12.0, 4.2$ Hz, 1H), 3.86 (dd, $J = 18.5, 9.5$ Hz, 3H), 3.75 (dd, $J = 10.7, 3.6$ Hz, 1H), 3.71 (t, $J = 9.3$ Hz, 2H), 3.67 – 3.63 (m, 3H), 3.51 – 3.45 (m, 1H).

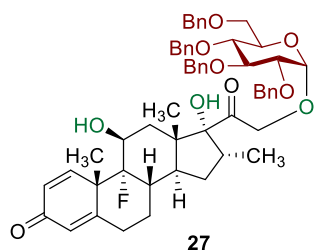
^{19}F NMR (564 MHz, CDCl_3) δ -136.94 (dd, $J = 52.9, 11.7$ Hz, β -isomer), -138.06 (dd, $J = 53.0, 12.3$ Hz, α -isomer).

^1H NMR matches with the literature report.²²⁸

5.2.5. Standard procedures for C14-catalyzed site-selective glycosylation (Scheme 32)



To a 10 mL oven-dried Schlenk flask, added Steroid-triol (0.1 mmol, 1.0 equiv.), catalyst (**C14**, 0.03 mmol, 30 mol%), DTBMP (0.2 mmol, 2.0 equiv.), then transferred glycosyl bromide **2** (0.2 mmol, 2 equiv.) with THF (0.2 mL). The resulting solution was stirred at 25 - 50 °C for 48 - 96 h, then directly subjected to Biotage Isolera One purification system to give desired products.



Reaction was conducted at 25 °C for 96 h.

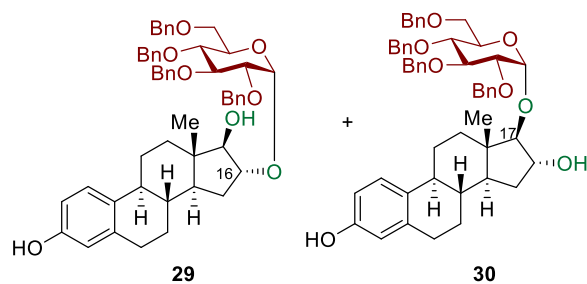
^1H NMR (600 MHz, C_6D_6) δ 7.45 (d, $J = 7.5$ Hz, 2H), 7.35 (d, $J = 7.4$ Hz, 2H), 7.30 (d, $J = 7.5$ Hz, 2H), 7.23 (d, $J = 7.4$ Hz, 2H), 7.21 – 7.13 (m, 7H), 7.12 – 7.06 (m, 5H), 6.91 (d, $J = 10.1$ Hz, 1H), 6.48 (dd, $J = 10.1, 1.6$ Hz, 1H), 6.23 (s, 1H), 5.27 (d, $J = 3.4$ Hz, 1H, H-1), 5.05 (d, $J = 11.4$ Hz, 1H), 4.95 (d, $J = 11.3$ Hz, 1H), 4.86 (d, $J = 11.4$ Hz, 1H), 4.82 (d, $J = 11.4$ Hz, 1H), 4.79 (d, $J = 17.1$ Hz, 1H), 4.63 (d, $J = 11.5$ Hz, 1H), 4.60 (d, $J = 11.3$ Hz, 1H), 4.54 (d, $J = 17.0$ Hz, 1H), 4.42 (d, $J = 12.2$ Hz, 1H), 4.38 (d, $J = 12.2$ Hz, 1H), 4.34 (t, $J = 9.3$ Hz, 1H), 4.21 – 4.16 (m, 1H), 4.00 – 3.98 (m, 1H), 3.75 – 3.67 (m, 3H), 3.65 (dd,

$J = 9.6, 3.5$ Hz, 1H), 3.21 – 3.10 (m, 2H), 2.41 – 2.39 (m, 1H), 2.25 – 2.15 (m, 1H), 2.11 – 1.92 (m, 2H), 1.91 – 1.84 (m, 2H), 1.46 – 1.30 (m, 4H), 1.28 (s, 3H), 1.27 – 1.20 (m, 1H), 1.06 (s, 3H), 1.03 – 0.94 (m, 2H), 0.83 (d, $J = 7.2$ Hz, 3H).

^{13}C NMR (151 MHz, C_6D_6) δ 207.62, 186.09, 165.50, 151.88, 139.72, 139.20, 138.99, 138.86, 130.28, 128.70, 128.65, 128.57, 128.56, 128.53, 128.35, 128.14, 127.98, 127.76, 127.61, 101.00, 99.83, 97.31, 91.57, 88.88, 82.19, 80.73, 78.39, 75.61, 75.17, 73.70, 72.89, 72.34, 72.08, 71.84, 71.07, 69.93, 48.68, 48.44, 48.28, 44.12, 37.03, 36.28, 34.99, 34.48, 34.35, 32.45, 31.02, 30.49, 30.23, 29.43, 27.58, 25.65, 23.07, 18.96, 17.32, 14.91, 11.67.

^{19}F NMR (564 MHz, C_6D_6) δ -165.18 (dd, $J = 28.9, 10.1$ Hz).

HRMS (ESI): calc. for $\text{C}_{56}\text{H}_{63}\text{O}_{10}\text{FNa}$ ($\text{M}+\text{Na}$): 937.4297; found: 937.4327.



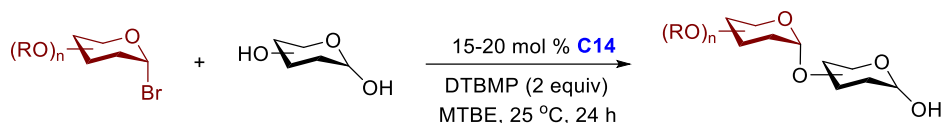
Reaction was conducted at 50 °C for 48 h.

29: ^1H NMR (600 MHz, CDCl_3) δ 7.42 – 7.26 (m, 18H), 7.17 – 7.13 (m, 2H), 7.10 (d, $J = 8.6$ Hz, 1H), 6.59 (dd, $J = 8.3, 2.4$ Hz, 1H), 6.53 (d, $J = 2.4$ Hz, 1H), 5.71 (brs, 1H, phenol-OH), 5.11 (d, $J = 3.6$ Hz, 1H), 5.02 (d, $J = 10.9$ Hz, 1H, H-1), 4.85 (d, $J = 11.4$ Hz, 2H), 4.81 (d, $J = 11.9$ Hz, 1H), 4.72 (d, $J = 11.9$ Hz, 1H), 4.62 (d, $J = 12.1$ Hz, 1H), 4.50 (dd, $J = 11.3, 9.0$ Hz, 2H), 4.08 (dd, $J = 11.8, 6.0$ Hz, 1H, H-16), 4.03 (t, $J = 9.3$ Hz, 1H), 3.92 – 3.89 (m, 1H), 3.74 (d, $J = 5.9$ Hz, 1H, H-17), 3.71 (dd, $J = 10.5, 4.3$ Hz, 1H), 3.67 (dd, $J = 10.4, 1.8$ Hz, 1H), 3.64 – 3.59 (m, 2H), 2.77 – 2.73 (m, 2H), 2.29 – 2.23 (m, 1H), 2.18 – 2.12 (m, 1H), 1.91 – 1.87 (m, 1H), 1.79 – 1.71 (m, 3H), 1.50 – 1.40 (m, 2H), 1.37 – 1.22 (m, 4H), 0.76 (s, 3H).

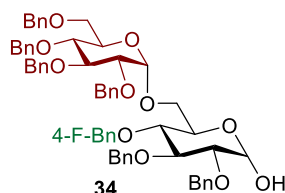
^{13}C NMR (151 MHz, CDCl_3) δ 153.41, 138.85, 138.13, 138.10, 137.88, 137.84, 132.39, 129.01, 128.52, 128.39, 128.38, 128.34, 128.22, 128.20, 127.98, 127.96, 127.88, 127.86, 127.74, 127.67, 127.56, 126.34, 125.27, 115.25, 112.69, 96.79, 87.84, 84.40, 82.00, 80.12, 77.96, 75.67, 75.16, 73.46, 73.18, 70.45, 68.69, 47.90, 43.79, 43.33, 38.24, 36.38, 31.25, 29.53, 27.06, 25.84, 21.43, 12.13.

Distinguished peak for **30**: ^1H NMR (600 MHz, CDCl_3) δ 4.31 – 4.27 (m, 1H, H-16), 3.98 – 3.95 (m, 1H, H-5), 3.51 (d, $J = 5.6$ Hz, 1H, H-17), 0.79 (s, 3H).

5.2.5. Standard procedures for C14-catalyzed chemoselective glycosylation (Table 10)



To a 10 mL oven-dried Schlenk flask, added Steroid-triol (0.15 – 0.3 mmol, 1.5 - 3 equiv.), catalyst (**C14**, 0.015 – 0.02 mmol, 15 - 20 mol%), DTBMP (0.2 mmol, 2.0 equiv.), then transferred glycosyl bromide (0.1 mmol, 1 equiv.) with MTBE (0.2 mL). The resulting solution was stirred at 25 - 50 °C for 24 h, then directly subjected to Biotage Isolera One purification system to give desired products.



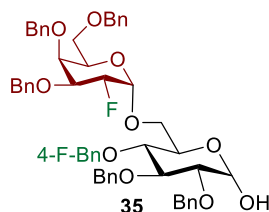
Reaction was conducted with 15 mol% catalyst at 25 °C.

^1H NMR (499 MHz, CDCl_3) δ 7.44 – 7.18 (m, 45H), 7.17 – 7.11 (m, 3H), 7.00 – 6.91 (m, 3H), 5.17 (d, $J = 3.4$ Hz, 1H), 5.06 – 4.93 (m, 4H), 4.93 – 4.79 (m, 6H), 4.79 – 4.66 (m, 6H), 4.65 – 4.56 (m, $J = 18.8, 6.7$ Hz, 4H), 4.52 – 4.44 (m, 3H), 4.08 (dd, $J = 9.8, 2.6$ Hz, 1H), 3.99 (t, $J = 9.0$ Hz, 2H), 3.87 – 3.76 (m, 4H), 3.70 – 3.52 (m, 9H), 3.46 (dd, $J = 9.4, 3.5$ Hz, 1H), 3.33 (t, $J = 7.8$ Hz, 1H).

^{13}C NMR (126 MHz, CDCl_3) δ 138.79, 138.76, 138.71, 138.58, 138.36, 138.25, 138.16, 137.89, 137.79, 137.77, 134.15, 134.12, 134.06, 134.03, 129.57, 129.53, 129.51, 129.47, 128.50, 128.49, 128.43, 128.39, 128.36, 128.34, 128.09, 127.99, 127.98, 127.97, 127.95, 127.91, 127.84, 127.82, 127.78, 127.74, 127.69, 127.66, 127.62, 127.59, 127.55, 115.29, 115.27, 115.12, 115.10, 97.56, 97.30, 91.05, 84.48, 83.33, 81.74, 81.69, 80.34, 80.08, 77.79, 77.70, 77.47, 75.63, 75.58, 75.55, 75.40, 75.14, 75.06, 74.65, 74.52, 74.16, 74.11, 73.46, 73.43, 73.19, 72.74, 72.45, 70.55, 70.34, 68.68, 67.04, 66.87.

^{19}F NMR (376 MHz, CDCl_3 , ^1H decoupled) δ -114.60, -114.74.

HRMS (ESI): calc. for $\text{C}_{61}\text{H}_{63}\text{O}_{11}\text{FNa}$ ($\text{M}+\text{Na}$): 1013.4247; found: 1013.4277.

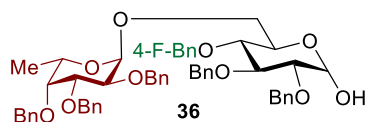


^1H NMR (600 MHz, CDCl_3) δ 7.39 – 7.21 (m, 60H), 7.17 (dd, $J = 13.9, 6.9$ Hz, 5H), 6.95 (td, $J = 8.6, 3.8$ Hz, 4H), 5.17 – 5.12 (m, 4H), 5.01 – 4.87 (m, 8H), 4.81 – 4.71 (m, 9H), 4.68 (dd, $J = 14.0, 6.0$ Hz, 5H), 4.55 – 4.48 (m, 4H), 4.46 (d, $J = 12.8$ Hz, 1H), 4.44 (d, $J = 11.9$ Hz, 2H), 4.37 (d, $J = 11.9$ Hz, 2H), 4.34 (d, $J = 11.7$ Hz, 1H), 4.07 (t, $J = 6.1$ Hz, 1H), 4.01 (dd, $J = 10.3, 4.4$ Hz, 2H), 3.99 – 3.85 (m, 11H), 3.79 – 3.71 (m, 3H), 3.63 (t, $J = 8.9$ Hz, 1H), 3.58 – 3.43 (m, 10H), 3.37 – 3.32 (m, 1H).

^{13}C NMR (151 MHz, CDCl_3) δ 163.10, 161.47, 138.64, 138.50, 138.36, 138.29, 138.26, 138.24, 138.20, 137.87, 137.59, 137.45, 134.06, 134.04, 133.86, 133.83, 129.61, 129.56, 129.51, 128.49, 128.44, 128.42, 128.40, 128.37, 128.33, 128.28, 128.24, 128.11, 128.07, 127.95, 127.93, 127.89, 127.86, 127.84, 127.76, 127.72, 127.69, 127.67, 127.65, 127.53, 127.49, 115.30, 115.27, 115.16, 115.13, 97.62, 97.48, 97.40, 90.95, 89.91, 89.86, 88.61, 88.60, 84.49, 83.47, 81.75, 80.36, 77.73, 77.68, 76.58, 76.48, 75.69, 75.57, 75.55, 75.51, 75.44, 75.39, 74.89, 74.86, 74.82, 74.53, 74.16, 74.11, 73.57, 73.48, 73.21, 72.89, 72.88, 72.77, 72.75, 70.83, 69.67, 68.91, 68.88, 67.65, 67.45.

^{19}F NMR (564 MHz, CDCl_3) δ -114.47 – -114.54 (m), -114.62 – -114.69 (m), -207.04 (ddd, $J = 50.4, 10.0, 4.1$ Hz), -207.25 (ddd, $J = 50.3, 10.2, 4.1$ Hz).

HRMS (ESI): calc. for $\text{C}_{54}\text{H}_{56}\text{O}_{10}\text{F}_2\text{Na}$ ($\text{M}+\text{Na}$): 925.3734; found: 925.3761.

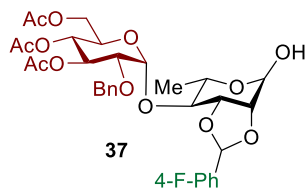


^1H NMR (600 MHz, CDCl_3) δ 7.45 – 7.26 (m, 36H), 7.25 – 7.18 (m, 5H), 7.17 – 7.12 (m, 3H), 6.96 (t, $J = 8.6$ Hz, 3H), 5.22 (d, $J = 3.2$ Hz, 1H), 5.00 (t, $J = 9.9$ Hz, 2H), 4.95 (d, $J = 11.5$ Hz, 1H), 4.91 (dd, $J = 8.5, 3.2$ Hz, 2H), 4.89 – 4.61 (m, 17H), 4.11 – 4.05 (m, 3H), 4.05 – 3.93 (m, 4H), 3.89 (dd, $J = 26.3, 10.9$ Hz, 2H), 3.72 – 3.60 (m, 6H), 3.55 (dd, $J = 9.4, 3.3$ Hz, 1H), 3.53 – 3.47 (m, 1H), 3.40 (t, $J = 8.1$ Hz, 1H), 1.14 (d, $J = 7.2$ Hz, 3H), 1.13 (d, $J = 6.8$ Hz, 3H).

^{13}C NMR (151 MHz, CDCl_3) δ 163.11, 163.06, 161.48, 161.44, 138.86, 138.84, 138.70, 138.67, 138.65, 138.63, 138.61, 138.56, 138.41, 138.00, 134.31, 134.29, 134.14, 134.12, 129.59, 129.53, 129.49, 129.44, 128.52, 128.42, 128.39, 128.27, 128.24, 128.22, 128.21, 128.09, 127.95, 127.91, 127.88, 127.81, 127.67, 127.61, 127.60, 127.49, 127.48, 115.26, 115.22, 115.12, 115.08, 98.04, 97.90, 97.47, 91.11, 84.50, 83.26, 81.72, 80.34, 79.32, 77.76, 77.72, 77.54, 76.42, 76.35, 75.75, 75.68, 74.89, 74.86, 74.73, 74.53, 74.15, 73.32, 73.25, 73.13, 72.93, 72.91, 70.20, 66.68, 66.49, 66.41, 66.30, 16.65, 16.63.

^{19}F NMR (564 MHz, CDCl_3) δ -114.62 – -114.69 (m), -114.80 – -114.88 (m).

HRMS (ESI): calc. for $\text{C}_{54}\text{H}_{57}\text{O}_{10}\text{FN}$ ($\text{M}+\text{Na}$): 907.3828; found: 907.3853.



Reaction was conducted with 15 mol% catalyst at 50 °C.

¹H NMR (500 MHz, CDCl₃) δ 7.45 – 7.37 (m, 2H), 7.36 – 7.25 (m, 6H), 7.10 – 7.01 (m, 2H), 5.85 (s, 1H), 5.49 (s, 1H), 5.39 (t, *J* = 9.7 Hz, 1H), 5.03 (d, *J* = 3.6 Hz, 1H), 5.00 (dd, *J* = 5.2, 2.4 Hz, 1H), 4.93 (t, *J* = 9.9 Hz, 1H), 4.75 (d, *J* = 5.5 Hz, 1H), 4.59 (dd, *J* = 23.2, 12.3 Hz, 2H), 4.31 – 4.25 (m, 1H), 4.20 – 4.11 (m, 2H), 3.97 (dd, *J* = 12.5, 3.2 Hz, 1H), 3.63 (dd, *J* = 12.5, 1.9 Hz, 1H), 3.58 (dd, *J* = 10.0, 3.7 Hz, 1H), 3.04 (brs, 1H), 2.01 (s, 3H), 1.97 – 1.95 (m, 6H), 1.31 (d, *J* = 5.0 Hz, 2H).

¹³C NMR (126 MHz, CDCl₃) δ 170.48, 170.13, 169.76, 164.48, 162.50, 137.50, 132.41, 132.39, 128.52, 128.45, 128.11, 127.92, 115.48, 115.30, 104.65, 100.98, 92.77, 85.22, 82.44, 79.36, 76.49, 72.98, 72.04, 69.02, 68.36, 67.27, 61.44, 20.83, 20.63, 20.61, 15.89.

¹⁹F NMR (376 MHz, CDCl₃, ¹H decoupled) δ -111.53.

HRMS (ESI): calc. for C₃₂H₃₇O₁₃FNa (M+Na): 671.2110; found: 671.2124.

5.3. Chapter 3 experimental section

5.3.1. Kinetic study

Rate equation derivation

Based on the mechanism outlined for phenanthroline-catalyzed glycosylation in **Scheme 31**, the overall reaction can be described as equation (1), wherein k_1 and k_{-1} defined the pre-equilibrium in the first nucleophilic substitution between the reactants, glycosyl bromide donor (D) and catalyst (C), and the intermediate (I). An irreversible nucleophilic attack (k_2) by a hydroxyl acceptor (A) then leads to formation of the coupling product (P) and regeneration of catalyst. Based on the assumption of steady-state approximation, the complete rate law can be derived as equation (2).



Therefore,

$$\frac{d[P]}{dt} = k_2[I][A] \quad (S1)$$

$$\frac{d[I]}{dt} = k_1[D][C] - k_{-1}[I] - k_2[I][A] \quad (S2)$$

In addition,

$$[C] = [C]_0 - [I] \quad (S3)$$

Applying steady-state approximation,

$$\frac{d[I]}{dt} = 0 \quad (S4)$$

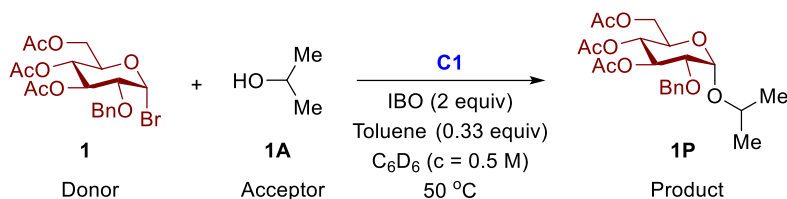
After incorporation of equation (S3):

$$[I] = \frac{k_1[D][C]_0}{k_{-1} + k_2[D] + k_2[A]} \quad (S5)$$

Substitute $[I]$ into rate equation (S1), the rate of product formation can be derived as:

$$\frac{d[P]}{dt} = \frac{k_1 k_2 [D][A][C]_0}{k_{-1} + k_1[D] + k_2[A]} \quad (2)$$

General experimental procedure for kinetic study with **1** as donor



A 10 mL scintillation vial was charged with glycosyl bromide **1** (fixed amount, 0.25 mmol, 1.0 equiv), isopropanol acceptor **1A** (vary amount from 0.5 to 5 equiv), catalyst **C1** (vary amount from 2 to 20 mol%), IBO (vary amount from 1.5 to 3 equiv), toluene (internal standard, 0.083mmol, 0.33 equiv), and C_6D_6 (0.5 mL). The resulting solution was then transferred to a 5 mm NMR tube. ^1H NMR spectrum was acquired on a 400 MHz instrument before heating. Then the mixture in NMR tube was then consistently shaken and heated in a 50 °C water bath. Between 3 and 60 hours, spectra were obtained depending on the experiment. Example spectra and example rate plot were based on standard condition: 0.25 mmol glycosyl bromide **1** (1.0 equiv), 0.75 mmol acceptor (3.0 equiv), 15 mol% catalyst **C1**, 0.5 mmol IBO (2 equiv), 0.083 mmol toluene (0.33 equiv) as an internal standard, and 0.5 mL C_6D_6 (0.5 M).

Spectra processing

The spectra for each kinetic experiment were processed using MestReNova (v. 6.0.2, Mestrelab Research S.L.). The concentrations of product were measured by integration of its H-1 proton against the toluene internal standard, $\delta = 2.1$ ppm. Peak fitting or deconvolution algorithms were not used for integration. An example of ^1H NMR spectra array is shown in Figure 33.

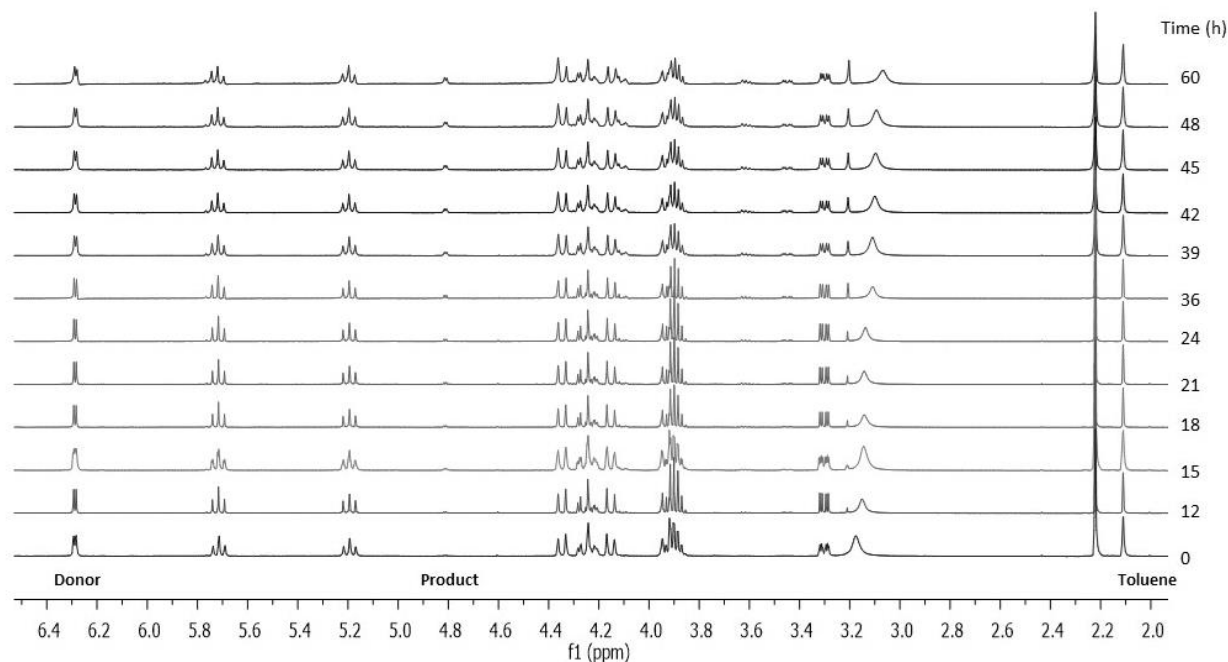


Figure 33. Example spectra array for a kinetic experiment with **1** as donor

Graphing

For each kinetic experiment, the concentration of product versus time were plotted on Excel 2016. Linear regression was obtained by best fitting with all points (Figure 34). Slope of the best-fit line represents the initial rate of reaction for each kinetic experiment. The initial rate was then graphed against catalyst concentration for fixed acceptor concentration (Figure 15a), and against acceptor concentration for fixed catalyst concentration (Figure 15b).

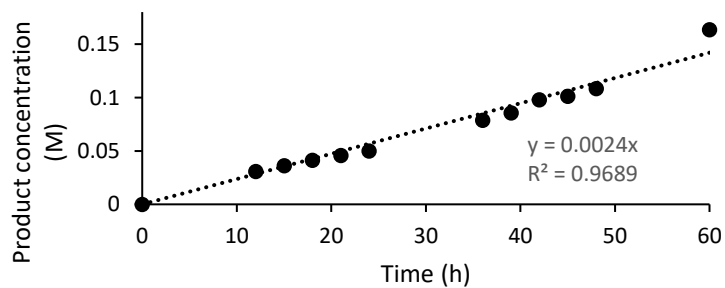


Figure 34. Example rate plot: product concentration versus time for a kinetic experiment

The product formation versus time was also compared at different equivalent of IBO (Figure 35). As shown in Figure 35, the rate of reactions does not change significantly with varying amounts of IBO.

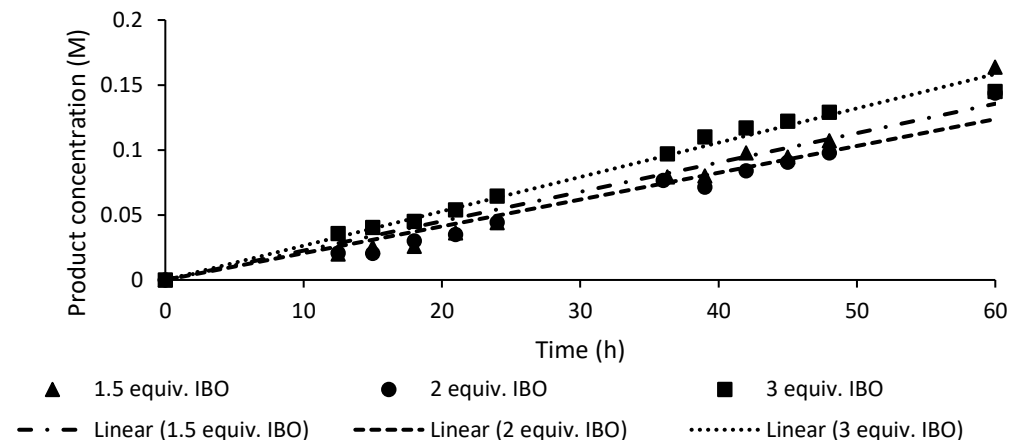


Figure 35. Product formation versus time at different equivalent of IBO

A control kinetic experiment was performed in the absence of catalyst (Figure 36). As shown in Figure 36, the desired product was not observed even after 24 h in the absence of catalyst. This result is consistent with our control experiment.¹²⁶ After 24 h, the desired product was slowly formed in the reaction. Until 60 h, only 3% conversion was observed. Collectively, these results suggest that the background reaction only takes place after a long period, and it would not affect the aforementioned kinetic experiment.

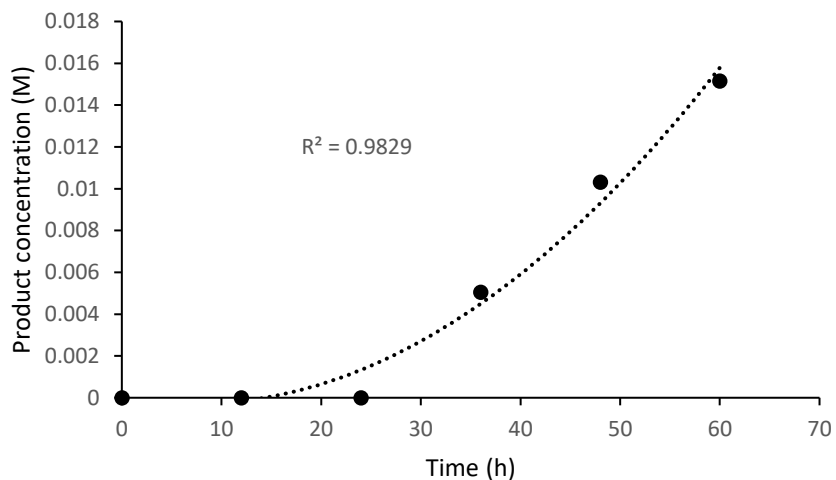
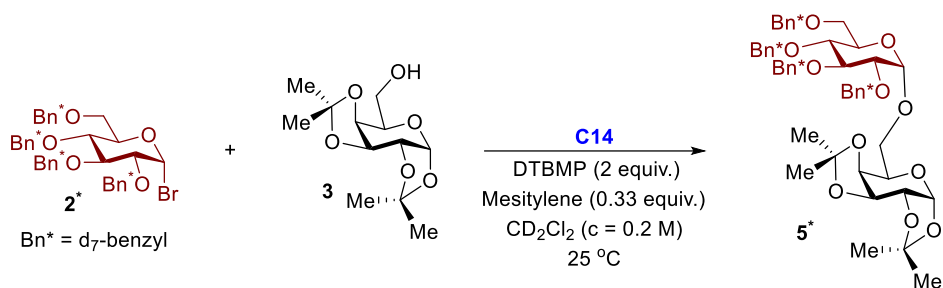


Figure 36. Product formation versus time at 0 mol% catalyst

General experimental procedure for kinetic study with **2*** as donor



All reagents were prepared into three stock solutions:

Solution A: 1 M donor **2*** stock solution. (1.2 mmol **2*** in 1.2 mL CDCl_2)

Solution B: 0.1 M Catalyst stock solution. (20.8mg (0.06 mmol) **C14** in 0.6 mL CDCl_2)

Solution C: 1 M acceptor **3** solution. (156 mg (0.6 mmol) **3**, 246.4 mg (1.2 mmol) DTBMP, and 27.8 μL (0.2 mmol) mesitylene in 0.6 mL CDCl_2)

0.1 mL of solution B and 0.1 mL of solution C were charged to a 1-dram scintillation, then added 0.1-0.3 mL solution A (vary amount of donor from 1 to 3 equiv.). CD_2Cl_2 was then added to the vial to bring the final volume to 0.5 mL. The reaction mixture was then transferred to an NMR tube, and immediately subjected to ^1H NMR to obtain spectrum at $t = 0$. Then a ^1H NMR spectrum was recorded every 30 minutes until 300 minutes.

For kinetic experiment with different catalyst, solution B was switched to 0.1 M stock solution with corresponding catalyst.

Spectra processing

The spectra for each kinetic experiment were processed using MestReNova (v. 6.0.2, Mestrelab Research S.L.). The concentrations of product were measured by integration of its H-1 proton against the mesitylene internal standard, $\delta = 6.85$ ppm. Peak fitting or deconvolution algorithms were not used for integration. An example of ^1H NMR spectra array is shown in Figure 37.

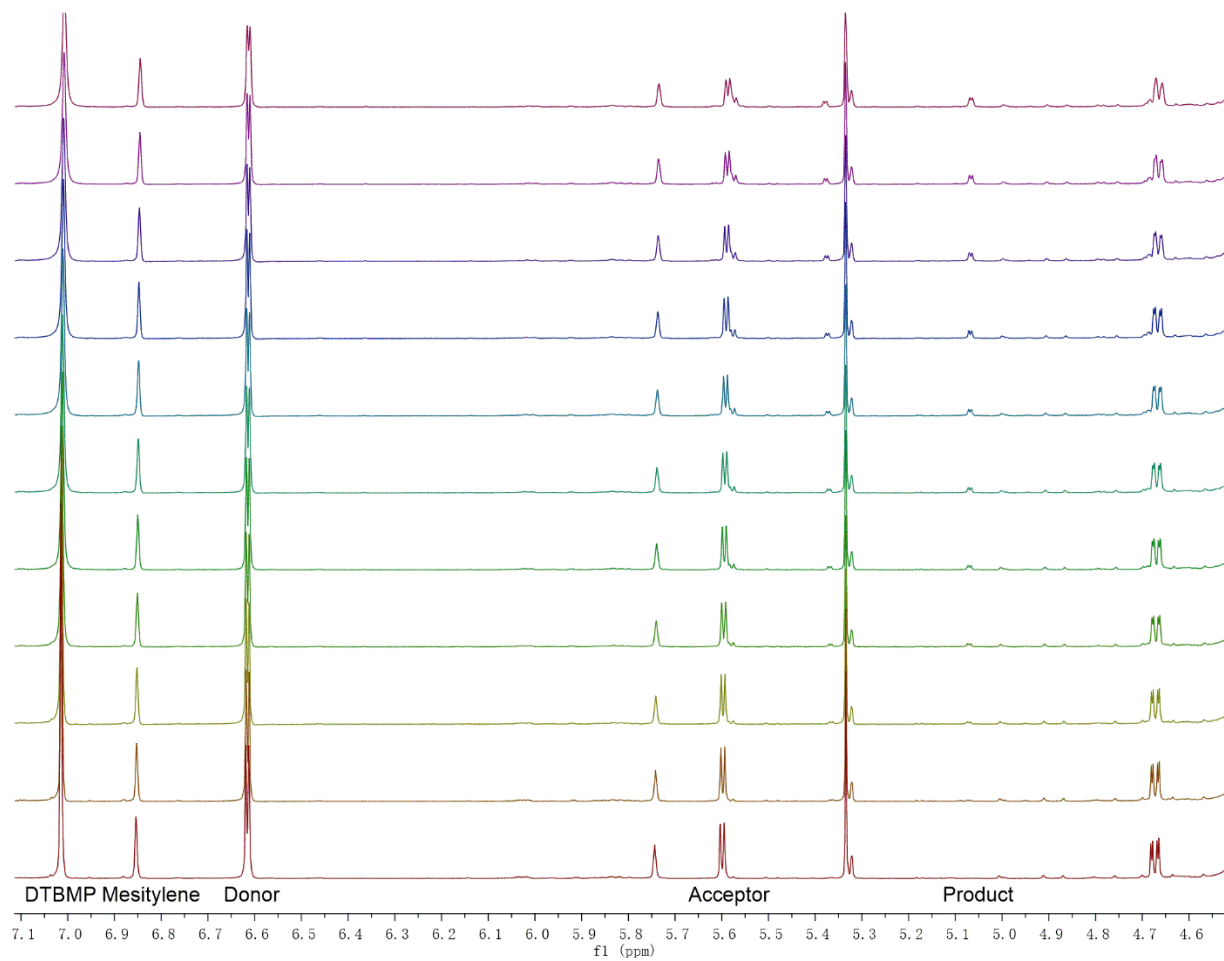
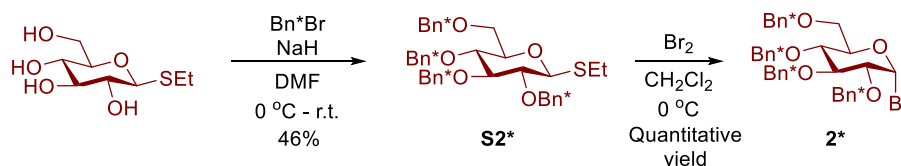


Figure 37. Example spectra array for a kinetic experiment with **2*** as donor

5.3.2. Mechanistic study

Preparation of 2,3,4,6-Tera-*O*-Benzyl-*d*₇- α -D-Glucopyranosyl Bromide (1*).



Ethyl 1-thio- β -D-Glucopyranoside (1.14 g, 5.08 mmol) was dissolved in 25 mL dry DMF in a 100 mL round-bottom flask, then benzyl bromide- d_7 (2.66 mL, 22.35 mmol, 4.4 equiv.) was added to the flask. The solution was then cooled to $0\text{ }^\circ\text{C}$ in an ice bath and sodium hydride (60% in mineral oil) (894 mg, 22.35 mmol, 4.4 equiv.) was added in 2 portions. The mixture was stirred in ice bath overnight. The resulting solution was poured into chipped ice ($\sim 100\text{ mL}$), and extracted with 200 mL ethyl acetate. The organic solution was washed with brine, dried over sodium sulfate, and then concentrated *in vacuo*. The residue was then subjected to Biotage Isolera One purification system to give 1.37 g (46%) of **S2*** as a white solid.

$^1\text{H NMR}$ (600 MHz, CDCl_3) δ 4.45 (d, $J = 9.8\text{ Hz}$, 1H, H-1 β), 3.73 (dd, $J = 10.9, 1.8\text{ Hz}$, 1H), 3.69 – 3.63 (m, 2H), 3.59 (t, $J = 9.4\text{ Hz}$, 1H), 3.49 – 3.39 (m, 2H), 2.83 – 2.68 (m, 2H), 1.32 (t, $J = 7.4\text{ Hz}$, 3H).

S2* (711.4 mg, 1.2 mmol) was charged to a 50 mL round-bottom flask equipped with nitrogen balloon, then 12 mL dry CH_2Cl_2 was added. The solution was cooled to $0\text{ }^\circ\text{C}$ in an ice bath, and Br_2 (0.12 mL, 2.4 mmol, 2 equiv.) was added. The reaction was stirred in ice bath, and monitored by TLC. Upon completion ($\sim 15\text{ minutes}$), the reaction was quenched with cyclohexene. The resulting residue was concentrated *in vacuo*, and yielded **2*** as pale-yellow syrup. This crude product was directly used for NMR study without further purification.

$^1\text{H NMR}$ (600 MHz, CD_2Cl_2) δ 6.53 (d, $J = 3.7\text{ Hz}$, 1H, H-1 α), 4.05 – 4.01 (m, 1H), 3.97 (t, $J = 9.1\text{ Hz}$, 1H), 3.76 (dd, $J = 11.0, 3.6\text{ Hz}$, 1H), 3.72 (t, $J = 9.6\text{ Hz}$, 1H), 3.65 (dd, $J = 11.0, 1.5\text{ Hz}$, 1H), 3.53 (dd, $J = 9.2, 3.7\text{ Hz}$, 1H). HR ESI-TOF MS (m/z): calcd for $\text{C}_{34}\text{H}_7\text{D}_{28}\text{BrO}_5\text{Na}$ [$\text{M} + \text{Na}$] $^+$, 653.3333; found, 653.3325.

Preparation of NMR samples.

All reagents were prepared into three stock solutions:

Solution A: 1 M donor **2*** stock solution. (1.2 mmol **2*** in 1.2 mL CDCl₂)

Solution B: 0.1 M Catalyst stock solution. (20.8mg (0.06 mmol) **C14** in 0.6 mL CDCl₂)

Solution C: 1 M acceptor **3** solution. (156 mg (0.6 mmol) **3**, 246.4 mg (1.2 mmol) DTBMP, and 27.8 μ L (0.2 mmol) mesitylene in 0.6 mL CDCl₂)

Detection of Glycosyl Phenanthrolium Intermediate. 0.1 mL solution A, 0.1 mL solution B and 0.3 mL CD₂Cl₂ was mixed in a 1-dram scintillation vial, then transferred to an oven-dried NMR tube, and sealed with a septum. The NMR tube was then purged with nitrogen. The tube was immediately placed into the NMR probe and the sample was locked and shimmed properly. ¹H NMR was taken at t = 0, then every 5 minutes. At t = 30 minutes, after the ¹H NMR was taken, 1 mL solution C was added to the NMR tube through the septum, and then purged with nitrogen. The solution was carefully mixed in the NMR tube by tightening the NMR tube to a stir bar retriever and stirred on a stir plate. ¹H NMR was then taken at t = 30 minutes and 300 minutes upon the addition of solution C. The full ¹H NMR spectra are shown in Figure 38 - Figure 42.

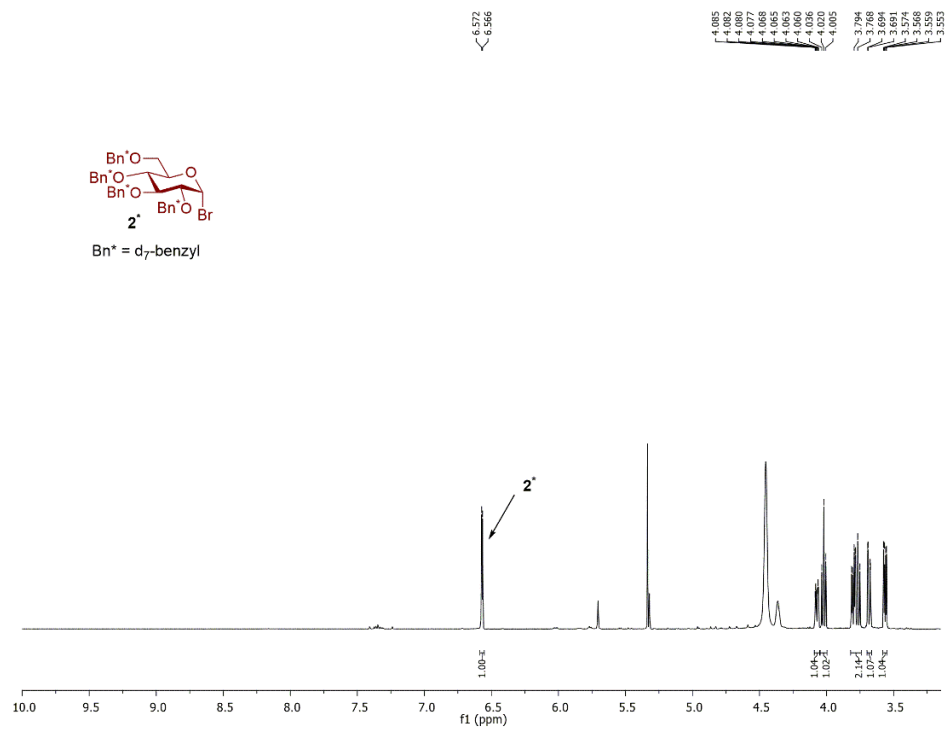


Figure 38. ^1H NMR of deuterated tetrabenzyl glucosyl bromide **2***

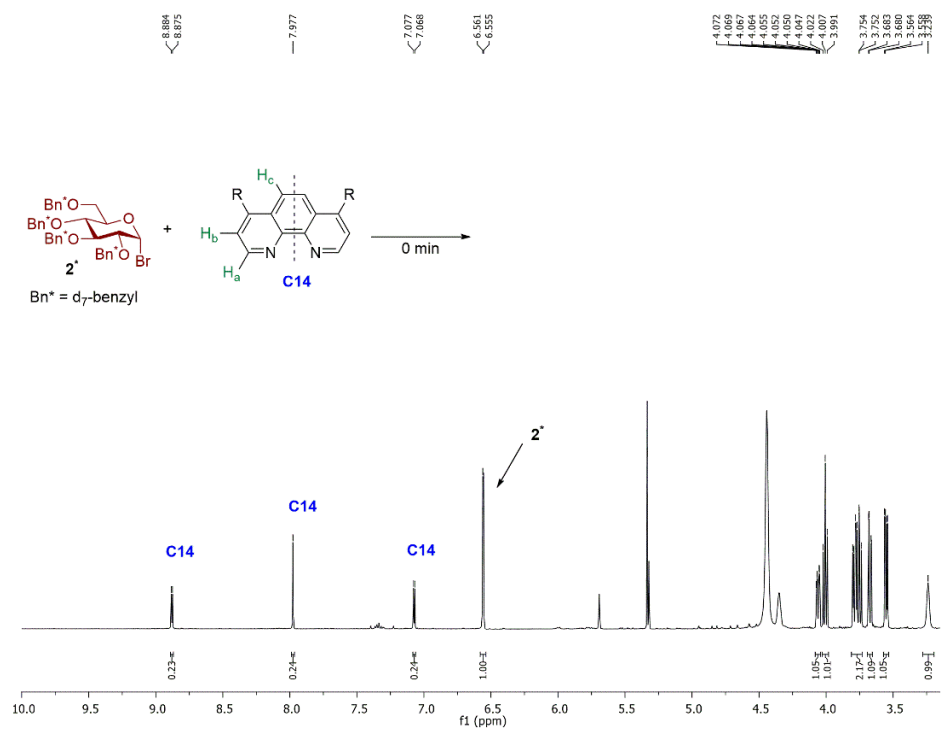


Figure 39. ^1H NMR of deuterated tetrabenzyl glucosyl bromide **2*** and **C14** at 0 min

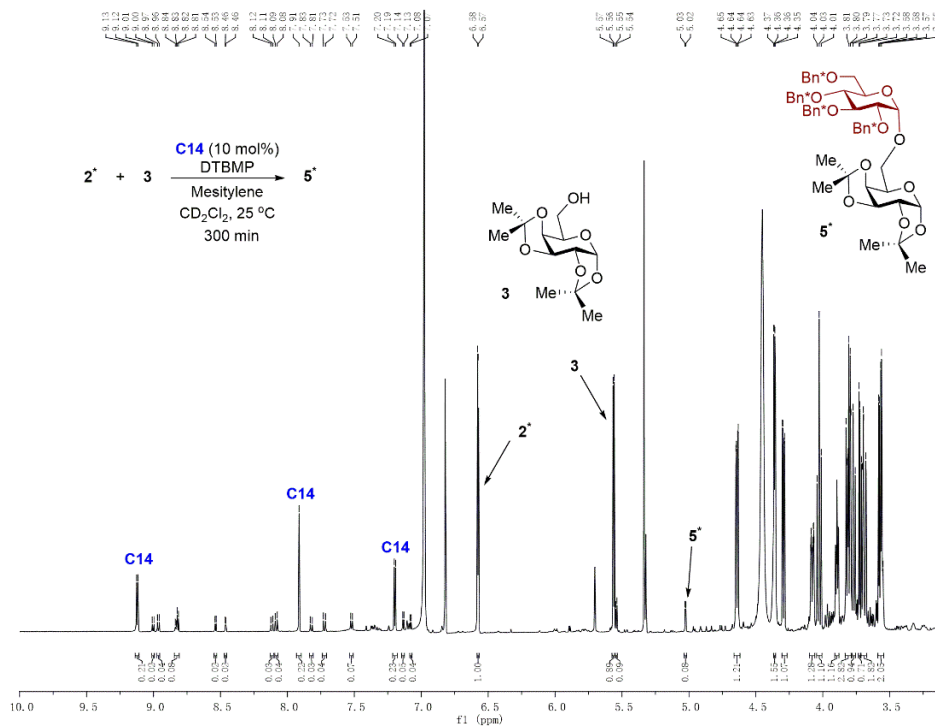


Figure 42. ^1H NMR of deuterated tetrabenzyl glucosyl bromide **2*** and **C14** with acceptor **3** at 300 min

Conformation of glycosyl phenanthrolium intermediates. 0.15 mmol of **2*** was prepared freshly from **S2***, then dissolved in 0.75 mL CD_2Cl_2 to make 0.2 M donor solution. **C14** (41.5 mg, 0.12 mmol) and mesitylene (5.6 μL , 0.04 mmol) was charged to a 1-dram scintillation vial, then 0.6 mL of the 0.2 M donor solution was added to the vial. After mixing, the solution was transferred to an oven-dried NMR tube, and purged with nitrogen. The tube was immediately placed into the NMR probe and the sample was locked and shimmed properly. Control ^1H NMR was taken every 5 minutes to ensure the intermediates was formed. Upon formation of intermediates (30 minutes), the NMR probe was cooled to $-60\text{ }^\circ\text{C}$ using liquid nitrogen and the sample was reshimmied, retuned, and the ^1H NMR spectrum was then recorded. The sample was warmed at intervals of $10\text{ }^\circ\text{C}$ and allowed to equilibrate for 10 minutes. A ^1H NMR spectrum was recorded at every interval. The collected spectra array was then combined using MestReNova 6.0.2 (Figure 22). As hydrogen bond scalar coupling were observable at $0\text{ }^\circ\text{C}$, ^1H - ^1H 2D COSY and ROESY spectra were recorded at $0\text{ }^\circ\text{C}$. The full spectra are shown in Figure 43 - Figure 49.

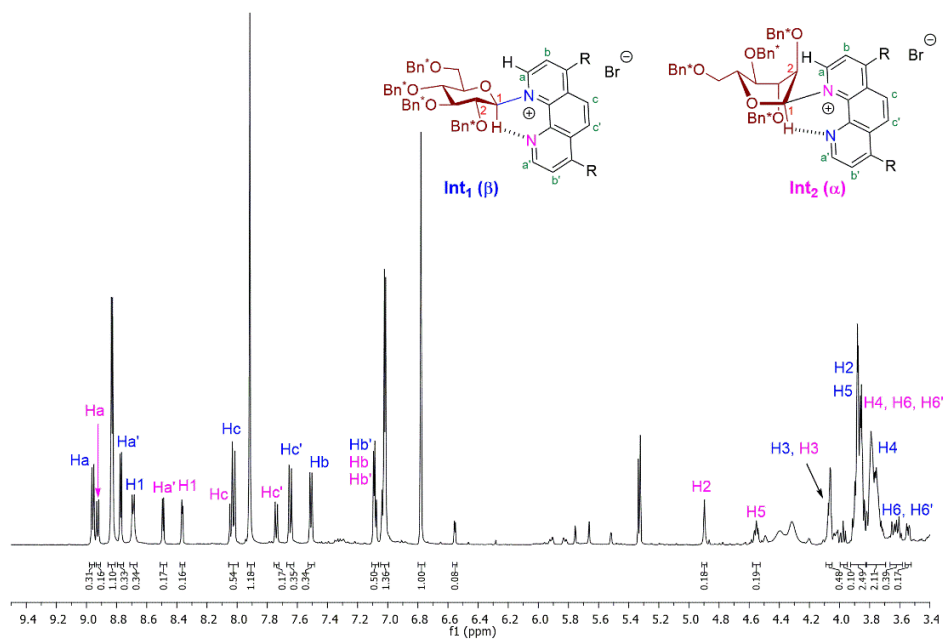


Figure 43. ^1H NMR of glucosyl phenanthrolium intermediates (**Int₁** and **Int₂**)

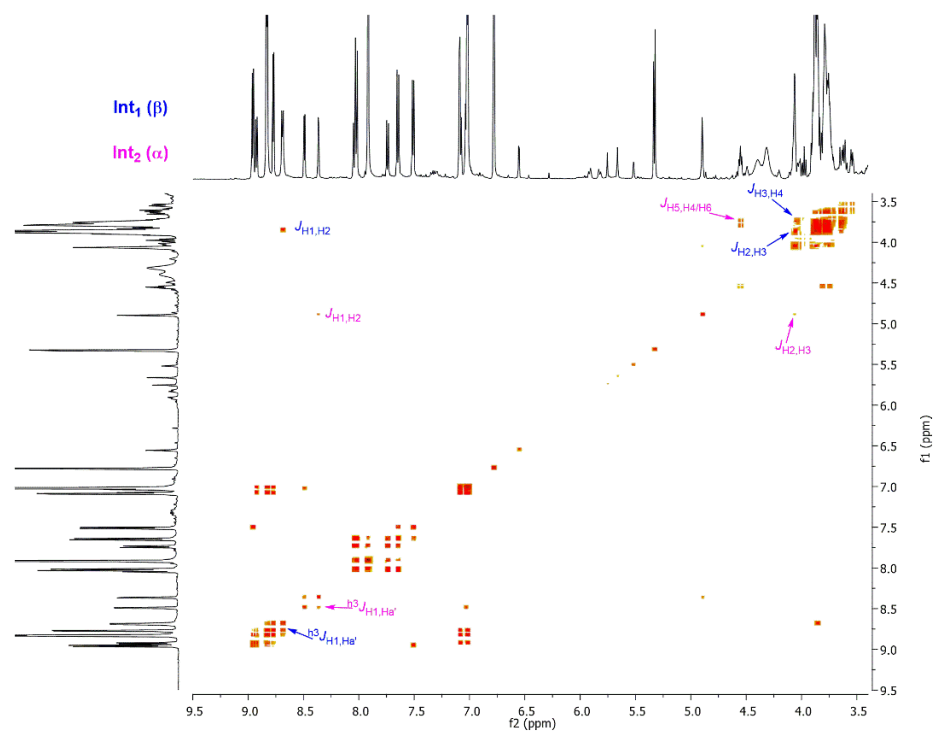


Figure 44. ^1H - ^1H 2D COSY NMR of glucosyl phenanthrolium intermediates (**Int₁** and **Int₂**)

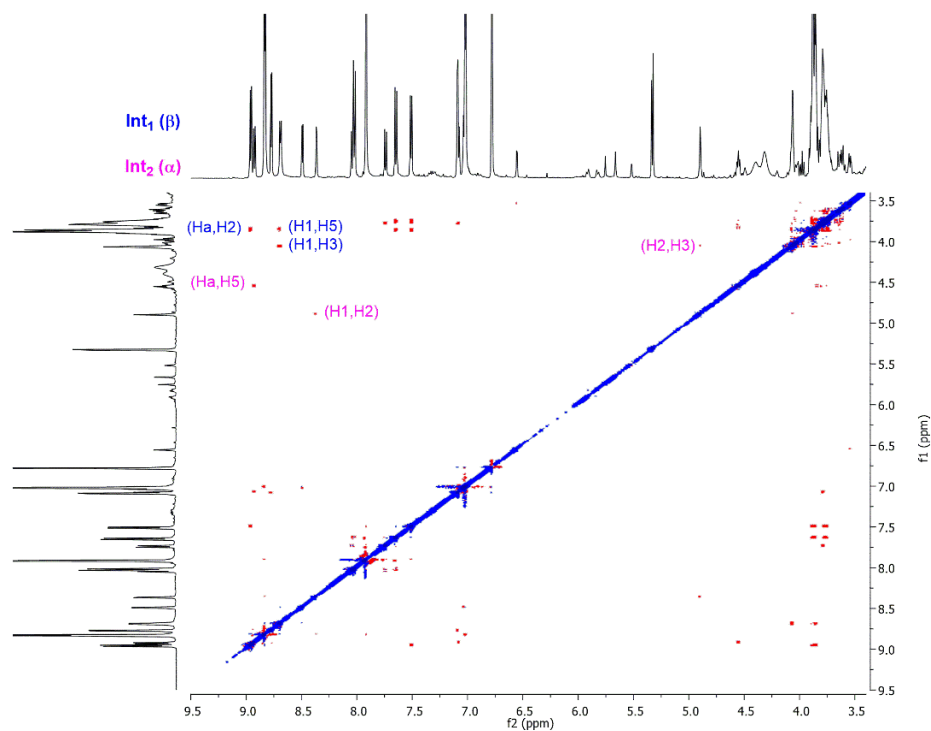


Figure 45. ^1H - ^1H 2D ROESY NMR of glucosyl phenanthrolium intermediates (**Int₁** and **Int₂**)

JL-7-73_intermediate_ESI-pos #41-52 RT: 1.20-1.50 AV: 12 NL: 1
T: FTMS + c ESI Full ms [150.00-2000.00]

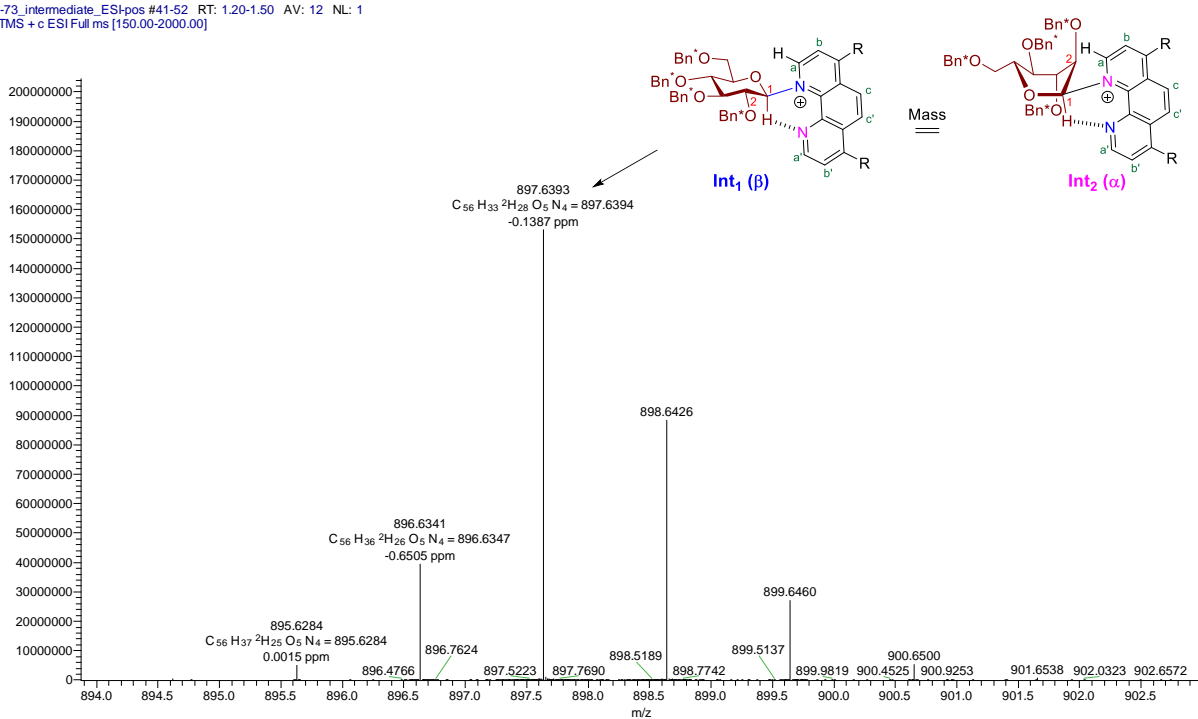


Figure 46. Mass spectrum detection of glucosyl phenanthrolium intermediates (**Int₁** and **Int₂**)

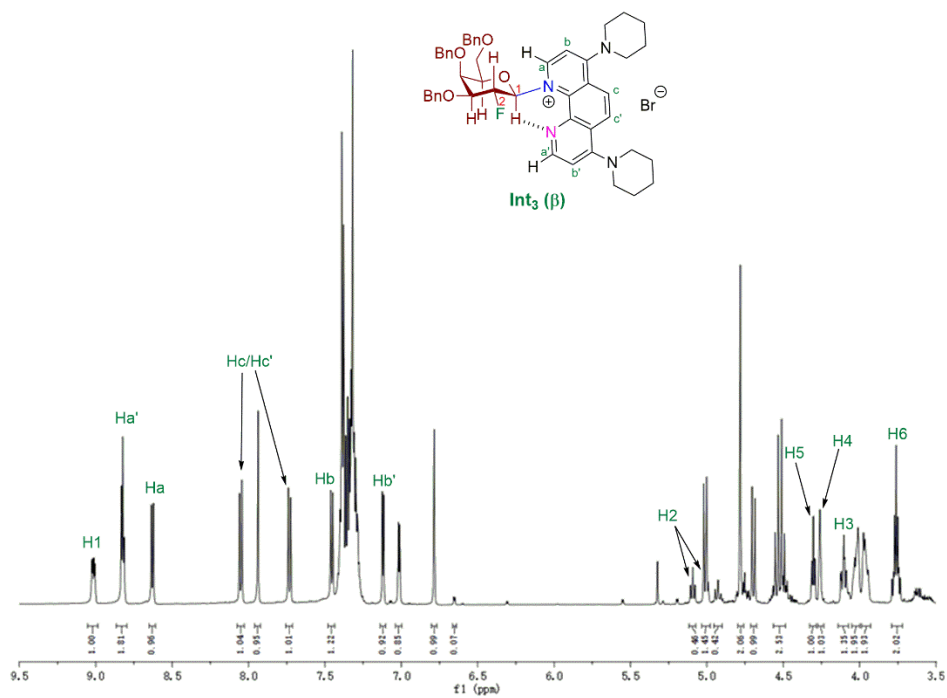


Figure 47. ^1H NMR of 2-deoxy-2-fluoro glucosyl phenanthrolium intermediate (**Int₃**)

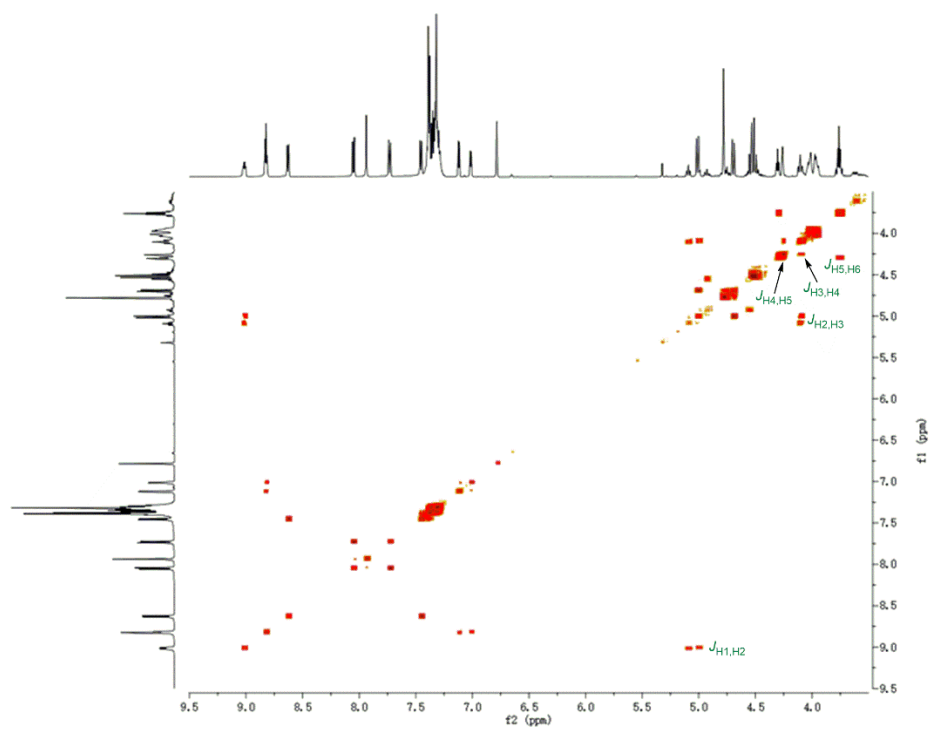


Figure 48. ^1H - ^1H 2D COSY NMR of 2-deoxy-2-fluoro glucosyl phenanthrolium intermediate (**Int₃**)

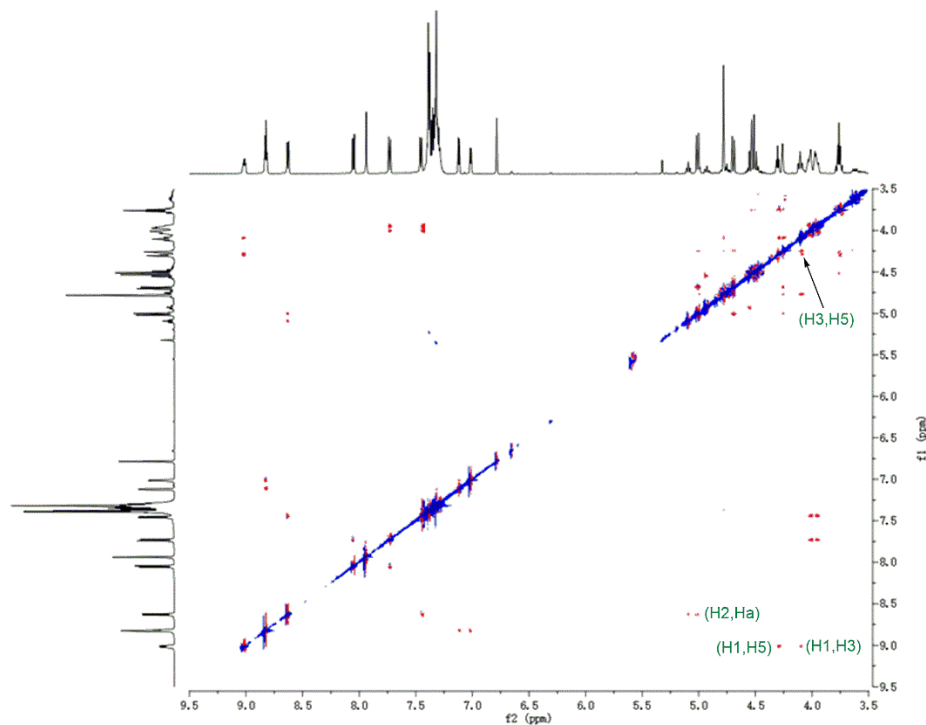


Figure 49. ^1H - ^1H 2D ROESY NMR of 2-deoxy-2-fluoro glucosyl phenanthrolium intermediate (**Int**₃)

5.3.3. Density Functional Theory (DFT) Calculations

Based on the observation from NMR studies, the β -glycosyl phenanthrolium ion was at $^4\text{C}_1$ chair conformation. However, both $\text{B}_{2,5}$ and $\text{B}_{1,4}$ boat conformations were fitted with the NMR observation for α -glycosyl phenanthrolium ion. As such, DFT calculations were performed to compare their energy level. All calculations were carried out with Gaussian 09.¹⁶⁰ Geometry optimization and vibrational frequency for these intermediates was computed at the B3LYP/6-31+G(d,p) level of theory¹⁴⁶⁻¹⁵⁶ with the SMD implicit solvation model¹⁵⁷ in diethyl ether and the GD3BJ empirical dispersion correction²²⁹⁻²³⁰. There is no imaginary frequency for these intermediates. The free energy of each optimized structure was in comparison with the β -glycosyl phenanthrolium ion. As shown in Figure 50, α -glycosyl phenanthrolium ion is more likely to be at $\text{B}_{2,5}$ boat conformation since its free energy is 7.9 kcal/mol lower than that of the $\text{B}_{1,4}$ boat conformation.

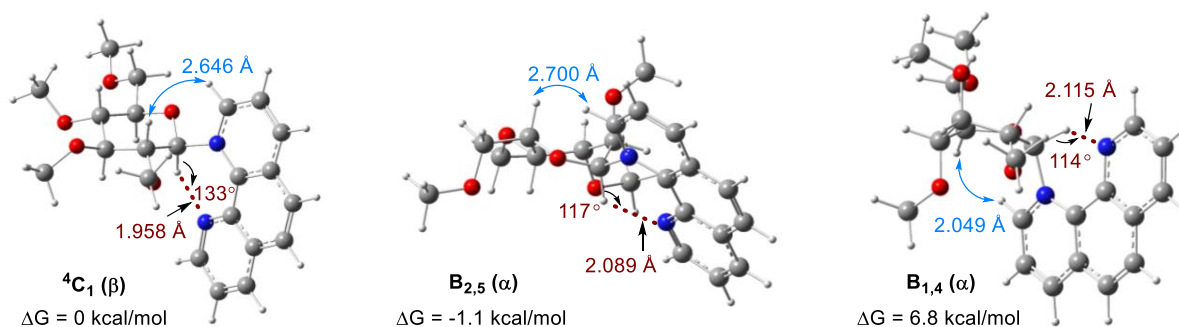
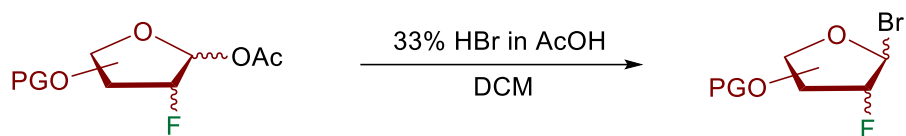


Figure 50. Optimized structures of β - and possible α -glycosyl phenanthrolium intermediates

The cartesian coordinates of these three structures was reported in the literature.²¹⁶

5.4. Chapter 4 experimental section

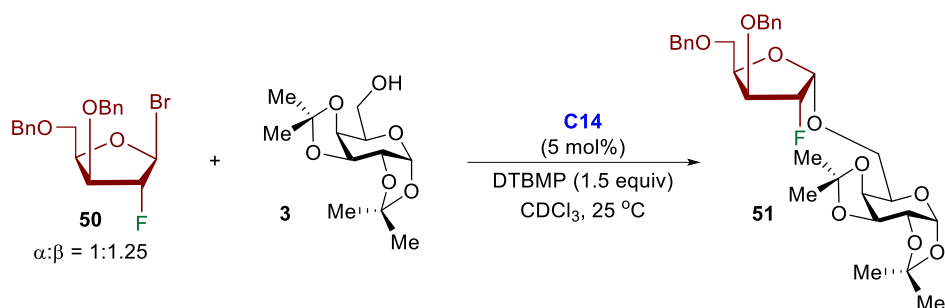
5.4.1. Preparation of 2-deoxy-2-fluoro-3,5-di-*O*-benzyl-D-furanosyl bromide donors



A solution of 1-acetate-2-deoxy-2-fluoro-3,5-bis-*O*-benzyl-D-furanose (1.0 equiv.) in dry CH_2Cl_2 (2.0 ml,) was placed in an ice bath to cool to 0°C and HBr (33% in acetic acid, 5.0 equiv.) was added in a dropwise manner. Then, the ice was removed and the mixture was allowed to warm up to ambient temperature while stirring, and continued reacting at this temperature for 1 h. The reaction mixture was then diluted with cold CH_2Cl_2 (50 mL) and washed with cold water (1 x 50 ml), cold saturated NaHCO_3 solution (2 x 50 ml), dried over Na_2SO_4 , filtered, and evaporated to yield the product as a brown oil. The product was immediately used without additional purification or characterization.

5.4.2. NMR study with 2-fluoro xylofuranosyl donor

NMR course of glycosylation with 2-fluoro xylofuranosyl bromide **50**



A 5 mm NMR tube was charged with 2-fluoro xylofuranosyl bromide **50** (3.0 equiv) and CDCl_3 (0.6 mL) (^1H and ^{19}F NMR were acquired). Then 5 mol% (according to donor) phenanthroline **C14** was added, ^1H and ^{19}F NMR were acquired after mixing for 30 min. After the NMR was taken, then the mixture in the NMR tube was added with acceptor **3** (1.0 equiv.) and DTBMP (1.5 equiv.). ^1H (Figure 51) and ^{19}F (Figure 52) NMR spectra were obtained at the given time (10 min -24 h) depending on the experiment.

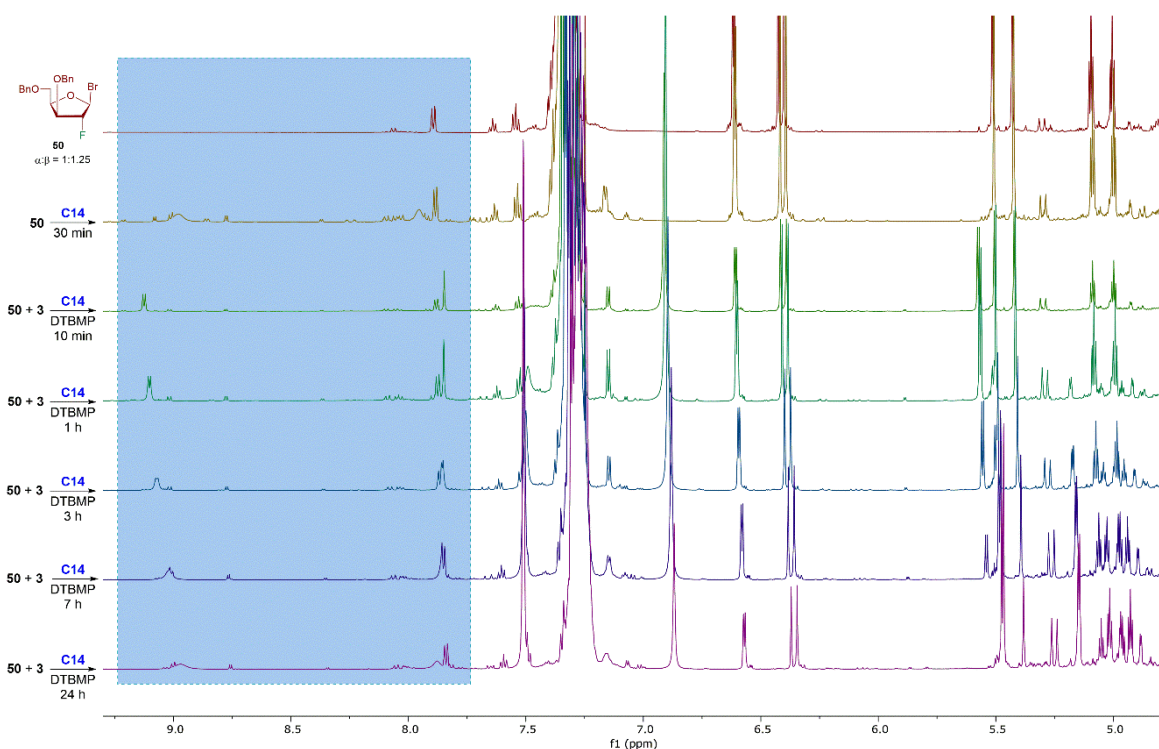


Figure 51. ^1H NMR course of furanosylation with 2-fluoro xylofuranosyl bromide **50**

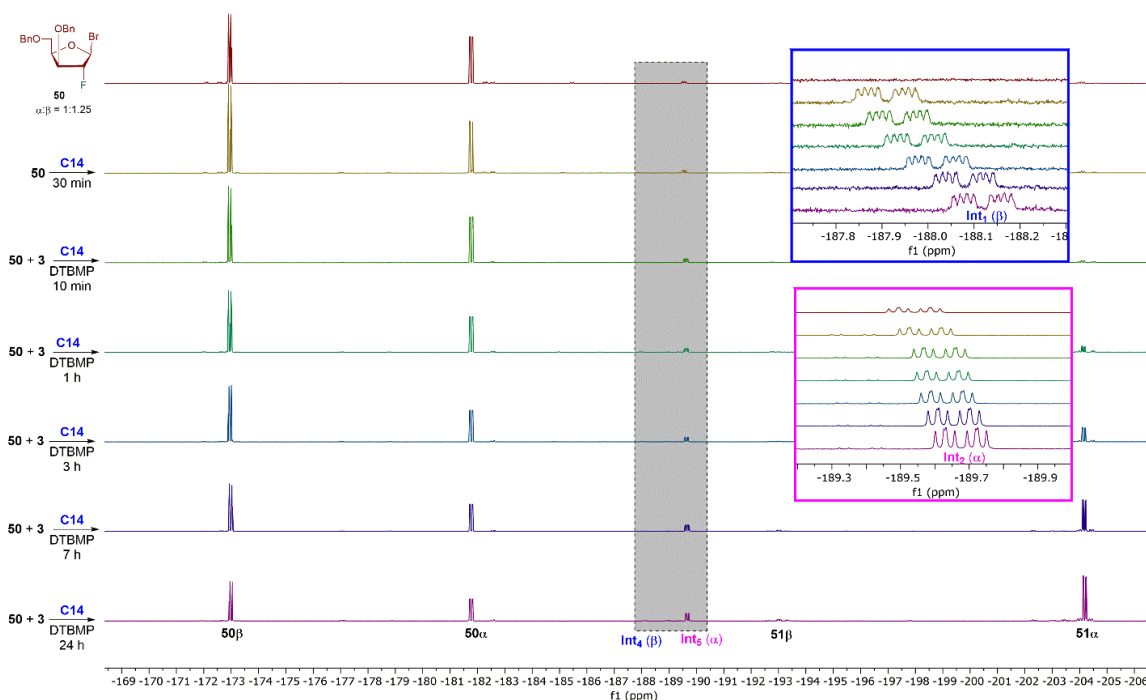
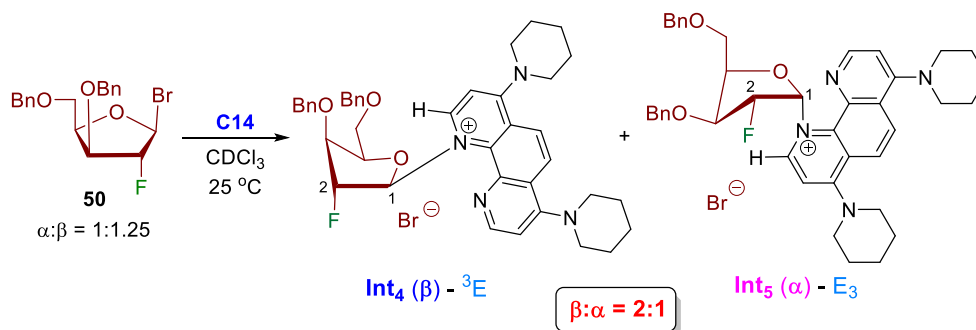


Figure 52. ^{19}F NMR course of furanosylation with 2-fluoro xylofuranosyl bromide **50**

NMR detection of xylofuranosyl phenanthrolium intermediates



A 5 mm NMR tube was charged with 2-fluoro xylofuranosyl bromide **50** (1.5 equiv.) and CDCl_3 (0.6 mL), ^1H and ^{19}F NMR were acquired. Then phenanthroline **C14** (1.0 equiv.) was added to the NMR tube. ^1H (Figure 53) and ^{19}F (Figure 54) NMR spectra were obtained at the given time (10 min -16 h) depending on the experiment. The full spectra of ^1H , ^1H - ^1H 2D COSY and ROESY NMR and mass spectrum are shown in Figure 55 - Figure 58.

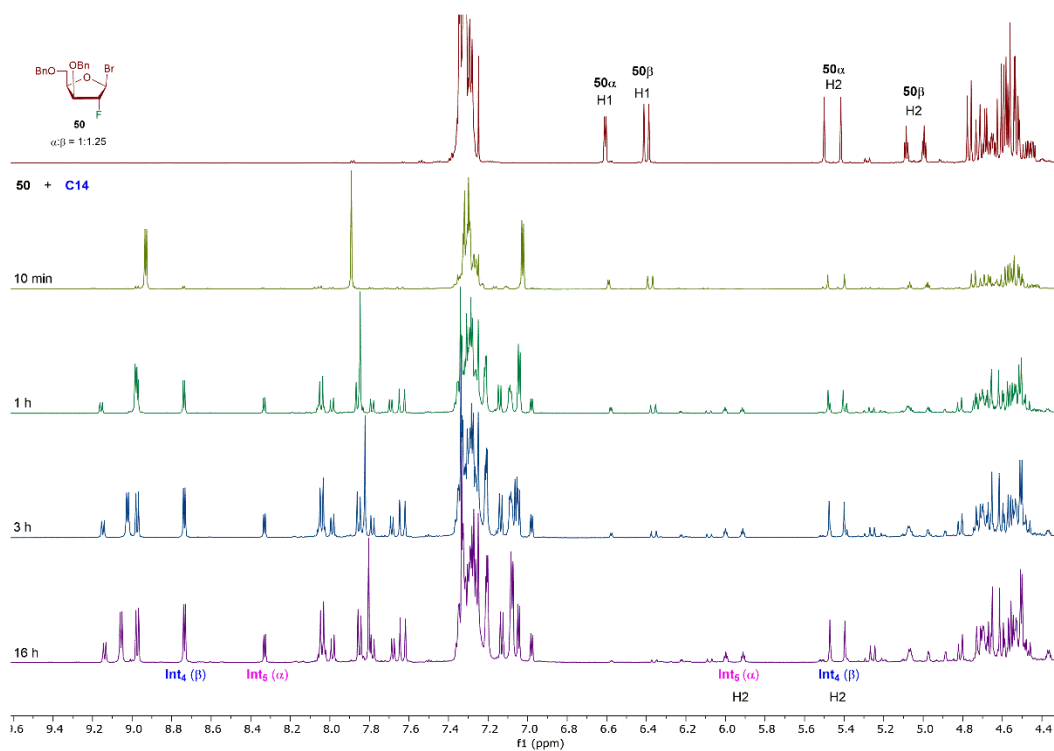


Figure 53. ^1H NMR detection of xylofuranosyl phenanthrolium intermediates (**Int₄** and **Int₅**)

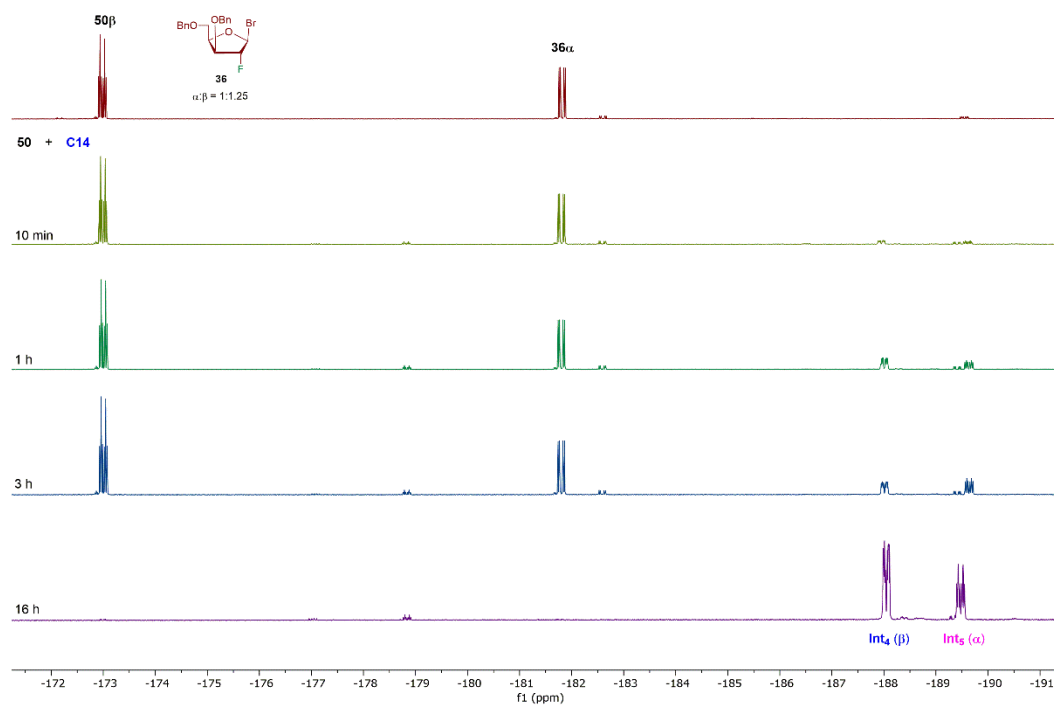


Figure 54. ^{19}F NMR detection of xylofuranosyl phenanthrolium intermediates (**Int₄** and **Int₅**)

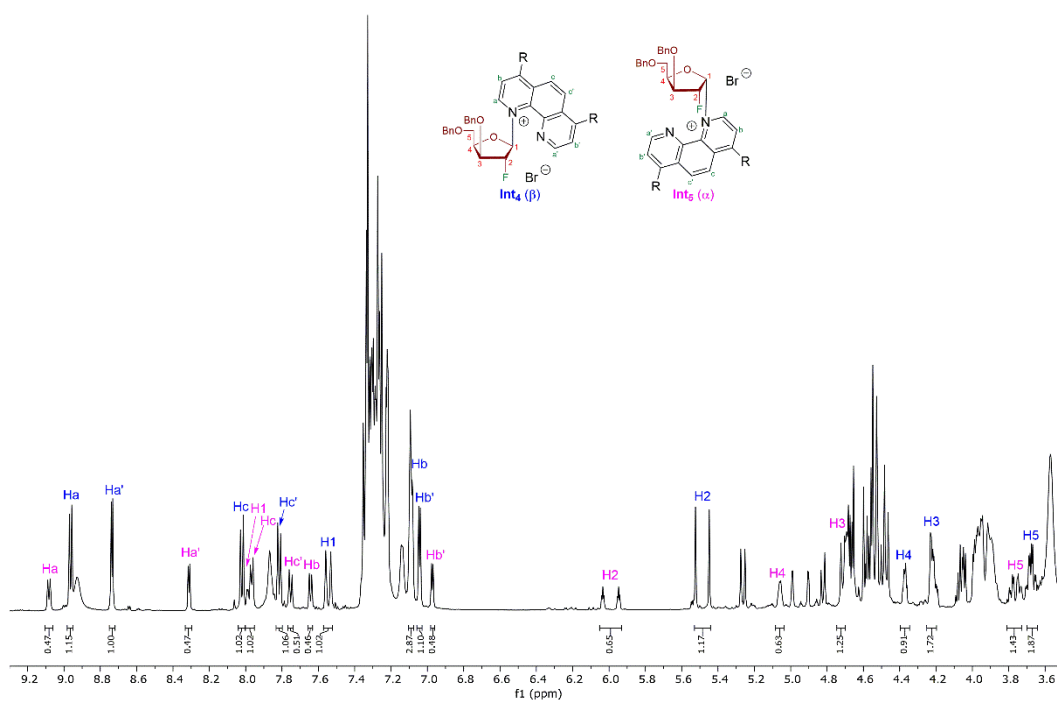


Figure 55. ^1H NMR of xylofuranosyl phenanthrolium intermediates (**Int₄** and **Int₅**)

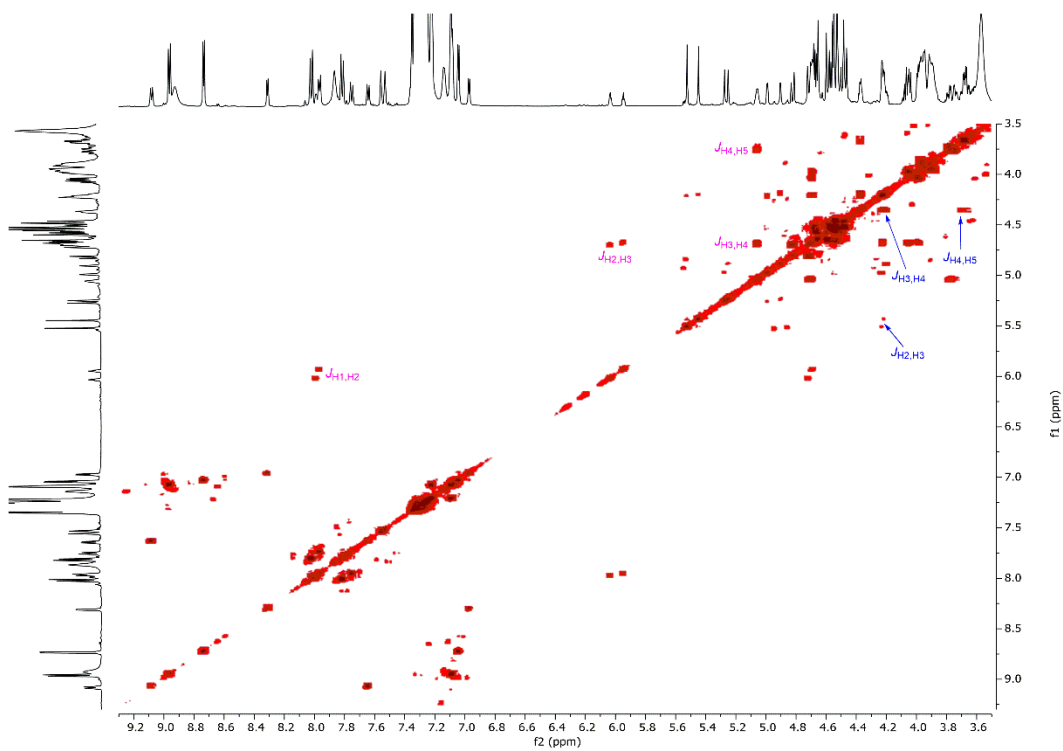


Figure 56. ^1H - ^1H COSY NMR of xylofuranosyl phenanthrolium intermediates (**Int₄** and **Int₅**)

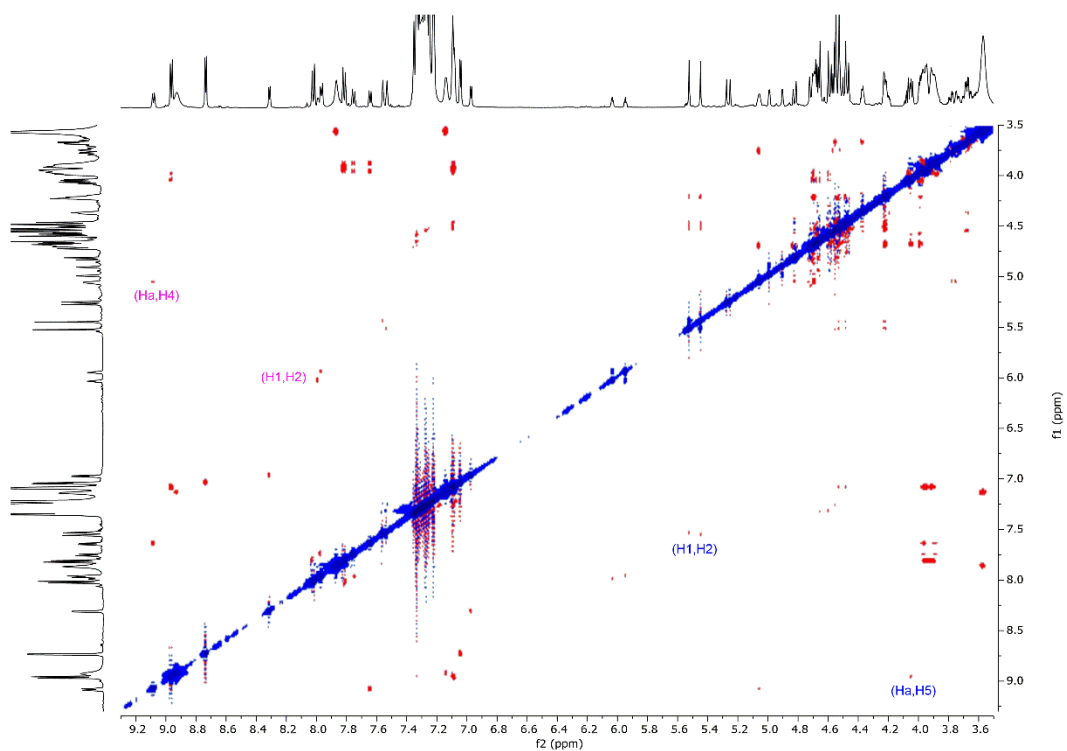


Figure 57. ^1H - ^1H ROESY NMR of xylofuranosyl phenanthrolium intermediates (**Int₄** and **Int₅**)

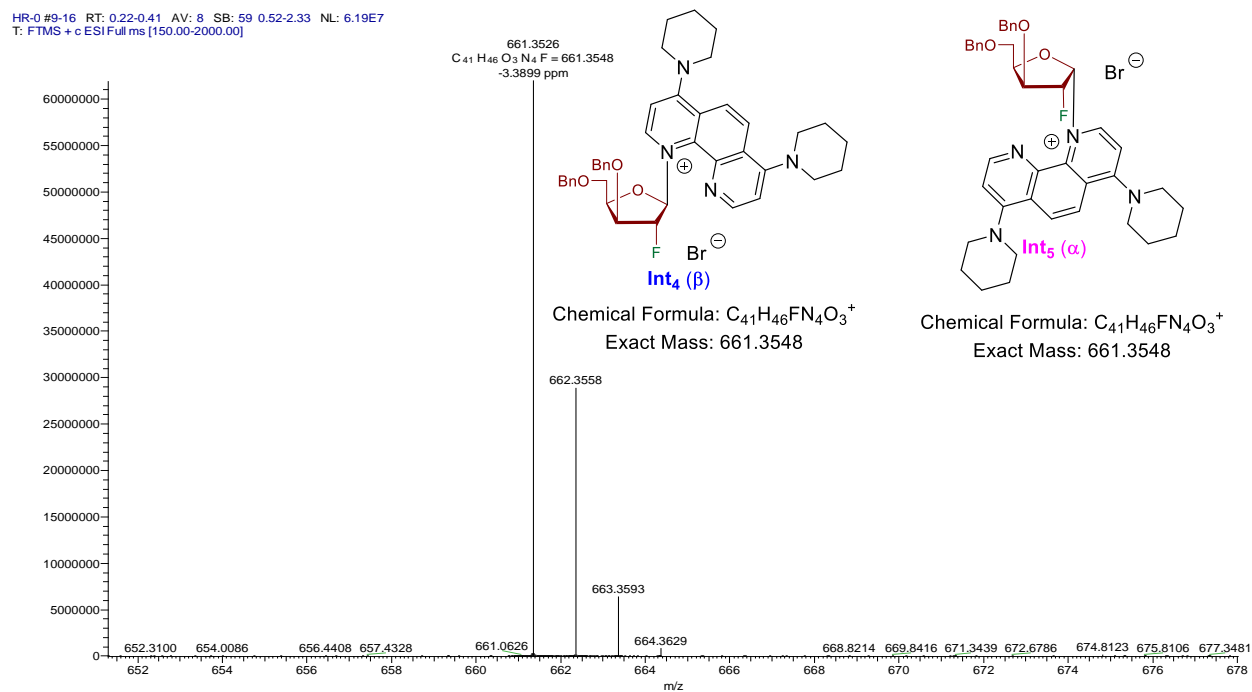
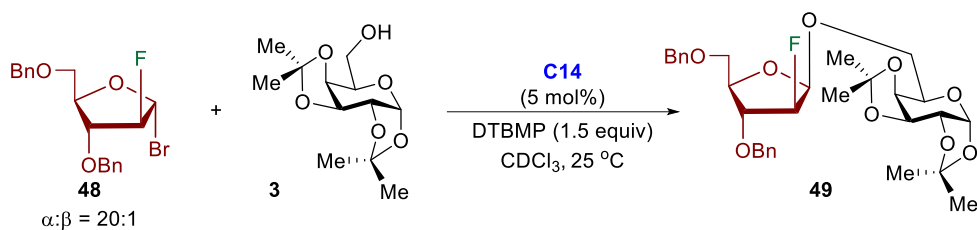


Figure 58. Mass Spectrum of xylofuranosyl phenanthrolium intermediates (**Int₄** and **Int₅**)

5.4.3. NMR study with 2-fluoro arabinofuranosyl donor

NMR course of glycosylation with 2-fluoro arabinofuranosyl bromide **48**



A 5 mm NMR tube was charged with 2-fluoro arabinosyl bromide **48** (3.0 equiv) and CDCl_3 (0.6 mL) (^1H and ^{19}F NMR were acquired). Then 5 mol% phenanthroline **C14** (with respect to donor) was added, ^1H and ^{19}F NMR were acquired after 30 min. After the NMR was taken, then the mixture in the NMR tube was added with acceptor **3** (1.0 equiv.) and DTBMP (1.5 equiv.). ^1H (Figure 59) and ^{19}F (Figure 60) NMR spectra were obtained at the given time (10 min -20 h) depending on the experiment.

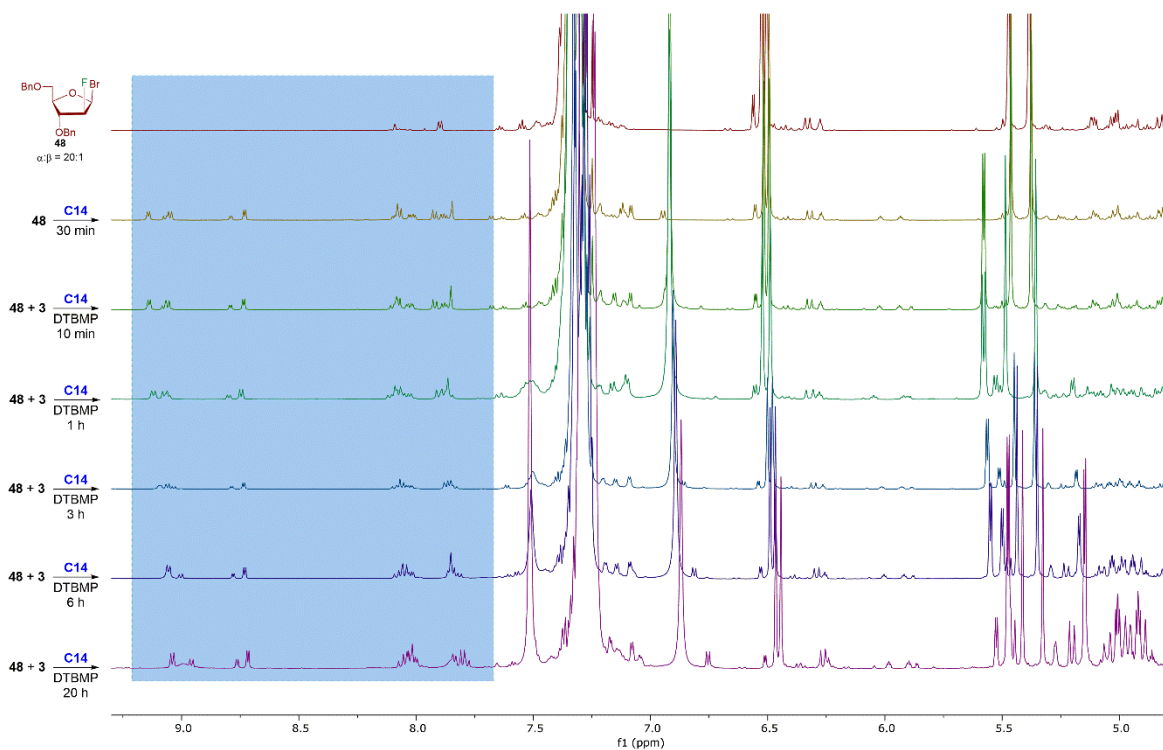


Figure 59. ^1H NMR course of furanosylation with 2-fluoro arabinofuranosyl bromide **48**

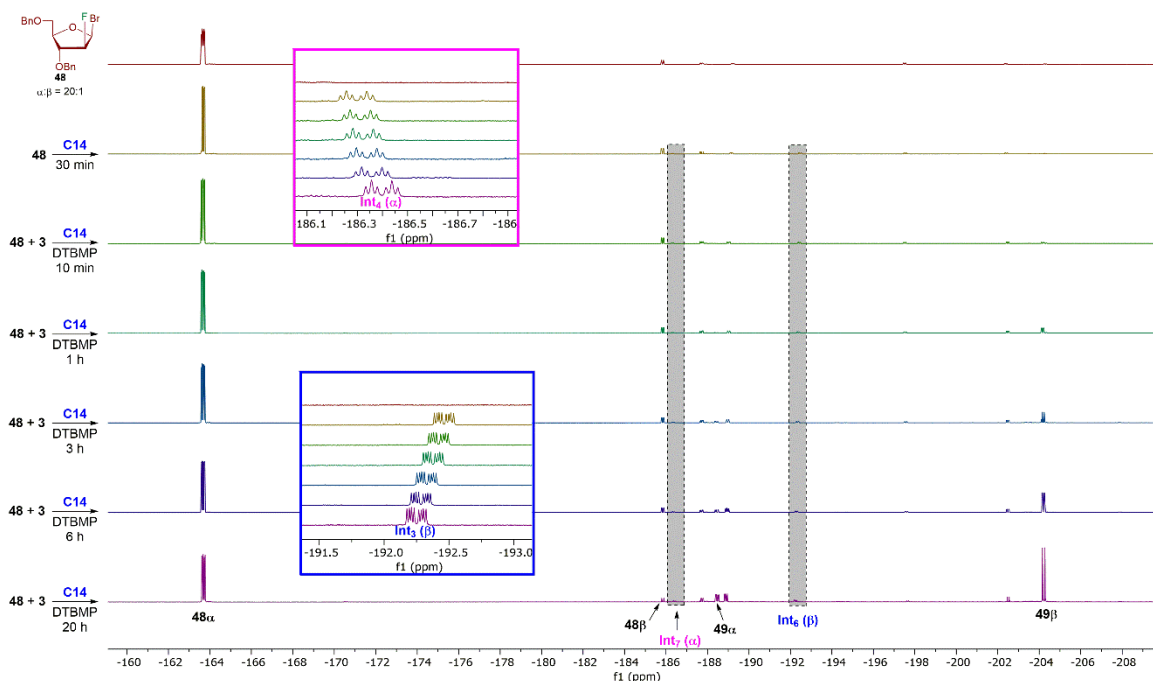
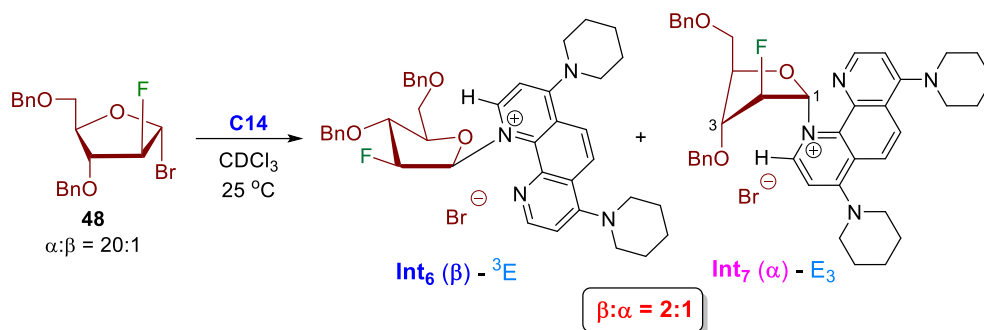


Figure 60. ^{19}F NMR course of furanosylation with 2-fluoro arabinofuranosyl bromide **48**

NMR detection of arabinofuranosyl phenanthrolium intermediates



A 5 mm NMR tube was charged with 2-fluoro arabinosyl bromide **48** (1.5 equiv.) and CDCl_3 (0.6 mL), ^1H and ^{19}F NMR were acquired. Then phenanthroline **C14** (1.0 equiv.) was added to the NMR tube. ^1H (Figure 61) and ^{19}F (Figure 62) NMR spectra were obtained at the given time (10 min -16 h) depending on the experiment. The full spectra of ^1H , ^1H - ^1H 2D COSY and NOESY NMR and mass spectrum are shown in Figure 63 - Figure 66.

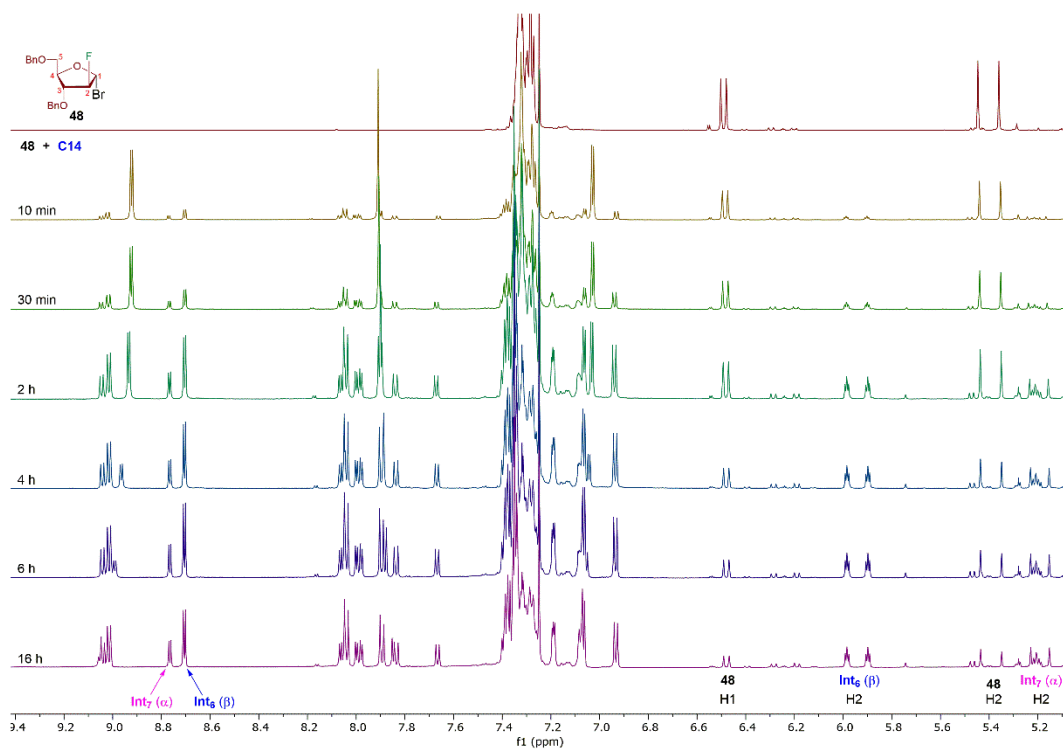


Figure 61. ^1H NMR detection of arabinofuranosyl phenanthrolium intermediates (**Int₆** and **Int₇**)

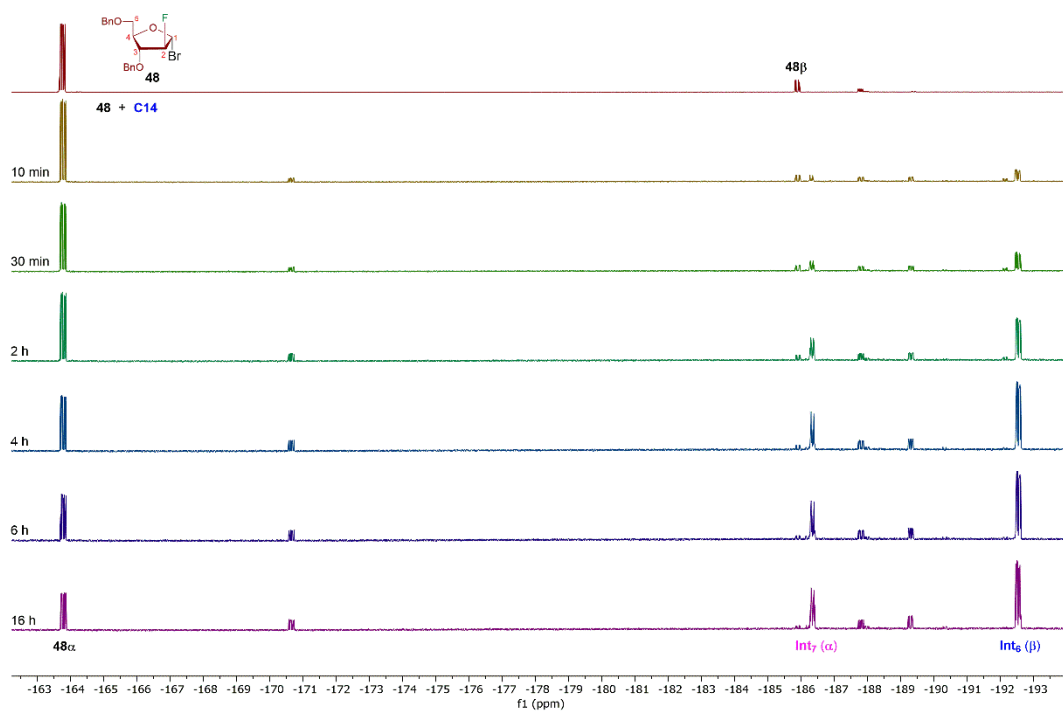


Figure 62. ^{19}F NMR detection of arabinofuranosyl phenanthrolium intermediates (**Int₆** and **Int₇**)

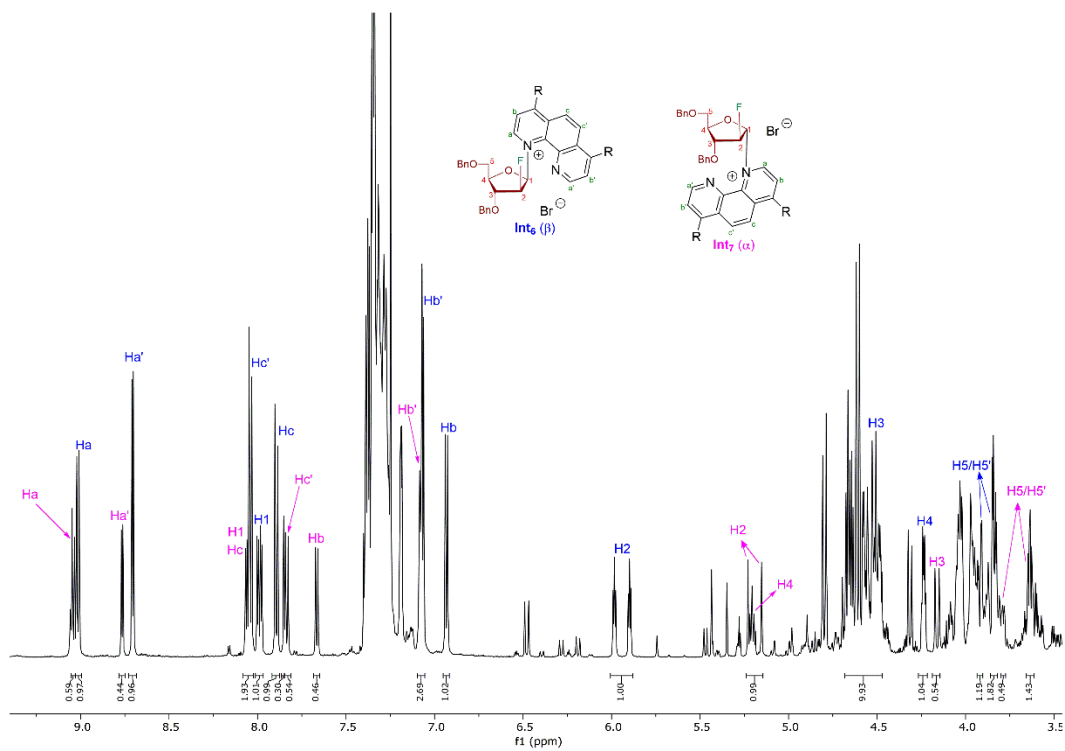


Figure 63. ^1H NMR of arabinofuranosyl phenanthrolium intermediates (**Int₆** and **Int₇**)

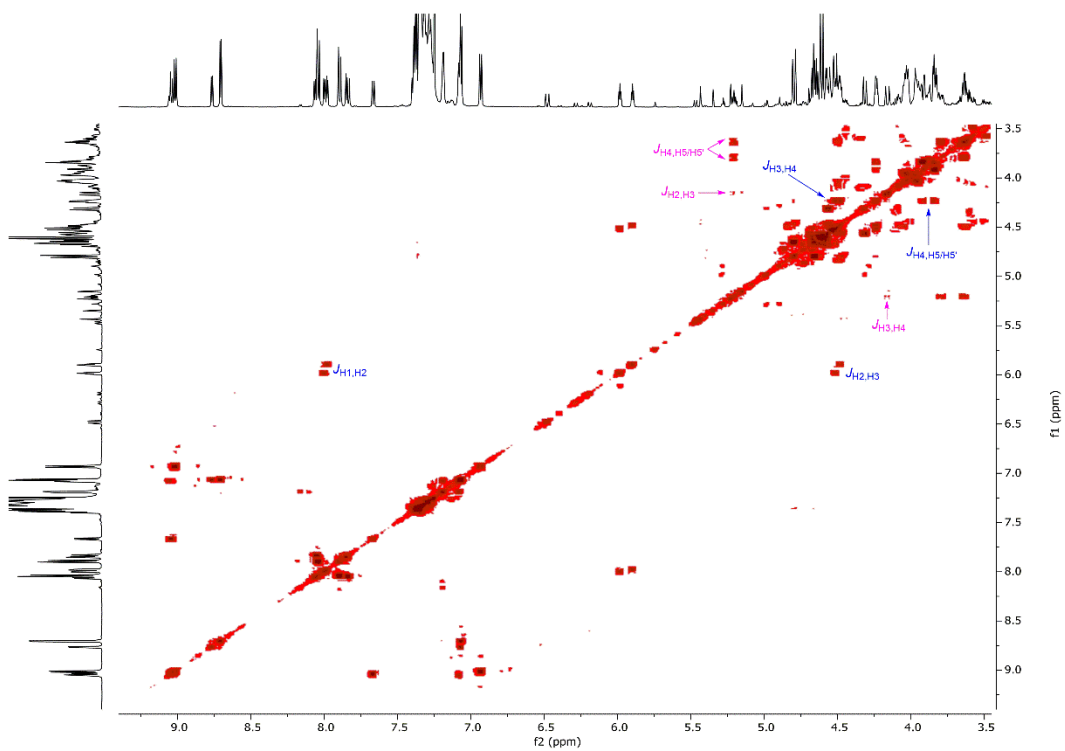


Figure 64. ^1H - ^1H COSY NMR of arabinofuranosyl phenanthrolium intermediates (**Int₆** and **Int₇**)

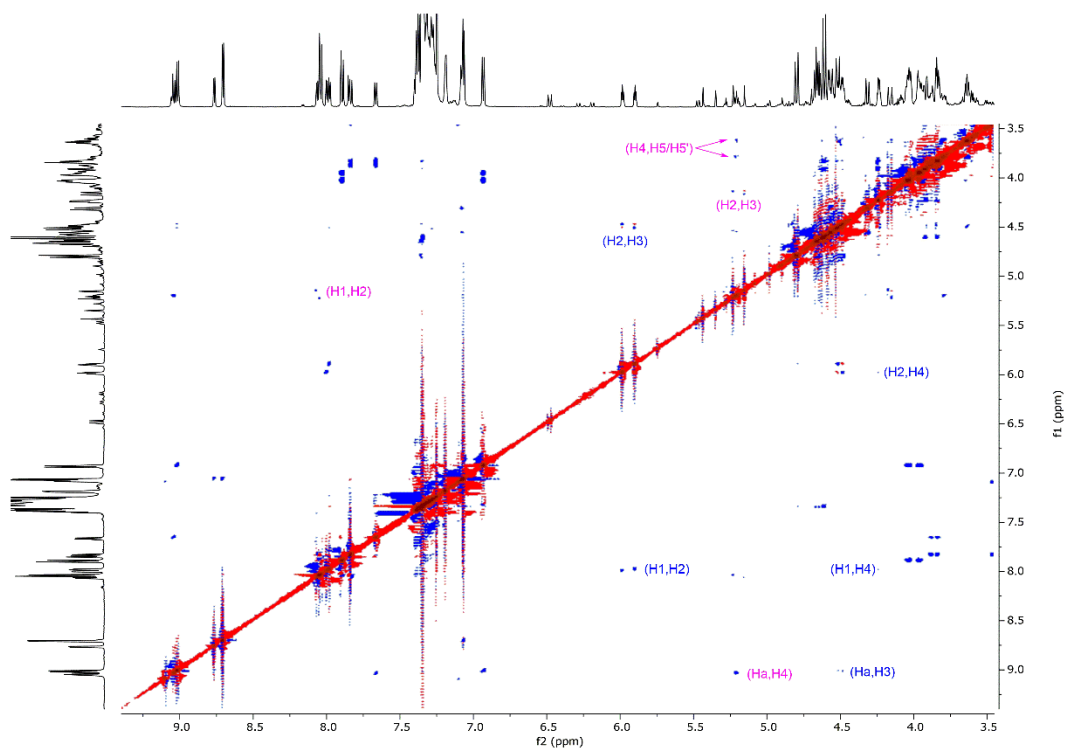


Figure 65. ^1H - ^1H NOESY NMR of arabinofuranosyl phenanthrolium intermediates (**Int₆** and **Int₇**)

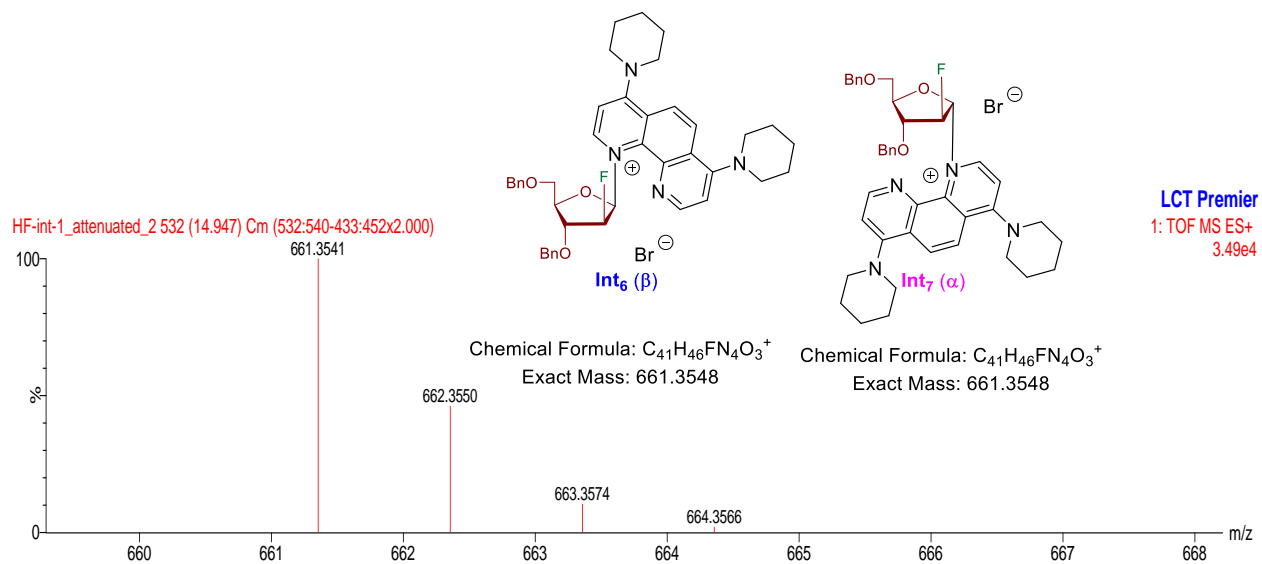
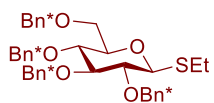
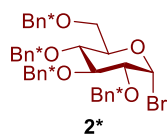
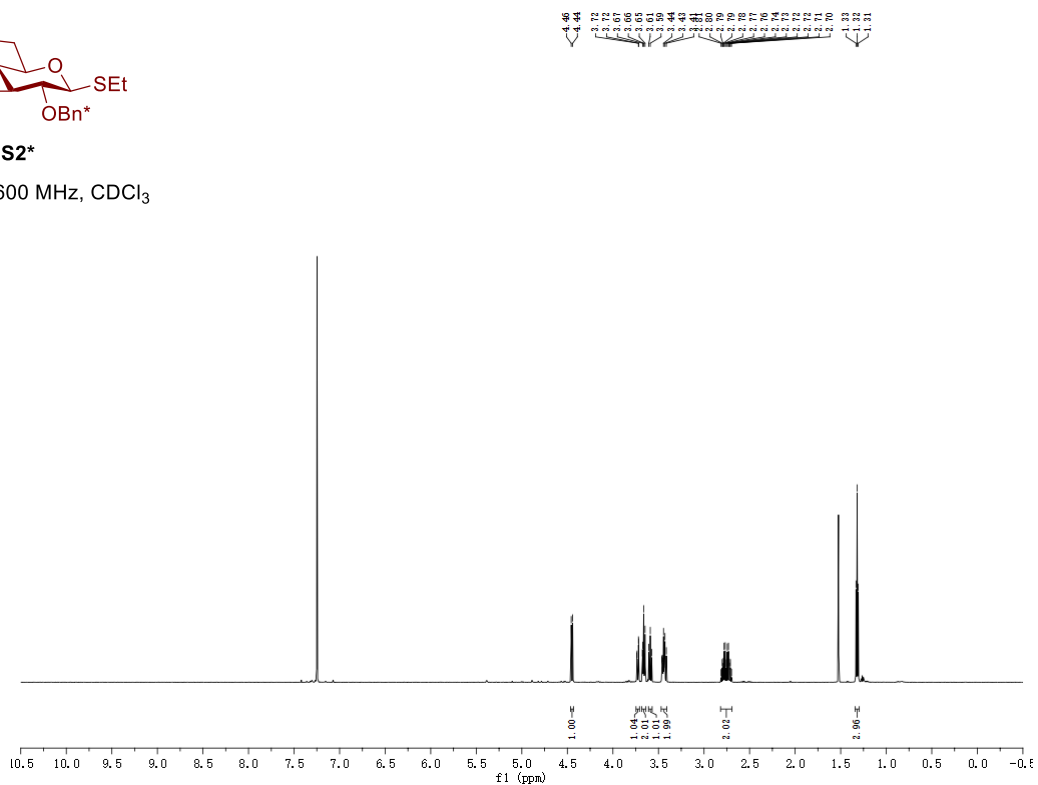
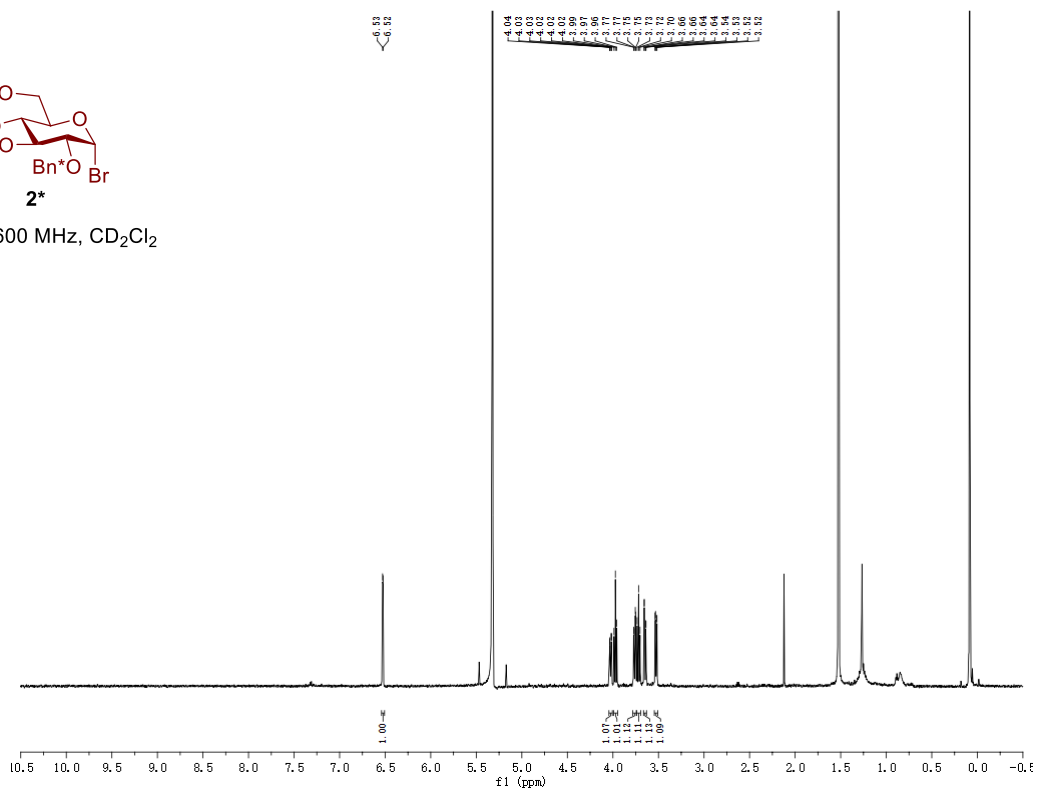
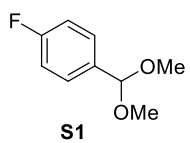


Figure 66. Mass Spectrum of xylofuranosyl phenanthrolium intermediates (**Int₆** and **Int₇**)

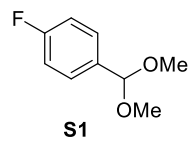
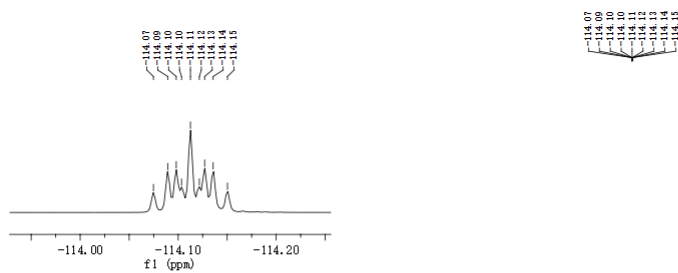
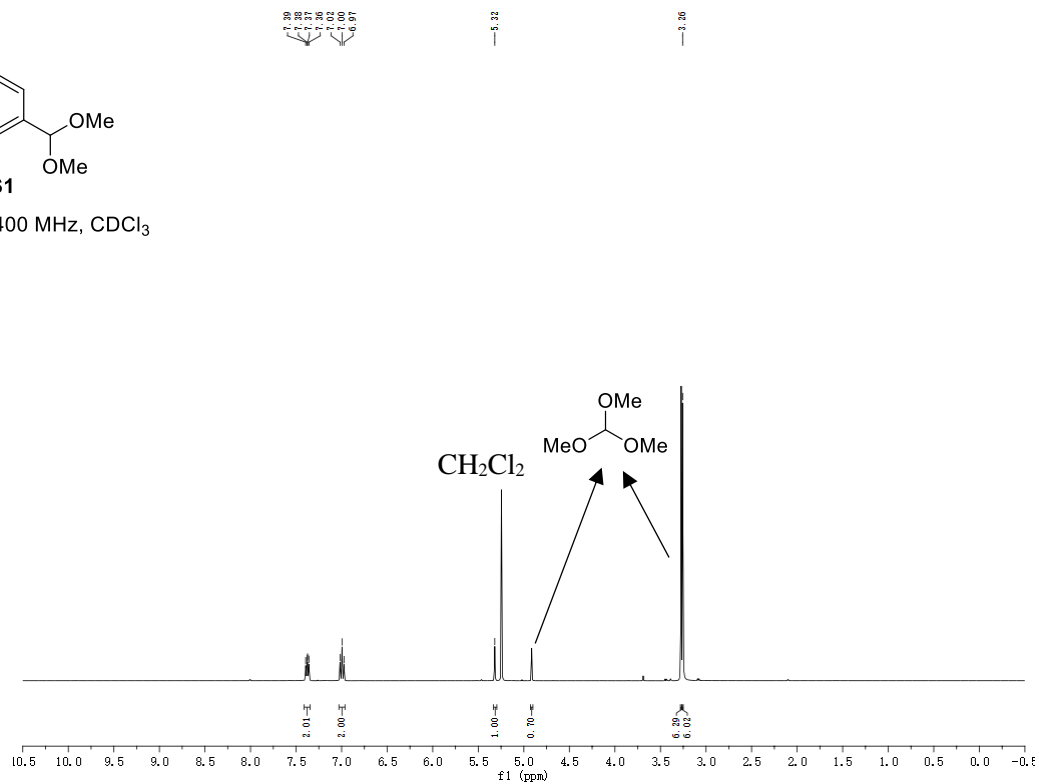
APPENDIX A: SYMBOL NOMENCLATURE FOR GLYCANS²²

SHAPE	White (Generic)	Blue	Green	Yellow	Orange	Pink	Purple	Light Blue	Brown	Red
Filled Circle	Hexose ○	Glc	Man	Gal	Gul	Alt	All	Tal	Ido	
Filled Square	HexNAc ◻	GlcNAc	ManNAc	GalNAc	GuINAc	AIINAc	AIINAc	TalNAc	IdoNAc	
Crossed Square	Hexosamine ◻	GlcN	Mann	GalN	GuIN	AIIN	AIIN	TalN	IdoN	
Divided Diamond	Hexurionate ◊	GlcA	ManA	GalA	GuIA	AIIA	AIIA	TalA	IdoA	
Filled Triangle	Deoxyhexose △	Qui	Rha		6dGul	6dAlt		6dTal		Fuc ▲
Divided Triangle	DeoxyhexNAc △	QuiNAc	RhaNAc			6dAIINAc		6dTalNAc		FucNAc ▲
Flat Rectangle	DJ-deoxyhexose ◻	Oli	Ivy		Abe	Par	Dig	Col		
Filled Star	Pentose ☆		Ara	Lvx	Xyl	Rib				
Filled Diamond	Deoxynonosonate ◊		Kdn				Neu5Ac	Neu5Gc	Neu	Sia ◆
Flat Diamond	DJ-deoxynonosonate ◊		Pse	Leg		Act		4eLeg		
Flat Hexagon	Unknown ◻	Bac	LDmanHep	Kdo	Dha	DDmanHep	MurNAc	MurNGc	Mur	
Pentagon	Assigned ◻	Api	Fru	Tag	Sor	Psi				

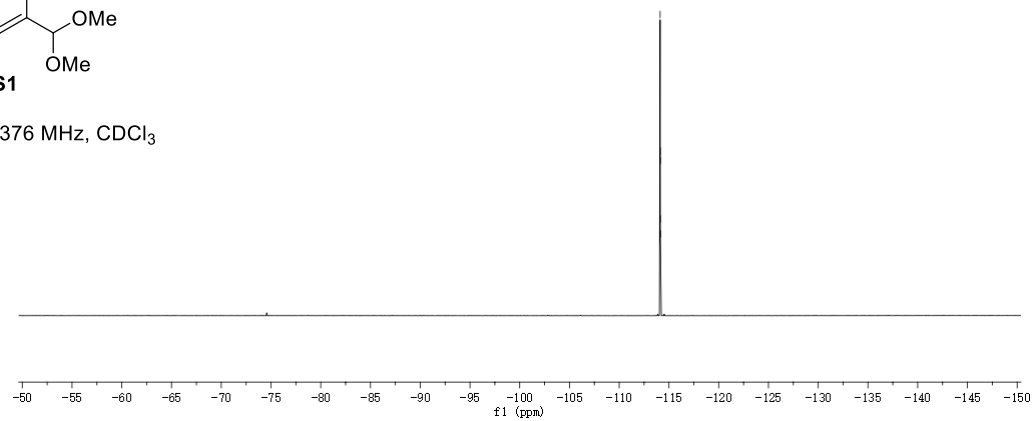
APPENDIX B: ^1H , ^{13}C AND ^{19}F NMR SPECTRA**S2*** ^1H NMR, 600 MHz, CDCl_3 **2*** ^1H NMR, 600 MHz, CD_2Cl_2 

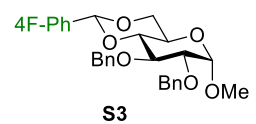
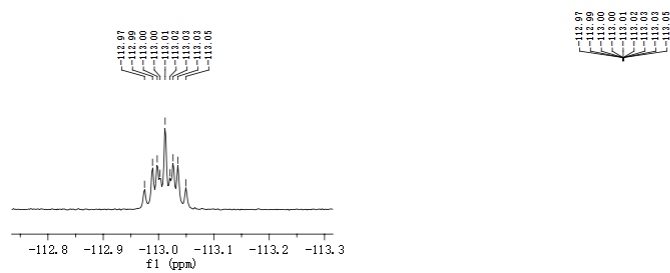


$^1\text{H NMR}$, 400 MHz, CDCl_3

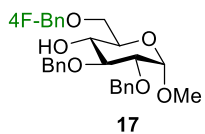
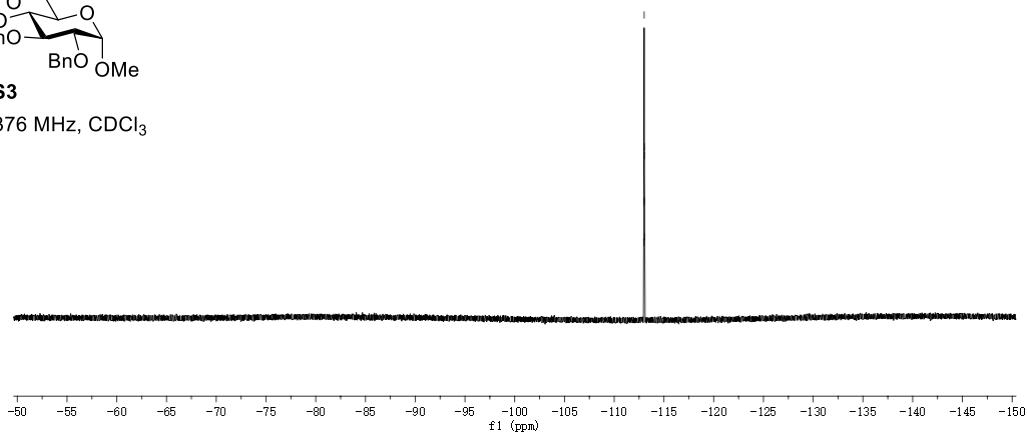


$^{19}\text{F NMR}$, 376 MHz, CDCl_3

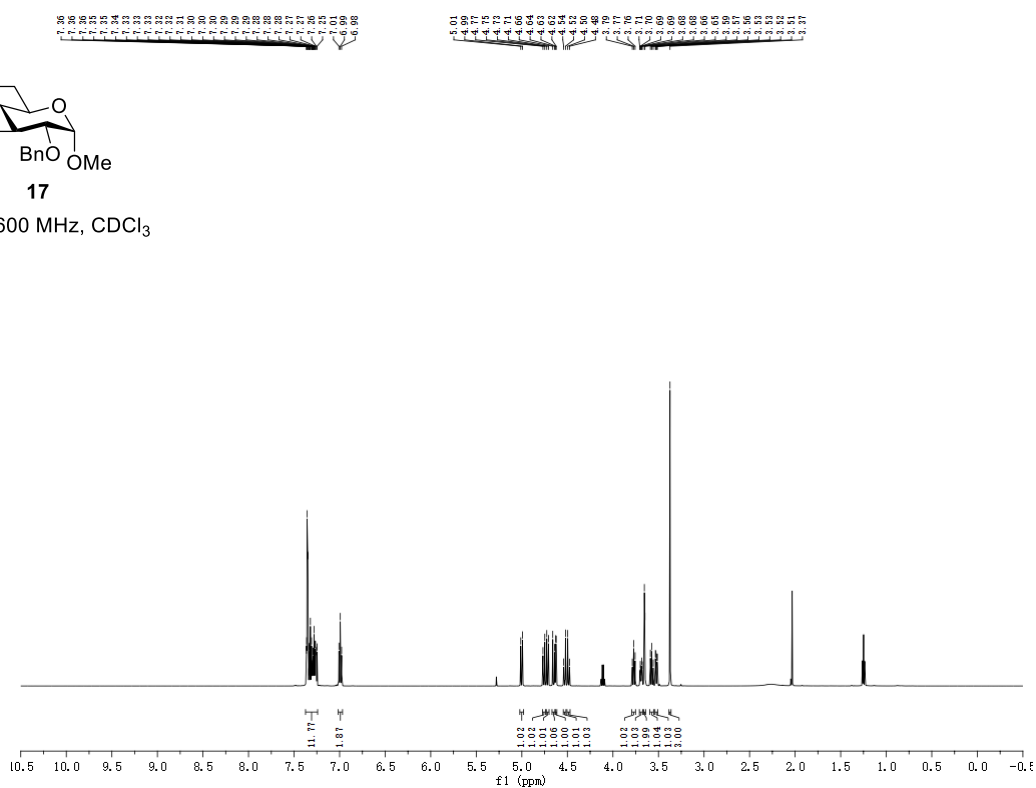


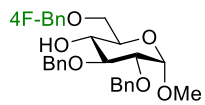


^{19}F NMR, 376 MHz, CDCl_3

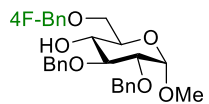
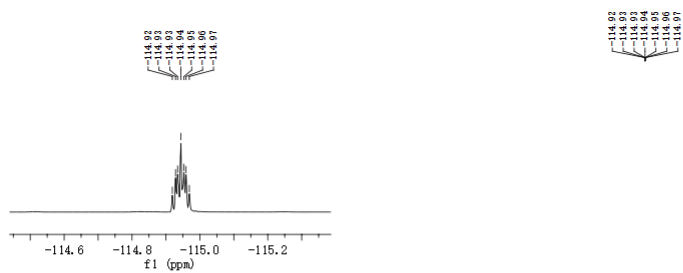
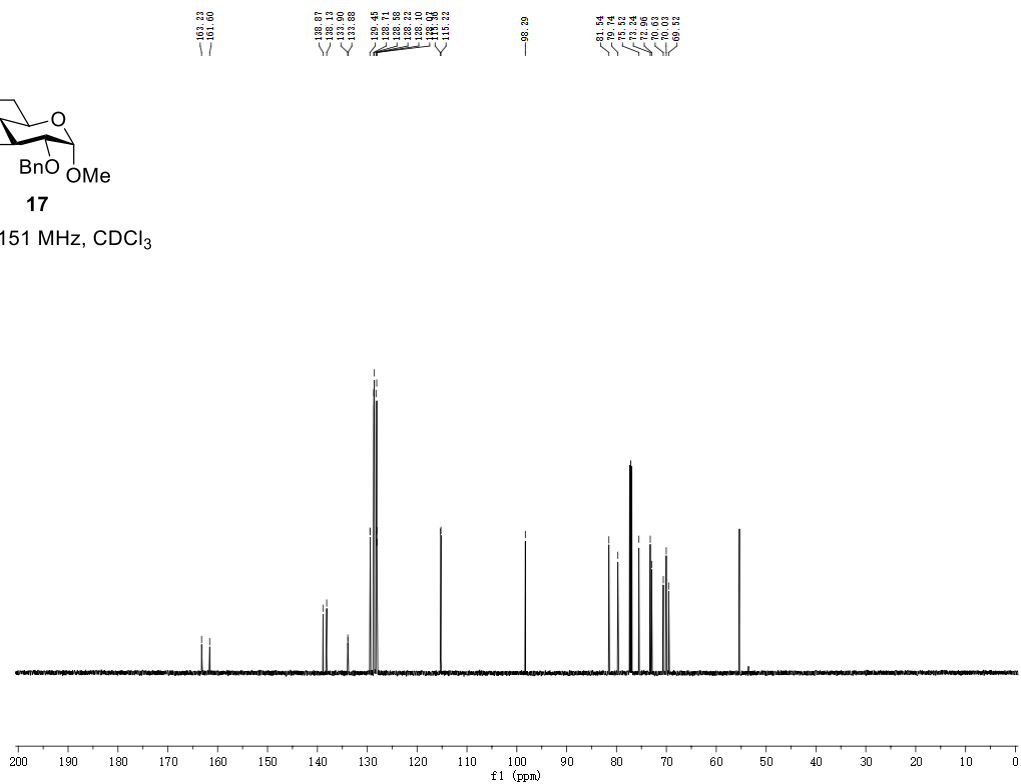


^1H NMR, 600 MHz, CDCl_3

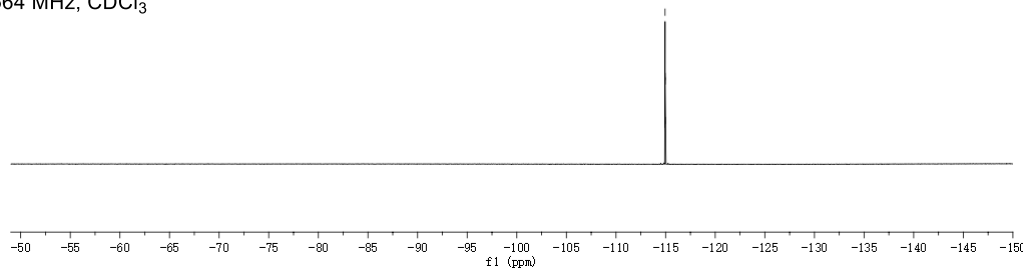


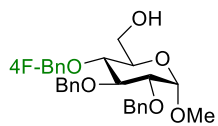
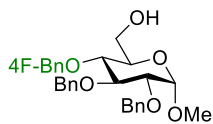
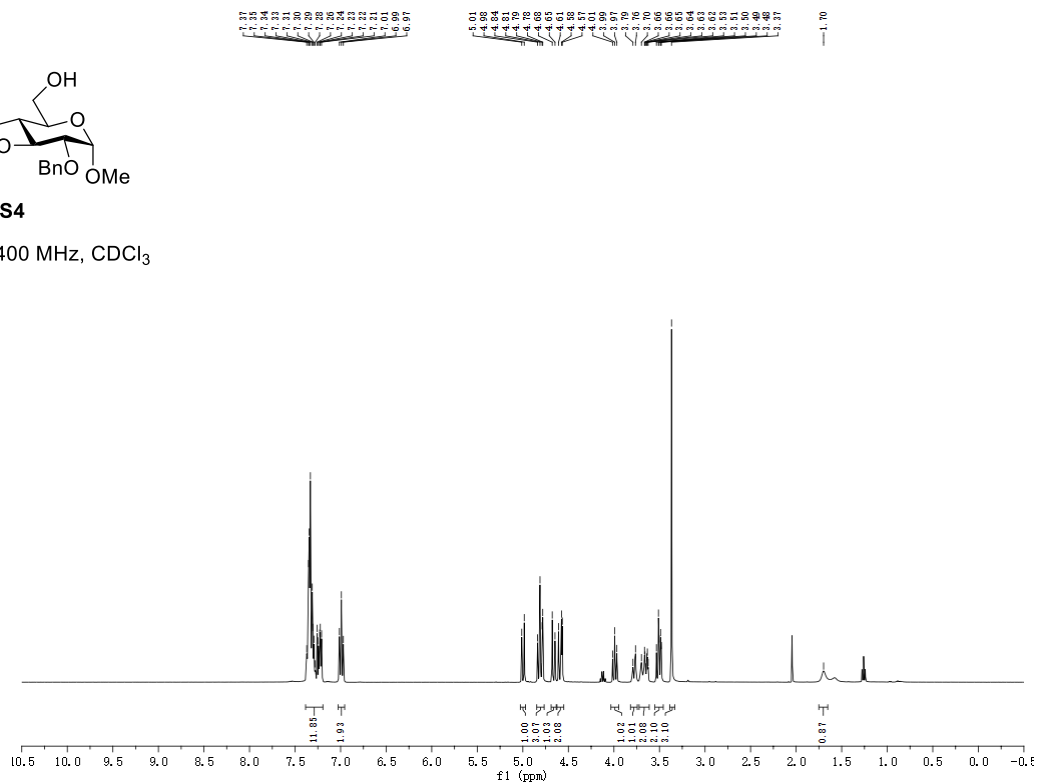
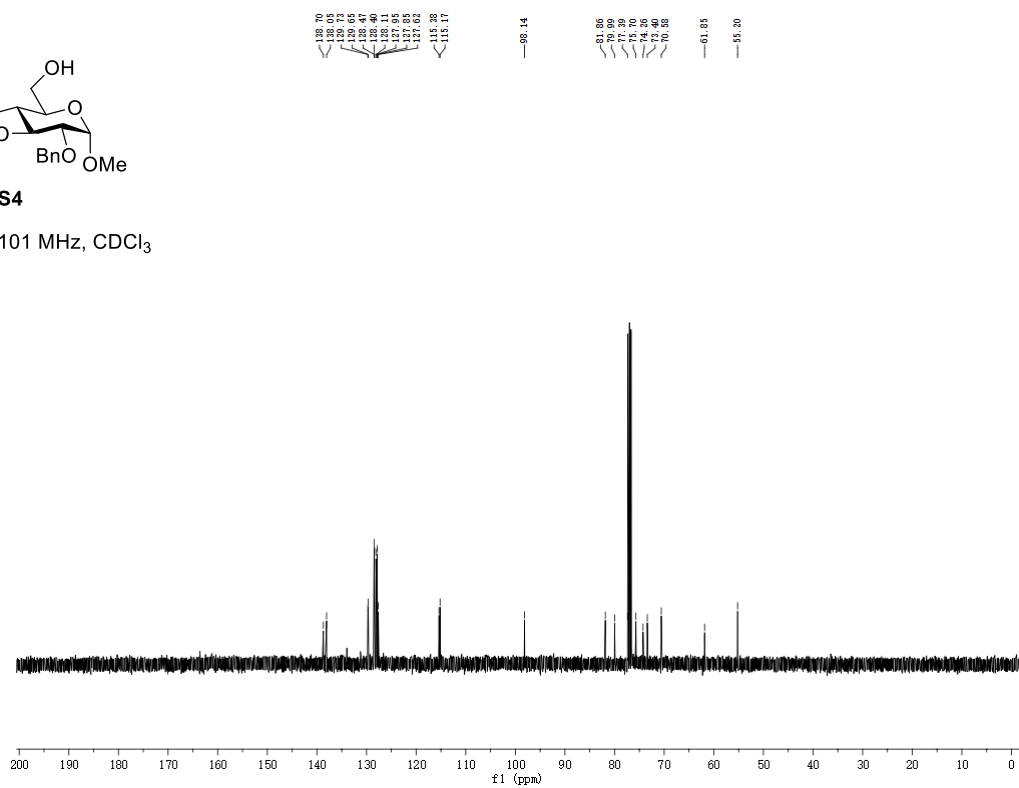


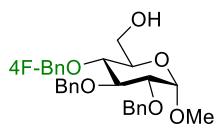
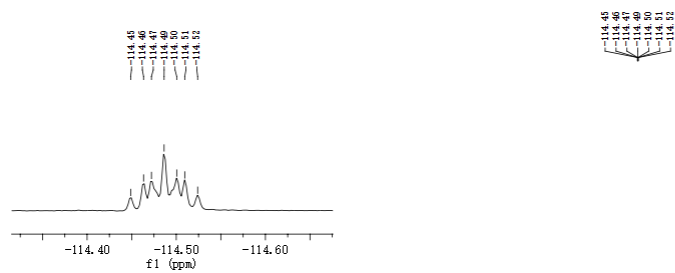
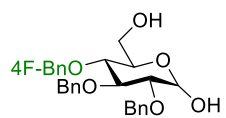
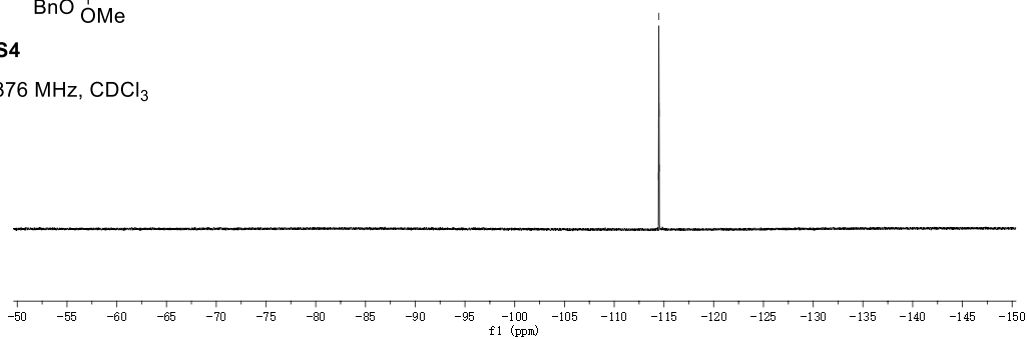
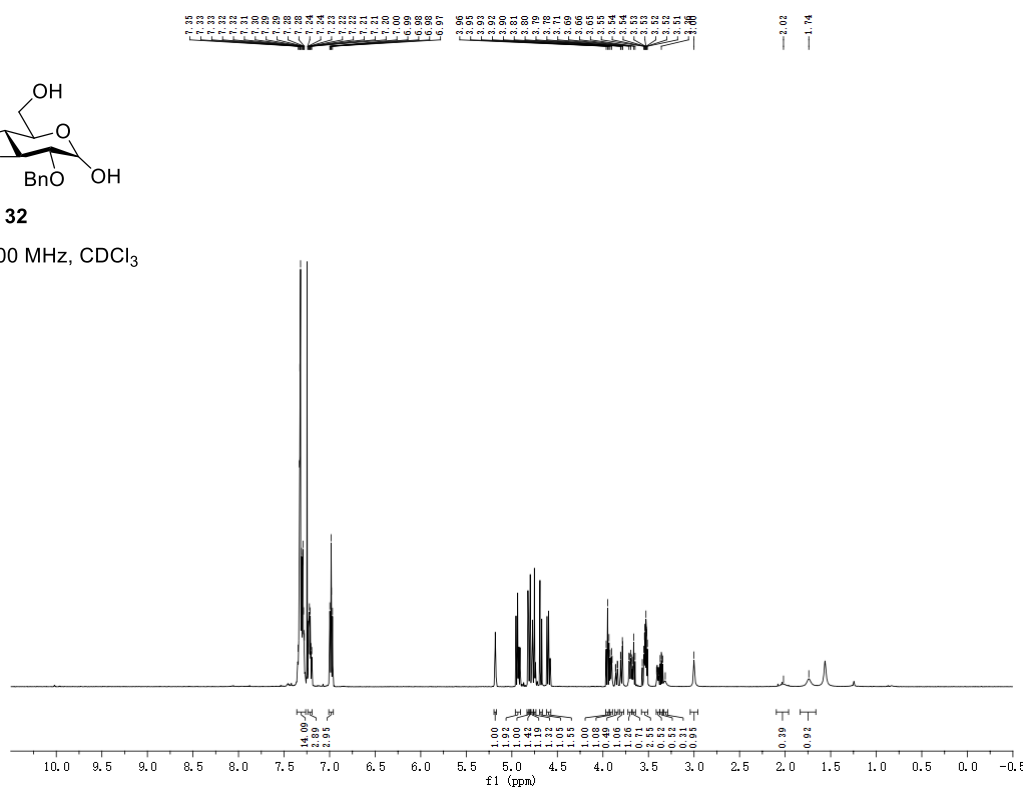
17

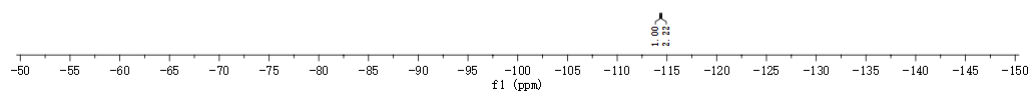
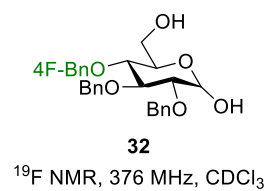
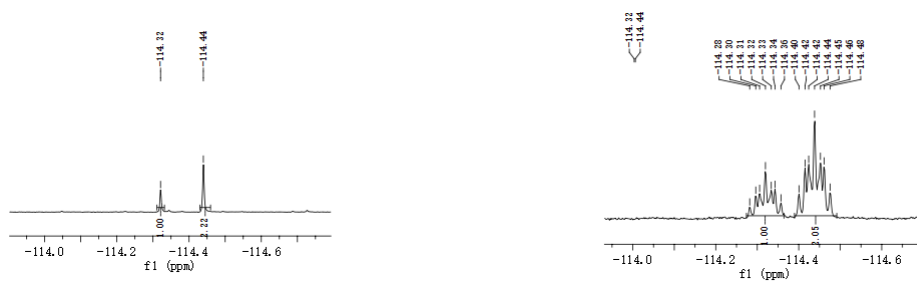
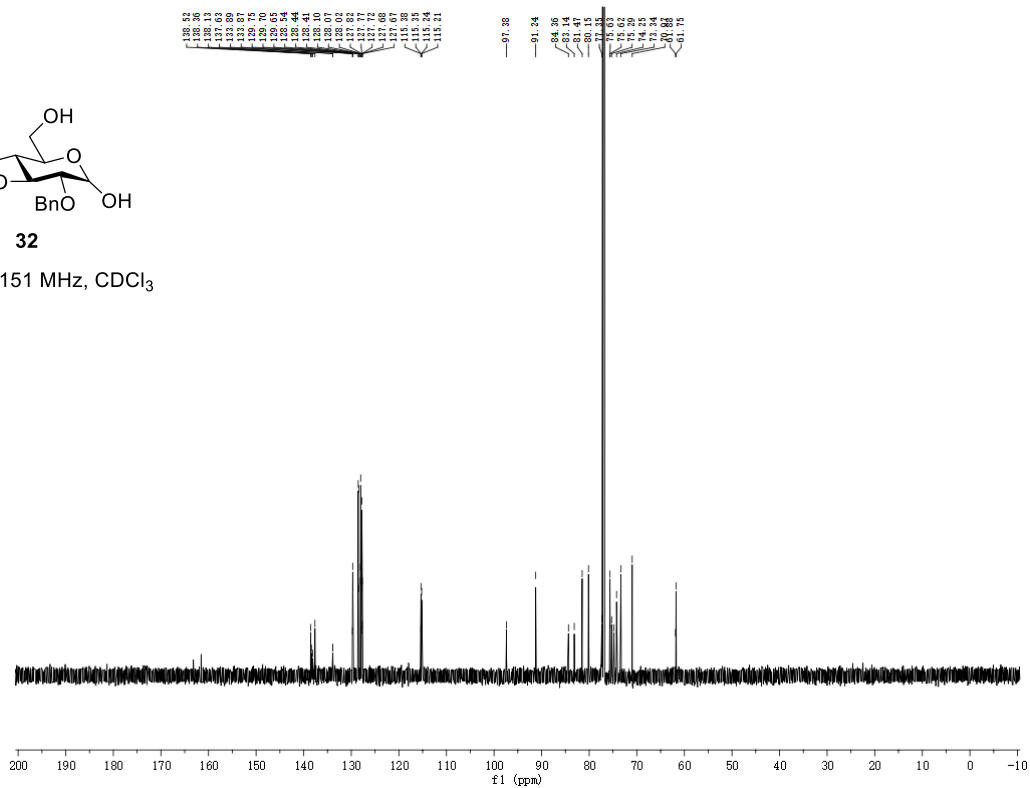
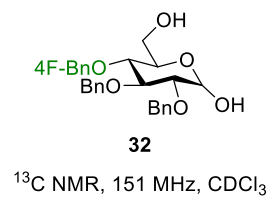
 ^{13}C NMR, 151 MHz, CDCl_3 

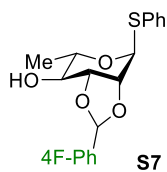
17

 ^{19}F NMR, 564 MHz, CDCl_3 

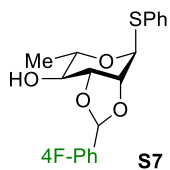
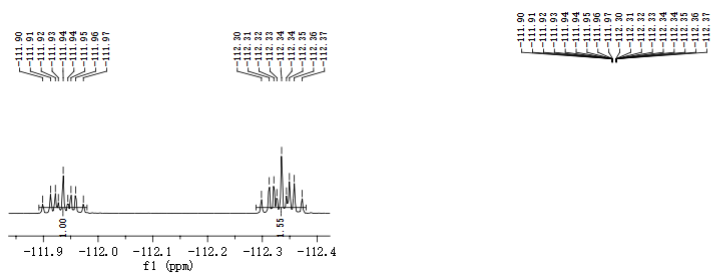
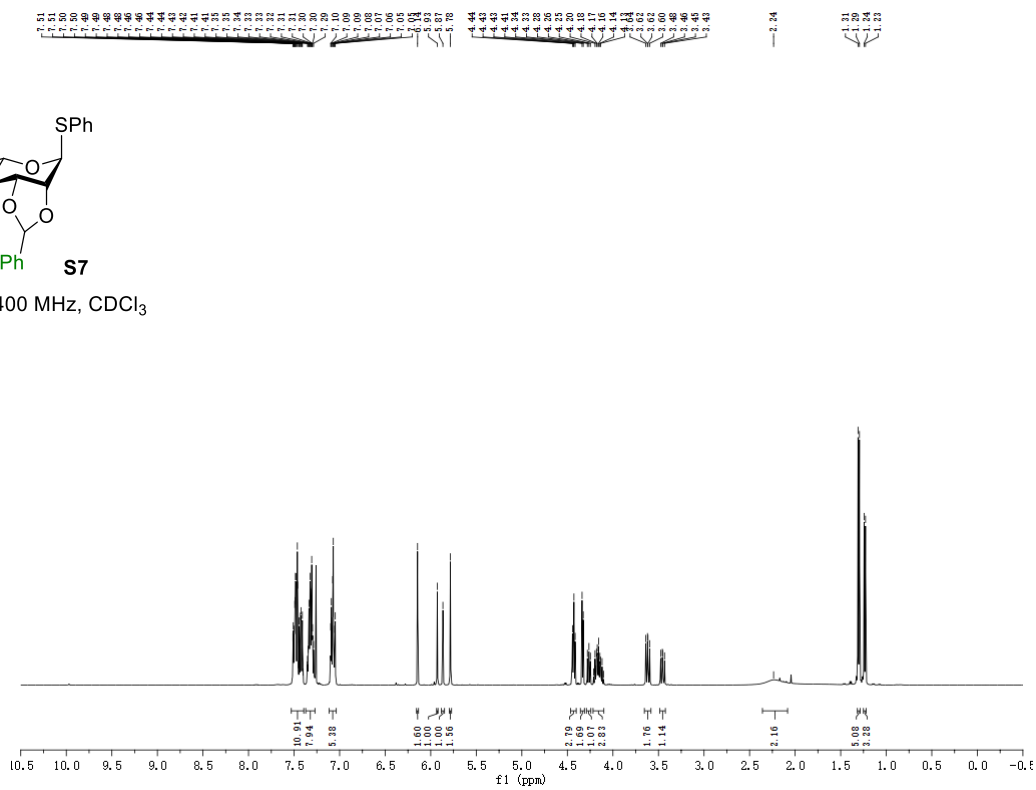
**S4** ^1H NMR, 400 MHz, CDCl_3 **S4** ^{13}C NMR, 101 MHz, CDCl_3 

**S4** ^{19}F NMR, 376 MHz, CDCl_3 **S2** ^1H NMR, 600 MHz, CDCl_3 

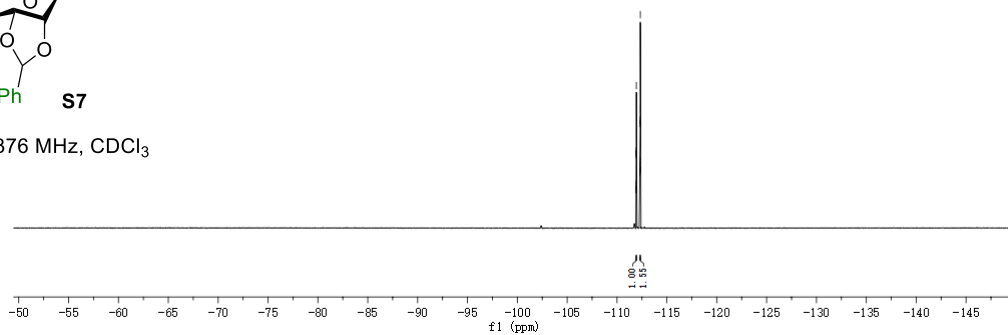


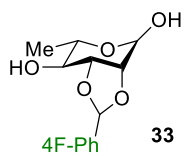


^1H NMR, 400 MHz, CDCl_3

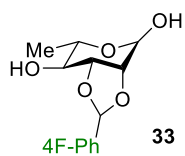
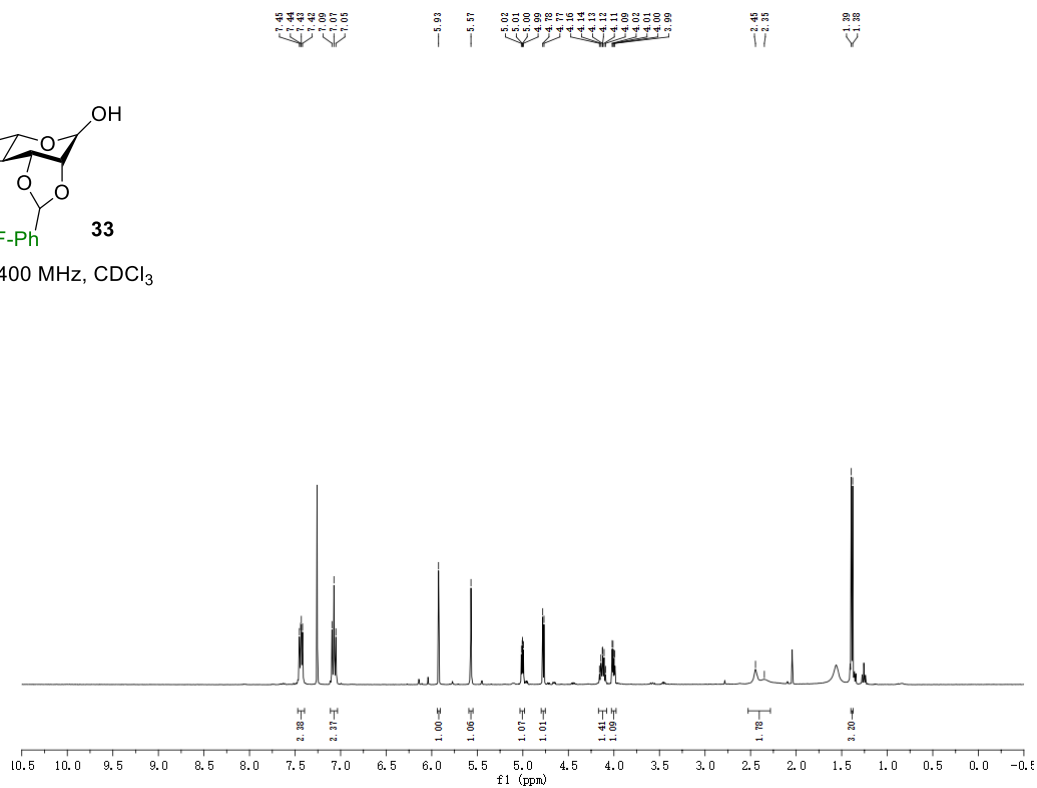


^{19}F NMR, 376 MHz, CDCl_3

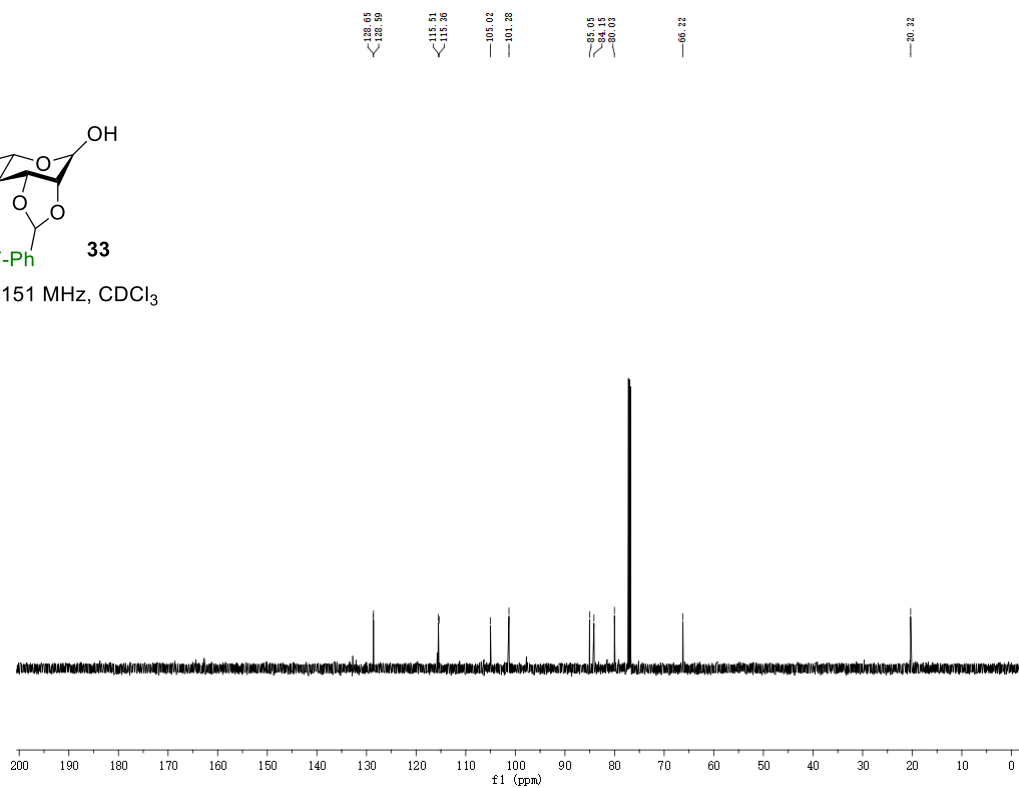


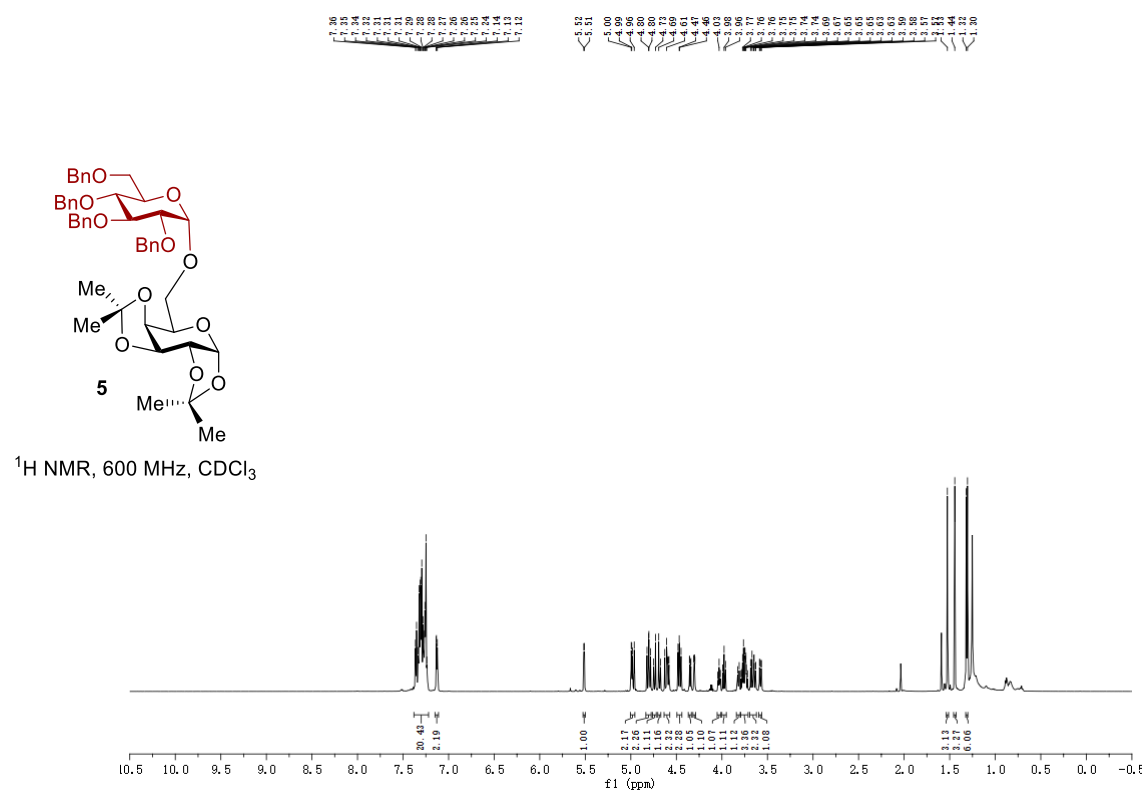
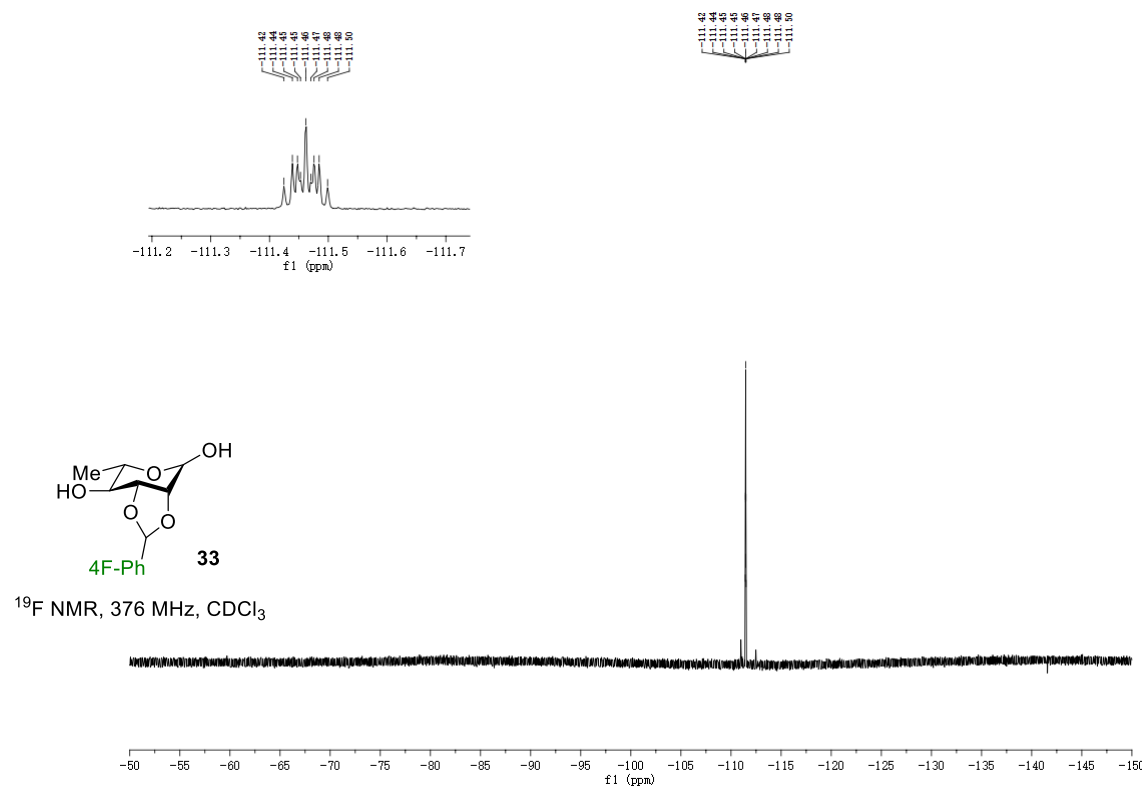


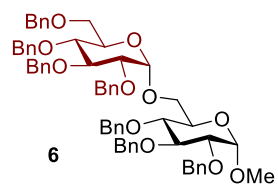
^1H NMR, 400 MHz, CDCl_3



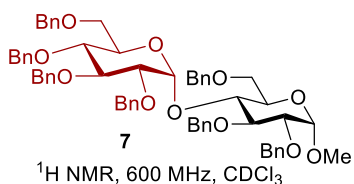
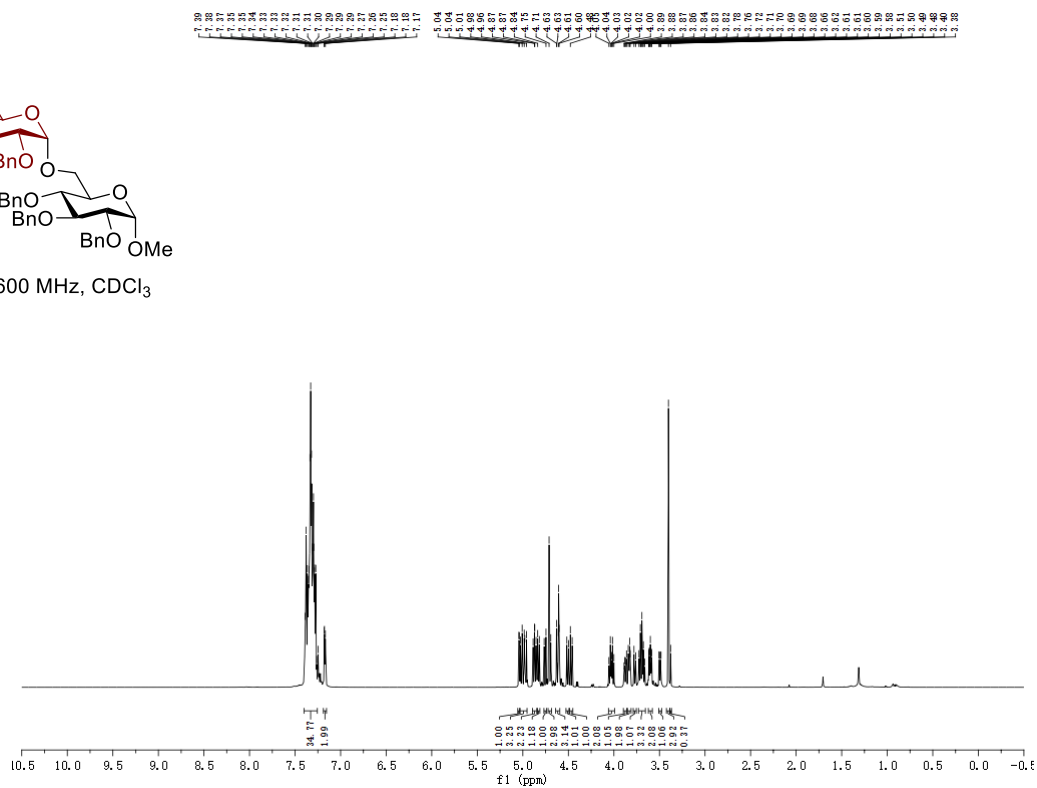
^{13}C NMR, 151 MHz, CDCl_3



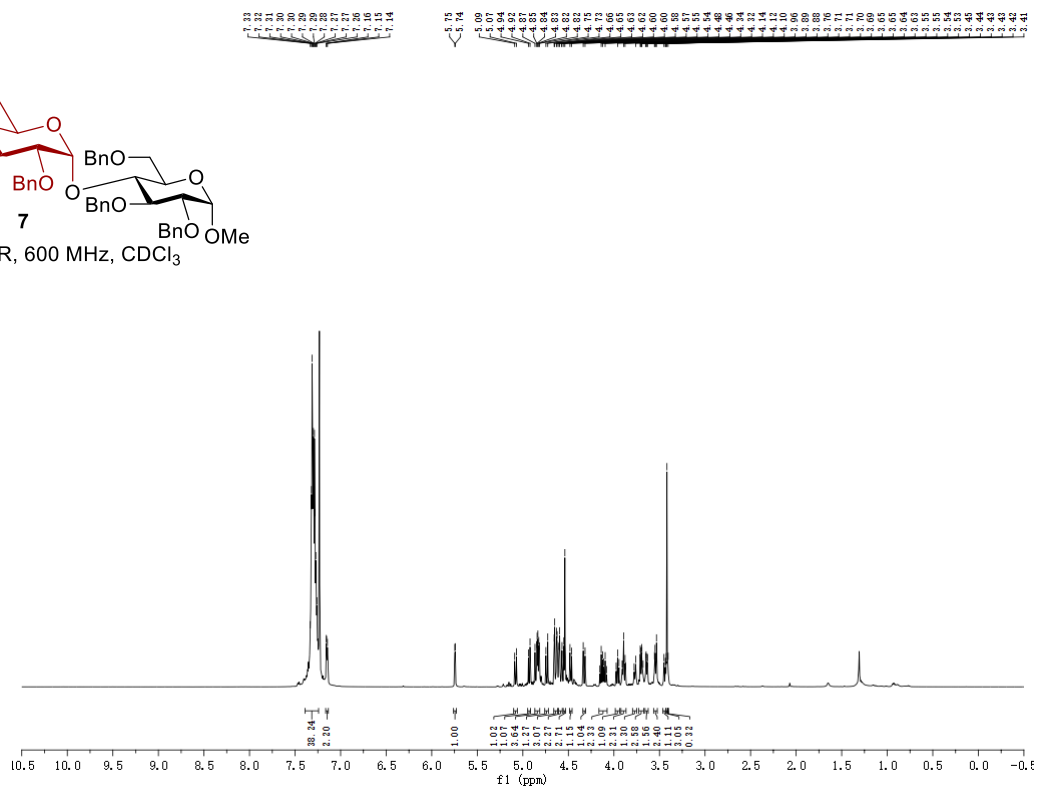


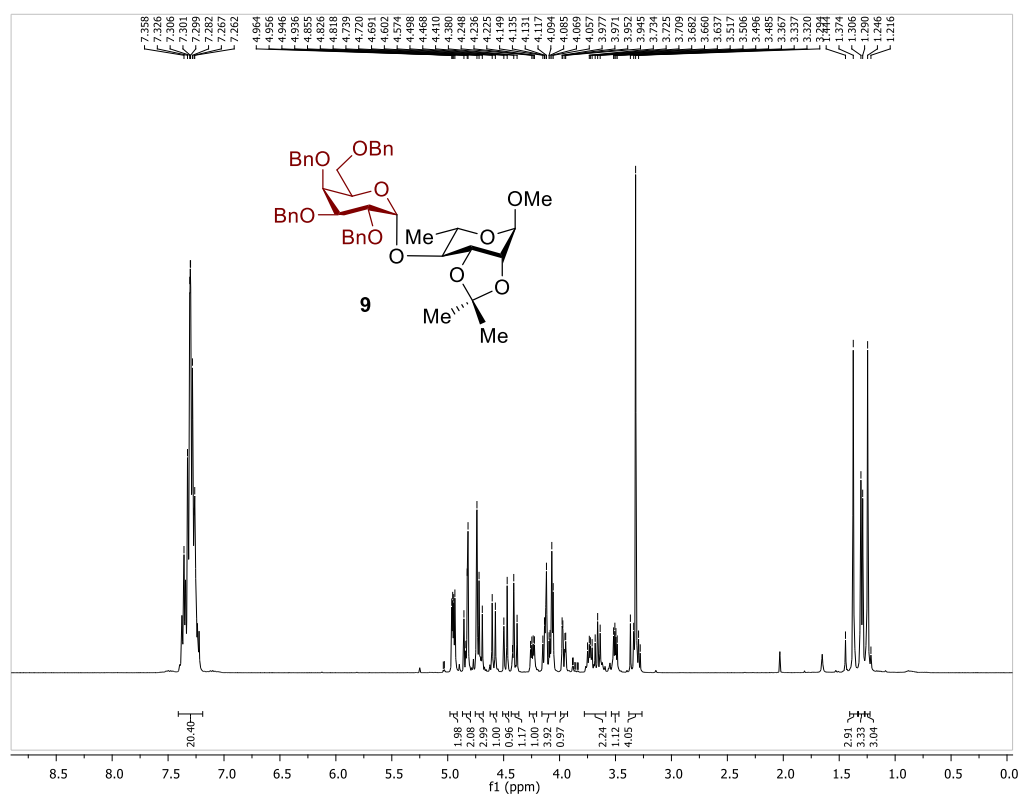
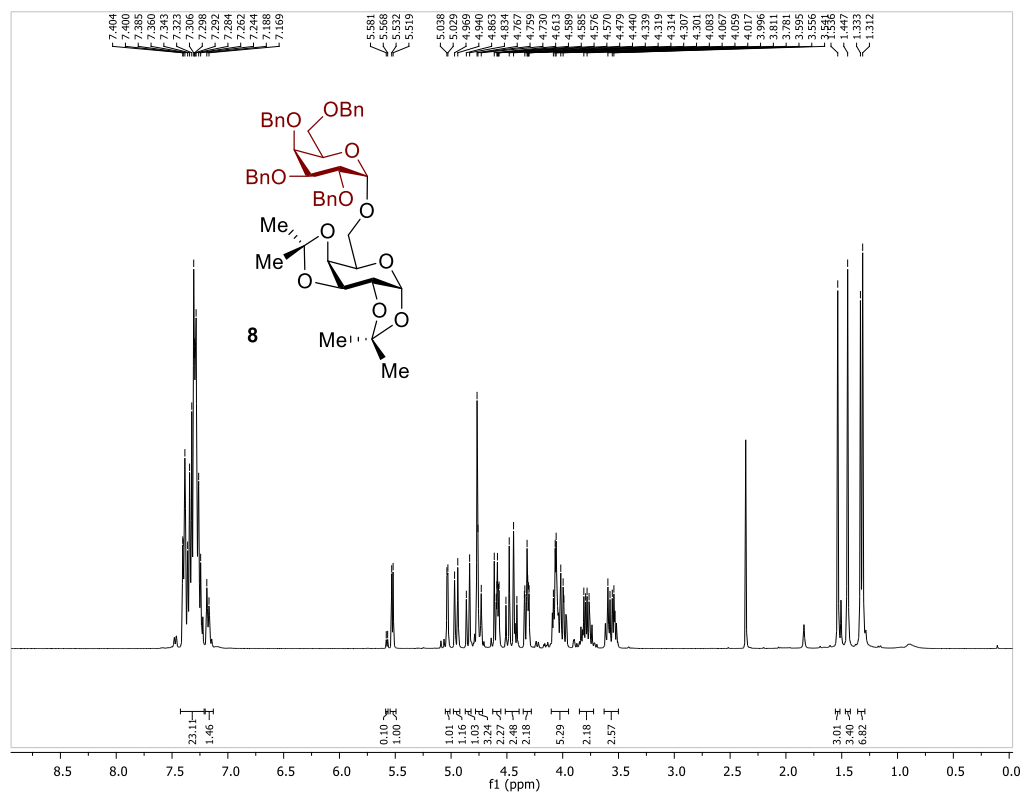


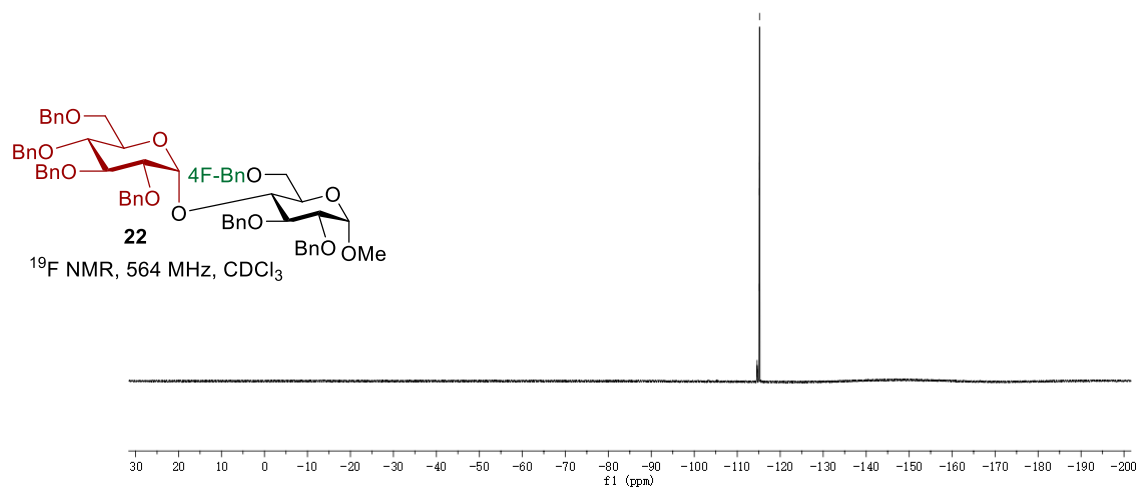
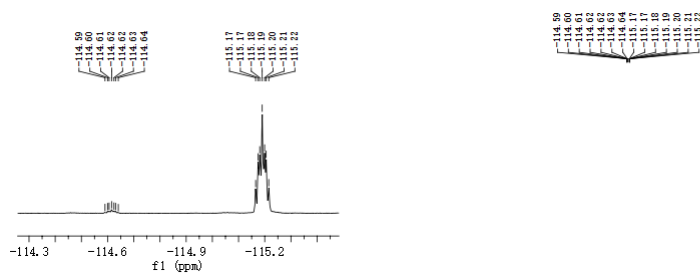
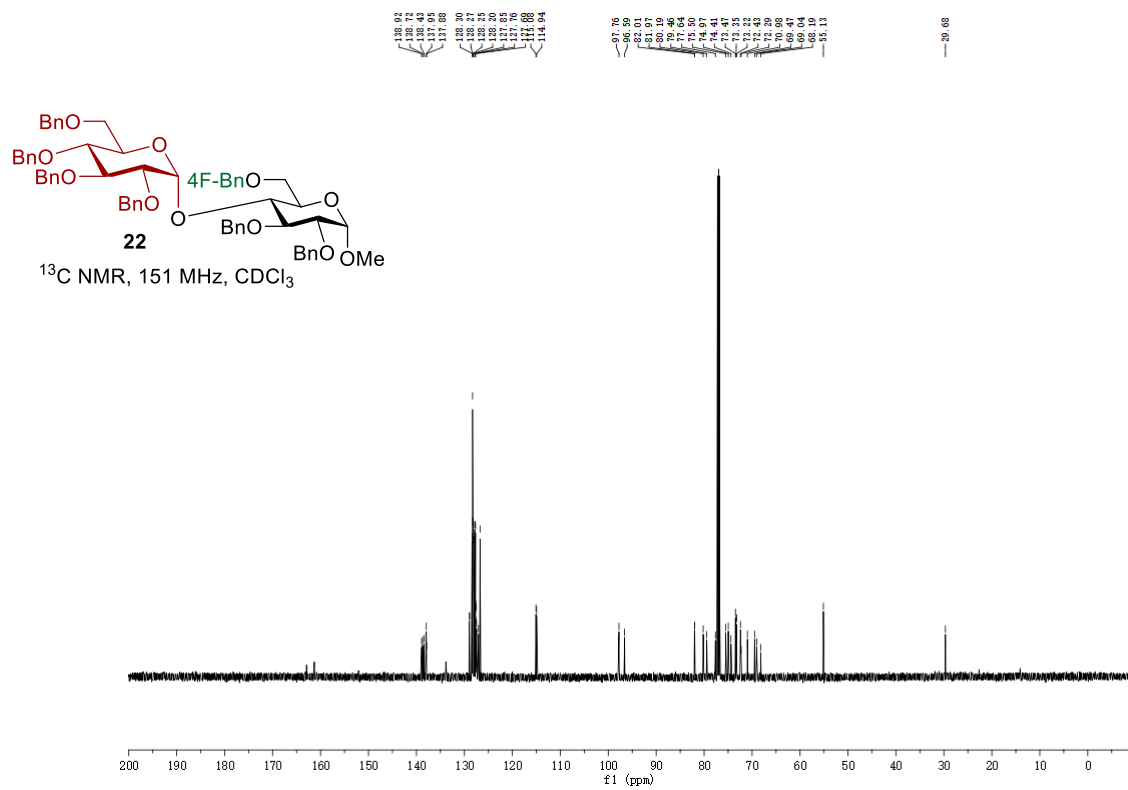
^1H NMR, 600 MHz, CDCl_3

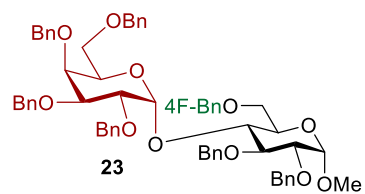


^1H NMR, 600 MHz, CDCl_3

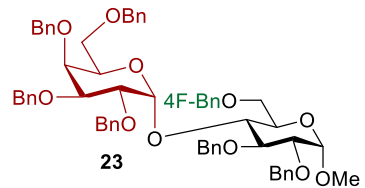
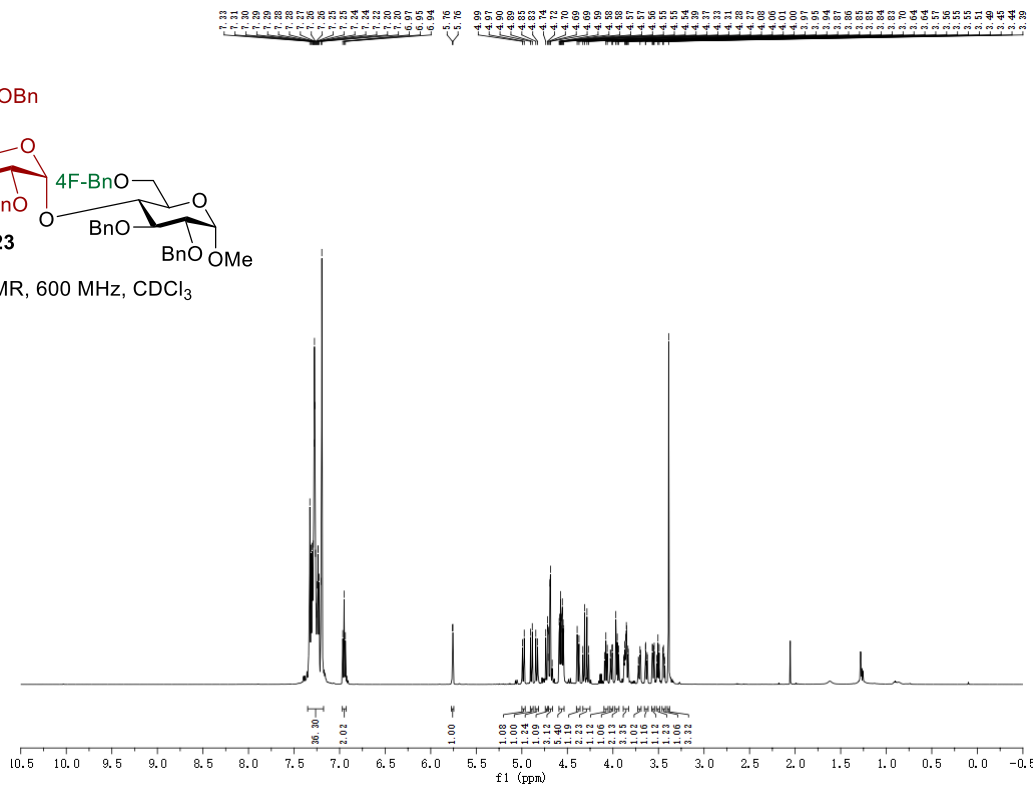




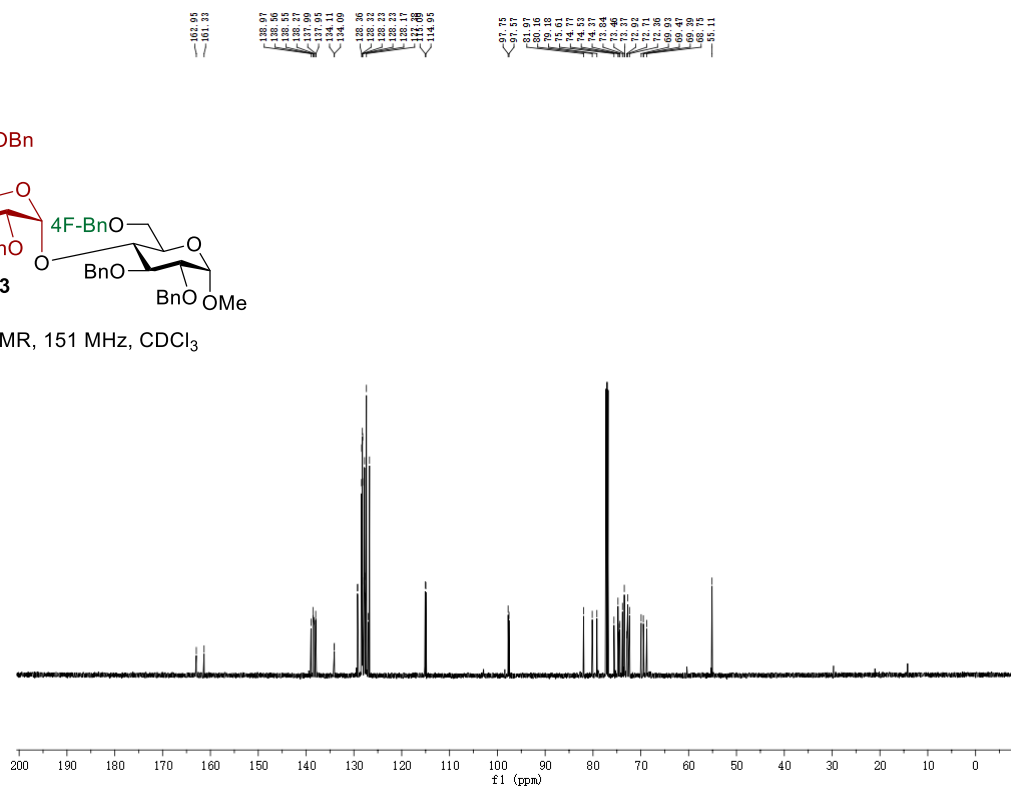


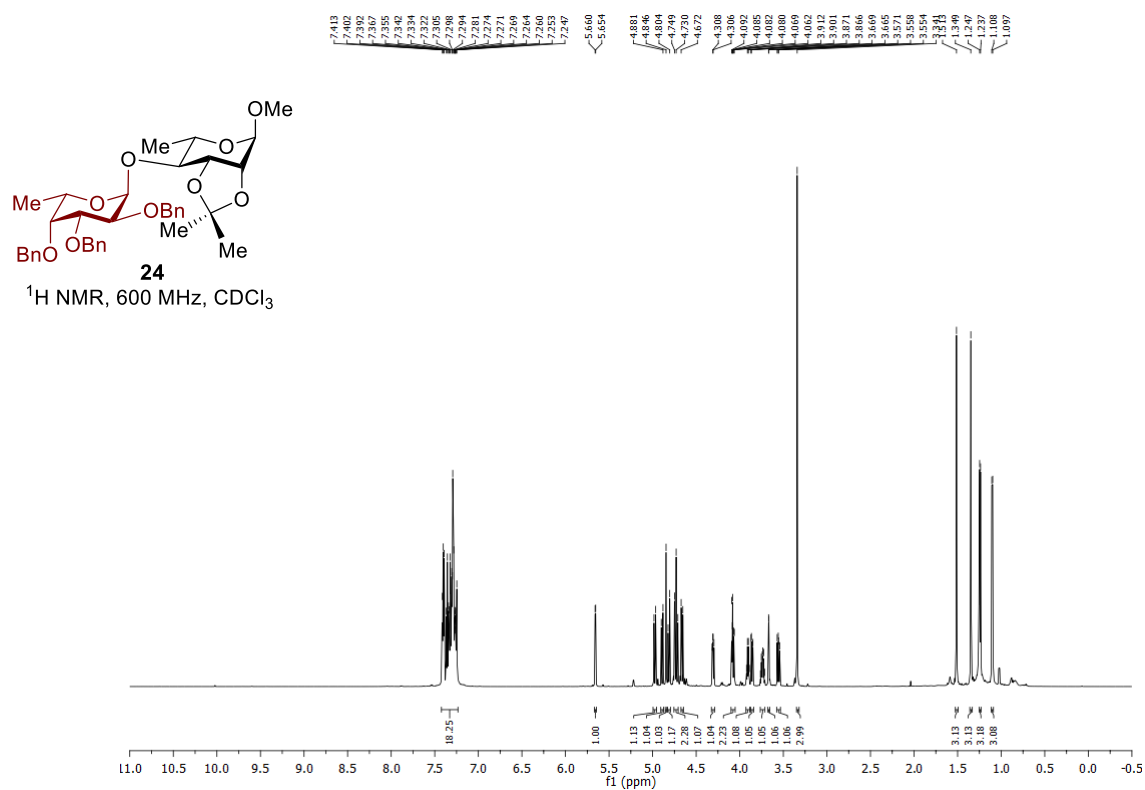
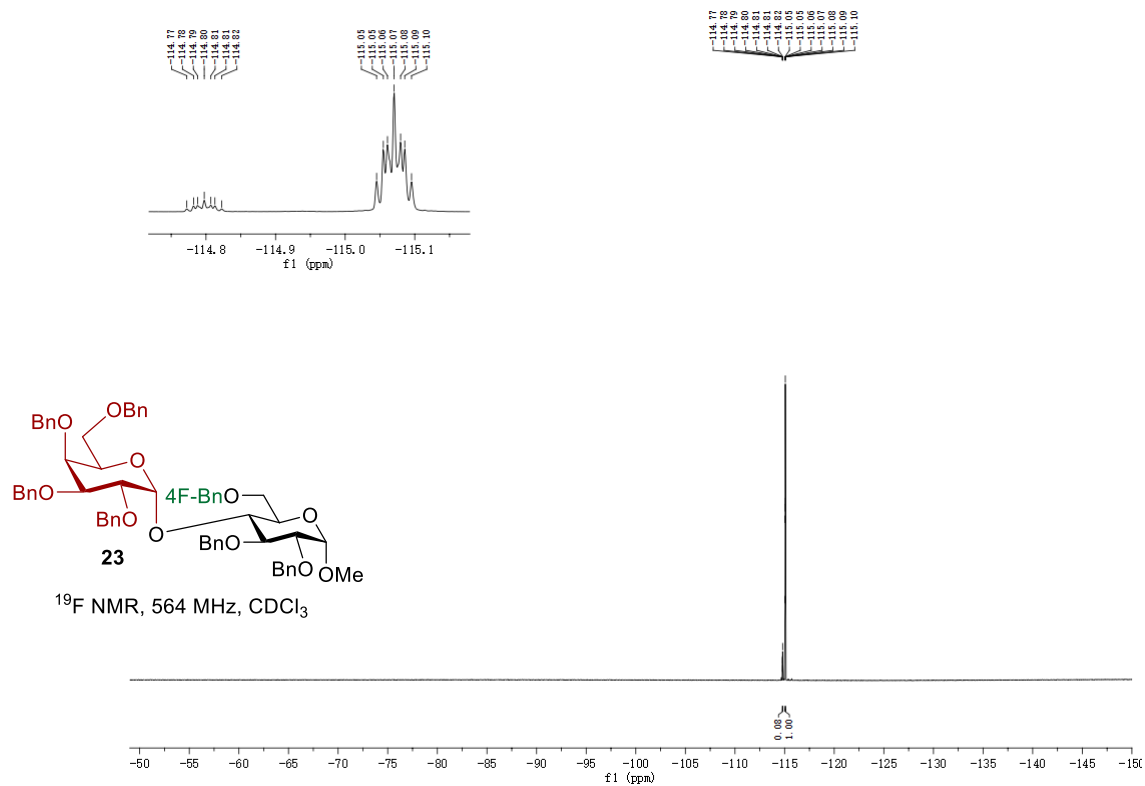


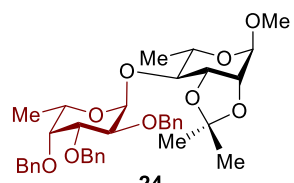
23
¹H NMR, 600 MHz, CDCl₃



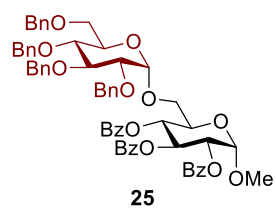
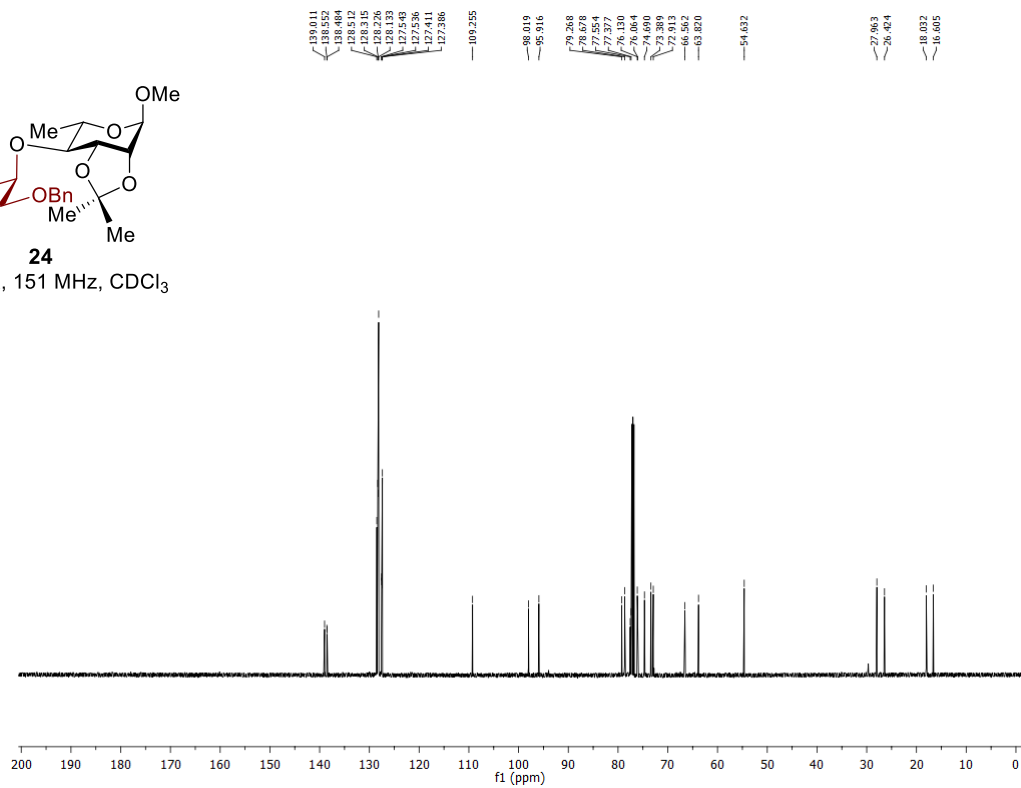
23
¹³C NMR, 151 MHz, CDCl₃



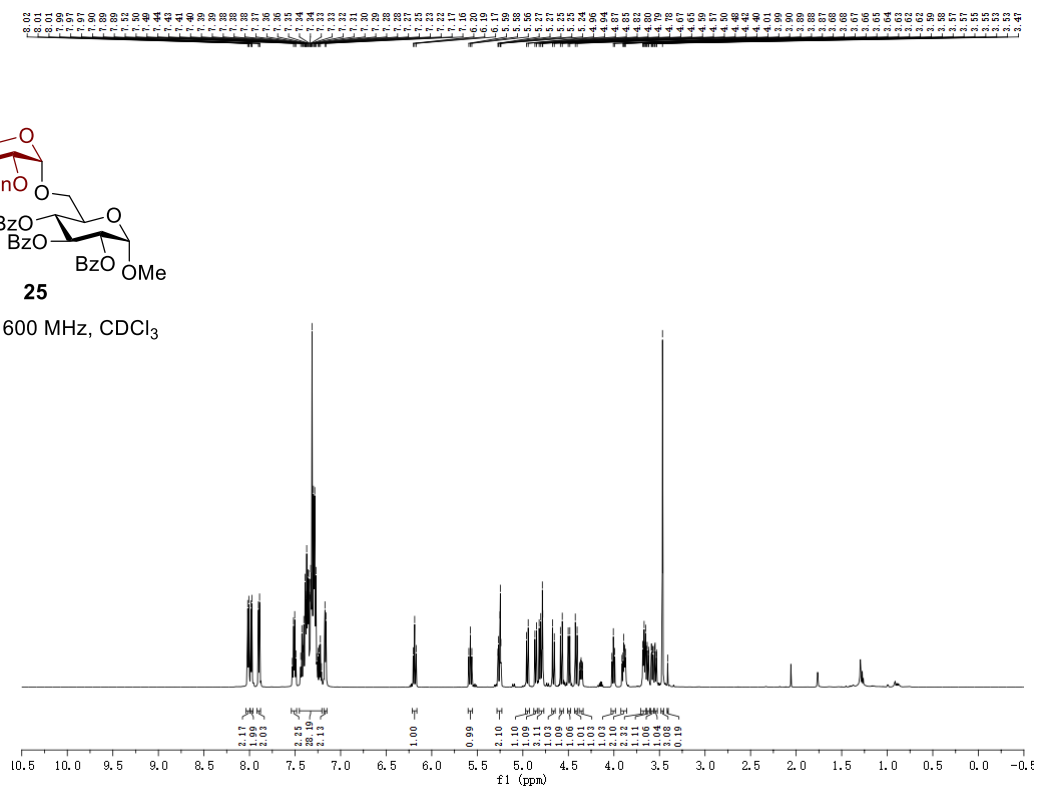


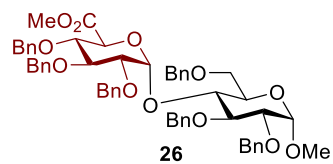


^{13}C NMR, 151 MHz, CDCl_3

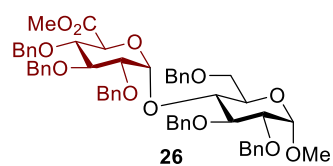
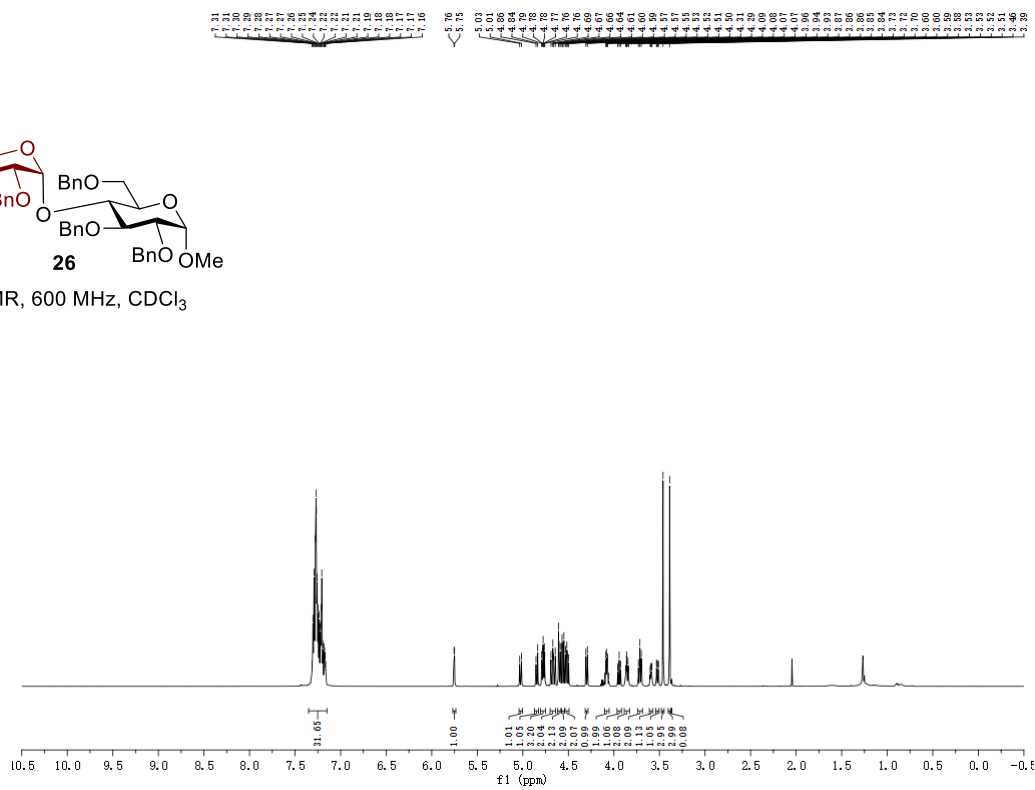


^1H NMR, 600 MHz, CDCl_3

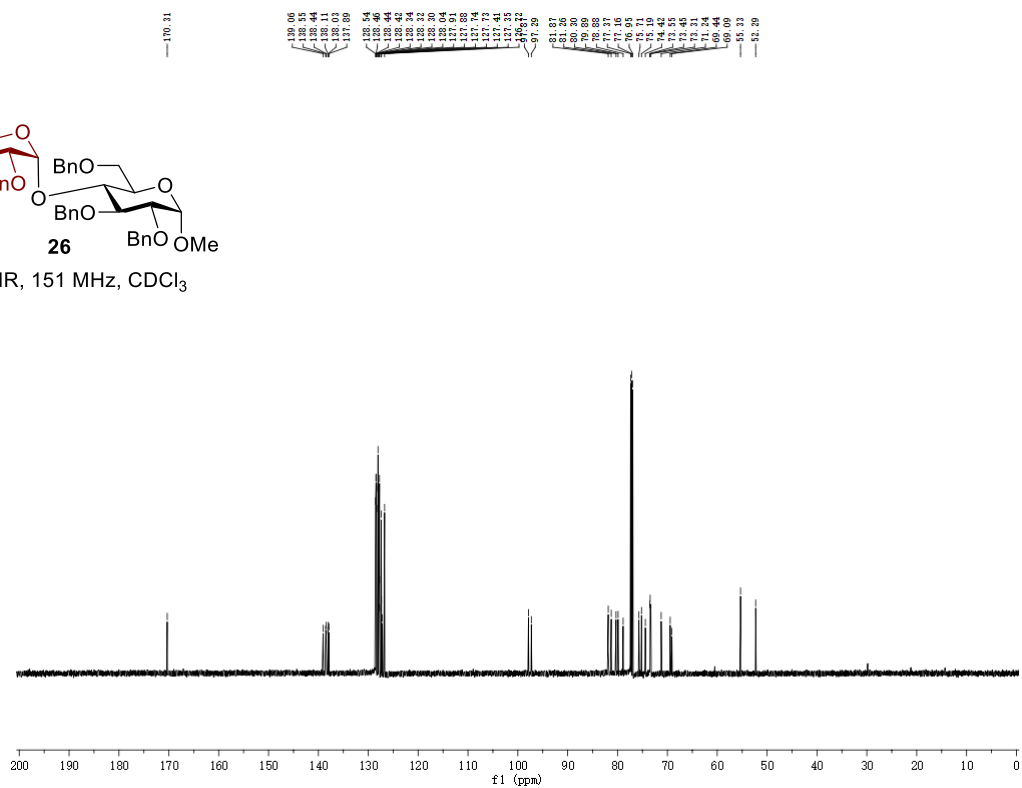


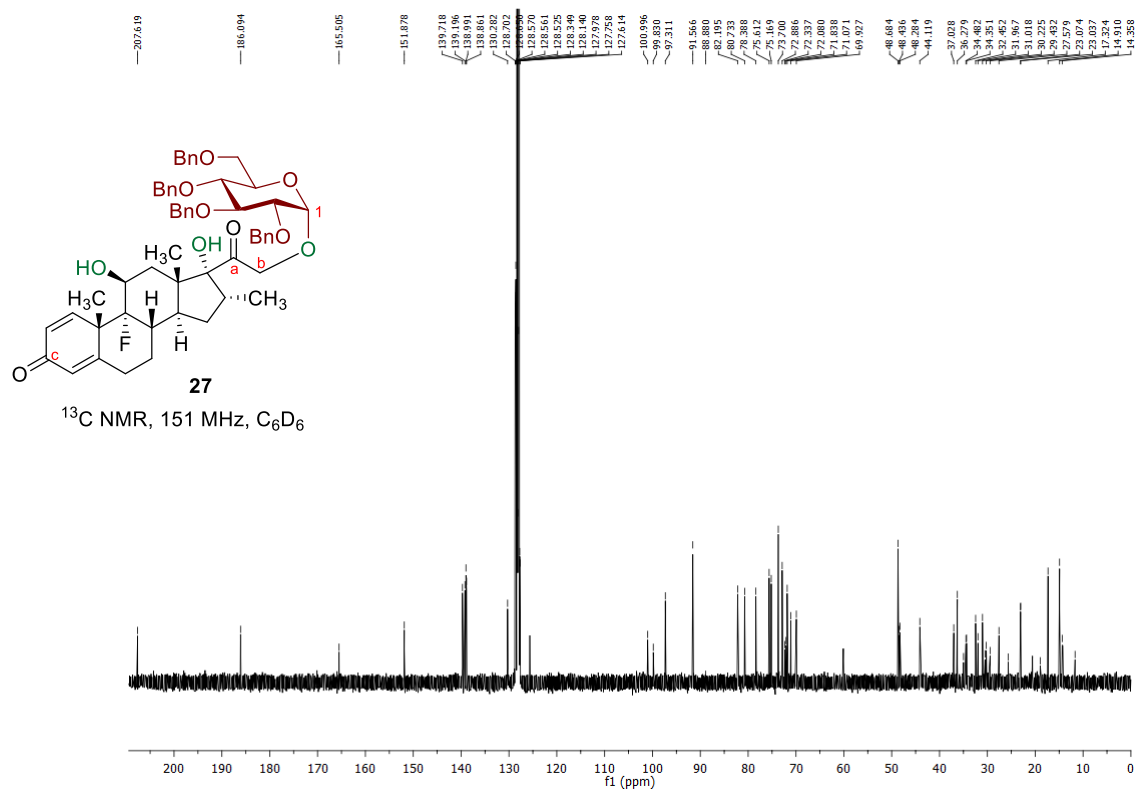
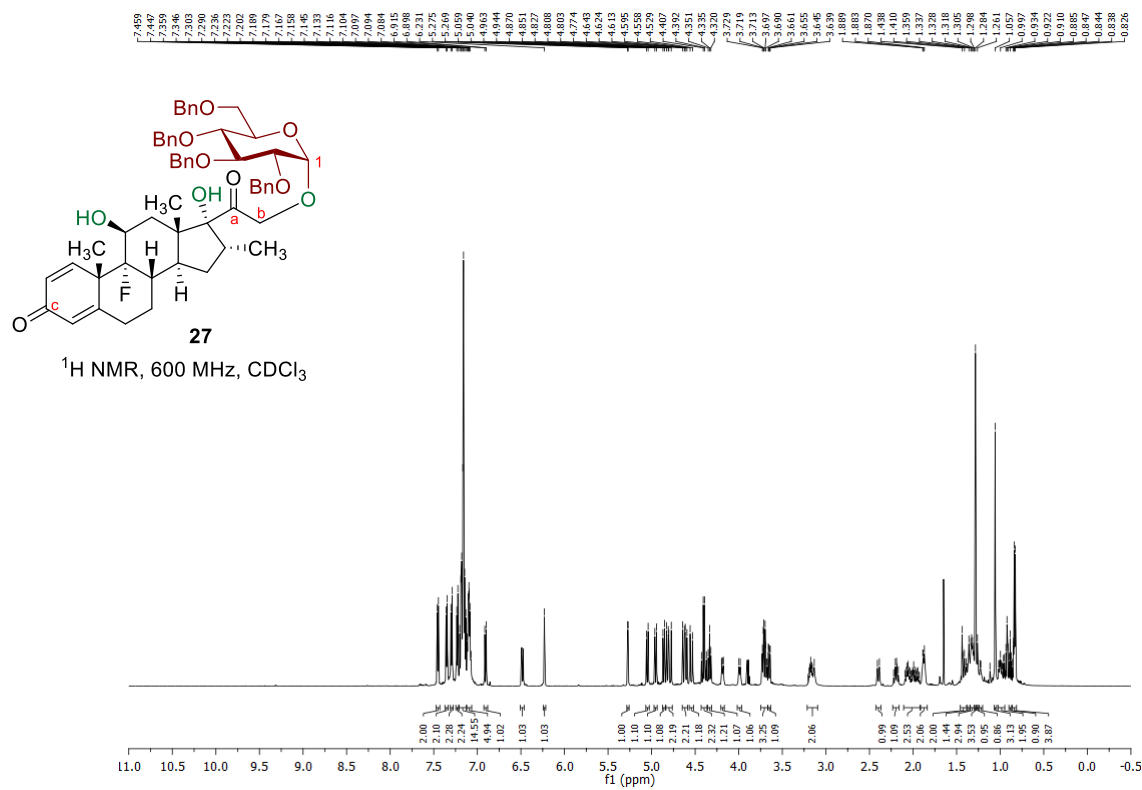


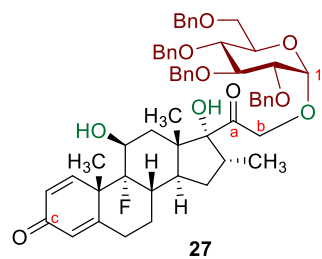
$^1\text{H NMR}$, 600 MHz, CDCl_3



$^{13}\text{C NMR}$, 151 MHz, CDCl_3

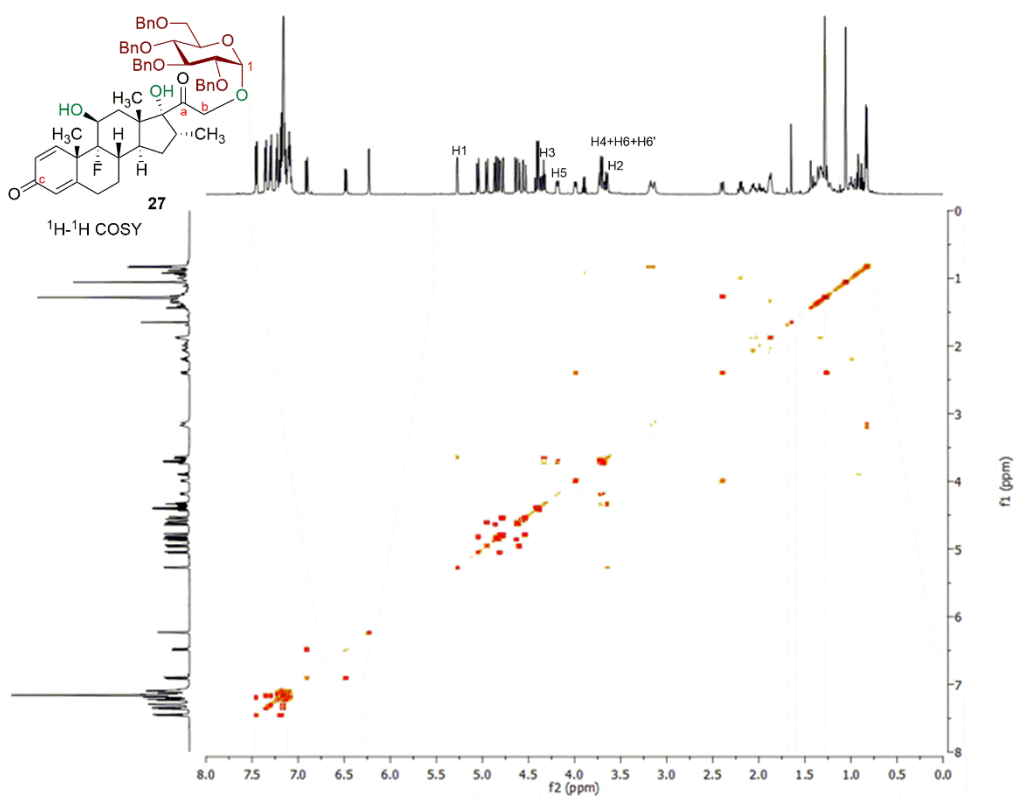
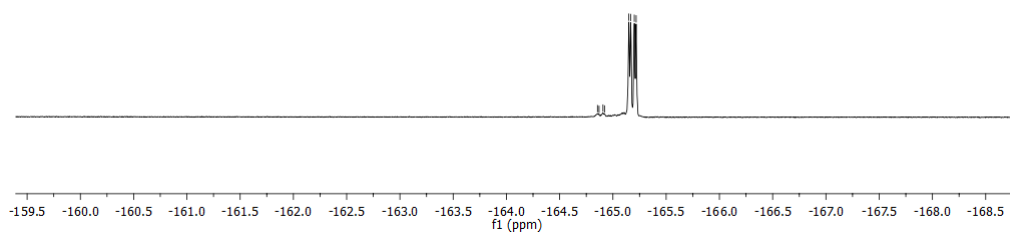


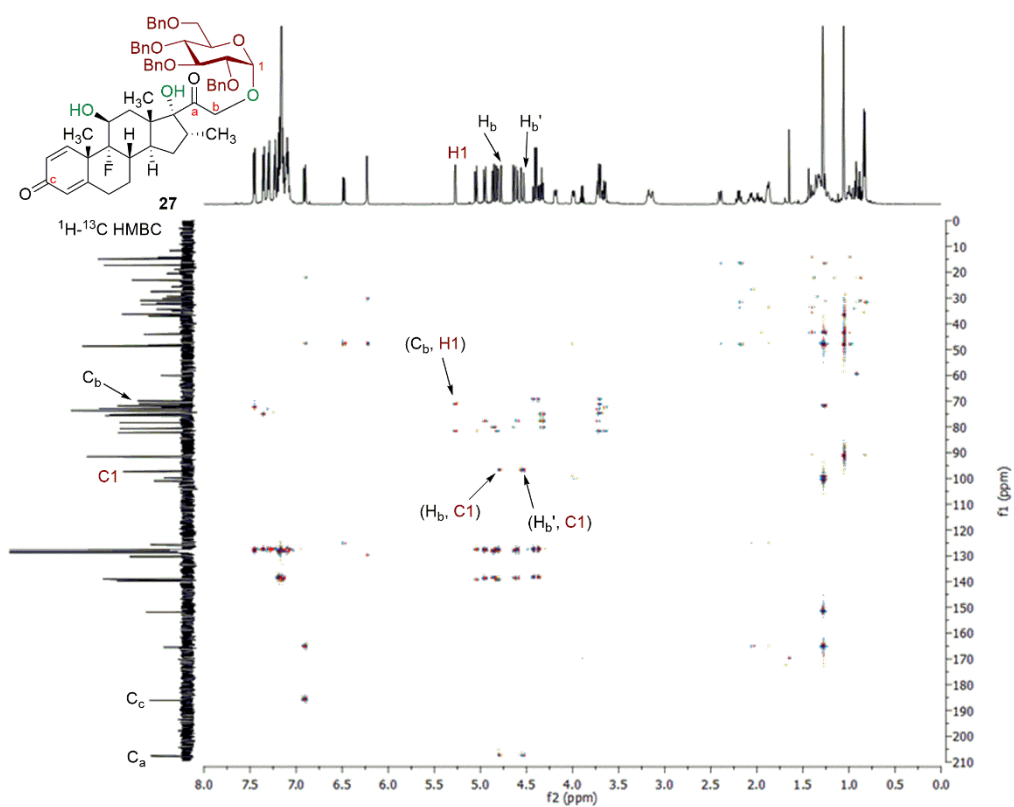
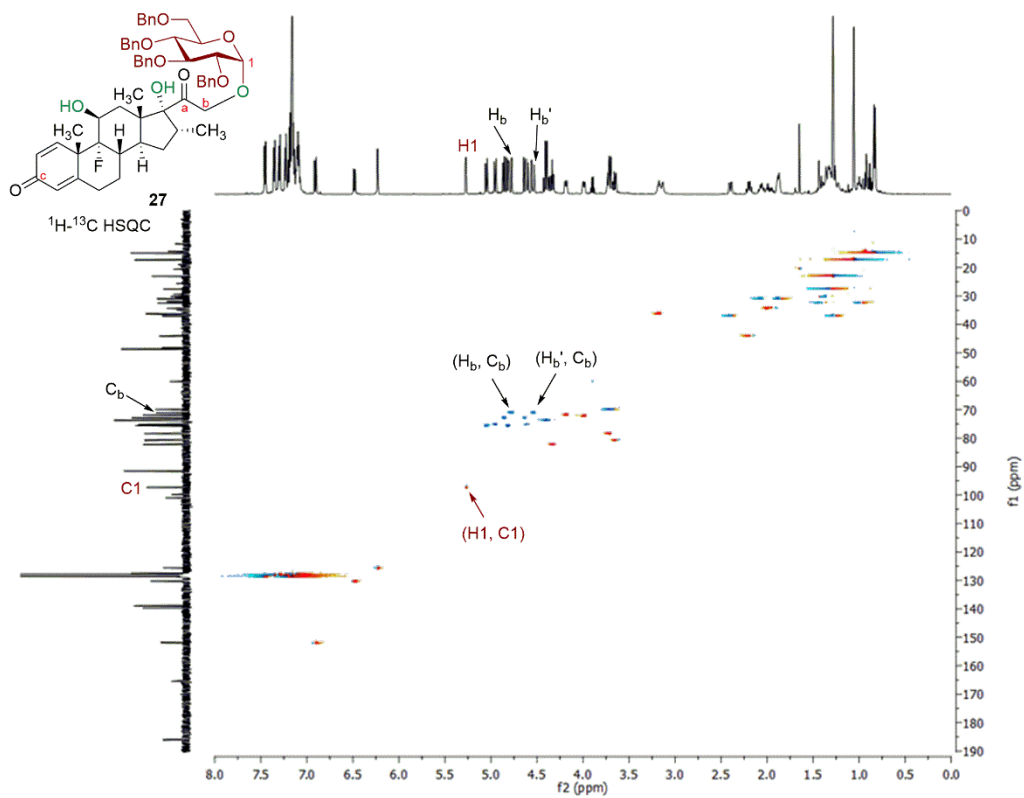


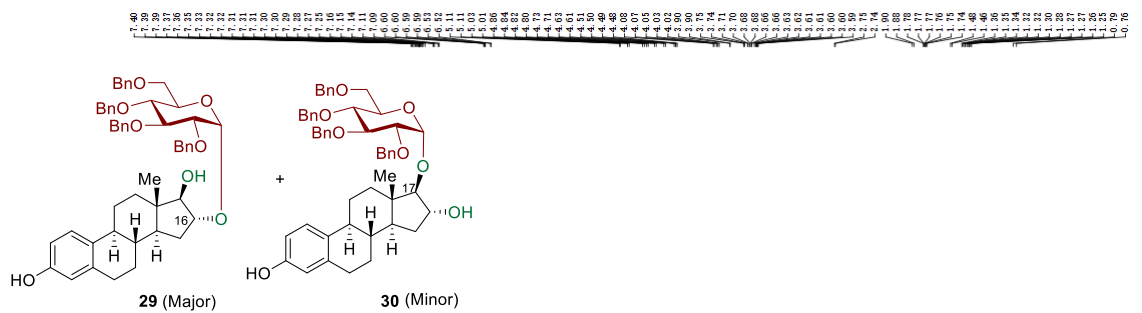


^{19}F NMR, 564 MHz, C_6D_6

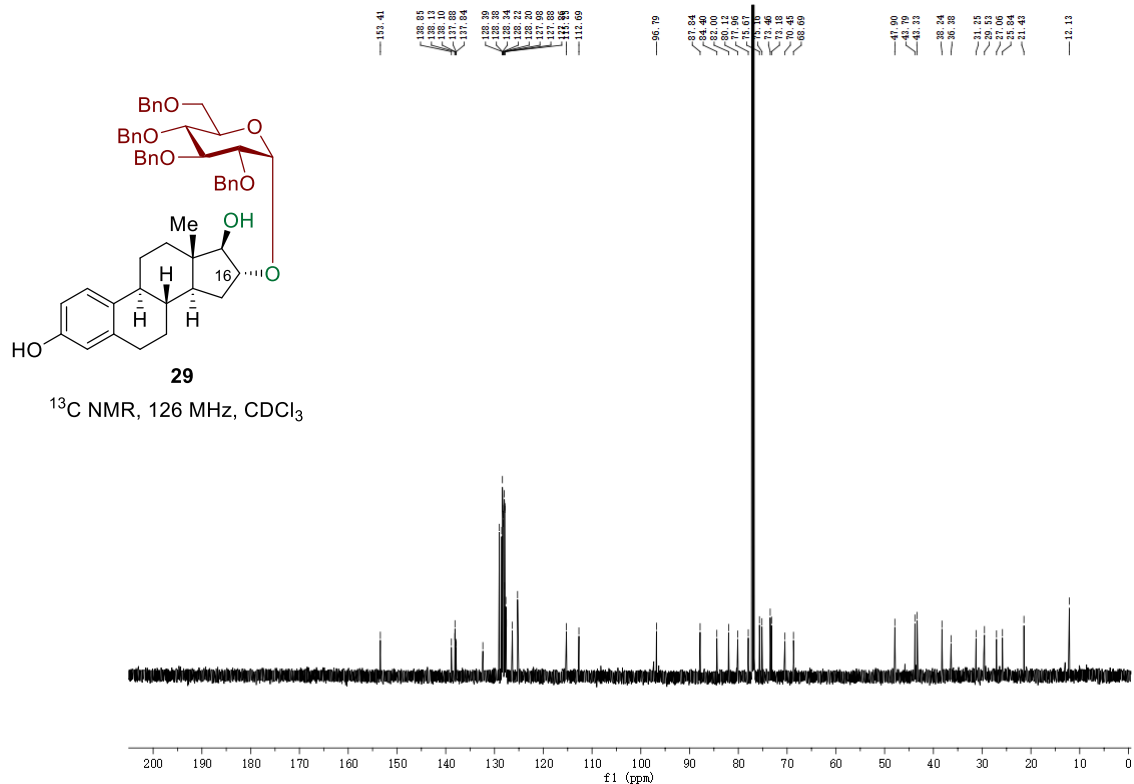
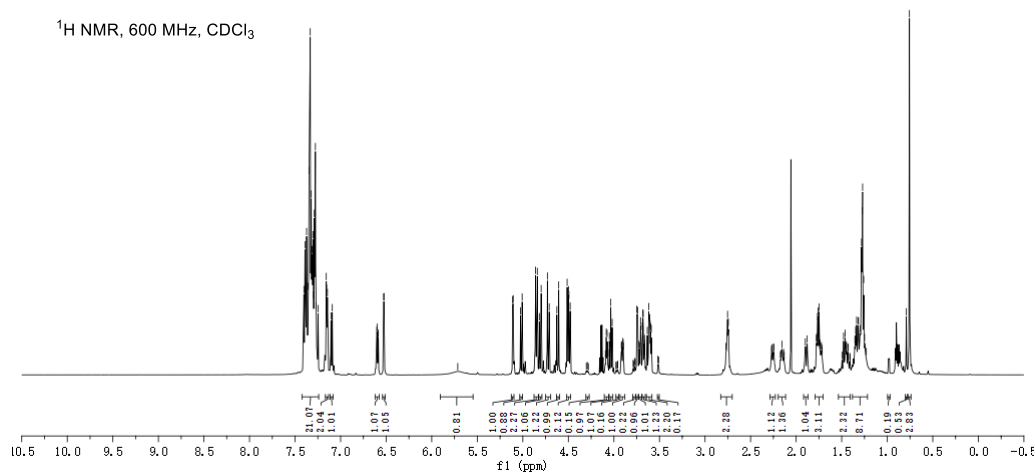
164.855
164.870
164.921
165.199
165.167
165.201
165.210

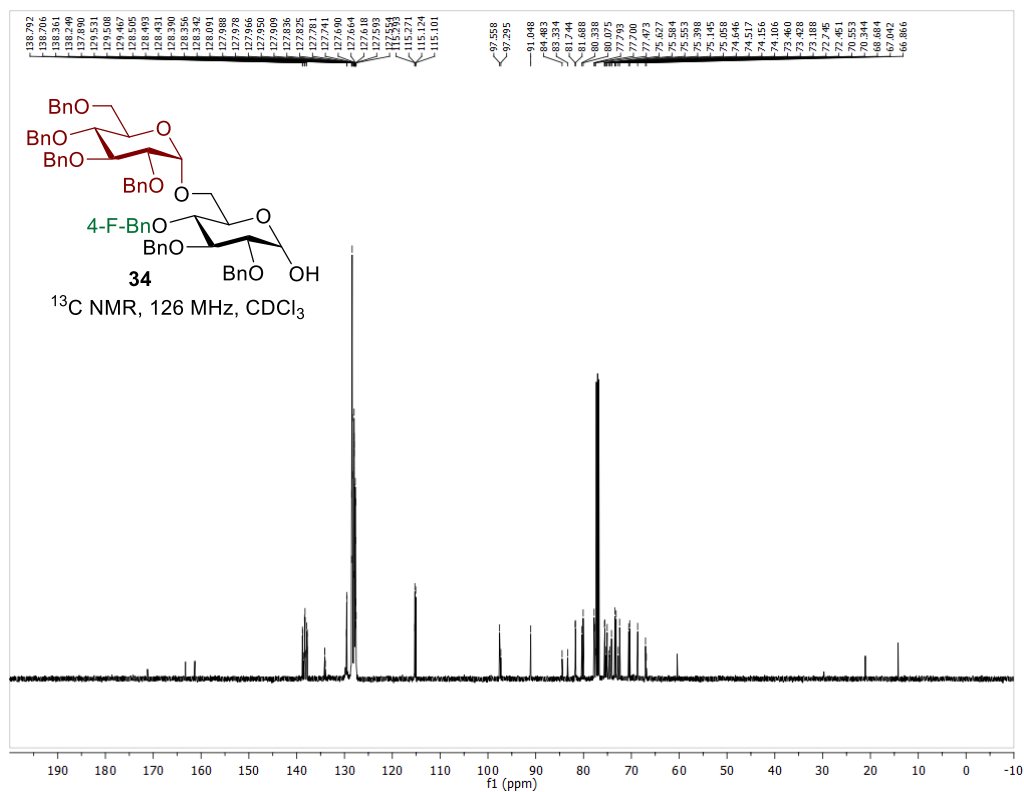
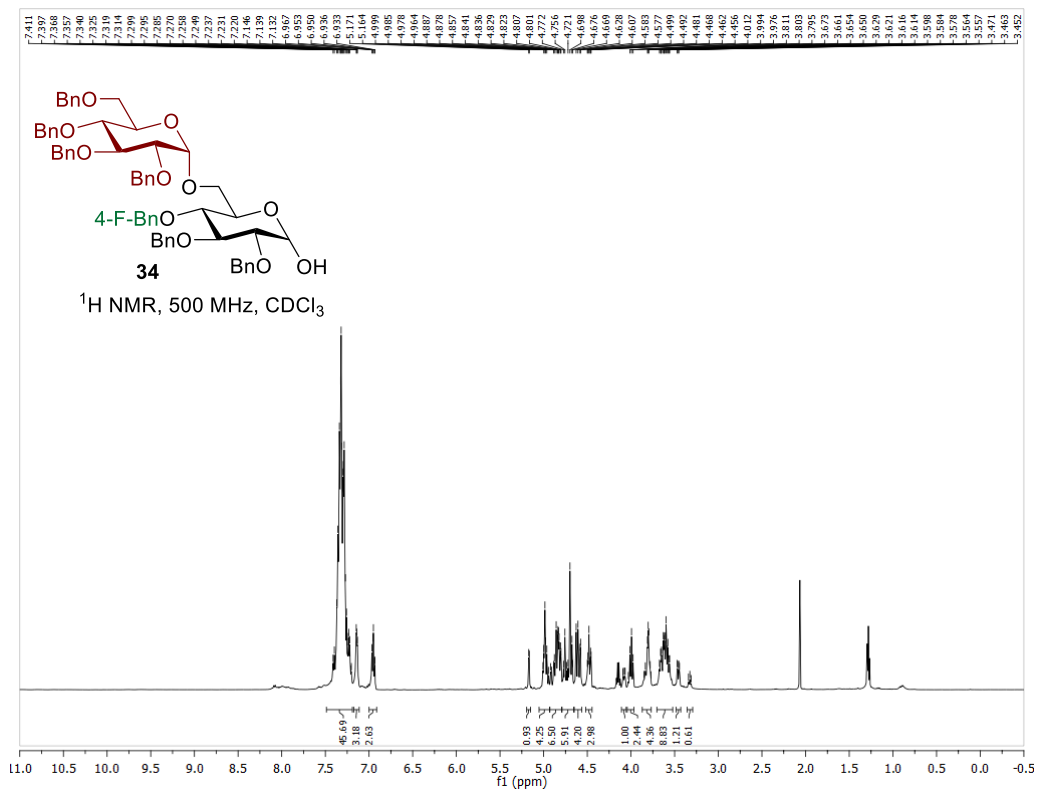


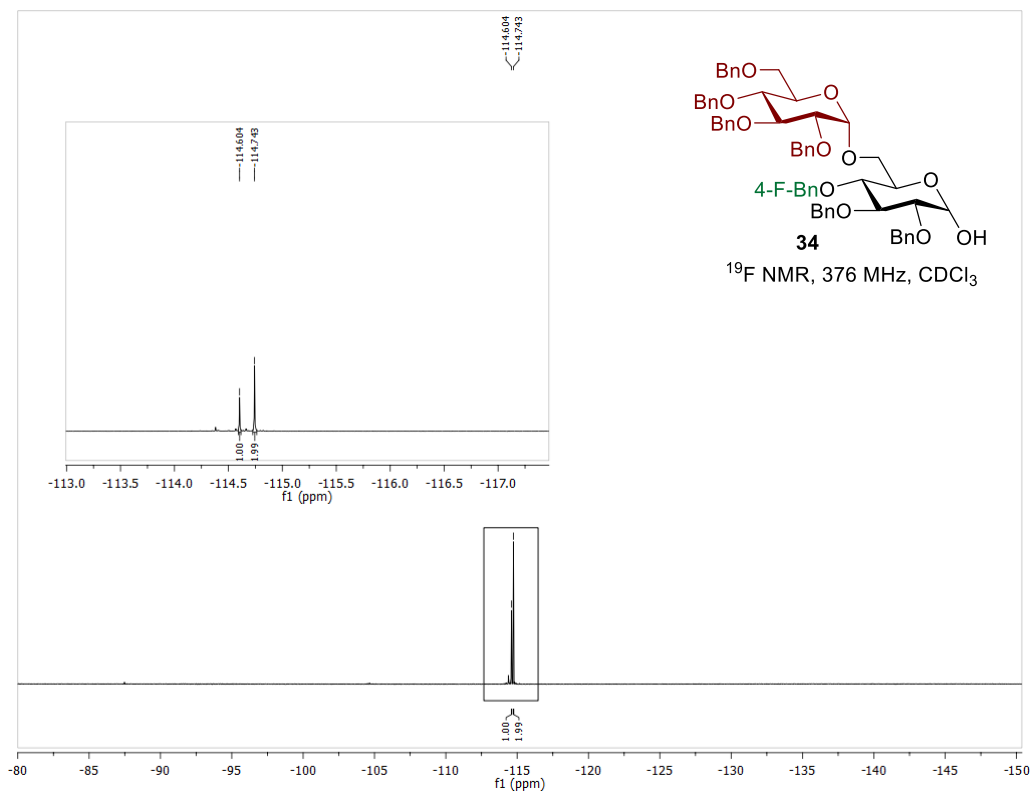




$^1\text{H NMR}$, 600 MHz, CDCl_3





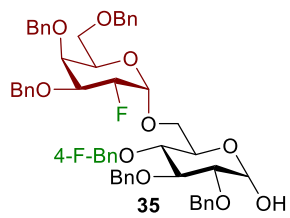


114.604
114.743

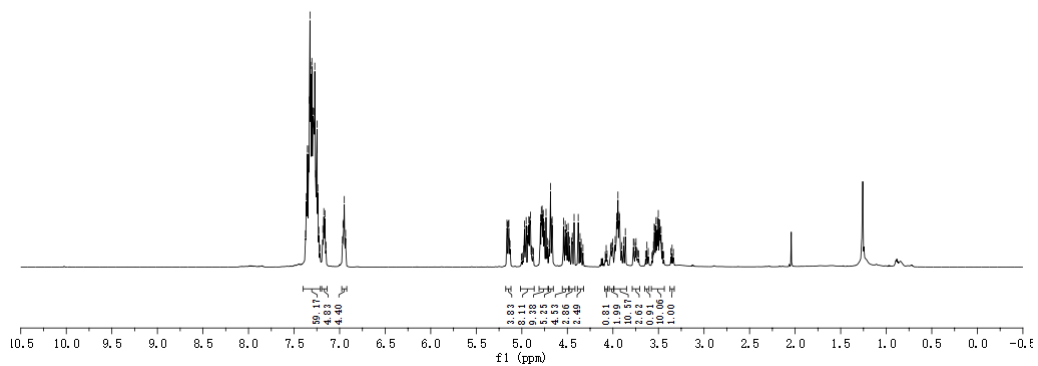
1.00
1.99

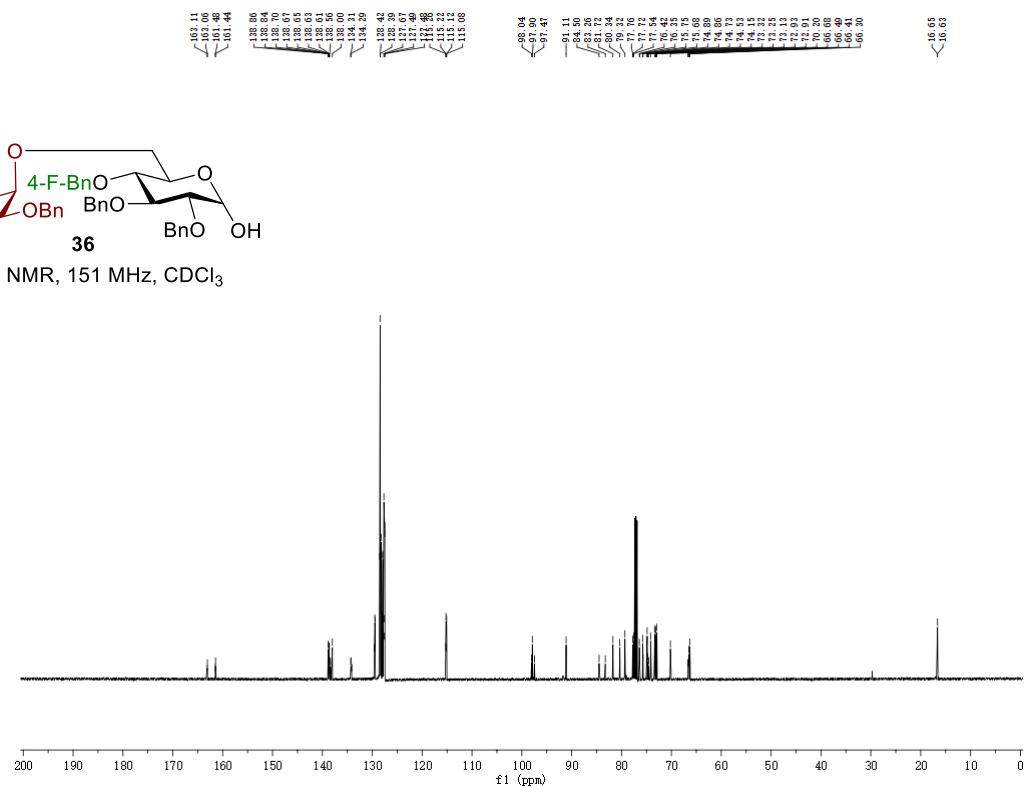
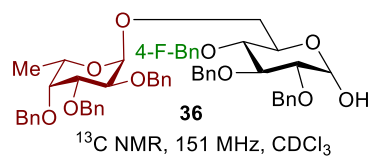
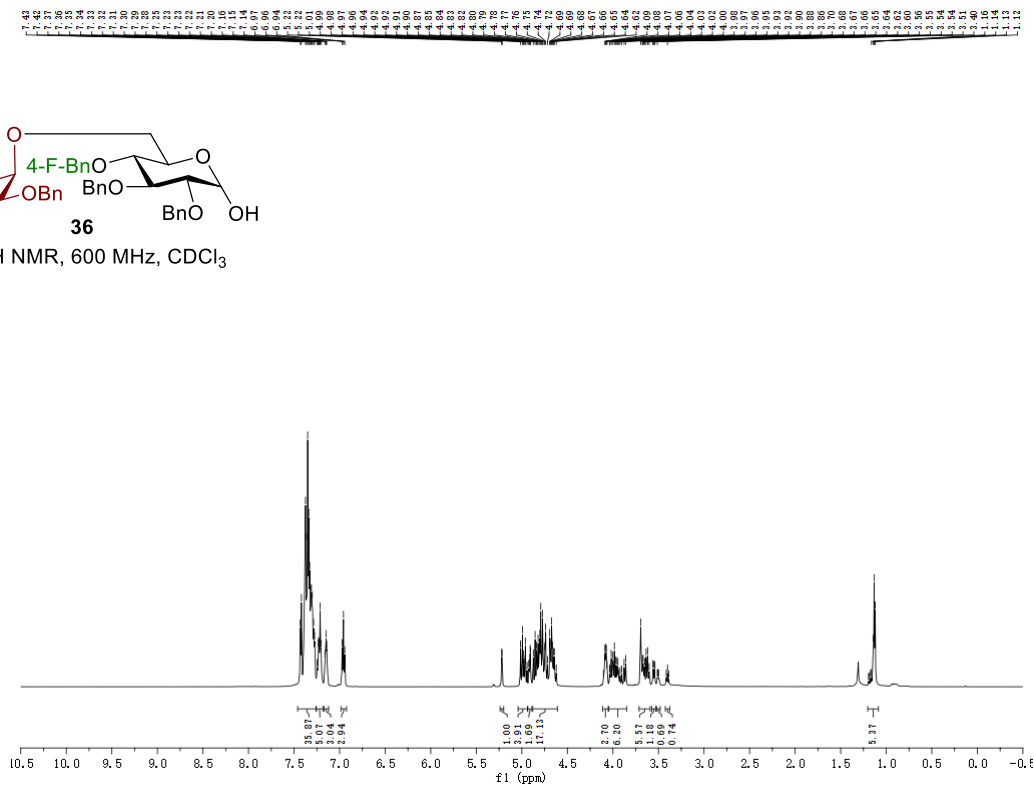
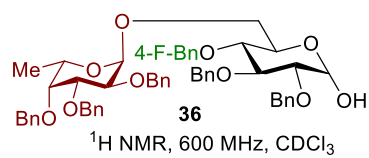
114.604
114.743

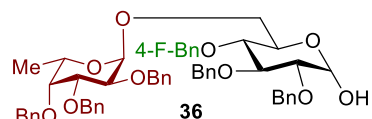
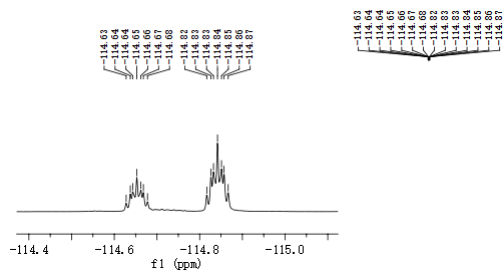
1.00
1.99



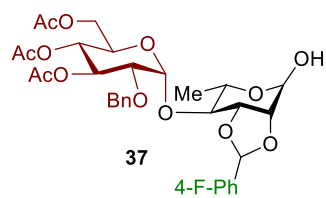
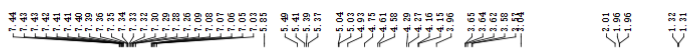
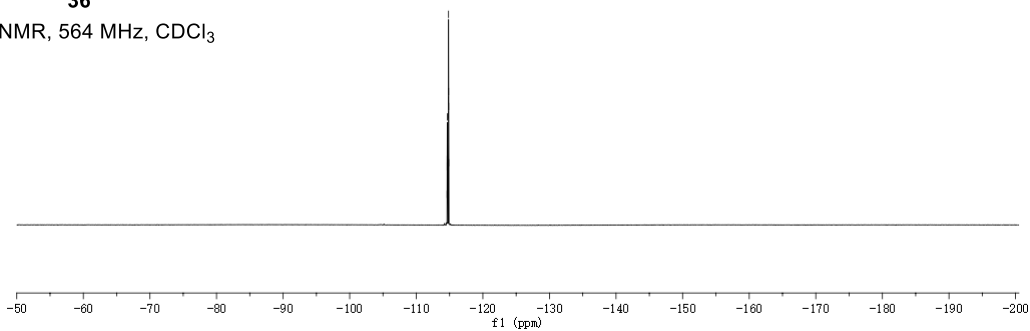
¹H NMR, 600 MHz, CDCl₃



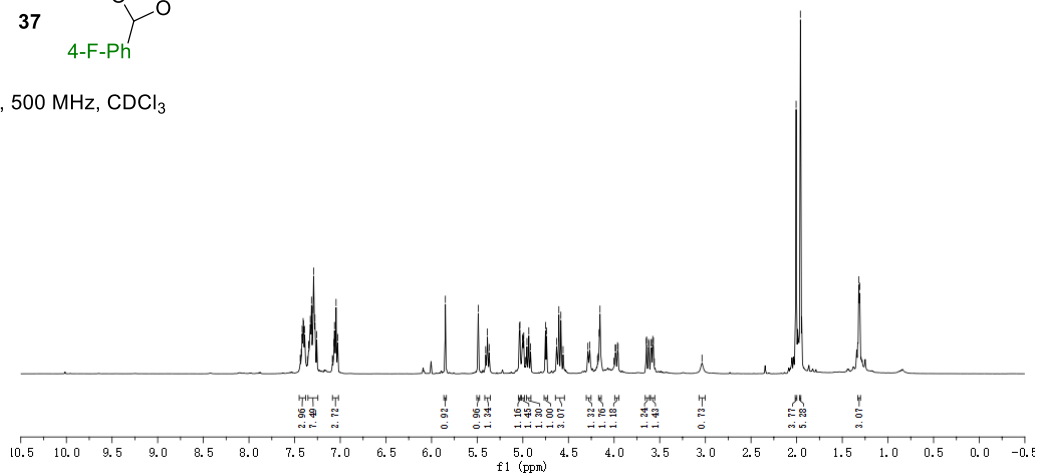


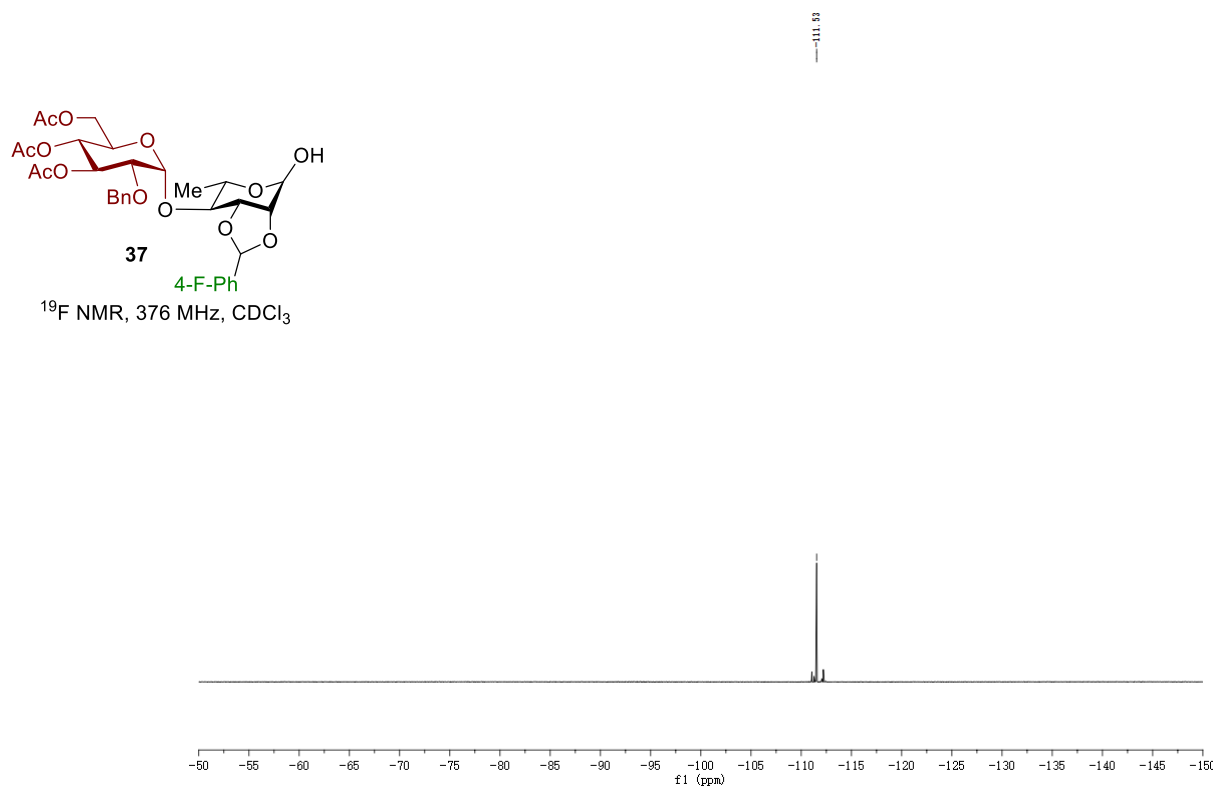
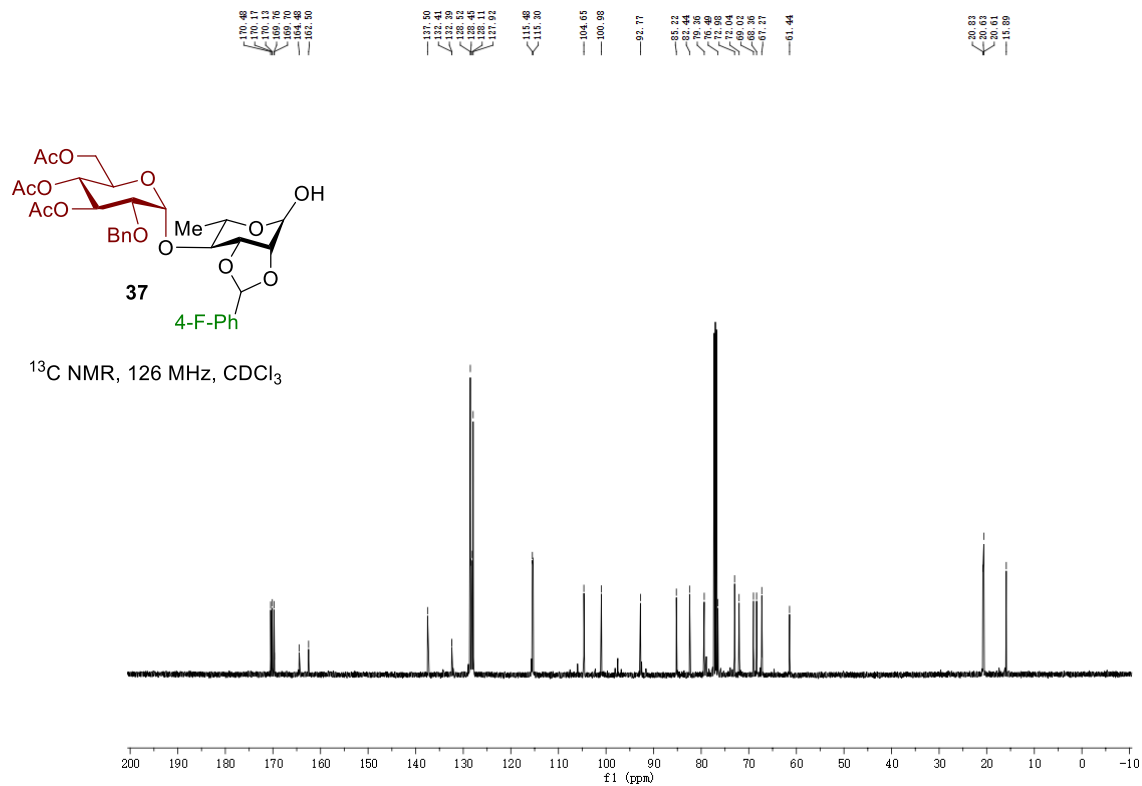


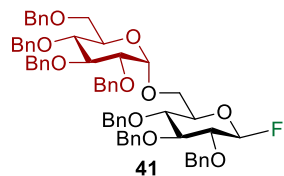
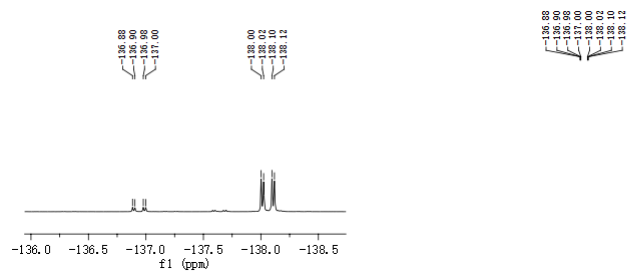
^{19}F NMR, 564 MHz, CDCl_3



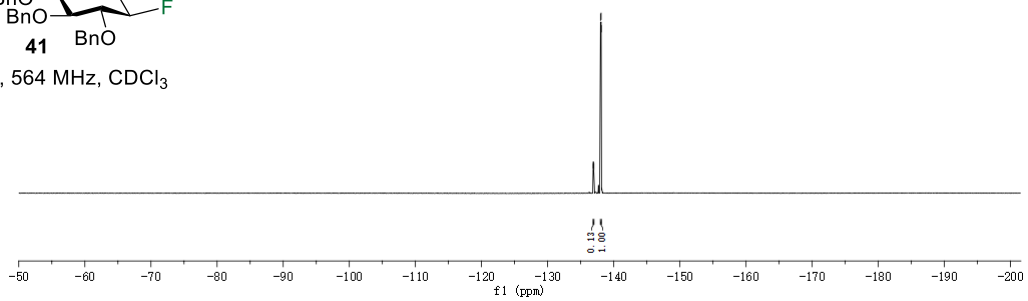
^1H NMR, 500 MHz, CDCl_3







^{19}F NMR, 564 MHz, CDCl_3



APPENDIX C: LICENSES FROM PUBLISHERS

JOHN WILEY AND SONS LICENSE TERMS AND CONDITIONS

Apr 04, 2022

This Agreement between Wayne State University -- Jiayi Li ("You") and John Wiley and Sons ("John Wiley and Sons") consists of your license details and the terms and conditions provided by John Wiley and Sons and Copyright Clearance Center.

License Number	5281960880859
License date	Apr 04, 2022
Licensed Content Publisher	John Wiley and Sons
Licensed Content Publication	Angewandte Chemie International Edition
Licensed Content Title	Phenanthroline-Catalyzed Stereoretentive Glycosylations
Licensed Content Author	Hien M. Nguyen, H. Bernhard Schlegel, Yi-Jung Tu, et al
Licensed Content Date	Apr 9, 2019
Licensed Content Volume	58
Licensed Content Issue	21
Licensed Content Pages	5
Type of Use	Dissertation/Thesis
Requestor type	Author of this Wiley article
Format	Electronic
Portion	Full article
Will you be translating?	No
Title	PHENANTHROLINE-CATALYZED 1,2-CIS GLYCOSYLATION: SCOPE AND MECHANISM
Institution name	Wayne State Univeristy
Expected presentation date	Jun 2022
Requestor Location	Wayne State University 5101 Cass. Ave DETROIT, MI 48202 United States Attn: Wayne State University
Publisher Tax ID	EU826007151
Total	0.00 USD
Terms and Conditions	

TERMS AND CONDITIONS

This copyrighted material is owned by or exclusively licensed to John Wiley & Sons, Inc. or one of its group companies (each a "Wiley Company") or handled on behalf of a society with which a Wiley Company has exclusive publishing rights in relation to a particular work (collectively "WILEY"). By clicking "accept" in connection with completing this licensing transaction, you agree that the following terms and conditions apply to this transaction (along with the billing and payment terms and conditions established by the Copyright Clearance Center Inc., ("CCC's Billing and Payment terms and conditions"), at the time that you opened your RightsLink account (these are available at any time at <http://myaccount.copyright.com>).

JOHN WILEY AND SONS LICENSE TERMS AND CONDITIONS

Apr 04, 2022

This Agreement between Wayne State University -- Jiayi Li ("You") and John Wiley and Sons ("John Wiley and Sons") consists of your license details and the terms and conditions provided by John Wiley and Sons and Copyright Clearance Center.

License Number	5281960698947
License date	Apr 04, 2022
Licensed Content Publisher	John Wiley and Sons
Licensed Content Publication	Advanced Synthesis & Catalysis
Licensed Content Title	A Mechanistic Probe into 1,2-cis Glycoside Formation Catalyzed by Phenanthroline and Further Expansion of Scope
Licensed Content Author	Hien M. Nguyen, Jiayi Li
Licensed Content Date	Jul 9, 2021
Licensed Content Volume	363
Licensed Content Issue	16
Licensed Content Pages	13
Type of Use	Dissertation/Thesis
Requestor type	Author of this Wiley article
Format	Electronic
Portion	Full article
Will you be translating?	No
Title	PHENANTHROLINE-CATALYZED 1,2-CIS GLYCOSYLATION: SCOPE AND MECHANISM
Institution name	Wayne State Univeristy
Expected presentation date	Jun 2022
Requestor Location	Wayne State University 5101 Cass Ave. DETROIT, MI 48202 United States Attn: Wayne State University
Publisher Tax ID	EU826007151
Total	0.00 USD
Terms and Conditions	

TERMS AND CONDITIONS

This copyrighted material is owned by or exclusively licensed to John Wiley & Sons, Inc. or one of its group companies (each a "Wiley Company") or handled on behalf of a society with which a Wiley Company has exclusive publishing rights in relation to a particular work (collectively "WILEY"). By clicking "accept" in connection with completing this licensing transaction, you agree that the following terms and conditions apply to this transaction (along with the billing and payment terms and conditions established by the Copyright Clearance Center Inc., ("CCC's Billing and Payment terms and conditions"), at the time that you opened your RightsLink account (these are available at any time at <http://myaccount.copyright.com>).

Stereoselective 1,2-cis Furanosylations Catalyzed by Phenanthroline

Author: Hengfu Xu, Richard N. Schaugaard, Jiayi Li, et al

Publication: Journal of the American Chemical Society

Publisher: American Chemical Society

Date: Apr 1, 2022

Copyright © 2022, American Chemical Society

PERMISSION/LICENSE IS GRANTED FOR YOUR ORDER AT NO CHARGE

This type of permission/license, instead of the standard Terms and Conditions, is sent to you because no fee is being charged for your order. Please note the following:

- Permission is granted for your request in both print and electronic formats, and translations.
- If figures and/or tables were requested, they may be adapted or used in part.
- Please print this page for your records and send a copy of it to your publisher/graduate school.
- Appropriate credit for the requested material should be given as follows: "Reprinted (adapted) with permission from {COMPLETE REFERENCE CITATION}, Copyright {YEAR} American Chemical Society." Insert appropriate information in place of the capitalized words.
- One-time permission is granted only for the use specified in your RightsLink request. No additional uses are granted (such as derivative works or other editions). For any uses, please submit a new request.

If credit is given to another source for the material you requested from RightsLink, permission must be obtained from that source.

[BACK](#)[CLOSE WINDOW](#)

REFERENCES

1. Davis, B. G.; Fairbanks, A. J., *Carbohydrate Chemistry*. Oxford University Press: 2002.
2. Prestegard, J. H.; Liu, J.; Widmalm, G., Oligosaccharides and Polysaccharides. In *Essentials of Glycobiology*, rd; Varki, A.; Cummings, R. D.; Esko, J. D.; Stanley, P.; Hart, G. W.; Aebi, M.; Darvill, A. G.; Kinoshita, T.; Packer, N. H.; Prestegard, J. H.; Schnaar, R. L.; Seeberger, P. H., Eds. Cold Spring Harbor (NY), 2015; pp 31-40.
3. O'Connor, C. M.; Adams, J. U., *Essentials of Cell Biology*. NPG Education: Cambridge, MA, 2010. <https://www.nature.com/scitable/ebooks/essentials-of-cell-biology-14749010/>.
4. Braidwood, L.; Breuer, C.; Sugimoto, K., My body is a cage: mechanisms and modulation of plant cell growth. *New Phytol* **2014**, *201* (2), 388-402.
5. Dick-Perez, M.; Zhang, Y. A.; Hayes, J.; Salazar, A.; Zobotina, O. A.; Hong, M., Structure and Interactions of Plant Cell-Wall Polysaccharides by Two- and Three-Dimensional Magic-Angle-Spinning Solid-State NMR. *Biochemistry-Us* **2011**, *50* (6), 989-1000.
6. Scheller, H. V.; Ulvskov, P., Hemicelluloses. *Annu Rev Plant Biol* **2010**, *61*, 263-289.
7. Mohnen, D., Pectin structure and biosynthesis. *Curr Opin Plant Biol* **2008**, *11* (3), 266-277.
8. Beveridge, T. J., Use of the Gram stain in microbiology. *Biotechnic & Histochemistry* **2001**, *76* (3), 111-118.
9. Coico, R., Gram Staining. *Current Protocols in Microbiology* **2006**, *00* (1), A.3C.1-A.3C.2.
10. Turner, R. D.; Vollmer, W.; Foster, S. J., Different walls for rods and balls: the diversity of peptidoglycan. *Molecular Microbiology* **2014**, *91* (5), 862-874.
11. Pasquina-Lemonche, L.; Burns, J.; Turner, R. D.; Kumar, S.; Tank, R.; Mullin, N.; Wilson, J. S.; Chakrabarti, B.; Bullough, P. A.; Foster, S. J.; Hobbs, J. K., The architecture of the Gram-positive bacterial cell wall. *Nature* **2020**, *582* (7811), 294-+.

12. Matias, V. R. F.; Beveridge, T. J., Native cell wall organization shown by cryo-electron microscopy confirms the existence of a periplasmic space in *Staphylococcus aureus*. *Journal of Bacteriology* **2006**, *188* (3), 1011-1021.
13. Beeby, M.; Gumbart, J. C.; Roux, B.; Jensen, G. J., Architecture and assembly of the Gram-positive cell wall. *Molecular Microbiology* **2013**, *88* (4), 664-672.
14. Misra, G.; Rojas, E. R.; Gopinathan, A.; Huang, K. C., Mechanical Consequences of Cell-Wall Turnover in the Elongation of a Gram-Positive Bacterium. *Biophys J* **2013**, *104* (11), 2342-2352.
15. Okuda, S.; Sherman, D. J.; Silhavy, T. J.; Ruiz, N.; Kahne, D., Lipopolysaccharide transport and assembly at the outer membrane: the PEZ model. *Nat Rev Microbiol* **2016**, *14* (6), 337-345.
16. Raetz, C. R. H., Biochemistry of Endotoxins. *Annu. Rev. Biochem.* **1990**, *59*, 129-170.
17. Reeves, P., Role of O-Antigen Variation in the Immune-Response. *Trends Microbiol* **1995**, *3* (10), 381-386.
18. Varki, A.; Kornfeld, S., Historical Background and Overview. In *Essentials of Glycobiology*, rd; Varki, A.; Cummings, R. D.; Esko, J. D.; Stanley, P.; Hart, G. W.; Aebi, M.; Darvill, A. G.; Kinoshita, T.; Packer, N. H.; Prestegard, J. H.; Schnaar, R. L.; Seeberger, P. H., Eds. Cold Spring Harbor (NY), 2015; pp 1-18.
19. Laine, R. A., A Calculation of All Possible Oligosaccharide Isomers Both Branched and Linear Yields 1.05×10^{12} Structures for a Reducing Hexasaccharide - the Isomer-Barrier to Development of Single-Method Saccharide Sequencing or Synthesis Systems. *Glycobiology* **1994**, *4* (6), 759-767.
20. Gabius, H. J.; Cudic, M.; Diercks, T.; Kaltner, H.; Kopitz, J.; Mayo, K. H.; Murphy, P. V.; Oscarson, S.; Roy, R.; Schedlbauer, A.; Toegel, S.; Romero, A., What is the Sugar Code? *Chembiochem* **2021**.
21. Kornfeld, S.; Li, E.; Tabas, I., The synthesis of complex-type oligosaccharides. II. Characterization of the processing intermediates in the synthesis of the complex oligosaccharide units of the vesicular stomatitis virus G protein. *J Biol Chem* **1978**, *253* (21), 7771-8.
22. Varki, A.; Cummings, R. D.; Aebi, M.; Packer, N. H.; Seeberger, P. H.; Esko, J. D.; Stanley, P.; Hart, G.; Darvill, A.; Kinoshita, T.; Prestegard, J. J.; Schnaar, R. L.; Freeze, H. H.; Marth, J. D.; Bertozzi,

- C. R.; Etzler, M. E.; Frank, M.; Vliegenthart, J. F.; Lutteke, T.; Perez, S.; Bolton, E.; Rudd, P.; Paulson, J.; Kanehisa, M.; Toukach, P.; Aoki-Kinoshita, K. F.; Dell, A.; Narimatsu, H.; York, W.; Taniguchi, N.; Kornfeld, S., Symbol Nomenclature for Graphical Representations of Glycans. *Glycobiology* **2015**, *25* (12), 1323-4.
23. Flynn, R. A.; Pedram, K.; Malaker, S. A.; Batista, P. J.; Smith, B. A. H.; Johnson, A. G.; George, B. M.; Majzoub, K.; Villalta, P. W.; Carette, J. E.; Bertozzi, C. R., Small RNAs are modified with N-glycans and displayed on the surface of living cells. *Cell* **2021**, *184* (12), 3109-+.
24. Stanley, P.; Taniguchi, N.; Aebi, M., N-Glycans. In *Essentials of Glycobiology*, rd; Varki, A.; Cummings, R. D.; Esko, J. D.; Stanley, P.; Hart, G. W.; Aebi, M.; Darvill, A. G.; Kinoshita, T.; Packer, N. H.; Prestegard, J. H.; Schnaar, R. L.; Seeberger, P. H., Eds. Cold Spring Harbor (NY), 2015; pp 99-111.
25. Brockhausen, I.; Stanley, P., O-GalNAc Glycans. In *Essentials of Glycobiology*, rd; Varki, A.; Cummings, R. D.; Esko, J. D.; Stanley, P.; Hart, G. W.; Aebi, M.; Darvill, A. G.; Kinoshita, T.; Packer, N. H.; Prestegard, J. H.; Schnaar, R. L.; Seeberger, P. H., Eds. Cold Spring Harbor (NY), 2015; pp 113-123.
26. Schnaar, R. L.; Kinoshita, T., Glycosphingolipids. In *Essentials of Glycobiology*, rd; Varki, A.; Cummings, R. D.; Esko, J. D.; Stanley, P.; Hart, G. W.; Aebi, M.; Darvill, A. G.; Kinoshita, T.; Packer, N. H.; Prestegard, J. H.; Schnaar, R. L.; Seeberger, P. H., Eds. Cold Spring Harbor (NY), 2015; pp 125-135.
27. Block, K. F.; Puerta-Fernandez, E.; Wallace, J. G.; Breaker, R. R., Association of OLE RNA with bacterial membranes via an RNA-protein interaction. *Mol Microbiol* **2011**, *79* (1), 21-34.
28. Sanders, W.; Laederach, A., Membrane RNAs in bacteria. *Mol Microbiol* **2011**, *79* (1), 1-2.
29. Taylor, M. E.; Drickamer, K.; Schnaar, R. L.; Etzler, M. E.; Varki, A., Discovery and Classification of Glycan-Binding Proteins. In *Essentials of Glycobiology*, rd; Varki, A.; Cummings, R. D.; Esko, J. D.; Stanley, P.; Hart, G. W.; Aebi, M.; Darvill, A. G.; Kinoshita, T.; Packer, N. H.; Prestegard, J. H.; Schnaar, R. L.; Seeberger, P. H., Eds. Cold Spring Harbor (NY), 2015; pp 361-372.

30. Walker, J. R.; Nagar, B.; Young, N. M.; Hiramata, T.; Rini, J. M., X-ray Crystal Structure of a Galactose-Specific C-Type Lectin Possessing a Novel Decameric Quaternary Structure. *Biochemistry-Us* **2004**, *43* (13), 3783-3792.
31. Melief, C. J. M.; van Hall, T.; Arens, R.; Ossendorp, F.; van der Burg, S. H., Therapeutic cancer vaccines. *The Journal of clinical investigation* **2015**, *125* (9), 3401-3412.
32. Astronomo, R. D.; Burton, D. R., Carbohydrate vaccines: developing sweet solutions to sticky situations? *Nat Rev Drug Discov* **2010**, *9* (4), 308-24.
33. Avery, O. T.; Goebel, W. F., CHEMO-IMMUNOLOGICAL STUDIES ON CONJUGATED CARBOHYDRATE-PROTEINS : II. IMMUNOLOGICAL SPECIFICITY OF SYNTHETIC SUGAR-PROTEIN ANTIGENS. *Journal of Experimental Medicine* **1929**, *50* (4), 533-550.
34. Grabenstein, J. D.; Klugman, K. P., A century of pneumococcal vaccination research in humans. *Clin Microbiol Infect* **2012**, *18 Suppl 5*, 15-24.
35. Ada, G.; Isaacs, D., Carbohydrate-protein conjugate vaccines. *Clin Microbiol Infect* **2003**, *9* (2), 79-85.
36. Galiza, E. P.; Heath, P. T., Pneumococcal conjugate vaccines. A review. *Minerva medica* **2007**, *98* (2), 131-43.
37. Gessner, B. D.; Adegbola, R. A., The impact of vaccines on pneumonia: Key lessons from Haemophilus influenzae type b conjugate vaccines. *Vaccine* **2008**, *26*, B3-B8.
38. Seeberger, P. H., Discovery of Semi- and Fully-Synthetic Carbohydrate Vaccines Against Bacterial Infections Using a Medicinal Chemistry Approach. *Chem Rev* **2021**, *121* (7), 3598-3626.
39. Crick, F., Central Dogma of Molecular Biology. *Nature* **1970**, *227* (5258), 561-563.
40. Global HIV Programme. <https://www.who.int/teams/global-hiv-hepatitis-and-stis-programmes/hiv/strategic-information/hiv-data-and-statistics> (accessed 12/28/2021).
41. Gilbert, M. T. P.; Rambaut, A.; Wlasiuk, G.; Spira, T. J.; Pitchenik, A. E.; Worobey, M., The emergence of HIV/AIDS in the Americas and beyond. *P Natl Acad Sci USA* **2007**, *104* (47), 18566-18570.

42. Esposito, C.; Escolino, M.; Troncoso Solar, B.; Iacona, R.; Esposito, R.; Settimi, A.; Mushtaq, I., Diagnosis and long-term outcome of renal cysts after laparoscopic partial nephrectomy in children. *BJU Int* **2017**, *119* (5), 761-766.
43. Quan, Y.; Rong, L.; Liang, C.; Wainberg, M. A., Reverse transcriptase inhibitors can selectively block the synthesis of differently sized viral DNA transcripts in cells acutely infected with human immunodeficiency virus type 1. *J Virol* **1999**, *73* (8), 6700-6707.
44. WHO Director-General's opening remarks at the media briefing on COVID-19 - 11 March 2020. <https://www.who.int/director-general/speeches/detail/who-director-general-s-opening-remarks-at-the-media-briefing-on-covid-19---11-march-2020> (accessed 12/28/2021).
45. Kupferschmidt, K.; Cohen, J., WHO launches global megatrial of the four most promising coronavirus treatments. *Science* 03/22/2020, 2020.
46. Scavone, C.; Brusco, S.; Bertini, M.; Sportiello, L.; Rafaniello, C.; Zoccoli, A.; Berrino, L.; Racagni, G.; Rossi, F.; Capuano, A., Current pharmacological treatments for COVID-19: What's next? *Brit J Pharmacol* **2020**, *177* (21), 4813-4824.
47. Warren, T. K.; Jordan, R.; Lo, M. K.; Ray, A. S.; Mackman, R. L.; Soloveva, V.; Siegel, D.; Perron, M.; Bannister, R.; Hui, H. C.; Larson, N.; Strickley, R.; Wells, J.; Stuthman, K. S.; Van Tongeren, S. A.; Garza, N. L.; Donnelly, G.; Shurtleff, A. C.; Retterer, C. J.; Gharaibeh, D.; Zamani, R.; Kenny, T.; Eaton, B. P.; Grimes, E.; Welch, L. S.; Gomba, L.; Wilhelmsen, C. L.; Nichols, D. K.; Nuss, J. E.; Nagle, E. R.; Kugelman, J. R.; Palacios, G.; Doerffler, E.; Neville, S.; Carra, E.; Clarke, M. O.; Zhang, L.; Lew, W.; Ross, B.; Wang, Q.; Chun, K.; Wolfe, L.; Babusis, D.; Park, Y.; Stray, K. M.; Trancheva, I.; Feng, J. Y.; Barauskas, O.; Xu, Y.; Wong, P.; Braun, M. R.; Flint, M.; McMullan, L. K.; Chen, S.-S.; Fearn, R.; Swaminathan, S.; Mayers, D. L.; Spiropoulou, C. F.; Lee, W. A.; Nichol, S. T.; Cihlar, T.; Bavari, S., Therapeutic efficacy of the small molecule GS-5734 against Ebola virus in rhesus monkeys. *Nature* **2016**, *531* (7594), 381-385.
48. Coronavirus (COVID-19) Update: FDA Authorizes Additional Oral Antiviral for Treatment of COVID-19 in Certain Adults. U.S. Food & Drug Administration: FDA News Release, 2021.

49. Kabinger, F.; Stiller, C.; Schmitzová, J.; Dienemann, C.; Kokic, G.; Hillen, H. S.; Höbartner, C.; Cramer, P., Mechanism of molnupiravir-induced SARS-CoV-2 mutagenesis. *Nat Struct Mol Biol* **2021**, 28 (9), 740-746.
50. Platt, F. M.; Neises, G. R.; Dwek, R. A.; Butters, T. D., N-butyldeoxynojirimycin is a novel inhibitor of glycolipid biosynthesis. *J Biol Chem* **1994**, 269 (11), 8362-8365.
51. Moyses, C., Substrate Reduction Therapy: Clinical Evaluation in Type 1 Gaucher Disease. *Philosophical Transactions: Biological Sciences* **2003**, 358 (1433), 955-960.
52. Ratner, L.; Vander Heyden, N., Mechanism of action of N-butyl deoxynojirimycin in inhibiting HIV-1 infection and activity in combination with nucleoside analogs. *AIDS research and human retroviruses* **1993**, 9 (4), 291-7.
53. Fischer, P. B.; Karlsson, G. B.; Dwek, R. A.; Platt, F. M., N-butyldeoxynojirimycin-mediated inhibition of human immunodeficiency virus entry correlates with impaired gp120 shedding and gp41 exposure. *J Virol* **1996**, 70 (10), 7153-7160.
54. Fanunza, E.; Frau, A.; Corona, A.; Tramontano, E., Chapter Four - Antiviral Agents Against Ebola Virus Infection: Repositioning Old Drugs and Finding Novel Small Molecules. In *Annual Reports in Medicinal Chemistry*, Botta, M., Ed. Academic Press: 2018; Vol. 51, pp 135-173.
55. Fischl, M. A.; Resnick, L.; Coombs, R.; Kremer, A. B.; Pottage, J. C., Jr.; Fass, R. J.; Fife, K. H.; Powderly, W. G.; Collier, A. C.; Aspinall, R. L.; et al., The safety and efficacy of combination N-butyl-deoxynojirimycin (SC-48334) and zidovudine in patients with HIV-1 infection and 200-500 CD4 cells/mm³. *Journal of acquired immune deficiency syndromes* **1994**, 7 (2), 139-47.
56. Zhu, Q.; Tong, Y.; Wu, T.; Li, J.; Tong, N., Comparison of the hypoglycemic effect of acarbose monotherapy in patients with type 2 diabetes mellitus consuming an Eastern or Western diet: a systematic meta-analysis. *Clin Ther* **2013**, 35 (6), 880-99.
57. Scheen, A. J., Clinical efficacy of acarbose in diabetes mellitus: a critical review of controlled trials. *Diabetes Metab* **1998**, 24 (4), 311-20.

58. McIver, L. A.; Tripp, J. Acarbose. <https://www.ncbi.nlm.nih.gov/books/NBK493214/> (accessed 12/30/2021).
59. Alquwaizani, M.; Buckley, L.; Adams, C.; Fanikos, J., Anticoagulants: A Review of the Pharmacology, Dosing, and Complications. *Curr Emerg Hosp Med Rep* **2013**, *1* (2), 83-97.
60. Seeberger, P. H.; Cummings, R. D., Glycans in Biotechnology and the Pharmaceutical Industry. In *Essentials of Glycobiology*, rd; Varki, A.; Cummings, R. D.; Esko, J. D.; Stanley, P.; Hart, G. W.; Aebi, M.; Darvill, A. G.; Kinoshita, T.; Packer, N. H.; Prestegard, J. H.; Schnaar, R. L.; Seeberger, P. H., Eds. Cold Spring Harbor (NY), 2015; pp 729-741.
61. Krasnova, L.; Wong, C. H., Understanding the Chemistry and Biology of Glycosylation with Glycan Synthesis. *Annu. Rev. Biochem.* **2016**, *85*, 599-630.
62. Guerrini, M.; Beccati, D.; Shriver, Z.; Naggi, A.; Viswanathan, K.; Bisio, A.; Capila, I.; Lansing, J. C.; Guglieri, S.; Fraser, B.; Al-Hakim, A.; Gunay, N. S.; Zhang, Z. Q.; Robinson, L.; Buhse, L.; Nasr, M.; Woodcock, J.; Langer, R.; Venkataraman, G.; Linhardt, R. J.; Casu, B.; Torri, G.; Sasisekharan, R., Oversulfated chondroitin sulfate is a contaminant in heparin associated with adverse clinical events. *Nature Biotechnology* **2008**, *26* (6), 669-675.
63. Boltje, T. J.; Buskas, T.; Boons, G. J., Opportunities and challenges in synthetic oligosaccharide and glycoconjugate research. *Nat. Chem.* **2009**, *1* (8), 611-622.
64. Leng, W.-L.; Yao, H.; He, J.-X.; Liu, X.-W., Venturing beyond Donor-Controlled Glycosylation: New Perspectives toward Anomeric Selectivity. *Acc. Chem. Res.* **2018**, *51* (3), 628-639.
65. Crich, D., Mechanism of a chemical glycosylation reaction. *Acc Chem Res* **2010**, *43* (8), 1144-53.
66. Andreana, P. R.; Crich, D., Guidelines for O-Glycoside Formation from First Principles. *Acs Central Sci* **2021**, *7* (9), 1454-1462.
67. Boons, G. J., Recent developments in chemical oligosaccharide synthesis. *Contemp Org Synth* **1996**, *3* (3), 173-200.
68. Kim, J. H.; Yang, H.; Boons, G. J., Stereoselective glycosylation reactions with chiral auxiliaries. *Angew. Chem., Int. Ed.* **2005**, *44* (6), 947-949.

69. Kim, J. H.; Yang, H.; Park, J.; Boons, G. J., A general strategy for stereoselective glycosylations. *J. Am. Chem. Soc.* **2005**, *127* (34), 12090-12097.
70. Yasomane, J. P.; Demchenko, A. V., Effect of Remote Picolinyl and Picoloyl Substituents on the Stereoselectivity of Chemical Glycosylation. *J. Am. Chem. Soc.* **2012**, *134* (49), 20097-20102.
71. Yasomane, J. P.; Demchenko, A. V., Hydrogen Bond Mediated Aglycone Delivery: Synthesis of Linear and Branched α -Glucans. *Angew. Chem., Int. Ed.* **2014**, *53* (39), 10453-10456.
72. Crich, D.; Sun, S. X., Direct synthesis of beta-mannopyranosides by the sulfoxide method. *J. Org. Chem.* **1997**, *62* (5), 1198-1199.
73. Nigudkar, S. S.; Demchenko, A. V., Stereocontrolled 1,2-cis glycosylation as the driving force of progress in synthetic carbohydrate chemistry. *Chem. Sci.* **2015**, *6* (5), 2687-2704.
74. Goodman, L., Neighboring-Group Participation in Sugars. In *Advances in Carbohydrate Chemistry*, Wolfrom, M. L.; Tipson, R. S., Eds. Academic Press: 1967; Vol. 22, pp 109-175.
75. Ding, F.; Ishiwata, A.; Ito, Y., Bimodal Glycosyl Donors Protected by 2-O-(ortho-Tosylamido)benzyl Group. *Org Lett* **2018**, *20* (14), 4384-4388.
76. Crich, D.; Sun, S., Direct Synthesis of β -Mannopyranosides by the Sulfoxide Method. *The Journal of Organic Chemistry* **1997**, *62* (5), 1198-1199.
77. Crich, D.; Sun, S., Formation of β -Mannopyranosides of Primary Alcohols Using the Sulfoxide Method. *The Journal of Organic Chemistry* **1996**, *61* (14), 4506-4507.
78. Huang, M.; Garrett, G. E.; Birlirakis, N.; Bohé, L.; Pratt, D. A.; Crich, D., Dissecting the mechanisms of a class of chemical glycosylation using primary ^{13}C kinetic isotope effects. *Nat Chem* **2012**, *4* (8), 663-667.
79. Loh, C. C. J., Exploiting non-covalent interactions in selective carbohydrate synthesis. *Nat Rev Chem* **2021**, *5* (11), 792-815.
80. Levi, S. M.; Jacobsen*, E. N., Catalyst-Controlled Glycosylation. In *Organic Reactions*, pp 801-852.
81. Michael, A., On the synthesis of helicin and phenolglucoside. *Am. Chem. J* **1879**, *1*, 305-312.

82. Koenigs, W.; Knorr, E., Ueber einige Derivate des Traubenzuckers und der Galactose. *Berichte der deutschen chemischen Gesellschaft* **1901**, 34 (1), 957-981.
83. Brigl, P.; Keppler, H., Carbohydrates, IV On the synthesis of alpha-glucosides. *Berichte Der Deutschen Chemischen Gesellschaft* **1926**, 59, 1588-1591.
84. Lemieux, R. U.; Hendriks, K. B.; Stick, R. V.; James, K., Halide Ion Catalyzed Glycosidation Reactions Syntheses of Alpha-Linked Disaccharides. *J Am Chem Soc* **1975**, 97 (14), 4056-4062.
85. Schombs, M.; Gervay-Hague, J., GLYCOCHEMISTRY. In *Glycochemical Synthesis*, 2016; pp 1-34.
86. Kaeothip, S.; Yasomane, J. P.; Demchenko, A. V., Glycosidation of Thioglycosides in the Presence of Bromine: Mechanism, Reactivity, and Stereoselectivity. *The Journal of Organic Chemistry* **2012**, 77 (1), 291-299.
87. Nogueira, J. M.; Nguyen, S. H.; Bennett, C. S., Cyclopropenium Cation Promoted Dehydrative Glycosylations Using 2-Deoxy- and 2,6-Dideoxy-Sugar Donors. *Org Lett* **2011**, 13 (11), 2814-2817.
88. Issa, J. P.; Lloyd, D.; Steliotes, E.; Bennett, C. S., Reagent Controlled β -Specific Dehydrative Glycosylation Reactions with 2-Deoxy-Sugars. *Org Lett* **2013**, 15 (16), 4170-4173.
89. Fischer, E., Ueber die Glucoside der Alkohole. *Berichte der deutschen chemischen Gesellschaft* **1893**, 26 (3), 2400-2412.
90. Nielsen, M. M.; Pedersen, C. M., Catalytic Glycosylations in Oligosaccharide Synthesis. *Chem Rev* **2018**, 118 (17), 8285-8358.
91. Schmidt, R. R.; Michel, J., Facile Synthesis of Alpha-O-Glycosyl and Beta-O-Glycosyl Imidates - Preparation of Glycosides and Disaccharides. *Angew Chem Int Edit* **1980**, 19 (9), 731-732.
92. Schmidt, R. R.; Stumpp, M.; Michel, J., α - and β -d-glucopyranosyl phosphates from O- α -D-glucopyranosyl trichloroacetimidates. *Tetrahedron Lett* **1982**, 23 (4), 405-408.
93. Schmidt, R. R.; Gaden, H.; Jatzke, H., New catalysts for the glycosyl transfer with O-glycosyl trichloroacetimidates. *Tetrahedron Lett* **1990**, 31 (3), 327-329.
94. Kumar, A.; Kumar, V.; Dere, R. T.; Schmidt, R. R., Glycoside Bond Formation via Acid-Base Catalysis. *Org Lett* **2011**, 13 (14), 3612-3615.

95. Gouliaras, C.; Lee, D.; Chan, L.; Taylor, M. S., Regioselective Activation of Glycosyl Acceptors by a Diarylborinic Acid-Derived Catalyst. *J. Am. Chem. Soc.* **2011**, *133* (35), 13926-13929.
96. Kumar, A.; Geng, Y.; Schmidt, R. R., Silicon Fluorides for Acid-Base Catalysis in Glycosidations. *Adv. Synth. Catal.* **2012**, *354* (8), 1489-1499.
97. Peng, P.; Schmidt, R. R., An Alternative Reaction Course in O-Glycosidation with O-Glycosyl Trichloroacetimidates as Glycosyl Donors and Lewis Acidic Metal Salts as Catalyst: Acid-Base Catalysis with Gold Chloride-Glycosyl Acceptor Adducts. *J. Am. Chem. Soc.* **2015**, *137* (39), 12653-12659.
98. Li, T.; Li, T.; Zhuang, H.; Wang, F.; Schmidt, R. R.; Peng, P., O-Glycosyl Trichloroacetimidates as Glycosyl Donors and Platinum(IV) Chloride as a Dual Catalyst Permitting Stereo- and Regioselective Glycosidations. *ACS Catal.* **2021**, *11* (16), 10279-10287.
99. Chuit, C.; Corriu, R. J. P.; Reye, C.; Young, J. C., Reactivity of penta- and hexacoordinate silicon compounds and their role as reaction intermediates. *Chem. Rev.* **1993**, *93* (4), 1371-1448.
100. Yang, J.; Cooper-Vanosdell, C.; Mensah, E. A.; Nguyen, H. M., Cationic Palladium(II)-Catalyzed Stereoselective Glycosylation with Glycosyl Trichloroacetimidates. *The Journal of Organic Chemistry* **2008**, *73* (3), 794-800.
101. Mensah, E. A.; Azzarelli, J. M.; Nguyen, H. M., Palladium-Controlled β -Selective Glycosylation in the Absence of the C(2)-Ester Participatory Group. *The Journal of Organic Chemistry* **2009**, *74* (4), 1650-1657.
102. McKay, M. J.; Naab, B. D.; Mercer, G. J.; Nguyen, H. M., Selective Formation of β -O-Aryl Glycosides in the Absence of the C(2)-Ester Neighboring Group. *The Journal of Organic Chemistry* **2009**, *74* (13), 4705-4711.
103. Terada, M., Binaphthol-derived phosphoric acid as a versatile catalyst for enantioselective carbon-carbon bond forming reactions. *Chem Commun* **2008**, (35), 4097-4112.
104. Akiyama, T., Stronger Brønsted Acids. *Chem. Rev.* **2007**, *107* (12), 5744-5758.

105. Hamilton, G. L.; Kanai, T.; Toste, F. D., Chiral Anion-Mediated Asymmetric Ring Opening of meso-Aziridinium and Episulfonium Ions. *J. Am. Chem. Soc.* **2008**, *130* (45), 14984-14986.
106. Cox, D. J.; Smith, M. D.; Fairbanks, A. J., Glycosylation Catalyzed by a Chiral Brønsted Acid. *Org Lett* **2010**, *12* (7), 1452-1455.
107. Kimura, T.; Sekine, M.; Takahashi, D.; Toshima, K., Chiral Brønsted Acid Mediated Glycosylation with Recognition of Alcohol Chirality. *Angewandte Chemie International Edition* **2013**, *52* (46), 12131-12134.
108. Tay, J.-H.; Argüelles, A. J.; DeMars, M. D.; Zimmerman, P. M.; Sherman, D. H.; Nagorny, P., Regiodivergent Glycosylations of 6-Deoxy-erythronolide B and Oleandomycin-Derived Macrolactones Enabled by Chiral Acid Catalysis. *J. Am. Chem. Soc.* **2017**, *139* (25), 8570-8578.
109. Wabnitz, T. C.; Yu, J.-Q.; Spencer, J. B., Evidence That Protons Can Be the Active Catalysts in Lewis Acid Mediated Hetero-Michael Addition Reactions. *Chemistry – A European Journal* **2004**, *10* (2), 484-493.
110. Taylor, J. G.; Adrio, L. A.; Hii, K. K., Hydroamination reactions by metal triflates: Brønsted acid vs. metal catalysis? *Dalton T* **2010**, *39* (5), 1171-1175.
111. Dang, T. T.; Boeck, F.; Hintermann, L., Hidden Brønsted Acid Catalysis: Pathways of Accidental or Deliberate Generation of Triflic Acid from Metal Triflates. *The Journal of Organic Chemistry* **2011**, *76* (22), 9353-9361.
112. Sletten, E. T.; Tu, Y.-J.; Schlegel, H. B.; Nguyen, H. M., Are Brønsted Acids the True Promoter of Metal-Triflate-Catalyzed Glycosylations? A Mechanistic Probe into 1,2-cis-Aminoglycoside Formation by Nickel Triflate. *ACS Catal.* **2019**, *9* (3), 2110-2123.
113. Parvin, T.; Yadav, R.; Choudhury, L. H., Recent applications of thiourea-based organocatalysts in asymmetric multicomponent reactions (AMCRs). *Org Biomol Chem* **2020**, *18* (29), 5513-5532.
114. Balmond, E. I.; Coe, D. M.; Galan, M. C.; McGarrigle, E. M., α -Selective Organocatalytic Synthesis of 2-Deoxygalactosides. *Angewandte Chemie International Edition* **2012**, *51* (36), 9152-9155.

115. Kotke, M.; Schreiner, P. R., Generally Applicable Organocatalytic Tetrahydropyranylation of Hydroxy Functionalities with Very Low Catalyst Loading. *Synthesis* **2007**, 2007 (05), 779-790.
116. Bradshaw, G. A.; Colgan, A. C.; Allen, N. P.; Pongener, I.; Boland, M. B.; Ortin, Y.; McGarrigle, E. M., Stereoselective organocatalyzed glycosylations – thiouracil, thioureas and monothiophthalimide act as Brønsted acid catalysts at low loadings. *Chem Sci* **2019**, 10 (2), 508-514.
117. Kimura, T.; Eto, T.; Takahashi, D.; Toshima, K., Stereocontrolled Photoinduced Glycosylation Using an Aryl Thiourea as an Organo photoacid. *Org Lett* **2016**, 18 (13), 3190-3193.
118. Reisman, S. E.; Doyle, A. G.; Jacobsen, E. N., Enantioselective Thiourea-Catalyzed Additions to Oxocarbenium Ions. *J. Am. Chem. Soc.* **2008**, 130 (23), 7198-7199.
119. Sun, L.; Wu, X.; Xiong, D.-C.; Ye, X.-S., Stereoselective Koenigs–Knorr Glycosylation Catalyzed by Urea. *Angewandte Chemie International Edition* **2016**, 55 (28), 8041-8044.
120. Park, Y.; Harper, K. C.; Kuhl, N.; Kwan, E. E.; Liu, R. Y.; Jacobsen, E. N., Macrocyclic bis-thioureas catalyze stereospecific glycosylation reactions. *Science* **2017**, 355 (6321), 162-166.
121. Levi, S. M.; Li, Q.; Rötheli, A. R.; Jacobsen, E. N., Catalytic activation of glycosyl phosphates for stereoselective coupling reactions. *Proceedings of the National Academy of Sciences* **2019**, 116 (1), 35.
122. Li, Q.; Levi, S. M.; Jacobsen, E. N., Highly Selective β -Mannosylations and β -Rhamnosylations Catalyzed by Bis-thiourea. *J. Am. Chem. Soc.* **2020**, 142 (27), 11865-11872.
123. Lairson, L. L.; Henrissat, B.; Davies, G. J.; Withers, S. G., Glycosyltransferases: Structures, functions, and mechanisms. *Annu. Rev. Biochem.* **2008**, 77, 521-555.
124. Lemieux, R. U.; Morgan, A. R., Mechanism for Formation of 1,2-Cis-Pyridine Nucleosides from 1,2-Cis-Acetohalogenosugars - a Novel Rearrangement. *J. Am. Chem. Soc.* **1963**, 85 (12), 1889-1890.
125. Lemieux, R. U.; Morgan, A. R., Abnormal Conformations of Pyridinium Alpha-Glycopyranosides. *Can. J. Chem.* **1965**, 43 (8), 2205-2213.
126. Yu, F.; Li, J.; DeMent, P. M.; Tu, Y.-J.; Schlegel, H. B.; Nguyen, H. M., Phenanthroline-Catalyzed Stereoretentive Glycosylations. *Angewandte Chemie-International Edition* **2019**, 58.

127. Taha, H. A.; Richards, M. R.; Lowary, T. L., Conformational Analysis of Furanoside-Containing Mono- and Oligosaccharides. *Chem. Rev.* **2013**, *113* (3), 1851-1876.
128. McKay, M. J.; Nguyen, H. M., Recent Advances in Transition Metal-Catalyzed Glycosylation. *ACS Catal.* **2012**, *2* (8), 1563-1595.
129. Kaeothip, S.; Pornsuriyasak, P.; Demchenko, A. V., Silver(I) tetrafluoroborate as a potent promoter for chemical glycosylation. *Tetrahedron Lett.* **2008**, *49* (9), 1542-1545.
130. Nigudkar, S. S.; Stine, K. J.; Demchenko, A. V., Regenerative Glycosylation under Nucleophilic Catalysis. *J. Am. Chem. Soc.* **2014**, *136* (3), 921-923.
131. Chatterjee, S.; Moon, S.; Hentschel, F.; Gilmore, K.; Seeberger, P. H., An Empirical Understanding of the Glycosylation Reaction. *J. Am. Chem. Soc.* **2018**, *140* (38), 11942-11953.
132. Lu, S. R.; Lai, Y. H.; Chen, J. H.; Liu, C. Y.; Mong, K. K., Dimethylformamide: an unusual glycosylation modulator. *Angew. Chem., Int. Ed.* **2011**, *50* (32), 7315-7320.
133. Vasudevan, D.; Takeuchi, H.; Johar, S. S.; Majerus, E.; Haltiwanger, R. S., Peters Plus Syndrome Mutations Disrupt a Noncanonical ER Quality-Control Mechanism. *Curr Biol* **2015**, *25* (3), 286-295.
134. DeMent, P. M.; Liu, C.; Wakpal, J.; Schaugaard, R. N.; Schlegel, H. B.; Nguyen, H. M., Phenanthroline-Catalyzed Stereoselective Formation of α -1,2-cis 2-Deoxy-2-Fluoro Glycosides. *ACS Catal.* **2021**, *11* (4), 2108-2120.
135. Saunders, C.; Khaled, M. B.; Weaver, J. D.; Tantillo, D. J., Prediction of F-19 NMR Chemical Shifts for Fluorinated Aromatic Compounds. *J. Org. Chem.* **2018**, *83* (6), 3220-3225.
136. Johnson, R. M.; Vinetz, J. M., Dexamethasone in the management of covid-19. *Bmj-Brit Med J* **2020**, *370*.
137. Lammers, T.; Sofias, A. M.; van der Meel, R.; Schiffelers, R.; Storm, G.; Tacke, F.; Koschmieder, S.; Brummendorf, T. H.; Kiessling, F.; Metselaar, J. M., Dexamethasone nanomedicines for COVID-19. *Nat. Nanotechnol.* **2020**, *15* (8), 622-624.

138. Fraser-Reid, B.; López, J. C., Armed–Disarmed Effects in Carbohydrate Chemistry: History, Synthetic and Mechanistic Studies. In *Reactivity Tuning in Oligosaccharide Assembly*, Fraser-Reid, B.; Cristóbal López, J., Eds. Springer Berlin Heidelberg: Berlin, Heidelberg, 2011; pp 1-29.
139. van der Vorm, S.; Hansen, T.; van Hengst, J. M. A.; Overkleeft, H. S.; van der Marel, G. A.; Codee, J. D. C., Acceptor reactivity in glycosylation reactions. *Chem. Soc. Rev.* **2019**, *48* (17), 4688-4706.
140. Nguyen, H. M.; Poole, J. L.; Gin, D. Y., Chemoselective iterative dehydrative glycosylation. *Angew. Chem., Int. Ed.* **2001**, *40* (2), 414-417.
141. Kanie, O.; Ito, Y.; Ogawa, T., Orthogonal Glycosylation Strategy in Oligosaccharide Synthesis. *J. Am. Chem. Soc.* **1994**, *116* (26), 12073-12074.
142. Ito, Y.; Kanie, O.; Ogawa, T., Orthogonal glycosylation strategy for rapid assembly of oligosaccharides on a polymer support. *Angew Chem Int Edit* **1996**, *35* (21), 2510-2512.
143. Kanie, O.; Ohtsuka, I.; Ako, T.; Daikoku, S.; Kame, Y.; Kato, R., Orthogonal glycosylation reactions on solid phase and synthesis of a library consisting of a complete set of fucosyl galactose isomers. *Angew. Chem., Int. Ed.* **2006**, *45* (23), 3851-3854.
144. Bencini, A.; Lippolis, V., 1,10-Phenanthroline: A versatile building block for the construction of ligands for various purposes. *Coord. Chem. Rev.* **2010**, *254* (17-18), 2096-2180.
145. Erkkila, K. E.; Odom, D. T.; Barton, J. K., Recognition and reaction of metallointercalators with DNA. *Chem. Rev.* **1999**, *99* (9), 2777-2795.
146. Stephens, P. J.; Devlin, F. J.; Chabalowski, C. F.; Frisch, M. J., Ab-Initio Calculation of Vibrational Absorption and Circular-Dichroism Spectra Using Density-Functional Force-Fields. *J. Phys. Chem.* **1994**, *98* (45), 11623-11627.
147. Becke, A. D., Density-Functional Thermochemistry .3. The Role of Exact Exchange. *J. Chem. Phys.* **1993**, *98* (7), 5648-5652.
148. Lee, C. T.; Yang, W. T.; Parr, R. G., Development of the Colle-Salvetti Correlation-Energy Formula into a Functional of the Electron-Density. *Phys. Rev. B* **1988**, *37* (2), 785-789.

149. Becke, A. D., Density-Functional Exchange-Energy Approximation with Correct Asymptotic-Behavior. *Phys. Rev. A* **1988**, 38 (6), 3098-3100.
150. Vosko, S. H.; Wilk, L.; Nusair, M., Accurate Spin-Dependent Electron Liquid Correlation Energies for Local Spin-Density Calculations - a Critical Analysis. *Can. J. Phys.* **1980**, 58 (8), 1200-1211.
151. Francl, M. M.; Pietro, W. J.; Hehre, W. J.; Binkley, J. S.; Gordon, M. S.; Defrees, D. J.; Pople, J. A., Self-Consistent Molecular-Orbital Methods .23. A Polarization-Type Basis Set for 2nd-Row Elements. *J. Chem. Phys.* **1982**, 77 (7), 3654-3665.
152. Gordon, M. S., The Isomers of Silacyclopropane. *Chem. Phys. Lett.* **1980**, 76 (1), 163-168.
153. Hariharan, P. C.; Pople, J. A., Accuracy of Ah Equilibrium Geometries by Single Determinant Molecular-Orbital Theory. *Mol. Phys.* **1974**, 27 (1), 209-214.
154. Harihara.Pc; Pople, J. A., Influence of Polarization Functions on Molecular-Orbital Hydrogenation Energies. *Theor. Chim. Acta* **1973**, 28 (3), 213-222.
155. Hehre, W. J.; Ditchfield, R.; Pople, J. A., Self-Consistent Molecular-Orbital Methods .12. Further Extensions of Gaussian-Type Basis Sets for Use in Molecular-Orbital Studies of Organic-Molecules. *J. Chem. Phys.* **1972**, 56 (5), 2257-2261.
156. Ditchfield, R.; Hehre, W. J.; Pople, J. A., Self-Consistent Molecular-Orbital Methods .9. Extended Gaussian-Type Basis for Molecular-Orbital Studies of Organic Molecules. *J. Chem. Phys.* **1971**, 54 (2), 724-728.
157. Marenich, A. V.; Cramer, C. J.; Truhlar, D. G., Universal Solvation Model Based on Solute Electron Density and on a Continuum Model of the Solvent Defined by the Bulk Dielectric Constant and Atomic Surface Tensions. *J. Phys. Chem. B* **2009**, 113 (18), 6378-6396.
158. Grimme, S.; Antony, J.; Ehrlich, S.; Krieg, H., A consistent and accurate ab initio parametrization of density functional dispersion correction (DFT-D) for the 94 elements H-Pu. *J. Chem. Phys.* **2010**, 132 (15), 154104.
159. Johnson, E. R.; Becke, A. D., A post-Hartree-Fock model of intermolecular interactions: Inclusion of higher-order corrections. *J. Chem. Phys.* **2006**, 124 (17), 024101.

160. Frisch, M. J.; Trucks, G. W.; Schlegel, H. B.; Scuseria, G. E.; Robb, M. A.; Cheeseman, J. R.; Scalmani, G.; Barone, V.; Petersson, G. A.; Nakatsuji, H.; Li, X.; Caricato, M.; Marenich, A. V.; Bloino, J.; Janesko, B. G.; Gomperts, R.; Mennucci, B.; Hratchian, H. P.; Ortiz, J. V.; Izmaylov, A. F.; Sonnenberg, J. L.; Williams; Ding, F.; Lipparini, F.; Egidi, F.; Goings, J.; Peng, B.; Petrone, A.; Henderson, T.; Ranasinghe, D.; Zakrzewski, V. G.; Gao, J.; Rega, N.; Zheng, G.; Liang, W.; Hada, M.; Ehara, M.; Toyota, K.; Fukuda, R.; Hasegawa, J.; Ishida, M.; Nakajima, T.; Honda, Y.; Kitao, O.; Nakai, H.; Vreven, T.; Throssell, K.; Montgomery Jr., J. A.; Peralta, J. E.; Ogliaro, F.; Bearpark, M. J.; Heyd, J. J.; Brothers, E. N.; Kudin, K. N.; Staroverov, V. N.; Keith, T. A.; Kobayashi, R.; Normand, J.; Raghavachari, K.; Rendell, A. P.; Burant, J. C.; Iyengar, S. S.; Tomasi, J.; Cossi, M.; Millam, J. M.; Klene, M.; Adamo, C.; Cammi, R.; Ochterski, J. W.; Martin, R. L.; Morokuma, K.; Farkas, O.; Foresman, J. B.; Fox, D. J. *Gaussian 09 Rev. E.01*, Wallingford, CT, 2013.
161. Lemieux, R. U., Newer developments in the conformational analysis of carbohydrates. *Pure Appl. Chem.* **1971**, *27* (4), 527-548.
162. Lemieux, R. U.; Morgan, A. R., The Mechanism for the Formation of 1,2-cis-Pyridine Nucleosides from 1,2-cis-Acethalogenosugars. A Novel Rearrangement. *J. Am. Chem. Soc.* **1963**, *85* (12), 1889-1890.
163. Lemieux, R. U.; Morgan, A. R., The Abnormal Conformations of Pyridinium α -Glycopyranosides. *Can. J. Chem.* **1965**, *43* (8), 2205-2213.
164. Dingley, A. J.; Cordier, F.; Grzesiek, S., An introduction to hydrogen bond scalar couplings. *Concepts Magn. Reson.* **2001**, *13* (2), 103-127.
165. Skorupowa, E.; Dmochowska, B.; Madaj, J.; Kasprzykowski, F.; Sokołowski, J.; Wiśniewski, A., Cyclization of N(Tetra-O-acetyl-d-gluco- and d-Mannopyranosyl)-Pyridinium Salts in a Methanolic Solution of Sodium Methylate. *J. Carbohydr. Chem.* **1998**, *17* (1), 49-59.
166. Garcia, B. A.; Gin, D. Y., Dehydrative glycosylation with activated diphenyl sulfonium reagents. Scope, mode of C(1)-hemiacetal activation, and detection of reactive glycosyl intermediates. *J. Am. Chem. Soc.* **2000**, *122* (18), 4269-4279.

167. Sorgenfrei, N.; Hioe, J.; Greindl, J.; Rothermel, K.; Morana, F.; Lokesh, N.; Gschwind, R. M., NMR Spectroscopic Characterization of Charge Assisted Strong Hydrogen Bonds in Bronsted Acid Catalysis. *J. Am. Chem. Soc.* **2016**, *138* (50), 16345-16354.
168. Ibba, F.; Pupo, G.; Thompson, A. L.; Brown, J. M.; Claridge, T. D. W.; Gouverneur, V., Impact of Multiple Hydrogen Bonds with Fluoride on Catalysis: Insight from NMR Spectroscopy. *J. Am. Chem. Soc.* **2020**, *142* (46), 19731-19744.
169. Mizan, T. I.; Savage, P. E.; Ziff, R. M., Temperature Dependence of Hydrogen Bonding in Supercritical Water. *J. Phys. Chem.* **1996**, *100* (1), 403-408.
170. Marino, C.; Gallo-Rodriguez, C.; Lederkremer, R. M. d., Galactofuranosyl-containing glycans: occurrence, synthesis and biochemistry. In *Glycans: Biochemistry, Characterization and Applications*, Mora-Montes, H. M., Ed. Nova Science Publishers, Inc.: Hauppauge, NY, 2012; pp 207-268.
171. Richards, M. R.; Lowary, T. L., Chemistry and biology of galactofuranose-containing polysaccharides. *Chembiochem* **2009**, *10* (12), 1920-38.
172. Tefsen, B.; van Die, I., Glycosyltransferases in chemo-enzymatic synthesis of oligosaccharides. *Methods Mol Biol* **2013**, *1022*, 357-67.
173. Lowary, T. L., Synthesis and conformational analysis of arabinofuranosides, galactofuranosides and fructofuranosides. *Curr Opin Chem Biol* **2003**, *7* (6), 749-56.
174. Imamura, A.; Lowary, T., Chemical Synthesis of Furanose Glycosides. *Trends Glycosci Glyc* **2011**, *23* (131), 134-152.
175. Gallo-Rodriguez, C.; Kashiwagi, G. A., Selective Glycosylations with Furanosides. In *Selective Glycosylations: Synthetic Methods and Catalysts*, Bennett, C. S., Ed. 2017; pp 297-326.
176. Angala, S. K.; Belardinelli, J. M.; Huc-Claustre, E.; Wheat, W. H.; Jackson, M., The cell envelope glycoconjugates of Mycobacterium tuberculosis. *Crit Rev Biochem Mol* **2014**, *49* (5), 361-399.
177. Lowary, T. L., Twenty Years of Mycobacterial Glycans: Furanosides and Beyond. *Acc. Chem. Res.* **2016**, *49* (7), 1379-1388.

178. Crick, D. C.; Mahapatra, S.; Brennan, P. J., Biosynthesis of the arabinogalactan-peptidoglycan complex of *Mycobacterium tuberculosis*. *Glycobiology* **2001**, *11* (9), 107r-118r.
179. Brennan, P. J.; Nikaido, H., THE ENVELOPE OF MYCOBACTERIA. *Annu. Rev. Biochem.* **1995**, *64* (1), 29-63.
180. Lowary, T. L., Recent Progress Towards the Identification of Inhibitors of Mycobacterial Cell Wall Polysaccharide Biosynthesis. *Mini-Rev Med Chem* **2003**, *3* (7), 689-702.
181. Pedersen, L. L.; Turco, S. J., Galactofuranose metabolism: a potential target for antimicrobial chemotherapy. *Cell Mol Life Sci* **2003**, *60* (2), 259-266.
182. Zhu, X. M.; Kawatkar, S.; Rao, Y.; Boons, G. J., Practical approach for the stereoselective introduction of beta-arabinofuranosides. *J. Am. Chem. Soc.* **2006**, *128* (36), 11948-11957.
183. Crich, D.; Pedersen, C. M.; Bowers, A. A.; Wink, D. J., On the use of 3,5-O-benzylidene and 3,5-O-(di-tert-butylsilylene)-2-O-benzylarabinothiofuranosides and their sulfoxides as glycosyl donors for the synthesis of beta-arabinofuranosides: Importance of the activation method. *J. Org. Chem.* **2007**, *72* (5), 1553-1565.
184. Wang, Y. X.; Maguire-Boyle, S.; Dere, R. T.; Zhu, X. M., Synthesis of beta-D-arabinofuranosides: stereochemical differentiation between D- and L-enantiomers. *Carbohydr. Res.* **2008**, *343* (18), 3100-3106.
185. Imamura, A.; Lowary, T. L., beta-Selective Arabinofuranosylation Using a 2,3-O-Xylylene-Protected Donor. *Org Lett* **2010**, *12* (16), 3686-3689.
186. Tilve, M. J.; Gallo-Rodriguez, C., Glycosylation studies on conformationally restricted 3,5-O-(di-tert-butylsilylene)-D-galactofuranosyl trichloroacetimidate donors for 1,2-cis alpha-D-galactofuranosylation. *Carbohydr. Res.* **2011**, *346* (18), 2838-2848.
187. Zhang, L.; Shen, K.; Taha, H. A.; Lowary, T. L., Stereocontrolled Synthesis of alpha-Xylofuranosides Using a Conformationally Restricted Donor. *J. Org. Chem.* **2018**, *83* (15), 7659-7671.

188. Bamhaoud, T.; Sanchez, S.; Prandi, J., 1,2,5-ortho esters of D-arabinose as versatile arabinofuranosidic building blocks. Concise synthesis of the tetrasaccharidic cap of the lipoarabinomannan of *Mycobacterium tuberculosis*. *Chem Commun* **2000**, (8), 659-660.
189. Sanchez, S.; Bamhaoud, T.; Prandi, J., A comprehensive glycosylation system for the elaboration of oligoarabinofuranosides. *Tetrahedron Lett* **2000**, 41 (39), 7447-7452.
190. Ishiwata, A.; Munemura, Y.; Ito, Y., NAP ether mediated intramolecular aglycon delivery: A unified strategy for 1,2-cis-glycosylation. *Eur. J. Org. Chem.* **2008**, 2008 (25), 4250-4263.
191. Argunov, D. A.; Krylov, V. B.; Nifantiev, N. E., Convergent synthesis of isomeric heterosaccharides related to the fragments of galactomannan from *Aspergillus fumigatus*. *Org Biomol Chem* **2015**, 13 (11), 3255-3267.
192. Lee, Y. J.; Lee, K.; Jung, E. H.; Jeon, H. B.; Kim, K. S., Acceptor-dependent stereoselective glycosylation: 2'-CB glycoside-mediated direct beta-D-arabinofuranosylation and efficient synthesis of the octaarabinofuranoside in mycobacterial cell wall. *Org Lett* **2005**, 7 (15), 3263-3266.
193. Liu, Q. W.; Bin, H. C.; Yang, J. S., beta-Arabinofuranosylation Using 5-O-(2-Quinolinecarbonyl) Substituted Ethyl Thioglycoside Donors. *Org Lett* **2013**, 15 (15), 3974-3977.
194. Gadikota, R. R.; Callam, C. S.; Wagner, T.; Del Fraino, B.; Lowary, T. L., 2,3-anhydro sugars in glycoside bond synthesis. Highly stereoselective syntheses of oligosaccharides containing alpha- and beta-arabinofuranosyl linkages. *J. Am. Chem. Soc.* **2003**, 125 (14), 4155-4165.
195. Gadikota, R. R.; Callam, C. S.; Lowary, T. L., Stereocontrolled synthesis of 2,3-anhydro-beta-D-lyxofuranosyl glycosides. *Org Lett* **2001**, 3 (4), 607-610.
196. Mereyala, H. B.; Hotha, S.; Gurjar, M. K., Synthesis of pentaarabinofuranosyl structure motif a of *Mycobacterium tuberculosis*. *Chem Commun* **1998**, (6), 685-686.
197. Désiré, J.; Prandi, J., Synthesis of methyl beta-D-arabinofuranoside 5-[1D (and L)-myo-inositol 1-phosphate], the capping motif of the lipoarabinomannan of *Mycobacterium smegmatis*. *Carbohydr Res* **1999**, 317 (1-4), 110-8.

198. Subramaniam, V.; Lowary, T. L., Synthesis of oligosaccharide fragments of mannosylated lipoarabinomannan from *Mycobacterium tuberculosis*. *Tetrahedron* **1999**, *55* (19), 5965-5976.
199. D'Souza, F. W.; Lowary, T. L., The first total synthesis of a highly branched arabinofuranosyl hexasaccharide found at the nonreducing termini of mycobacterial arabinogalactan and lipoarabinomannan. *Org Lett* **2000**, *2* (10), 1493-1495.
200. Yin, H. F.; D'Souza, F. W.; Lowary, T. L., Arabinofuranosides from mycobacteria: Synthesis of a highly branched hexasaccharide and related fragments containing beta-arabinofuranosyl residues. *J. Org. Chem.* **2002**, *67* (3), 892-903.
201. Joe, M.; Sun, D.; Taha, H.; Completo, G. C.; Croudace, J. E.; Lammas, D. A.; Besra, G. S.; Lowary, T. L., The 5-deoxy-5-methylthio-xylofuranose residue in mycobacterial lipoarabinomannan. Absolute stereochemistry, linkage position, conformation, and immunomodulatory activity. *J. Am. Chem. Soc.* **2006**, *128* (15), 5059-5072.
202. Thadke, S. A.; Mishra, B.; Hotha, S., Facile Synthesis of beta- and alpha-Arabinofuranosides and Application to Cell Wall Motifs of *M. tuberculosis*. *Org Lett* **2013**, *15* (10), 2466-2469.
203. Erkkila, A.; Majander, I.; Pihko, P. M., Iminium catalysis. *Chem. Rev.* **2007**, *107* (12), 5416-5470.
204. Mukherjee, S.; Yang, J. W.; Hoffmann, S.; List, B., Asymmetric enamine catalysis. *Chem. Rev.* **2007**, *107* (12), 5471-5569.
205. Wurz, R. P., Chiral dialkylaminopyridine catalysts in asymmetric synthesis. *Chem. Rev.* **2007**, *107* (12), 5570-5595.
206. Gaunt, M. J.; Johansson, C. C. C., Recent developments in the use of catalytic asymmetric ammonium enolates in chemical synthesis. *Chem. Rev.* **2007**, *107* (12), 5596-5605.
207. Enders, D.; Niemeier, O.; Henseler, A., Organocatalysis by N-heterocyclic, carbenes. *Chem. Rev.* **2007**, *107* (12), 5606-5655.
208. Hashimoto, T.; Maruoka, K., Recent development and application of chiral phase-transfer catalysts. *Chem. Rev.* **2007**, *107* (12), 5656-5682.

209. Atodiresei, L.; Schiffers, I.; Bolm, C., Stereoselective anhydride openings. *Chem. Rev.* **2007**, *107* (12), 5683-5712.
210. Doyle, A. G.; Jacobsen, E. N., Small-molecule H-bond donors in asymmetric catalysis. *Chem. Rev.* **2007**, *107* (12), 5713-5743.
211. Akiyama, T., Stronger bronsted acids. *Chem. Rev.* **2007**, *107* (12), 5744-5758.
212. Davie, E. A. C.; Mennen, S. M.; Xu, Y. J.; Miller, S. J., Asymmetric catalysis mediated by synthetic peptides. *Chem. Rev.* **2007**, *107* (12), 5759-5812.
213. Kamber, N. E.; Jeong, W.; Waymouth, R. M.; Pratt, R. C.; Lohmeijer, B. G. G.; Hedrick, J. L., Organocatalytic ring-opening polymerization. *Chem. Rev.* **2007**, *107* (12), 5813-5840.
214. McGarrigle, E. M.; Myers, E. L.; Illa, O.; Shaw, M. A.; Riches, S. L.; Aggarwal, V. K., Chalcogenides as organocatalysts. *Chem. Rev.* **2007**, *107* (12), 5841-5883.
215. Mayfield, A. B.; Metternich, J. B.; Trotta, A. H.; Jacobsen, E. N., Stereospecific Furanosylations Catalyzed by Bis-thiourea Hydrogen-Bond Donors. *J. Am. Chem. Soc.* **2020**, *142* (8), 4061-4069.
216. Li, J. Y.; Nguyen, H. M., A Mechanistic Probe into 1,2-cis Glycoside Formation Catalyzed by Phenanthroline and Further Expansion of Scope. *Adv. Synth. Catal.* **2021**, *363* (16), 4054-4066.
217. Larsen, C. H.; Ridgway, B. H.; Shaw, J. T.; Smith, D. M.; Woerpel, K. A., Stereoselective C-glycosylation reactions of ribose derivatives: Electronic effects of five-membered ring oxocarbenium ions. *J. Am. Chem. Soc.* **2005**, *127* (31), 10879-10884.
218. Aiguabella, N.; Holland, M. C.; Gilmour, R., Fluorine-directed 1,2-trans glycosylation of rare sugars. *Org Biomol Chem* **2016**, *14* (24), 5534-5538.
219. Koshiha, M.; Suzuki, N.; Arihara, R.; Tsuda, T.; Nambu, H.; Nakamura, S.; Hashimoto, S., Catalytic stereoselective glycosidation with glycosyl diphenyl phosphates: Rapid construction of 1,2-cis-alpha-glycosidic linkages. *Chem-Asian J* **2008**, *3* (8-9), 1664-1677.
220. Lafont, D.; Carriere, F.; Ferrato, F.; Boullanger, P., Syntheses of an alpha-D-Gal-(1 -> 6)-beta-D-Gal diglyceride, as lipase substrate. *Carbohydr. Res.* **2006**, *341* (6), 695-704.

221. Smith, B. M.; Graham, A. E., Indium triflate mediated acetalization of aldehydes and ketones. *Tetrahedron Lett* **2006**, *47* (52), 9317-9319.
222. Sakai, N.; Moritaka, K.; Konakahara, T., A Novel Approach to the Practical Synthesis of Sulfides: An InBr₃-Et₃SiH Catalytic System Promoted the Direct Reductive Sulfidation of Acetals with Disulfides. *Eur. J. Org. Chem.* **2009**, *2009* (24), 4123-4127.
223. Garegg, P. J.; Hultberg, H.; Wallin, S., A Novel, Reductive Ring-Opening of Carbohydrate Benzylidene Acetals .2. *Carbohydr. Res.* **1982**, *108* (1), 97-101.
224. Shie, C. R.; Tzeng, Z. H.; Kulkarni, S. S.; Uang, B. J.; Hsu, C. Y.; Hung, S. C., Cu(OTf)₂ as an efficient and dual-purpose catalyst in the regioselective reductive ring opening of benzylidene acetals. *Angew. Chem., Int. Ed.* **2005**, *44* (11), 1665-1668.
225. Yu, F.; Li, J. Y.; DeMent, P. M.; Tu, Y. J.; Schlegel, H. B.; Nguyen, H. M., Phenanthroline-Catalyzed Stereoretentive Glycosylations. *Angew. Chem. Int. Ed.* **2019**, *58* (21), 6957-6961.
226. Vidadala, S. R.; Hotha, S., Methyl glycosides are identified as glycosyl donors for the synthesis of glycosides, disaccharides and oligosaccharides. *Chem Commun* **2009**, (18), 2505-2507.
227. Chu, A. H.; Nguyen, S. H.; Sisel, J. A.; Minciunescu, A.; Bennett, C. S., Selective synthesis of 1,2-*cis*- α -glycosides without directing groups. Application to iterative oligosaccharide synthesis. *Org Lett* **2013**, *15* (10), 2566-9.
228. Chiba, H.; Funasaka, S.; Mukaiyama, T., Catalytic and stereoselective glycosylation with glucosyl thioformimidates. *B Chem Soc Jpn* **2003**, *76* (8), 1629-1644.
229. Grimme, S.; Antony, J.; Ehrlich, S.; Krieg, H., A consistent and accurate ab initio parametrization of density functional dispersion correction (DFT-D) for the 94 elements H-Pu. *J. Chem. Phys.* **2010**, *132* (15).
230. Johnson, E. R.; Becke, A. D., A post-Hartree-Fock model of intermolecular interactions: Inclusion of higher-order corrections. *J. Chem. Phys.* **2006**, *124* (17).

ABSTRACT**PHENANTHROLINE-CATALYZED 1,2-*CIS* GLYCOSYLATION: SCOPE AND MECHANISM**

by

JIAYI LI**August 2022****Advisor:** Dr. Hien M. Nguyen**Major:** Organic Chemistry**Degree:** Doctor of Philosophy

Phenanthroline, a rigid and planar organic compound with two fused pyridine rings, has been used as a powerful ligand for metals and a binding agent for DNA/RNA. We recently discovered that phenanthroline could be used as a nucleophilic catalyst to access high yielding and diastereoselective α -1,2-*cis* glycosides through the coupling of hydroxyl acceptors with α -glycosyl bromide donors. The utility of the phenanthroline catalysis is expanded to sterically hindered hydroxyl nucleophiles and chemoselective coupling of an alkyl hydroxyl group in the presence of a free C1-hemiacetal functionality. In addition, the phenanthroline-based catalyst has a pronounced effect on site-selective couplings of triol motifs and orthogonally activates the anomeric bromide leaving group over the anomeric fluoride and sulfide counterparts.

An extensive mechanistic investigation showed two glycosyl phenanthrolium ion intermediates, a 4C_1 chair-like β -conformer and a $B_{2,5}$ boat-like α -conformer, in a ratio of 2:1 (β : α). Further, NMR studies show that a hydrogen bonding is formed between the second nitrogen atom of phenanthroline and the C1-anomeric hydrogen of sugar moiety to stabilize the phenanthrolium ion intermediates. To obtain high levels of α -1,2-*cis* stereoselectivity, a Curtin-Hammett scenario was proposed wherein interconversion of the 4C_1 β -conformer and $B_{2,5}$ α -conformer is more rapid than nucleophilic addition. Hydroxyl attack takes

place from the α -face of the more reactive 4C_1 chair-like β -phenanthroline intermediate to give an α -anomeric product.

The phenanthroline catalysis system is applicable to a number of furanosyl bromide donors to provide the challenging 1,2-*cis* substitution products in good yield with high anomeric selectivity. While arabinofuranosyl bromide provides β -1,2-*cis* products, xylo- and ribofuranosyl bromides favor α -1,2-*cis* products. NMR experiments and density-functional theory calculations support an associative mechanism in which the rate-determining step occurs from an invertive displacement of the faster reacting phenanthroline ion intermediate with alcohol nucleophile.

AUTOBIOGRAPHICAL STATEMENT

JIAYI LI

EDUCATION

- 2018-2022 Ph.D., Organic Chemistry
Wayne State University, Detroit, MI, USA
Advisor: Prof. Hien M. Nguyen
- 2013-2017 B. S., Chemical Engineering
University of Iowa, Iowa City, IA, USA,

PUBLICATIONS

1. Yu, F., **Li, J.**, DeMent, P. M., Tu, Y., Schlegel, H. B., Nguyen, H. M. "Phenanthroline-Catalyzed Stereoretentive Glycosylations." *Angew. Chem. Int. Ed.* **2019**, 58(21), 6957-6961
2. Zhu, S., **Li, J.**, Loka, R. S., Vlodayvsky, I., Zhang, K., Nguyen, H. M. "Modulating Heparanase Activity: Tuning Sulfation Pattern and Glycosidic Linkage of Oligosaccharides." *J. Med. Chem.* **2020**, 63(8), 4227-4255
3. **Li, J.**, Nguyen, H. M. "A Mechanistic Probe into 1,2-cis Glycoside Formation Catalyzed by Phenanthroline and Further Expansion of Scope." *Adv. Synth. Catal.* **2021**, 363(16), 4054-4066
4. Xu, H., Schaugaard, R. N.*, **Li, J.***, Schlegel, H. B., Nguyen, H. M. "Phenanthroline-Catalyzed Stereoselective 1,2-cis Furanosylations." *J. Am. Chem. Soc.* **2022**, 144, 7441-7456

PRESENTATIONS

- 02/2021 ACS CARB Glycoscience Meetings, Online
- 08/2021 AbbVie Scholars Symposium, Online
- 03/2022 ACS Spring 2022, Division of Carbohydrate Chemistry, San Diego, CA